Quantum Dynamics, Thermalization and Black holes

A thesis submitted to
Tata Institute of Fundamental Research, Mumbai
for the degree of
Doctor of Philosophy in Physics

by
Sorokhaibam Nilakash Singh

Department of Theoretical Physics, School of Natural Sciences
Tata Institute of Fundamental Research, Mumbai
February, 2017
[Final version submitted in Febraury, 2018]

Declaration

This thesis is a presentation of my original research work. Wherever contributions of others are involved, every effort is made to indicate this clearly, with due reference to the literature, and acknowledgement of collaborative research and discussions.

The work was done under the guidance of Prof. Gautam Mandal, at the Tata Institute of Fundamental Research, Mumbai.

S. Nilakash

Sorokhaibam Nilakash Singh

In my capacity as supervisor of the candidates thesis, I certify that the above statements are true to the best of my knowledge.

Gautam M

Prof. Gautam Mandal

Date:

To my mother, brother and Lydia.

Acknowledgements

First, I would like to thank my supervisor, Prof. Gautam Mandal. None of these works in this thesis would have been possible without his constant guidance, encouragement and motivation. It is needless to mention that I learnt from him almost all of the research level physics that I have learnt so far. The wisdoms that he shared with me are life lessons. He once told me,"Give your talk as if you are teaching the audience". It completely changed my perspective on giving talks. There were many more such stark realizations during the endless conversations and discussions with Prof. Mandal. Equally important for the completion of my PhD journey is the inquisitive atmosphere created by the presence of Prof. Shiraz Minwalla and Prof. Sandip Trivedi. I will miss the seminars which usually go beyond lunchtime.

I would also like to thank my two other collaborators and friends, Ritam Sinha and Shruti Paranjape. The innumerable hours spent together with them are some of my sweetest memories in TIFR.

As in the saying *'It takes a village to raise a child'*, this thesis is a result of the cumulative efforts of many people who have taught me throughout the various stages of my education. To use modern computer parlance, my school teachers gave me the instruction set, my teachers in HRD Academy instilled in me the operating system kernel. The love for Physics shared with my college teachers was like the drivers necessary to run a computer. And finally, in TIFR, I got the various applications which do meaningful works.

I would also like to take the opportunity to thank three authors who inspired me from a very early age with their books. My first encounter with exciting physics was from an old B.Sc. physics book by C.L. Arora. Physics was linear and predictable to me until my encounter with the second book - Chaos, Fractals and Self-Organisation by Arvind Kumar, published by National Book Trust. And the third author who boosted me to the fancy, imaginative realm of present day theoretical physics is Stephen Hawking with his book - A Brief History of Time.

Lastly, I want to thank the Almighty for showing me the path so far. Working on my favourite topics of theoretical physics and finishing this thesis is like a dream come true. Perhaps, my yearning backreacts strongly and constructively to the wavefunction of the Universe.

S.N.S.
February 9, 2018

List of publications

1. G. Mandal, R. Sinha, and N. Sorokhaibam, *The inside outs of AdS(3)/CFT(2): Exact AdS wormholes with entangled CFT duals*, JHEP 1501 (2014) p. 036, [arXiv:1405.6695].

2. G. Mandal, R. Sinha, and N. Sorokhaibam, *Thermalization with chemical potentials, and higher spin black holes*, JHEP 08 (2015) p. 013, [arXiv:1501.0458].

3. G. Mandal, S. Paranjape, and N. Sorokhaibam, *Thermalization in 2D critical quench and UV/IR mixing*, JHEP 01 (2018) p. 027, [arXiv:1512.02187].

4. S. Paranjape, and N. Sorokhaibam, *Exact Growth of Entanglement and Dynamical Phase Transition in Global Fermionic Quench*, arXiv:1609.02926, prepared for submission to JHEP.

The synopsis is based on the first three papers. The results of the fourth paper have also been included in this thesis. Papers 1 and 2 are based on joint work which have partial overlap with the thesis work of Ritam Sinha. The contents of paper 3 are exclusive to this thesis. Some parts of the contents of paper 4 have appeared in the M.Sc. thesis of Shruti Paranjape.

Contents

Synopsis

1 Introduction:

Black holes have always been a fascinating object of study since the Schwarzchild metric was found, shortly after the formulation of general theory of relativity. It is the region of the Universe which essentially marks the closest encounter between quantum mechanics and the general theory of relativity: the two cornerstones of modern science. It is natural to expect such regions of space to provide the most stringent test to any putative Theory of Everything. This viewpoint indeed has been especially fruitful. Although incomplete yet, study of black holes in the context of string theory in fact gives a unified view of the Natural world and provides relation between widely separated models and fields of Physics, the most prominent recent developments being the AdS/CFT correspondence, or the Gauge/Gravity duality. The basic idea of the AdS/CFT correspondence is that gravity in AdS space is dual to a CFT living in the AdS boundary. The standard view of a black hole is that it has a singularity and a horizon which is a null hypersurface enclosing the singularity, and represents the limiting surface from within which even light cannot escape. In recent years, there has been a lively debate on whether quantum mechanics is consistent with a smooth horizon, or in other words whether the inside of a black hole makes sense. Maldacena and Susskind [4] have suggested that the region inside the horizon is a geometric representation of quantum mechanical entanglement. The proposal of [4], summarized by the symbolic equation ER = EPR,[1] is illustrated by the eternal black hole geometry which is dual to the thermofield state [5]. It has been argued in several papers that although the proposal holds for this illustrative special case, it does not hold in general.

Although, ER=EPR has been very interesting for the formalism, the more interesting aspects of black holes are their formation and dynamics. In AdS/CFT correspondence, black holes are dual to microcanonical (or, the equivalent canonical) ensembles in the boundary CFT. Hence, according to AdS/CFT, the dynamical problem of thermalization where a pure quantum mechanical state appears to evolve into a micro-canonical ensemble is analogous to black hole formation. More generally, the question of whether a pure state can evolve non-trivially into a stationary state is the larger issue of equilibration. In fact, in a broad class of statistical mechanics and condensed matter examples, thermalization is said to occur when the final state is effectively a microcanonical ensemble, that is, for a large number of observables, the expectation values asymptote to those in a microcanonical ensemble with an equivalent canonical temperature $T = 1/\beta$. Analytic examples of such asymptotia have been found by Calabrese and Cardy [6] in two dimensional CFT's following a quantum quench where the quenching of the Hamiltonian to a critical Hamiltonian H is assumed to lead to a boundary state normalized by the insertion of $\mathrm{e}^{-\kappa_2 H}$ where H is the CFT Hamiltonian. These special states (which we will call the CC states, for Calabrese-Cardy) were shown by Hartman and Maldacena [7] to be dual to a segment of an eternal black hole geometry.

[1] ER signifies Einstein-Rosen bridge which is a spacelike surface connecting the two asymptotic exterior regions of an eternal black hole. EPR stands for 'spooky action at a distance' of Einstein, Podolsky and Rosen in quantum mechanics, which is now known as quantum entanglement.

The 'thermalization' explored here is limited to entanglement entropy or one- or two-point functions.

In this thesis, we address the above issues. The pertinent results are contained in [1], [2] and [3]. The present synopsis which gives a technical summary of these results, is organized as follows.

In section 2, based on [1], we address the question of eternal black hole geometry being dual to the thermofield state is a fine-tuned example of ER=EPR which is generically untrue. We explicitly constructed a general class of two-sided geometries which represent entangled CFTs. We compute correlators between general operators at the two boundaries and find perfect agreement between CFT and bulk calculations. We calculate and match the CFT entanglement entropy (EE) with the holographic EE which involves geodesics passing through the wormhole. We also compute a holographic, non-equilibrium entropy for the CFT using properties of the regular horizon. The construction of the bulk solutions here uses an exact version of Brown-Henneaux type diffeomorphisms which are asymptotically nontrivial and transform the CFT states by two independent unitary operators on the two sides. Our solutions provide an infinite family of explicit examples of the ER=EPR relation. This part does not appear in any other thesis/dissertation.

In section 3, based on [2], a definition of thermalization is adopted which is robust with respect to specific choices of observables. We define thermalization as the approach of the reduced density matrix of a finite subsystem, althought the full system is in a pure state, to the reduced density matrix of the same subsystem when the full system is in a thermal ensemble.[2] We prove such thermalizations to occur under rather general assumptions, for the special CC state described above, as well as for an infinite generalization of these states (which we call generalized Calabrese-Cardy (gCC) states) characterizing additional conserved charges $W_3, W_4, \ldots$ besides the Hamiltonian. In the latter case, the 'thermalization' leads to a Generalized Gibbs Ensemble (GGE) defined by the density matric $\mathrm{e}^{-\kappa_2 H - \kappa_3 W_3 - \kappa_4 W_4 - \cdots}/Z$. Similar results have also been subsequently reproduced by Cardy [8]. We proposed that the bulk or gravity dual of this evolution is the formation of a higher spin(hs) black hole. The equilibrium expectation values of observables match between AdS and CFT because the GGE is the CFT dual of a higher-spin blackhole. We also showed (a) the thermalization rate of the pure initial states, (b) the relaxation time of perturbation in a GGE and (c) that the relaxation rate and the (imaginary part of the) quasinormal frequency of a higher spin black hole match.

In the above work, we had to make certain assumptions to prove thermalization. In section 4, based on [3], we examine quantum quenches to criticality in specific field theories. In this work, we work without the assumptions. We calculate the exact wavefunction that results from a quantum quench to a vanishing mass in a large class of examples: (i) in theories of scalars and fermions, (ii) starting from various pre-quench states (e.g. ground state or squeezed states), (iii) from an initially massive or critical Hamiltonian, and (iv) with a variety of quench protocols. In all these situations, for quadratic theories, the resulting wavefunction is of a generalized Calabrese-Cardy form $|\psi\rangle = \exp[-\sum_{n=2}^{\infty} \kappa_n W_n]|Bd\rangle$ $(W_2 = H)$, *i.e.*, it is a conformal boundary state deformed by an infinite number of $\mathbb{W}_\infty$ charges. We find

[2] In Statistical Mechanics literature, this is called subsystem thermalization.

special squeezed states in the pre-quench phase which lead to small $\kappa_{n>2}$; in these cases, the exact correlators, in agreement with the analysis of [2], show equilibration to a GGE with a relaxation rate determined up to $O(\kappa_{n>2})$. By contrast, with general pre-quench states, including the ground state, we find the $\kappa_{n>2}$ are not small; exact correlators in these cases, although equilibrating at long times, do not generically have a simple thermal or GGE form even at large distances. The main lesson we draw is that in 2D critical quench, long time and large distance physics can be sensitive to perturbations by high dimension operators, in apparent contrast with general Wilsonian lore.

2 AdS3/CFT2(based on [1])

The objective is to explicitly construct a general class of time dependent two-sided geometries [3] which represent entangled time dependent states in a CFT. A useful approach to construct the geometric dual to a CFT state is by using a Fefferman-Graham (FG) expansion, with boundary data provided by the CFT state. To begin with, let us consider the case of a single CFT. Since we are primarily interested in the metric, let us focus, for simplicity, on states in which only the stress tensor is excited. The dual geometry would then be given by the solution to the appropriate Einstein equations subject to the boundary data provided by the stress tensor. This approach has been particularly fruitful in the context of the $\mathrm{AdS}_3/\mathrm{CFT}_2$ duality where the Fefferman-Graham expansion has been shown, for pure gravity, to terminate [9] , yielding the following exact metric derived by Banados *et al.* [10]

$$ds^2 = \frac{dz^2}{z^2} - dx_+dx_-\left(\frac{1}{z^2} + z^2\frac{L(x_+)\bar{L}(x_-)}{16}\right) + \frac{1}{4}\left(L(x_+)dx_+^2 + \bar{L}(x_-)dx_-^2\right) \tag{1}$$

The boundary data ($z \to 0$) is represented by the following holographic stress tensors (we choose $-\Lambda = 1/\ell^2 = 1$)

$$8\pi G_3 T_{++}(x_+) = \frac{L(x_+)}{4},\, 8\pi G_3 T_{--}(x_-) = \frac{\bar{L}(x_-)}{4} \tag{2}$$

The above metric becomes singular at the horizon

$$z = z_0 \equiv 2\left(L(x_+)\bar{L}(x_-)\right)^{-1/4}, \tag{3}$$

and therefore the metric (1), describes only an exterior geometry. When L and $\bar{L}$ are constants, the metric corresponds to the eternal BTZ blackhole solution [11] which has a maximal extension with two exteriors(left and right) joined to the interior region across a smooth horizon. There is also a past interior corresponding to a whitehole. The maximal extension is obtained by transforming to Eddington-Finkelstein(EF) coordinate patches. We will be using five coordinate patches.

[3]By *two-sided*, we mean geometries which have two asymptotically AdS regions.

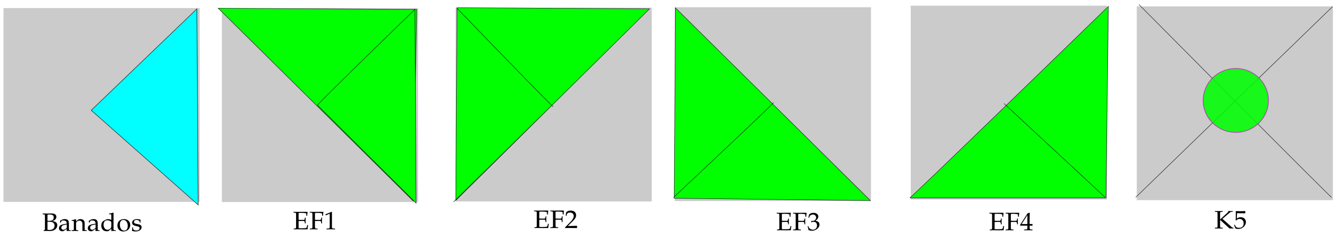

Figure 1: The (green parts of) the five figures on the right depict the five coordinate charts used in [1] to cover the eternal BTZ solution. The coordinate chart K5 is needed to cover the "bifurcation surface" where the past and future horizons meet (it is a point in the Penrose diagram). The leftmost diagram (in blue) represents the coordinate chart used in (1). Each of the coordinate charts is shown, for facility of comparison, within a Penrose diagram where the parts not within the chart are shown in gray.

The EF1 coordinates represented in figure 1, are obtained from the coordinates of (1) by the transformations

$$\frac{z}{z_0} = \sqrt{\frac{1}{\lambda_0}\left(\lambda - \sqrt{\lambda^2 - \lambda_0^2}\right)} \tag{4}$$
$$x_+ = v - \frac{1}{2\sqrt{L}} \ln\left(\frac{\lambda - \lambda_0}{\lambda + \lambda_0}\right), \; x_- = w - \frac{1}{2\sqrt{\bar{L}}} \ln\left(\frac{\lambda - \lambda_0}{\lambda + \lambda_0}\right)$$

The metric, in these coordinates, becomes

$$ds^2 = \frac{d\lambda^2}{4(\lambda + \lambda_0)^2} + \frac{L}{4}dv^2 + \frac{\bar{L}}{4}dw^2 - \lambda\, dvdw + \frac{\sqrt{L}}{2(\lambda + \lambda_0)}dvd\lambda + \frac{\sqrt{\bar{L}}}{2(\lambda + \lambda_0)}dwd\lambda \tag{5}$$

The subleading term in the metric corresponds to the normalizable metric fluctuation, which gives the expectation value of the stress tensor; this is the holographic stress tensor [12], and is given here by

$$8\pi G_3 T_{vv}(x_+) = \frac{L}{4}, \; 8\pi G_3 T_{ww}(x_-) = \frac{\bar{L}}{4} \tag{6}$$

The IR cutoff surface and the boundary metric are

$$\lambda_{ir} = 1/\epsilon^2, \qquad ds^2_{bdry} = -dvdw \tag{7}$$

The event horizon λ_H, the inner horizon λ_i, and the singularity λ_s are at

$$\lambda_H = \lambda_0 \equiv \frac{\sqrt{L\bar{L}}}{2}, \; \lambda_i = -\lambda_0, \; \lambda_s = -\frac{1}{4}(L + \bar{L}) \tag{8}$$

Note that for BTZ black holes without angular momentum $\bar{L} = L$ and $\lambda_i = \lambda_s$. The other coordinate systems - EF2, EF3, etc., are similar and details are in [1].

2.1 Solution generating diffeomorphisms (SGD)

We will now proceed to construct new solutions with arbitrary boundary data at the two boundaries (represented by two arbitrary holographic stress tensors $T_{R,\mu\nu}(x)$ and $T_{L,\mu\nu}(x)$) by applying the method of solution generating diffeomorphisms to the above geometry. Normally one considers a geometry obtained by a diffeomorphism as indistinguishable from the original one. However, this statement is untrue for diffeomorphisms which are symptotically non-trivial(do not die off sufficiently fast).

The diffeomorphism in the EF1 coordinate chart is given by

$$\lambda = \frac{\tilde{\lambda}}{G'_+(\tilde{v})G'_-(\tilde{w})},\ v = G_+(\tilde{v}),\ w = G_-(\tilde{w}) \tag{9}$$

The new metric $\tilde{g}_{MN}$, written in terms of $\tilde{x}^M = (\tilde{\lambda}, \tilde{v}, \tilde{w})$, is

$$\begin{aligned}\tilde{g}_{MN}(\tilde{x})d\tilde{x}^M d\tilde{x}^N \equiv ds^2 = \frac{1}{B^2}\Big[& d\tilde{\lambda}^2 + A_+^2 d\tilde{v}^2 + A_-^2 d\tilde{w}^2 + 2A_+ d\tilde{v}d\tilde{\lambda} + 2A_- d\tilde{w}d\tilde{\lambda} \\ &- \tilde{\lambda}\Big(B^2 + 2\Big(A_+\frac{G''_-(\tilde{w})}{G'_-(\tilde{w})} + A_-\frac{G''_+(\tilde{v})}{G'_+(\tilde{v})} + \tilde{\lambda}\frac{G''_+(\tilde{v})G''_-(\tilde{w})}{G'_+(\tilde{v})G'_-(\tilde{w})}\Big)\Big)d\tilde{v}d\tilde{w}\Big]\end{aligned} \tag{10}$$

where

$$A_+ = \sqrt{L}G'_+(\tilde{v})(\tilde{\lambda}+\tilde{\lambda}_0) - \tilde{\lambda}\frac{G''_+(\tilde{v})}{G'_+(\tilde{v})},\ A_- = \sqrt{\bar{L}}G'_-(\tilde{w})(\tilde{\lambda}+\tilde{\lambda}_0) - \tilde{\lambda}\frac{G''_-(\tilde{w})}{G'_-(\tilde{w})},\ B = 2(\tilde{\lambda}+\tilde{\lambda}_0)$$

The new IR cutoff surface and the boundary metric are

$$\tilde{\lambda}_{ir} = (1/\epsilon^2) \Rightarrow \lambda = 1/(\epsilon^2 G'_+(\tilde{v})G'_-(\tilde{w})), \qquad ds^2_{bdry} = -d\tilde{v}d\tilde{w} \tag{11}$$

The diffeomorphism (SGD) used in the coordinate chart EF2 (see Fig 1), which is independent of the one above used in EF1, is given by

$$\lambda_1 = \frac{\tilde{\lambda}_1}{H'_+(\tilde{u})H'_-(\tilde{\omega})},\ u = H_+(\tilde{u}),\ \omega = H_-(\tilde{v}) \tag{12}$$

In a manner similar to the above, we apply the SGD characterized by $G_\pm$ on EF4 and the SGD characterized by $H_\pm$ on EF3 (which shares the left exterior with EF2). We use the identity diffeomorphism of Kruskal patch K5 (with $\xi_5^M = 0$). Away from the boundary, the metrics obtained in the various EF coordinate charts differ from each other only by trivial diffeomorphisms which become the identity transformation at infinity. Since the physical content of each of these metrics is represented only by the boundary data, it ensures that all the different metrics represent the same single spacetime metric in different charts. It is clear that the SGDs lead to a *smooth metric* in each chart and their overlaps, provided $G_\pm(x), H_\pm(x)$ are differentiable and invertible functions. We will only consider such functions. It can be verified that such a class of functions is sufficiently general to generate any pair of physically sensible holographic stress tensors at both boundaries.

So far we have viewed the SGDs as a coordinate transformation. Alternatively, however, we can also view the diffeomorphism as an active movement of points: $x^M \to \tilde{x}^M = x^M + \xi^M$. In this viewpoint, the future horizon $\lambda = \lambda_H = \lambda_0$ (see (8)) on the right moves to

$$\tilde{\lambda}_H = G'_+(\tilde{v})\ G'_-(\tilde{w})\lambda_0,\ \tilde{\lambda}_{1,H} = H'_+(\tilde{u})\ H'_-(\tilde{\omega})\lambda_0 \tag{13}$$

Similar statements can be made in the other coordinate charts. The horizons represented this way are smooth but undulating.

2.2 The Dual Conformal Field Theory

The eternal BTZ black hole geometry corresponds to the following thermofield double state [5, 7, 13, 14]

$$|\psi_0\rangle = Z(\beta_+, \beta_-)^{-1/2} \sum_n \exp[-\beta_+ E_{+,n}/2 - \beta_- E_{-,n}/2]|n\rangle|n\rangle \tag{14}$$

The states $|n\rangle$ denote all simultaneous eigenstates of $H_\pm = (H \pm J)/2$ with eigenvalues $E_{\pm,n}$. $|\psi_0\rangle$ here is a pure state in $\mathcal{H} \otimes \mathcal{H}$ obtained by the 'purification' of the thermal ensemble with inverse temperature β and angular velocity Ω and $\beta_\pm = \beta(1 \pm \Omega)$. For non-spinning BTZ black hole ($\Omega = 0 = J$), the CFT dual is the standard thermofield double:

$$|\psi_{0,0}\rangle = Z(\beta)^{-1/2} \sum_n \exp[-\beta E_n/2]|n\rangle|n\rangle \tag{15}$$

CFT duals of our new solutions The SGD's reduce to conformal transformations at the boundary. So, we claim that the CFT-duals to the new solutions obtained using SDG are described by the pure states $|\psi\rangle = U_L U_R|\psi_0\rangle$ where U_R is the unitary transformation which implements the conformal transformations on the CFT on the right boundary (characterized by $G_\pm$), and U_L is the unitary transformation which implements the conformal transformations on the CFT on the left boundary (characterized by $H_\pm$). This is the Schrödinger picture of the conformal transformations. However, it is easier and more illuminating if we work in Heisenberg picture. Here, we note that stress tensors and primary operators transform under a conformal transformation $(v, w) \to (\tilde{v}, \tilde{w})$ as

$$T_{\tilde{v}\tilde{v}}(P) = \left(\frac{\partial \tilde{v}}{\partial v}\right)^{-2} [T_{\tilde{v}\tilde{v}}(\tilde{v}) - \frac{c}{12} S(v, \tilde{v})], \quad O(\tilde{v}, \tilde{w}) = O(v, w) \left(\frac{dv}{d\tilde{v}}\right)^h \left(\frac{dw}{d\tilde{w}}\right)^{\bar{h}} \tag{16}$$

where $S(v, \tilde{v})$ is the usual Schwarzian derivative.

2.3 Duality Matching

Stress Tensor

We will first consider the stress tensor of the boundary theory on the right. The generalization to the stress tensor on the left is trivial.We use the definition of holographic stress tensor in

[12, 15]. We find that

$$
\begin{aligned}
8\pi G_3 T_{\tilde{v}\tilde{v}} &= \frac{L}{4}G'_+(\tilde{v})^2 + \frac{3G''_+(\tilde{v})^2 - 2G'_+(\tilde{v})G'''_+(\tilde{v})}{4G'_+(\tilde{v})^2}, \\
8\pi G_3 T_{\tilde{w}\tilde{w}} &= \frac{\bar{L}}{4}G'_-(\tilde{w})^2 + \frac{3G''_-(\tilde{w})^2 - 2G'_-(\tilde{w})G'''_-(\tilde{w})}{4G'_-(\tilde{w})^2}
\end{aligned}
\tag{17}
$$

This clearly is the original stress tensor (6) under the conformal transformations $v = G_+(\tilde{v})$ and $w = G_-(\tilde{w})$ of CFT stress tensor (16).

General two-point correlators

The holographic correspondence for the two point functions of scalar operators of large conformal dimension in semiclassical limit can be written simply as [16]:

$$
\langle\psi_0|O(P)O(Q)|\psi_0\rangle_{CFT} = \exp[-2hL(\mathbf{P},\mathbf{Q})] \tag{18}
$$

where $L(\mathbf{P},\mathbf{Q})$ is the length of the extremal geodesic connecting the two points $\mathbf{P}$ and $\mathbf{Q}$, which can be on the boundary of same exterior region(RR or LL) or on boundaries of different exterior regions(RL or LR).

Gravity side The geodesic length from $\mathbf{P}(1/\epsilon_R^2, v, w)$ on the right boundary to a point $\mathbf{Q} = (1/\epsilon_L^2, u, \omega)$ on the left boundary is given by

$$
L(\mathbf{P},\mathbf{Q}) = \log\left[\frac{4\cosh[\sqrt{L}(v-u)/2]\cosh[\sqrt{L}(w-\omega)/2]}{L\epsilon_R\epsilon_L}\right] \tag{19}
$$

With SGDs, the new geodesic length is given by the active transformation of the u,v,w and ω and the new IR cutoff given by (11). Similar, results are also obtained when $\mathbf{P}$ and $\mathbf{Q}$ are on same side.

CFT side Using Minkowski to Rindler coordinate transformation as done in [7], we get the following result

$$
\langle\psi_0|O(X_{+R},X_{-R})\,O(X_{+L},X_{-L})|\psi_0\rangle = \Big(\frac{4\cosh\left[\sqrt{L}(v-u)/2\right]\,\cosh\left[\sqrt{L}(w-\omega)/2\right]}{L\epsilon^2}\Big)^{-2h} \tag{20}
$$

where (X_{+R}, X_{-R}) and (X_{+L}, X_{-L}) are the boundary points corresponding to the bulk points $\mathbf{P}$ and $\mathbf{Q}$ respectively. Operator O is assumed to have dimensions $(h,\bar{h})$ and ϵ is a real space field theory cut-off. We have related the temperature of the CFT to $L(=\bar{L})$ by the equation $\sqrt{L} = 2\pi/\beta$. It is easy to see that this correlator satisfies the relation (18) using $\epsilon_R = \epsilon_L = \epsilon$.

In the new states, the correlators are found from (20) by a conformal transformation of the boundary coordinates. The Jacobian factors have the effect of the replacement $\epsilon^2 \to \epsilon^2\sqrt{G'_+(\tilde{v})G'_-(\tilde{w})H'_+(\tilde{u})H'_-(\tilde{\omega})}$. With these ingredients, it is straightforward to verify that (18) is satisfied with the new geodesics. Similar arguments apply to RR and LL correlators.

Entanglement entropy: We can calculate entanglement entropy(EE) of a region $A = A_R \cup A_L$, where A_R is a half line $(v-w)/2 > x_R$ on the right boundary at 'time' $(v+w)/2 = t_R$ and A_L is a half line $(u-\omega)/2 > x_L$ of the left boundary at 'time' $(u+\omega)/2 = t_L$. The boundary of the region A consists of a point $P(v_{\partial A}, w_{\partial A})$ on the right and a point $Q'(u_{\partial A}, \omega_{\partial A})$ on the left, with coordinates

$$\begin{aligned} P: \quad v_{\partial A} &= t_R + x_R, \quad w_{\partial A} = t_R - x_R \\ Q': \quad u_{\partial A} &= t_L + x_L, \quad \omega_{\partial A} = t_L - x_L \end{aligned} \tag{21}$$

The CFT EE is given by the logarithm of expectation value of twist operators, which are primary operators, inserted at $\mathbf{P}$ and $\mathbf{Q'}$, while the bulk EE is given by the extremal geodesic length anchored at $\mathbf{P}$ and $\mathbf{Q'}$. From RL two point function matching, it automatically follows that CFT EE and bulk EE match perfectly.

Entropy

Inspecting (5), the entropy density matches the result from CFT using Cardy's formula, using the expression of stress tensor in (6). In the non-equlibrium situation, from the metric (10) the entropy density is then given by

$$\tilde{s} = \frac{1}{4G_3}\left(\frac{1}{2}\sqrt{L}G'_+(\tilde{v}) + \frac{1}{2}\sqrt{\bar{L}}G'_-(\tilde{w})\right) \tag{22}$$

And from CFT, in adiabatic approximation, the leading $G'_+(\tilde{v})$ and $G'_-(\tilde{w})$ parts of the stress tensors are

$$8\pi G_3 T_{\tilde{v}\tilde{v}} = \frac{L}{4}G'_+(\tilde{v})^2, \quad 8\pi G_3 T_{\tilde{w}\tilde{w}} = \frac{\bar{L}}{4}G'_-(\tilde{w})^2 \tag{23}$$

With this the same non-equilibrium entropy (22) is reproduced.

2.4 Conclusion

We have solved the boundary value problem for 3D gravity (with $\Lambda < 0$) with independent boundary data on two asymptotically AdS_3 exterior geometries. The boundary data, specified in the form of arbitrary holographic stress tensors, yields spacetimes with wormholes, *i.e.* with exterior regions connected across smooth horizons. The explicit metrics are constructed by the technique of solution generating diffeomorphisms (SGD) from the eternal BTZ black string. By using the fact that the SGD's reduce to conformal transformations at both boundaries, we claim that the dual CFT states are specific time-dependent entangled states which are conformal transformations of the standard thermofield double. We compute various correlators and a dynamical entanglement entropy, in the bulk and in the CFT, to provide evidence for the duality. We also arrive at an expression for a non-equilibrium entropy function from the area-form on the horizon of these geometries.

3 Thermalisation with Chemical Potentials(based on [2])

The dynamics of systems undergoing a quantum quench has been extensively studied in recent years[17]. In a quantum quench, some parameter of the Hamiltonian changes over a brief period of time. The initial wavefunction in the pre-quench phase, whether it is a ground state or otherwise, typically evolves to a non-stationary state, which then evolves by the post-quench Hamiltonian which is time-dependent. An important question in such a dynamics is whether correlators equilibrate at long times, and if so, whether the equilibrium is described by a thermal ensemble or otherwise [17, 18, 19]. As mentioned in the Introduction, Calabrese and Cardy [6] had found such thermalization in two dimensional quantum quench where the quenching of the Hamiltonian to a critical Hamiltonian is assumed to lead to a boundary state normalized by the insertion of $e^{-\kappa_2 H}$ where H is the CFT Hamiltonian. Generalizing [20], we will consider the system at $t = 0$ to be in a "quenched state"

$$|\psi_0\rangle = \exp[-\kappa_2 H - \sum_{n=3}^{\infty} \kappa_n W_n]|Bd\rangle \tag{24}$$

Here $|Bd\rangle$ is a conformal invariant boundary state; the exponential factors cut off the UV modes to make the state normalizable. W_n denote the additional conserved charges in the final theory. It has been argued in [8] that any CFT has an infinite number of conserved charges. In the work presented below, we will assume that these charges correspond to local conserved charges like charges of $\mathcal{W}_\infty$ currents. More generally, our work applies also to a finite number of conserved charges. We will focus on two-dimensional conformal field theories (CFTs) on an infinite line $\sigma \in \mathbb{R}$.

We find that the expectation values of local observables supported on a finite interval $A : \sigma \in [-l/2, l/2])$ asymptotically approach their values in a Generalized Gibbs ensemble(GGE),

$$\rho_{eqm} = \frac{1}{Z} \exp[-\beta H - \sum_n \mu_n W_n], \quad Z = \mathrm{Tr} \exp[-\beta H - \sum_n \mu_n W_n] \tag{25}$$

whose temperature and chemical potentials are related to the cutoff scales in (24) as follows

$$\beta = 4\kappa_2, \quad \mu_n = 4\kappa_n, \quad n = 3, 4, ... \tag{26}$$

With the above identification of parameters, we will rewrite the initial quenched state (24) henceforth as

$$|\psi_0\rangle = \exp[-(\beta H - \sum_{n=3}^{\infty} \mu_n W_n)/4]|Bd\rangle \tag{27}$$

For single local observables, we find that at large times

$$\langle\psi(t)|\phi_k(\sigma)|\psi(t)\rangle = \mathrm{Tr}\,(\phi_k(0)\rho_{eqm}(\beta, \mu_i)) + a_k\, e^{-\gamma_k t} + ... \tag{28}$$

where $\phi_k(\sigma)$ is an arbitrary quasiprimary field (labelled by an index k). Below we compute the thermalization exponent γ_k in a perturbation in the chemical potentials and to linear order it is given by

$$\gamma_k = \frac{2\pi}{\beta}\left[\Delta_k + \sum_n \tilde{\mu}_n Q_{n,k} + O(\tilde{\mu}^2)\right], \ \tilde{\mu}_n \equiv \frac{\mu_n}{\beta^{n-1}}, \tag{29}$$

Here $\Delta_k = h_k + \bar{h}_k$ is the scaling dimension and $Q_{n,k}$ are the (shifted) W_n-charges (see (40) for the full definition) of the field ϕ_k (in case of primary fields) or of the minimum-dimension field which appears in the conformal transformation of ϕ_k. More generally, we found

$$\rho_{gCC,A}(t) = \rho_{GGE,A} + a(t)e^{-\gamma_{min} t} \tag{30}$$

where $\rho_{gCC,A}(t)$ and $\rho_{GGE,A}$ are the reduced density matrices of a subsystem A in the gCC state and GGE respectively. And γ_{min} is the lowest value of γ_k among the operators of the theory considered.

Our work, described above, constitutes a general proof of thermalization[4] for integrable systems in case of 2D conformal models. Thermalization in integrable systems is a relatively new area of research. Earlier works include various isolated examples, e.g., (a) one-dimensional hardcore bosons [21], (b) transverse field Ising model [22], and (c) matrix quantum mechanics models [23]. The equilibrium ensembles in this context have been called a generalized Gibbs ensemble (GGE).

One of the main technical advances made in this work is the resummation of leading-log terms at large times, which leads to exponentiation of the perturbation series, leading to the thermalization rate, presented in (28), (29), as a function of chemical potentials. This allows us to also compute the effect of chemical potentials on the relaxation times of thermal Green's functions. Another technical advance consists of the computation of the long-time reduced density matrix, using a short-interval expansion, which allows us to prove thermalization of an arbitrary string of local observables.

3.1 Thermalization time scale for single local observables

We will briefly recall how these are computed in the absence of the chemical potentials [20, 24]. The expectation value on r.h.s. of (28) corresponds to the one-point function on a strip geometry, with complex coordinate $w = \sigma + i\tau$, $\sigma \in (-\infty, \infty)$, $\tau \in (-\beta/4, \beta/4)$ where τ is eventually to be analytically continued to $\tau = it$. This can be conformally transformed to an upper half plane by using the map

$$z = ie^{(2\pi/\beta)w} = ie^{2\pi(\sigma+i\tau)/\beta} = ie^{2\pi(\sigma-t)/\beta} \xrightarrow{t\to\infty} z \to 0 \tag{31}$$

$$\bar{z} = -ie^{2\pi(\sigma-i\tau)/\beta} = -ie^{2\pi(\sigma+t)/\beta} \xrightarrow{t\to\infty} \bar{z} \to -i\infty \tag{32}$$

For a primary field with $h_k = \bar{h}_k$ (of the form $\phi_k(w, \bar{w}) = \varphi_k(w)\varphi_k(\bar{w})$),

$$\begin{aligned}\langle\phi_k(\sigma, t)\rangle_{dyn} = \langle\phi_k(w, \bar{w})\rangle_{str} &= \left(\frac{\partial z}{\partial w}\right)^{h_k}\left(\frac{\partial \bar{z}}{\partial \bar{w}}\right)^{\bar{h}_k}\langle\phi_k(z, \bar{z})\rangle_{UHP} \\ &= a_k\left(e^{2\pi t/\beta} + e^{-2\pi t/\beta}\right)^{-2h_k} \sim a_k e^{-\gamma_k^{(0)} t} + ..., \ \gamma_k^{(0)} = 2\pi\Delta_k/\beta = 4\pi h_k/\beta\end{aligned} \tag{33}$$

[4]in the sense of subsystem thermalization.

where in going from the first line to the second line, we have used the method of images [25, 24] with $h_k = \bar{h}_k,\ z' = \bar{z}$. In the above a_k, A_k are known numerical constants.

Equilibrium expectation value in (28), for $\mu_n = 0$, corresponds to a cylindrical geometry in the w-plane, with $\tau = 0$ identified with $\tau = \beta$. By using the same conformal map (31) this can be transformed to a one-point function on the plane. For a primary field the latter vanishes. Hence (28) is trivially satisfied. For a quasiprimary field ϕ_k, its conformal transformation generates additional terms, including possibly a c-number term.

For the general case with $\mu_n \neq 0$, we will regard the W_n as conserved charges of a W-algebra, although the results we derive will be equally valid as long as these charges, together with H, form a mutually commuting set, and the currents $(\mathcal{W}_n(w), \bar{\mathcal{W}}_n(\bar{w}))$ are quasiprimary fields.

$$W_n = \frac{1}{2\pi}\int_\Gamma W_{\tau\tau\ldots\tau} d\sigma = \frac{1}{2\pi}\int_\Gamma \big(i^n dw_1\, \mathcal{W}_n(w_1) + (-i)^n d\bar{w}_1\, \bar{\mathcal{W}}_n(\bar{w}_1)\big) \tag{34}$$

Here the contour Γ is taken to be a $\tau =$ constant line along which $dw_1 = d\bar{w}_1 = d\sigma$. Under the conformal transformation (31) to the plane/UHP, the holomorphic part of the contour integral becomes

$$W_n|_{hol} = \frac{i^n}{2\pi}\left(\frac{2\pi}{\beta}\right)^{n-1}\int_{\Gamma_1} dz_1 \left[z_1^{n-1}\mathcal{W}_n(z_1) + \sum_{m=1}^{\lfloor n/2\rfloor} a_{n,n-2m} z_1^{n-2m-1}\mathcal{W}_{n-2m}(z_1)\right] \tag{35}$$

where the $a_{n,n-2m}$ denote the mixing of $\mathcal{W}_n(z_1)$ with lower order W-currents under conformal transformations [26, 27]. The contour Γ_1 is an image of the contour Γ onto the plane. The expression for the antiholomorphic part $W_n|_{antihol}$ is similar.

One-point function on the strip with chemical potentials

Consider only a single chemical potential μ_3, using perturbation theory Feynman diagrams:

$$\begin{aligned}\langle \phi_k(w,\bar{w})\rangle^{\mu}_{str} &= \langle \phi_k(w,\bar{w})\rangle_{str} - \frac{\mu_3}{4}\langle \{W_3, \phi_k(w,\bar{w})\}\rangle^{conn}_{str} \\ &+ \left(\frac{\mu_3}{4}\right)^2 \frac{1}{2!}(\langle \{W_3 W_3, \phi_k(w,\bar{w})\}\rangle^{conn}_{str} + 2\langle W_3\phi_k(w,\bar{w})W_3\rangle^{conn}_{str}) + \mathcal{O}(\mu_n^3)\end{aligned} \tag{36}$$

The $\{\ ,\}$ denotes an anticommutator. The operator ordering implies the following: when W_3 appears on the left of $\phi_k(w,\bar{w})$, e.g., in $\langle W_3\phi_k(w,\bar{w})\rangle$, the integration contour (34) for W_3 on the strip lies above the point $(w,\bar{w})$; similarly when W_3 appears on the right of $\phi_k(w,\bar{w})$, e.g. in $\langle \phi_k(w,\bar{w})W_3\rangle$, the contour for W_3 is below the point $(w,\bar{w})$.

The first, μ-independent, term in the above expansion is already calculated in (33).

After conformally transforming to the UHP, we regard $\bar{\varphi}_k$ on the UHP as φ_k^* at the image point on the LHP (up to a constant). Combining with the arguments used for the holomorphic operators, we eventually get

$$\begin{aligned}\frac{\langle \{W_3, \phi_k(w,\bar{w})\}\rangle^{conn}_{str}}{\langle \phi_k(w,\bar{w})\rangle_{str}} &= i^3\frac{2\pi}{\beta^2}(z\bar{z})^h I_3(z,z'), \\ I_3(z,z') &\equiv \int_{\Gamma_1+\Gamma_1'+\tilde{\Gamma}_1+\tilde{\Gamma}_1'} dz_1\ z_1^2 \langle \mathcal{W}_3(z_1)\varphi_k(z)\varphi_k^*(z')\rangle^{conn}_{\mathbb{C}} / \langle \varphi_k(z)\varphi_k^*(z')\rangle^{conn}_{\mathbb{C}}\end{aligned} \tag{37}$$

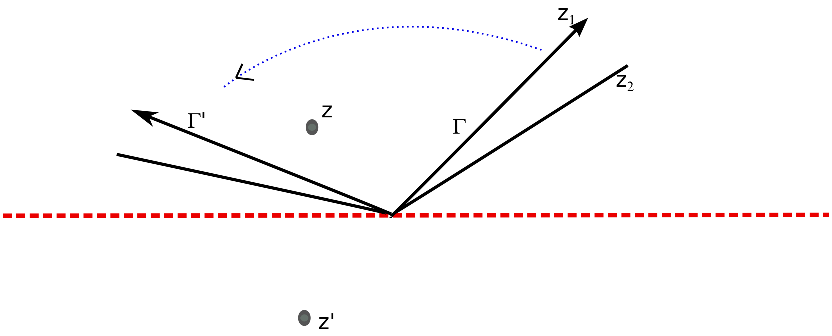

Figure 2: Various contours needed to compute the W_n insertions in (36). At late times, the insertion of each contour, irrespective of the position of the contour, amounts to insertion of a given factor linear in t. This allows to resum arbitrary orders of arbitrary W_n-charge insertions, leading to the exponential time-dependence as in (28).

In the long time limit, $O(\mu_3)$ correction is given by (using that all four contours $\Gamma_1, \tilde{\Gamma}_1, \Gamma_1', \tilde{\Gamma}_1'$ contribute equally, cancelling the $1/4$ in $-\mu_3/4$)

$$\begin{aligned}\langle\phi_k(\sigma,t)\rangle_{dyn} &= a_k e^{-2\pi\Delta_k t/\beta}\left(1 - Q_{3,k}\tilde{\mu}_3\ (\frac{2\pi t}{\beta} + \text{constant}) + O(\mu_3^2)\right) + \ldots,\\ Q_{3,k} &= i^3 2q_{3,k}(2\pi),\ \tilde{\mu}_3 = \frac{\mu_3}{\beta^2},\ \Delta_k = 2h_k \end{aligned}\tag{38}$$

where q_3 is the $\mathcal{W}_3$-charge of the field ϕ_k. For higher order μ_3 terms, closing the contour integrals and using the leading OPE terms and we find the re-exponentiation and get (28). We note that the leading contribution had been isolated by considering a scaling

$$\tilde{\mu}_n \to 0, \tilde{t} \equiv \frac{t}{\beta} \to \infty,\ \text{such that}\ \tilde{\mu}_n\tilde{t} = \text{constant}.\tag{39}$$

For higher W_n charges, due to the quasiprimary nature (35), the $O(\mu)$ correction with all chemical potentials is given by

$$\begin{aligned}\langle\phi_k(\sigma,t)\rangle_{dyn} &= a_k e^{-2\pi\Delta_k t/\beta}\left(1 - \sum_{n=3} Q_{n,k}\tilde{\mu}_n\ (\frac{2\pi t}{\beta} + \text{constant}) + O(\mu^2)\right) + \ldots,\\ \tilde{\mu}_n &= \frac{\mu_n}{\beta^{n-1}},\ \Delta_k = h_k + \bar{h}_k = 2h_k\\ Q_{n,k} &= 2\sum_{m=0}^{\lfloor n/2-1\rfloor} a_{n,m} i^{n-2m}(2\pi)^{n-2m-2} q_{n-2m,k}\\ &\qquad = i^n(2\pi)^{n-2}2q_{n,k} + i^{n-2}(2\pi)^{n-4}a_{n,2}\,2q_{n-2,k} + \ldots,\end{aligned}\tag{40}$$

3.2 Proof of thermalization: Reduced density matrix, Multiple local observables

Besides the one-point functions discussed above, it turns our that we can demonstrate thermalization of *all operators in an interval A of length l*. It is convenient to define a 'thermalization function' $I_A(t)$ [28] as

$$I_A(t) = \text{Tr}(\hat{\rho}_{dyn,A}(t)\hat{\rho}_{eqm,A}(\beta,\mu_n)) = \frac{\text{Tr}(\rho_{dyn,A}(t)\rho_{eqm,A}(\beta,\mu_n))}{[\text{Tr}(\rho_{dyn,A}(t)^2)\text{Tr}(\rho_{eqm,A}(\beta,\mu_i)^2)]^{1/2}}$$
$$\rho_{dyn,A}(t) = \text{Tr}_{\bar{A}}\ |\psi(t)\rangle\langle\psi(t)|,\ \rho_{eqm,A}(\beta,\mu_n) = \text{Tr}_{\bar{A}}\ \rho_{eqm}(\beta,\mu_i) \tag{41}$$

Here $\hat{\rho} = \rho/\sqrt{\text{Tr}\rho^2}$ denotes a 'square-normalized' density matrix. Using the short-interval expansion above, and the long time behaviour of one-point functions, it is easy to prove that the system thermalizes

$$I(t) = 1 - \alpha \exp[-2\gamma_m t] + ... \quad \Rightarrow \rho_{dyn,A}(t) \xrightarrow{t\to\infty} \rho_{eqm,A}(\beta,\mu_n) + \mathcal{O}(e^{-\gamma_{min} t}) \tag{42}$$

This implies thermalization for an arbitrary string of local operators (with $\sigma_1, \sigma_2, ... \in A$).

$$\langle\psi(t)|\mathcal{O}_1(x_1)\mathcal{O}_2(x_2)....\mathcal{O}_n(x_n)|\psi(t)\rangle \xrightarrow{t\to\infty} Tr\left(\rho_{GGE}\mathcal{O}_1(x_1)\mathcal{O}_2(x_2)....\mathcal{O}_n(x_n)\right) \tag{43}$$

3.3 Decay of perturbations of a thermal state

We find that the long time behaviour (28) of an operator $\phi_k(0,t)$ in the quenched state is the same as that of its two-point function (44) in the thermal state (25) (with chemical potentials). The latter measures the thermal decay of a perturbation and is more directly related to a black hole quasinormal mode.

We define the thermal two-point function as [5]

$$G_+(t,l;\beta,\mu) \equiv \frac{1}{Z}\text{Tr}(\phi_k(l,t)\phi_k(0,0)e^{-\beta H - \sum_n \mu_n W_n}) \tag{44}$$

For $\mu = 0$, with ϕ_k of conformal dimensions $h_k = \bar{h}_k$,

$$G_+(t,l;\beta,0) \xrightarrow{t,l\gg\beta} \begin{cases} \text{const } e^{-2\pi t\Delta_k/\beta}, & (t-l) \gg \beta \\ \text{const } e^{-2\pi l\Delta_k/\beta}, & (l-t) \gg \beta \end{cases} \tag{45}$$

The effect of turning on the chemical potentials can be dealt with as in the previous sections. By resumming the perturbative series in a straightforward fashion, we get,

$$G_+(t,0;\beta,\mu) \xrightarrow{t\to\infty} G_+(0,0;\beta,0)b(\mu)e^{-\gamma_k t} \tag{46}$$

where $b(\mu)$ is time-independent, and is of the form $b(\mu) = 1 + O(\mu)$. This long time decay is the same as that of the one-point function (28) in the quenched state, as claimed above.

3.4 Holography and higher spin black holes

Zero chemical potential: A global quantum quench described by an initial state of the form (27), for large central charges and zero chemical potentials, has been shown in [5, 7, 14] to be dual to one half of the eternal BTZ (black string) geometry, whose boundary represents an end-of-the-world brane.

[5] We use the same notations as in [29].

In an independent development, it was found in [30] that the quasinormal mode of a scalar field $\Phi_k(\sigma, t, z)$ of mass m in a BTZ background (dual to a CFT operator ϕ_k of dimension $\Delta_k \equiv 1 + \sqrt{1+m^2}$) is of the form $\exp[-2\pi\Delta t/\beta]$ at large times. This time-dependence agrees with the CFT exponent in (45) exactly. This shows that the exponential decay of a CFT perturbation to a thermal state corresponds to the decay of the corresponding scalar field in the bulk geometry. This result has been extended to higher spin fields in the BTZ background in [31].

Non-zero chemical potentials: In case the CFT has additional conserved charges, in particular if it has a representation of a W_∞ algebra (and consequently the hs(λ) algebra [32]), then the bulk dual corresponding to those conserved charges have been conjectured to be the conserved higher spin charges of higher spin gravity. In particular, [33, 34] have shown that if one interprets the grand canonical ensemble (26) (more generally, the GGE) in the framework of an hs(λ) representation, then the bulk dual corresponds to a higher spin black hole.

Thus, we would like to conjecture that the bulk dual of the quantum quench with chemical potentials, would correspond to a gravitational collapse to a higher spin black hole.

As an important consistency check, by analogy with the case with zero potential, in the present case too, the leading quasinormal mode (QNM) of a scalar field $\Phi_k(\sigma, t, z)$ should have a time-dependence given by (46). Following the results in [35] we find that at late times $t \gg \beta$ the QNM for the hs(λ) scalar field Φ_+ behaves, up to $O(\mu_3)$, as $e^{-i\omega_{k,0}t}$, where

$$\omega_{k,0} = -i\frac{2\pi}{\beta}\left(1 + \lambda + \tilde{\mu}_3\frac{1}{3}(1+\lambda)(2+\lambda)\right) \tag{47}$$

where the index k here refers to the operator ϕ_k dual to the scalar field Φ_+. Noting that for this operator we have $\Delta_k = 1 + \lambda$, and $Q_{3,k} = \frac{1}{3}(1+\lambda)(2+\lambda)$ [36, 37], we see that the QNM frequency $\omega_{k,0}$ agrees, to the relevant order, with the pole of the thermal 2-point function which, in turn, is related to the thermalization exponent by the relation $\omega_{k,0} = -i\gamma_k$, with γ_k given in (28).

3.5 Conclusion

We considered 2D conformal field theories with additional conserved charges besides the energy. We probed non-equilibrium physics starting from global quenches described by conformal boundary states modified by multiple UV cut-off parameters. It was found that local observables in such a state thermalize to an equilibrium described by a grand canonical ensemble (26) with temperature and chemical potentials related to the cut-off parameters. We computed the thermalization rate for various observables, including the reduced density matrix for an interval. It was found that the same rate appears also in the long time decay of two-point functions in equilibrium. In the context where the number of conserved charges is infinite, and they are identified with commuting W_∞ charges, the equilibrium ensemble (a generalized Gibbs ensemble, GGE) corresponds to a higher spin black hole [33, 34]. We found that the thermalization rate found above agrees with the leading quasinormal frequency of the higher spin black hole; this constitutes an additional, dynamical, evidence for the holographic correspondence between the global quenches in this paper and the evolution into the higher spin black hole.

4 Free Scalar and Fermion Quenches(based on [3])

In the previous section 3, the proof of thermalization required certain assumptions:
(a) the post-quench wavefunction is of the generalized Calabrese-Cardy (gCC) form.

$$|\psi\rangle = \exp[-\kappa_2 H - \sum_{n>2} \kappa_n W_n]|Bd\rangle \tag{48}$$

where W_n are additional conserved charges in the system (the results are valid even without the additional charges present in the system). It was assumed that the charges are obtained from local currents. For specificity, we have assumed that the system is integrable, with a $\mathbb{W}_\infty$ algebra and the W_n, $n = 2, 3, ...$ $(W_2 = H)$ are $\mathbb{W}_\infty$ charges.
(b) The spectrum of conformal dimensions in the post-quench critical theory has a gap.
(c) The dimensionless parameters $\tilde{\kappa}_n = \kappa_n/\kappa_2^{n-1}, n > 2$ are small and can be treated perturbatively.
(d) The size l of the interval is small compared to κ_2.
In this section we will focus on our work [3] where working with theories of free scalars or fermions with a time-dependent mass $m(t)$ quenched to $m = 0$. we extend the proof of thermlization, without making the assumptions above. One of the technical advances in this paper is the use of nontrivial pre-quench states, which we take to be squeezed states. The motivation for considering this class of states is that besides being technically accessible, these states are experimentally realizable (see, e.g. [38, 39]) and carry non-trivial quantum entanglement encoded by the squeezing function.

4.1 Critical quench of a scalar field: general strategy

An important example of quantum quench is provided by free scalar field theories with time-dependent mass (our notations will closely follow [40]). We will consider critical quench, the mass gap asymptotically vanishes following the quench.

The equations of motion of various Fourier modes get decoupled, where each mode satisfies a Schrödinger-type equation with $-m^2(t)$ playing the role of a potential:

$$-\frac{d^2\phi(k,t)}{dt^2} + V(t)\phi(k,t) = E\phi(k,t), \quad V(t) = -m^2(t),\ E = k^2. \tag{49}$$

The solution for the field $\phi(k,t) = \int dx\, \phi(x,t)\, e^{-ikx}$ can be expressed in two distinct bases,

$$\begin{aligned}\phi(k,t) &= a_{in}(k)u_{in}(k,t) + a_{in}^\dagger(-k)u_{in}^*(-k,t)\\ &= a_{out}(k)u_{out}(k,t) + a_{out}^\dagger(-k)u_{out}^*(-k,t),\end{aligned} \tag{50}$$

where the 'in' and 'out' wavefunctions $u_{in,out}(k,t)$ are related by a Bogoluibov transformation. The in- and out- oscillators are related to each other through the Bogoliubov coefficients

$\alpha(k), \beta(k)$

$$a_{in}(k) = \alpha^*(k) a_{out}(k) - \beta^*(k) a^\dagger_{out}(-k),$$
$$a_{out}(k) = \alpha(k) a_{in}(k) + \beta^*(k) a^\dagger_{in}(-k) \tag{51}$$

The Bogoliubov coefficients are actually functions of $|k|$.

General proof of the gCC ansatz [2] for the ground state The two sets of oscillators define two distinct vacua $|0, in\rangle$ and $|0, out\rangle$, defined by $a_{in}(k)|0, in\rangle = 0$ and $a_{out}(k)|0, out\rangle = 0$. Using the first line of (51), we can express the in-vacuum in terms of the out-vacua as follows

$$|0, in\rangle = \exp[\frac{1}{2}\sum_k \gamma(k) a^\dagger_{out}(k) a^\dagger_{out}(-k)]|0, out\rangle, \tag{52}$$
$$= \exp[-\sum_k \kappa(k) a^\dagger_{out}(k) a_{out}(k)]|D\rangle, \tag{53}$$
$$\text{where} \quad \gamma(k) = \beta^*(k)/\alpha^*(k) \qquad \kappa(k) = -\frac{1}{2}\log(-\gamma(k)) \tag{54}$$

where in the second line we have used Baker-Campbell-Hausdorff formula and $|D\rangle$ is a Dirichlet boundary state defined in terms of the 'out' Fock space. Using the propeties of quantum mechanical scattering problem, we find that $\gamma(k)$ admits a small-momentum expansion of the form

$$\gamma(k) = -1 + \gamma_1|k| + \gamma_2|k|^2 + \gamma_3|k|^3 + ..., \ Re(\gamma_1) \geq 0 \tag{55}$$
$$\Rightarrow \kappa(k) = \kappa_2|k| + \kappa_3|k|^2 + \kappa_4|k|^3 - ..., \tag{56}$$

hence, this proves the ansatz (48), where $W_{2n}, n = 1, 2, ..., (W_2 = H)$ are the even W_∞ charges[6] [41] of the final massless scalar field theory.

4.2 Thermalization to GGE

As we have shown in section 3, the post-quench state, which is of the form (48) shows subsystem thermalization to the GGE:

$$|\psi(k_2, \{k_n\})\rangle_{\rm gCC} \xrightarrow[\text{thermalization}]{\text{subsystem}} \rho_{\rm GGE}(\beta, \{\mu_n\}), \quad \beta = 4\kappa_2, \mu_n = 4\kappa_n \tag{57}$$

A reduced density matrix on the LHS asymptotically approaches that in the RHS. We will compute explicit correlators below which satisfy the same property.

The energy and W-charges (as well as the number operator) are conserved in the post-quench CFT dynamics, we have

$$\langle H\rangle_{\rm gCC} = \langle H\rangle_{\rm GGE}, \ \langle W_n\rangle_{\rm gCC} = \langle W_n\rangle_{\rm GGE}, \ \langle N(k)\rangle_{\rm gCC} = \langle N(k)\rangle_{\rm GGE} \tag{58}$$

[6] $H \equiv W_2 = \sum_k |k| a^\dagger_{out}(k) a_{out}(k)$, $W_{2n} = \sum_k |k|^{2n-1} a^\dagger_{out}(k) a_{out}(k)$, $n = 2, 3, ...$

Thus, the charges measured for the post-quench state also refer to those of the GGE. In particular, note that

$$\langle N(k)\rangle = |\beta(k)|^2 = \frac{|\gamma(k)|^2}{1-|\gamma(k)|^2} = \frac{1}{e^{4\kappa(k)-1}} \tag{59}$$

This relation can be identified with a similar relation in [21].

4.3 Specific quench protocols

Massive to critical scalar quench: For the specific mass function

$$m^2(t) = m_0^2(1-\tanh(\rho t))/2 \tag{60}$$

$$\xrightarrow{\rho\to\infty} m_0^2\Theta(-t) \tag{61}$$

$\rho \to \infty$ is the sudden limit. Solving (49), we find the following Bogoliubov coefficients

$$\alpha(k) = \sqrt{\frac{\omega_{out}}{\omega_{in}}}\,\frac{\Gamma\left(-\frac{i\omega_{out}}{\rho}\right)\Gamma\left(1-\frac{i\omega_{in}}{\rho}\right)}{\Gamma\left(-\frac{i\omega_{+}}{2\rho}\right)\Gamma\left(1-\frac{i\omega_{+}}{2\rho}\right)} \xrightarrow{\rho\to\infty} \frac{1}{2}\frac{|k|+\omega_{in}}{\sqrt{|k|\omega_{in}}} \tag{62}$$

$$\beta(k) = \sqrt{\frac{\omega_{out}}{\omega_{in}}}\,\frac{\Gamma\left(\frac{i\omega_{out}}{\rho}\right)\Gamma\left(1-\frac{i\omega_{in}}{\rho}\right)}{\Gamma\left(\frac{i\omega_{-}}{2\rho}\right)\Gamma\left(1+\frac{i\omega_{-}}{2\rho}\right)} \xrightarrow{\rho\to\infty} \frac{1}{2}\frac{|k|-\omega_{in}}{\sqrt{|k|\omega_{in}}} \tag{63}$$

Using these values, and the general method of Section 4.1, we find that the ground state is of the gCC form (48) where

$$\kappa_2 = \frac{1}{m_0}\left(1+\frac{\pi^2}{12}\frac{m_0^2}{\rho^2} - i\frac{\zeta(3)}{4}\frac{m_0^3}{\rho^3}+...\right),\ \kappa_4 = \frac{1}{m_0^3}\left(-\frac{5}{160}+\frac{\pi^2}{288}\frac{m_0^2}{\rho^2}+...\right),\ ... \tag{64}$$

Comparison with CC state ansatz of [20]: The propagator can be calculated in terms of Meijer G-function. In the asymptotic limit $t \to \infty$, it becomes

$$\begin{aligned} G_{q,0}(0,t;r,t) &= \frac{1}{8}\left(m_0(2t-r)\right) + \frac{1}{8\sqrt{2\pi m_0}}\left(\frac{e^{-m_0(2t-r)}}{\sqrt{2t-r}} + \frac{e^{-m_0(r+2t)}}{\sqrt{r+2t}} + \frac{2e^{-m_0 r}}{\sqrt{r}}\right) + ... \quad & r<2t \\ &= \frac{1}{8\sqrt{2\pi m_0}}\left(\frac{e^{-m_0(r-2t)}}{\sqrt{r-2t}} + \frac{e^{-m_0(r+2t)}}{\sqrt{r+2t}} + \frac{2e^{-m_0 r}}{\sqrt{r}}\right) + ... \quad & r>2t \end{aligned}$$

Using this, we can calculate $\langle\partial\phi\partial\phi\rangle$ and $\langle\partial\phi\bar{\partial}\phi\rangle$ and it does not matches with the CC state value calculated by BCFT techniques in [20] even in high effective temperature limit. The Energy density in the $t \to \infty$ limit is,

$$H = m_0^2/(16\pi) \tag{65}$$

Again it does not agree with the thermal value[28] with $\beta = 4/m_0$. In other words, the higher chemical potentials affect the asymptotic energy density.

We also consider critical to critical scalar quench with the mass function[40] given by $m^2(t) = m_0^2 \,\text{sech}^2(\rho t)$ and found the various parameters. We also considered massive to critical fermionic quench with the mass profile[42, 40] given by $\frac{m_0}{2}\,(1 - \tanh(\rho t))$ and identified various κ_n's.

4.4 Quenching squeezed states

Suppose, instead of the ground state we start with a squeezed state[7] of the pre-quench Hamiltonian:[8]

$$|\psi, in\rangle = |f\rangle \equiv \exp\left[\frac{1}{2}\sum_k f(k) a_{in}^\dagger(k) a_{in}^\dagger(-k)\right] |0, in\rangle \tag{66}$$

This is clearly a Bogoliubov transformation of $|0, in\rangle$. And the quench process is another further bogoluibov transformation. So, the final state is a gCC state (48) where now the $\gamma(k)$ and $\kappa(k)$ in (54) are modified due to the non-trivial initial state as

$$\gamma_{\text{eff}}(k) = \frac{\beta^*(k) + f(k)\alpha(k)}{\alpha^*(k) + f(k)\beta(k)}, \qquad \kappa_{\text{eff}}(k) \equiv -\frac{1}{2}\log\left(-\gamma_{\text{eff}}(k)\right) \tag{67}$$

Using elements of scattering theory and assuming $f(k)$ to be regular at $k = 0$ so that it admits an expansion $f(k) = f(0) + O(k)$, we find that the first factor in the RHS has an expansion $-1 + O(k)$. This ensures an expansion of κ_{eff} in the form (56).

Explicit Examples: Starting from the squeezed state define by

$$f(k) = 1 - \frac{2|k|}{\sqrt{|k|^2 + {m_0}^2}\tanh\left(\kappa_{2,0}k + \kappa_{4,0}k^3\right) + k} \tag{68}$$

the quench protocol of 'tanh' function (61), in the sudden limit $\rho \to \infty$ yields[9]

$$|f\rangle = \exp[-\left(\kappa_{2,0}H + \kappa_{4,0}W_4\right)|D\rangle \tag{69}$$

$\kappa_{4,0} = 0$ is the special case which yields CC state.

Correlators in Squeezed States

The propagator and other correlators in a squeezed state (69) is given by

$$\begin{aligned}
\langle\phi\phi\rangle &= \int \frac{dk}{4\pi}\frac{e^{ikr}}{k}\left(\coth\left(2k\left(\kappa_2 + \kappa_4 k^2\right)\right) - \cos(2kt)\text{cosech}\left(2k\left(\kappa_2 + \kappa_4 k^2\right)\right) - 1\right) \\
\langle\partial\phi\partial\phi\rangle &= \int \frac{dk}{8\pi} e^{ikr} k\left(\coth\left(2k\kappa_2 + 2k^3\kappa_4\right) - 1\right) \\
\langle\partial\phi\bar{\partial}\phi\rangle &= \int \frac{dk}{8\pi} e^{-2ikt} k\ \text{cosech}\left(2\kappa_2 k + 2k^3\kappa_4\right)
\end{aligned} \tag{70}$$

[7]These states have importance in diverse contexts [38, 43] including quantum entanglement [39]. Time-development of these states can address the issue of dynamical evolution of quantum entanglement, among other things.

[8]We assume that the norm of the squeezed state is finite, which is ensured by the finiteness of the integral $\int dk/(2\pi)\log(1 - |f(k)|^2)$.

[9]Note that we choose here $\kappa_{2,0}$, $\kappa_{4,0}$ to be positive to ensure that the gCC state is of finite norm.

The first two equations describe two-point functions with $(x_1, t_1) = (0, t)$, $(x_2, t_2) = (r, t)$, whereas the third equation is a one-point function at a point (x, t) (which is independent of x by translational invariance). For CC state($\kappa_4 = 0$), the fourier transforms can be easily calculated, the results exactly match the results obtained using BCFT in [44]. The equilibrium energy can also be calculated in the $t \to \infty$ limit as

$$H = \frac{\pi}{96\kappa_2^2} \tag{71}$$

This agrees with the thermal energy density with $\beta = 4\kappa_2$.

With non-zero κ_4, let us first consider $\langle \partial\phi\bar{\partial}\phi \rangle$. The associated Fourier transform can be computed by contour integration. Note that the cosech function has simple poles in the k-plane at $2\kappa_4 k^3 + 2\kappa_2 k = i\pi n$. Thus, there are three simple poles for each n. Out of these poles, there is only one perturbative($\kappa_4 \ll \kappa_2^3$) branch, the total residue in this branch for $n = \pm 1$ poles is

$$\langle \partial\phi\bar{\partial}\phi \rangle_{gCC} = -\frac{\pi}{16\kappa_2^2}\left(1 + 4\pi^2\tilde{\kappa}_4 + 48\pi^4\tilde{\kappa}_4^2\right)\exp\left(-\frac{4\left(\pi + 4\pi^3\tilde{\kappa}_4 + 48\pi^5\tilde{\kappa}_4^2\right)t}{4\kappa_2}\right) \tag{72}$$

where $\tilde{\kappa}_4 = \frac{\kappa_4}{4^2\kappa_2^3}$.

Comparison with MSS: Using the charge under the μ_4 current $q_4 = 3$, $\beta = 4\kappa_2$ and $\tilde{\kappa}_4 = \tilde{\mu}_4$, we match the results of MSS exactly. Note that above, $\tilde{\mu}_4^2 t$ also exponentiates, so this gives the behaviour expected by MSS and higher orders.

The computation of $\langle \partial\phi\partial\phi \rangle$ follows along similar lines. Here, the poles are the same. The only difference is the residue of coth.

Comparison with equilibrium GGE calculation: Using the Wightman function in a GGE, the holomorphic two-point function is now given by

$$\begin{aligned}\frac{1}{Z}\mathrm{Tr}\left(\partial\phi(x_2,t_2)\partial\phi(x_1,t_1)e^{-\beta H-\mu_4 W_4}\right) &= \frac{1}{2}\int\frac{dk}{2\pi}\frac{k\ e^{-ik(x+t)}}{e^{\beta|k|+\mu_4|k|^3}-1}\\ &= \frac{1}{4}\int\frac{dk}{2\pi}k\ e^{-ik(x+t)}\left(\coth(\beta|k|/2+\mu_4|k|^3/2)-1\right)\end{aligned} \tag{73}$$

which exactly matches (70) provided we define $\beta = 4\kappa_2$, $\mu_4 = 4\kappa_4$.

4.5 Conclusion

We found an exact agreement between $t \to \infty$ correlators in the gCC state (68) and in the corresponding GGE (*cf.* equations (70) and (73)) with chemical potentials $\mu_n = 4\kappa_2$. The relaxation rate of one-point functions is seen to exactly exponentiate (see (72)), and its perturbation expansion in the higher κ_n coefficients agrees with the value from section 3 calculation by CFT techniques. We also found that generically GGE correlators (equivalently, late time correlators in a gCC state) and thermal correlators (equivalently late time correlators in a CC state), characterized by the same temperature (equivalently same κ_2 are different, even at large distance scales (e.g. κ_4 appears in the correlation length in (72)). So, it is clear that while the fact of thermalization is true, the late time exponents depend nontrivially on the higher chemical potentials (or higher κ_n's), even though these correspond to perturbation by irrelevant operators in an Wilsonian RG sense.

At least for the free theories that we considered, the equilibrium chemical potentials allow a reconstruction of the quench protocol (completely or partially depending on the situation). Now, it is well-known that the potential of a one-dimensional Schrodinger problem [45] can be reconstructed from the reflection amplitude. This implies, for the ground state quench, that through correspondence between the quench problem and the scattering problem, $m(t)$ can be reconstructed from $\kappa(k)$. This, in turn, means that the μ_n's carry complete knowledge of the quench protocol $m(t)$. In case we consider a squeezed pre-quench state, the GGE is characterized by the function $\kappa_{eff}(k)$ which is given by a combination of the knowledge of the squeezing function $f(k)$ and the quench protocol $m(t)$. Thus, in case the pre-quench initial state as well as the quench protocol are unknown, the equilibrium ensemble has an imperfect recollection of the history.

Chapter I

AdS_3/CFT_2: Geometry of entanglement[1]

1 Introduction and Summary

It has been a matter of lively debate whether the standard description of a large black hole with a smooth horizon is quantum mechanically consistent, and is, in fact, consistent with AdS/CFT. While the firewall hypothesis [46, 47] [2] argues against the validity of the standard description, Maldacena and Susskind [4] have suggested that the region inside the horizon is a geometric representation of quantum mechanical entanglement. Both the above proposals, and related issues, are discussed in a number of papers; for a partial list, related to the discussion in this chapter, see [46, 47, 49, 50, 51, 52, 53, 54, 55, 56]. The proposal of [4], summarized by the symbolic equation ER = EPR, [3] is illustrated by the eternal black hole geometry which is dual to the thermofield state [5].[4] It has been argued in several papers (see, e.g., [51, 56]) that although the proposal holds for this illustrative case, it does not hold in general. One of the objectives of this chapter is to explicitly construct a general class of two-sided geometries [5] which represent entangled CFT's.

A useful approach to construct the geometric dual to a CFT state is by using a Fefferman-Graham (FG) expansion, with boundary data provided by the CFT state. To begin with, let us consider the case of a single CFT. Since we are primarily interested in the metric, let us focus, for simplicity, on states in which only the stress tensor is excited. The dual geometry would then be given by the solution to the appropriate Einstein equations subject to the boundary data provided by the stress tensor. This approach has been particularly fruitful in the context of the AdS_3/CFT_2 duality where the Fefferman-Graham expansion has been

[1] The contents of this chapter have partial overlap with Ritam Sinha's thesis work.

[2] See also [48].

[3] Einstein-Rosen (wormhole) = Einstein-Podolsky-Rosen (entangled state).

[4] See [7] for an AdS/CFT check on the dynamical entanglement entropy which involves the wormhole region, and [14] for generalization to include angular momentum and charge.

[5] By *two-sided*, we mean geometries which have two asymptotically AdS regions.

shown, for pure gravity, to terminate [9] , yielding the following exact metric [6]

$$ds^2 = \frac{dz^2}{z^2} - dx_+ dx_- \left(\frac{1}{z^2} + z^2 \frac{L(x_+)\bar{L}(x_-)}{16} \right) + \frac{1}{4} \left(L(x_+) dx_+^2 + \bar{L}(x_-) dx_-^2 \right) \tag{I.1}$$

The boundary data ($z \to 0$) is represented by the following holographic stress tensors (we choose $-\Lambda = 1/\ell^2 = 1$)

$$8\pi G_3 T_{++}(x_+) = \frac{L(x_+)}{4},\ 8\pi G_3 T_{--}(x_-) = \frac{\bar{L}(x_-)}{4} \tag{I.2}$$

The above metric becomes singular at the horizon

$$z = z_0 \equiv 2 \left(L(x_+)\bar{L}(x_-) \right)^{-1/4}, \tag{I.3}$$

and therefore the metric (I.1), describes only an exterior geometry. [7]

How does one carry out such a construction with two boundaries, with two sets of boundary data? Indeed, it is not even clear, *a priori*, whether simultaneously specifying two independent pieces of boundary data can always lead to a consistent solution in the bulk (this question has been raised in several recent papers, e.g. see [50]). A possible approach to this problem is suggested by the fact that the eternal BTZ solution, which contains (I.1) with constant stress tensors, admits a maximal extension with two exteriors, which are joined to an interior region across a smooth horizon. The maximal extension is constructed by transforming, e.g., to various Eddington-Finkelstein (EF) coordinate patches (described in Appendix I.A). A naive generalization of such a procedure in case of variable $L, \bar{L}$, of transforming the metric (I.1) to EF type coordinates, does not seem to work since it leads to a complex metric in the interior region [8]. A second approach could be to solve Einstein's equations, by using the constant $L, \bar{L}$ (eternal BTZ) solution as a starting point and, incorporate the effect of variable $L, \bar{L}$ perturbatively, either in a derivative expansion or an amplitude expansion. While this method may indeed work, at the face of it, it is far from clear how the variation in $L, \bar{L}$ can be chosen to be different at the two boundaries.

We will use the method of solution generating diffeomorphisms (SGD). In gauge theory terms, these are asymptotically nontrivial gauge transformations which correspond to global charge rotations; the use of these objects was introduced in [58, 59, 60], and used crucially by Brown and Henneaux[61] to generate 'Virasoro charges' through asymptotically nontrivial SGDs that reduced at the AdS boundary to conformal transformations. (We discuss these in more detail in Section 2). Brown and Henneaux had discussed only the asymptotic form of the SGDs. We apply two independent, exact Brown-Henneaux SGDs [9] to different

[6] In (I.1), $x_\pm = t \pm x$, with $x \in \mathbb{R}$. For $L, \bar{L}$ constant, this corresponds to the BTZ black string.

[7] The inverse metric g^{MN} blows up at the horizon, as in case of Schwarzschild geometry. However, unlike there, here the other region $z > z_0$ does *not* represent the region behind the horizon; rather it gives a second coordinatization of the exterior region again. We will use a different set of coordinate systems to probe the interior and a second exterior region.

[8] Such a coordinate transformation has been discussed in [57] in an asymptotic series near the boundary.

[9] It has been shown by Roberts [62] that the exterior metric (I.1) can be obtained by an exact Brown-Henneaux type diffeomorphism applied to the Poincare metric. See Appendix I.D for a discussion on this and a different, new, transformation which is closer to the ones we use here.

coordinate patches of the eternal BTZ geometry, yielding a black hole spacetime with two completely general stress tensors on the two boundaries. In other words, our strategy for solving the boundary value problem can be summarized as: given arbitrary boundary data in terms of stress tensors $T_R, \bar{T}_R$, and $T_L, \bar{T}_L$, we (i) find the two specific sets of conformal transformations (which we are going to call G_+, G_- and H_+, H_-) which, when acting on a constant stress tensor, gives rise to these stress tensors, (ii) find the SGD's which reduce to these conformal transformations and (iii) apply the SGD's to the eternal BTZ metric.

This solves the boundary value problem we posed above.

The results are organized as follows:

(1) The new solutions: In Section 2 we describe the explicit *solution generating diffeomorphisms* (SGDs) and construct the resulting two-sided black hole geometries. The diffeomorphisms reduce to conformal transformations at each boundary, parameterized by functions $G_\pm$ on the right and $H_\pm$ on the left. The SGD parameterized by $G_\pm$ is applied to the Eddington-Finkelstein coordinate chart EF1 (which covers the right exterior and the black hole interior, see Figure I.1) and to EF4 (right exterior + white hole interior), whereas the SGD parameterized by $H_\pm$ is applied to the Eddington-Finkelstein coordinate chart EF2 (left exterior + black hole interior) and to EF3 (left exterior + white hole interior). To cover the entire spacetime we also use a Kruskal chart K5 which covers an open neighbourhood of the bifurcate Killing horizon; here we leave the original Kruskal metric unaltered. The effect of the above SGDs is that we have a description of different metric tensors in different charts. In Section 2.3 we show that all these can be pieced together to give a single (pseudo-)Riemannian manifold; we prove this by showing that in the pairwise overlap of any two charts $N_1 \cap N_2$ the different metrics constructed above differ only by a trivial diffeomorphism (see the definition 2.5); the full metric, specified with the help of the various charts, is schematically represented in Figure I.3. An important manifestation of the asymptotic nontriviality of the SGDs is to move and warp the infra-red regulator surface (see Figure I.2); the change in the boundary properties, as found in later sections, can be directly attributed to this.

The new spacetime so constructed inherits the original causal structure, with the event horizon, the bifurcation surface, and the two exterior and interior regions (see also footnotes 10 and 32). The horizon is, therefore, regular by construction. In the new EF coordinates (the *tilded* coordinates) the horizon consists of smoothly undulating surfaces (see Fig I.4).

(2) The CFT duals: In Section 3 the fact that the SGDs reduce asymptotically to conformal transformations is used to infer that the CFT duals to our geometries are given by conformal unitary transformations $U_L \otimes U_R$ to the thermofield double state. The correspondence between various AdS and CFT quantities, implied by this, is explicitly verified in the next few sections.

(3) The AdS/CFT checks: In section 4 we carry out this test for the stress tensor. We compute the holographic stress tensor [12, 15] in the new geometry and show that it exactly matches with the expectation value of the conformally transformed (including the Schwarzian derivative) stress tensor in the thermofield double state. In section 5 we compare AdS and CFT results for both $\langle O_L O_R \rangle$ and $\langle O_R O_R \rangle$ types of correlators. The holographic two-point function is found by computing geodesic lengths in the new geometries and we find that it correctly matches with the two-point function of transformed operators. This can be

regarded as an evidence for the ER=EPR relation in the presence of probes.

(4) Entanglement entropy: As a further check, in section 6 we apply the above result for two-point functions to show that the entanglement entropy EE in CFT matches the holographic EE [63, 13] including when the Ryu-Takayanagi geodesic passes through the wormhole. This constitutes a direct proof of the ER=EPR conjecture for the entire class of geometries constructed here. We work out the dynamical entanglement entropy in an example (see fig I.5).

(5) Holographic entropy from horizon: In section 7, we make crucial use of the existence of smooth horizons on both sides to compute a holographic entropy along the lines of [64]. We are able to compute the entropy in the CFT by using the Cardy formula and an adiabatic limit (which allows the use of the 'instantaneous' energy eigenvalues to compute degeneracies); the holographic entropy agrees with this. The entropy turns out to be divergenceless, reflecting the dissipationless nature of 2D CFT. There is, however, a nontrivial local flow of entropy (see fig I.6).

(6) ER=EPR: In Section 8 we discuss some implications of our solutions *vis-a-vis* the ER=EPR relation of Maldacena and Susskind [4]. Our solutions establish an infinite family of quantum states entangling two CFTs which are represented in the bulk by wormhole geometries. We show, in particular, that out of a given set of quantum states we consider, all characterized by the same energy, there are states with low entanglement entropies, which nevertheless are still represented by wormhole geometries; this is in keeping with the picture of geometric entanglement suggested in [4].

2 The solutions

In this section we obtain the new solutions by carrying out the procedure outlined in the Introduction. As explained in Section I.A, for constant $L, \bar{L}$, the metric (I.1) represents a BTZ black hole of constant mass and angular momentum (I.83). In that case, one can construct EF coordinates (see Section I.A) to extend the spacetime to include the region behind the horizon and a second exterior. We will, in fact, use five charts to cover the extended geometry (see Fig I.1).

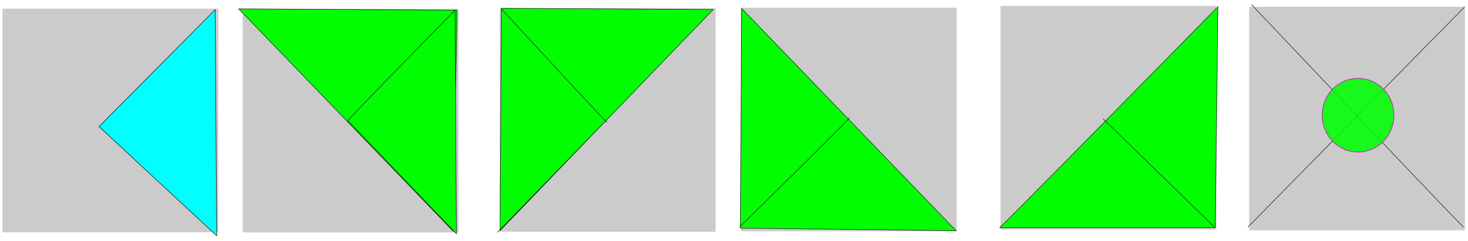

Figure I.1: The (green parts of) the five figures on the right depict the five coordinate charts used to cover the eternal BTZ solution.[10]The coordinate chart K5 is needed to cover the "bifurcation surface" where the past and future horizons meet (it is a point in the Penrose diagram). The leftmost diagram (in blue) represents the coordinate chart used in (I.1). Each of the coordinate charts is shown, for facility of comparison, within a Penrose diagram where the parts not within the chart are shown in gray.

2.1 The eternal BTZ geometry

We will now briefly review some properties of the eternal BTZ geometry. The maximal extension of the eternal BTZ geometry, starting from (I.1) is described in detail in Section I.A. We will briefly reproduce some of the formulae relevant to the coordinate system ("EF1") describing the right exterior and the interior. The EF1 coordinates are obtained from the coordinates of (I.1) by the transformations

$$\frac{z}{z_0} = \sqrt{\frac{1}{\lambda_0}\left(\lambda - \sqrt{\lambda^2 - \lambda_0^2}\right)} \tag{I.4}$$

$$x_+ = v - \frac{1}{2\sqrt{L}} \ln\left(\frac{\lambda - \lambda_0}{\lambda + \lambda_0}\right), \quad x_- = w - \frac{1}{2\sqrt{\bar{L}}} \ln\left(\frac{\lambda - \lambda_0}{\lambda + \lambda_0}\right)$$

The metric, in these coordinates, becomes

$$ds^2 = \frac{d\lambda^2}{4(\lambda + \lambda_0)^2} + \frac{L}{4}dv^2 + \frac{\bar{L}}{4}dw^2 - \lambda\, dvdw + \frac{\sqrt{L}}{2(\lambda + \lambda_0)}dvd\lambda + \frac{\sqrt{\bar{L}}}{2(\lambda + \lambda_0)}dwd\lambda \tag{I.5}$$

The event horizon λ_H, the inner horizon λ_i, and the singularity λ_s are at

$$\lambda_H = \lambda_0 \equiv \frac{\sqrt{L\bar{L}}}{2}, \ \lambda_i = -\lambda_0, \ \lambda_s = -\frac{1}{4}(L + \bar{L}) \tag{I.6}$$

[10] This is the entire geometry for the non-spinning BTZ; for spinning BTZ solutions, we do not attempt to cover the region beyond the inner horizon, since we are interested in the asymptotic properties in the two exteriors mentioned above. See also footnote 32.

Note that for BTZ black holes without angular momentum $\bar{L} = L$ and $\lambda_i = \lambda_s$. The location of the event horizon corresponds to (I.3).

In order to regulate IR divergences coming from $\lambda \to \infty$, we define a cut-off surface Σ_B at a constant large $\lambda = \lambda_{ir}$; the metric (I.5) on Σ_B turns out to be

$$\lambda = \lambda_{ir} = 1/\epsilon^2 \Rightarrow ds^2|_{\Sigma_B} = -(1/\epsilon^2)\ dv\ dw(1 + O(\epsilon^2)) \tag{I.7}$$

By the usual AdS/CFT correspondence the leading term defines the boundary metric (see Section I.C)

$$ds^2_{bdry} = -dv\ dw \tag{I.8}$$

The subleading term in the metric corresponds to the normalizable metric fluctuation, which gives the expectation value of the stress tensor; this is the holographic stress tensor [12], and is given here by

$$8\pi G_3 T_{vv}(x_+) = \frac{L}{4},\ 8\pi G_3 T_{ww}(x_-) = \frac{\bar{L}}{4} \tag{I.9}$$

It is easy to see that we will get the same boundary metric and stress tensor from an analysis of the coordinate chart EF4. It is also straightforward to derive similar results for the left exterior (which represent a state with the same mass and angular momentum) using EF2 and EF3.

2.2 Solution generating diffeomorphisms (SGD)

We will now proceed to construct new solutions with arbitrary boundary data at the two boundaries (represented by two arbitrary holographic stress tensors $T_{R,\mu\nu}(x)$ and $T_{L,\mu\nu}(x)$) by applying the method of solution generating diffeomorphisms to the above geometry, as explained in the introduction.

The solution generating diffeomorphisms can be described as follows. Suppose we start with a certain metric $g_{MN}(x)dx^M dx^N$ [11] in a certain coordinate chart $\mathcal{U}_P$ containing a point P. The new metric $\tilde{g}_{MN}$, in this coordinate chart, is given in terms of a diffeomorphism (active coordinate transformation) $f : \tilde{x}^M = \tilde{x}^M(x)$, by the definition

$$g \to \tilde{g} \equiv f^* g : \quad \tilde{g}_{MN}(\tilde{x}) \equiv \frac{\partial x^P}{\partial \tilde{x}^M} \frac{\partial x^Q}{\partial \tilde{x}^N} g_{PQ}(x) \tag{I.10}$$

In the above, $f^* g$ is a standard mathematical notation for the pullback of the metric g under the diffeomorphism f. For diffeomorphisms differing infinitesimally from the identity map: $\tilde{x}^M = x^M - \xi^M(x)$, we, of course, have the familiar relation

$$\delta g_{MN}(x) = D_M \xi_N + D_N \xi_M \tag{I.11}$$

Normally, a diffeomorphism is considered giving rise to a physically indistinguishable solution; this, however, is not true when the diffeomorphism is non-trivial at infinity (this is explained in more detail in Section 2.5).

As explained in Section I.A, we use five charts to cover the entire eternal BTZ geometry (see Fig I.1). These charts are labelled as EF1, EF2, EF3, EF4 and K5. We use a nontrivial diffeomorphism in each of EF1, EF2, EF3 and EF4, which overlap with the boundary and the identity transformation in the Kruskal patch K5.

[11] Notation: $x^M = \{\lambda, x^\mu\},\ x^\mu = \{v, w\}$.

The metric in the coordinate chart EF1

The diffeomorphism in the EF1 coordinate chart is given by

$$\lambda = \frac{\tilde{\lambda}}{G'_+(\tilde{v})G'_-(\tilde{w})},\ v = G_+(\tilde{v}),\ w = G_-(\tilde{w}) \tag{I.12}$$

The new metric $\tilde{g}_{MN}$, written in terms of $\tilde{x}^M = (\tilde{\lambda}, \tilde{v}, \tilde{w})$, is

$$\begin{aligned}\tilde{g}_{MN}(\tilde{x})d\tilde{x}^M d\tilde{x}^N \equiv ds^2 = \frac{1}{B^2}\Big[&d\tilde{\lambda}^2 + A_+^2 d\tilde{v}^2 + A_-^2 d\tilde{w}^2 + 2A_+ d\tilde{v}d\tilde{\lambda} + 2A_- d\tilde{w}d\tilde{\lambda} \\ &- \tilde{\lambda}\Big(B^2 + 2\Big(A_+\frac{G''_-(\tilde{w})}{G'_-(\tilde{w})} + A_-\frac{G''_+(\tilde{v})}{G'_+(\tilde{v})} + \tilde{\lambda}\frac{G''_+(\tilde{v})G''_-(\tilde{w})}{G'_+(\tilde{v})G'_-(\tilde{w})}\Big)\Big)d\tilde{v}d\tilde{w}\Big]\end{aligned} \tag{I.13}$$

where

$$A_+ = \sqrt{L}G'_+(\tilde{v})(\tilde{\lambda}+\tilde{\lambda}_0) - \tilde{\lambda}\frac{G''_+(\tilde{v})}{G'_+(\tilde{v})},\ A_- = \sqrt{L}G'_-(\tilde{w})(\tilde{\lambda}+\tilde{\lambda}_0) - \tilde{\lambda}\frac{G''_-(\tilde{w})}{G'_-(\tilde{w})},\ B = 2(\tilde{\lambda}+\tilde{\lambda}_0)$$

For infinitesimal transformations $G_\pm(x) \equiv x + \epsilon_\pm(x)$, this amounts to an asymptotically nontrivial diffeomorphism ξ^M (see (I.11))[12]

$$\xi_1^v = \epsilon_+(v),\ \xi_1^w = \epsilon_-(w),\ \xi_1^\lambda = -\lambda\left(\epsilon'_+(v) + \epsilon'_-(w)\right) \tag{I.14}$$

The behaviour of the metric (I.13) at a constant large λ surface is given by

$$ds^2 = -\tilde{\lambda}\ d\tilde{v}d\tilde{w}\ (1 + O(1/\tilde{\lambda})) \tag{I.15}$$

This, by following arguments similar to the previous case (see Section 2.1), identifies the IR cutoff surface as

$$\tilde{\lambda}_{ir} = (1/\epsilon^2) \tag{I.16}$$

and the boundary metric as

$$ds^2_{bdry} = -d\tilde{v}d\tilde{w} \tag{I.17}$$

The subleading term in (I.15), as explored in Section 4, gives the holographic stress tensor. We will see there that the subleading term depends on the SGD functions $G_\pm$; this feature is what makes the SGD's asymptotically nontrivial (see Section 2.5 for a more detailed discussion on this).

In terms of the old λ-coordinate, the surface (I.16) is

$$\lambda = 1/(\epsilon^2 G'_+(\tilde{v})G'_-(\tilde{w})) \tag{I.18}$$

Note that this surface is different from (I.7), and is nontrivially warped, as in Figure I.2. This is another manifestation of the asymptotic non-triviality of the diffeomorphism (I.12), which is responsible for nontrivial transformation of bulk quantities, such as geodesic lengths.

[12] The subscript in ξ_1^M refers to the chart EF1.

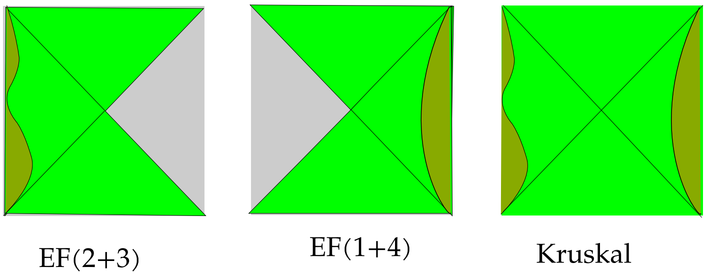

Figure I.2: This figure shows the IR cut-off (I.16) in the new geometries. The effect of the SGDs, in the old (un-tilded) coordinates, is to deform the IR cut-off surfaces. The surface deformation on the right exterior is given by the change from (I.7) to (I.18); there is a similar surface deformation on the left exterior.

We note that the leading large $\tilde{\lambda}$ behaviour of (I.13) is that of AdS$_3$

$$ds^2 = \frac{d\tilde{\lambda}^2}{4\tilde{\lambda}^2} - \tilde{\lambda}\; d\tilde{v}\; d\tilde{w} + ... \tag{I.19}$$

As mentioned before, and will be explored in detail in Section 4, the subleading terms, represented by the ellipsis ..., are nontrivially different from that of AdS$_3$.

The metric in the coordinate chart EF2

The diffeomorphism (SGD) used in the coordinate chart EF2 (see Fig I.1), which is independent of the one above used in EF1, is given by

$$\lambda_1 = \frac{\tilde{\lambda}_1}{H'_+(\tilde{u})H'_-(\tilde{\omega})},\; u = H_+(\tilde{u}),\; \omega = H_-(\tilde{v}) \tag{I.20}$$

which leads to the metric

$$\begin{aligned} ds^2 = \frac{1}{B^2}\Big[& d\tilde{\lambda}_1^2 + A_+^2 d\tilde{u}^2 + A_-^2 d\tilde{\omega}^2 - 2A_+ d\tilde{u}d\tilde{\lambda}_1 - 2A_- d\tilde{\omega}d\tilde{\lambda}_1 \\ & - \tilde{\lambda}_1\Big(B^2 - 2\Big(A_+\frac{H''_-(\tilde{\omega})}{H'_-(\tilde{\omega})} + A_-\frac{H''_+(\tilde{u})}{H'_+(\tilde{u})} - \tilde{\lambda}_1\frac{H''_+(\tilde{u})H''_-(\tilde{\omega})}{H'_+(\tilde{u})H'_-(\tilde{\omega})}\Big)\Big)d\tilde{\omega}d\tilde{u}\Big] \end{aligned} \tag{I.21}$$

where

$$A_+ = \sqrt{L}H'_+(\tilde{u})(\tilde{\lambda}_1 + \tilde{\lambda}_0) + \tilde{\lambda}_1\frac{H''_+(\tilde{u})}{H'_+(\tilde{u})},\; A_- = \sqrt{\bar{L}}H'_-(\tilde{\omega})(\tilde{\lambda}_1 + \tilde{\lambda}_0) + \tilde{\lambda}_1\frac{H''_-(\tilde{\omega})}{H'_-(\tilde{\omega})},\; B = 2(\tilde{\lambda}_1 + \tilde{\lambda}_0)$$

For infinitesimal transformations $H_\pm(x) = x + \varepsilon_\pm(x)$, this implies a diffeomorphism ξ_2^M where

$$\xi_2^u = -\varepsilon_+(u),\; \xi_2^\omega = -\varepsilon_-(\omega),\; \xi_2^\lambda = -\lambda\left(\varepsilon'_+(u) + \varepsilon'_-(\omega)\right) \tag{I.22}$$

Note, once again, the asymptotic nontriviality of the above diffeomorphism.

2.3 The full metric

In a manner similar to the above, we apply the SGD characterized by $G_\pm$ on EF4 (which shares the right exterior with EF1, see Appendix I.A.1): and the SGD characterized by $H_\pm$ on EF3 (which shares the left exterior with EF2):

$$\begin{aligned}
\text{EF4}: \quad & \lambda = \frac{\tilde{\lambda}}{G'_+(\tilde{u}_1)G'_-(\tilde{\omega}_1)}, \; u_1 = G_+(\tilde{u}_1), \; \omega_1 = G_-(\tilde{\omega}_1) \\
& \qquad \text{infinitesimally} \quad \left(\xi_4^\lambda, \xi_4^{u_1}, \xi_4^{\omega_1}\right) = \left(-\lambda(\epsilon'_+(u_1) + \epsilon'_-(\omega_1)), \epsilon_+(u_1), \epsilon_-(\omega_1)\right) \\
\text{EF3}: \quad & \lambda = \frac{\tilde{\lambda}_1}{H'_+(\tilde{v}_1)H'_-(\tilde{w}_1)}, \; v_1 = H_+(\tilde{v}_1), \; w_1 = H_-(\tilde{w}_1) \\
& \qquad \text{infinitesimally} \quad \left(\xi_4^\lambda, \xi_4^{v_1}, \xi_4^{w_1}\right) = \left(-\lambda(\varepsilon'_+(v_1) + \varepsilon'_-(w_1)), \varepsilon_+(v_1), \varepsilon_-(w_1)\right) \quad \text{(I.23)}
\end{aligned}$$

The infinitesimal transformations are similar to those in eqs. (I.14) and (I.22). As mentioned above, we use the identity diffeomorphism of Kruskal patch K5 (with $\xi_5^M = 0$). The expressions for the metric in various coordinate charts are given in (I.13), (I.21), (I.114), (I.115) and (I.104).

We will now show that the five different metrics in the five coordinate charts define a single metric in the entire spacetime. To see this, note that although the SGD's applied on the five charts are different, (equivalently, for infinitesimal transformations, the diffeomorphisms ξ_i^M in the five charts differ from each other), they satisfy the following sufficient criteria:

(i) At both the right (and left) exterior boundary, the diffeomorphisms coincide. For example, in case of the right exterior (see (I.100)), as $\lambda \to \infty$, $u_1 \to v$, $\omega_1 \to w$. Hence $\tilde{u}_1 = G_+^{-1}(u_1) \to G_+^{-1}(v) = \tilde{v}$. In other words, for infinitesimal transformations $\xi_4^M(P) \to \xi_1^M(P)$ for a given point P with $\lambda \to \infty$. This implies that the metric (I.13) coincides at the right boundary with the similar metric(I.114) obtained by applying the $G_\pm$ transformations on the coordinate chart EF4. Similarly, the metric (I.21) obtained by the $H_\pm$ transformations in EF2 and the similar metric (I.115) obtained by the $H_\pm$ transformations in EF3 coincide at the left exterior boundary.

(ii) Away from the boundary, the metrics obtained in the various EF coordinate charts differ from each other only by trivial diffeomorphisms which become the identity transformation at infinity. Since the physical content of each of these metrics is represented only by the boundary data, the above point (i) ensures that all the different metrics represent the same single spacetime metric in different charts (see Figure I.3).

(iii) It is clear that the SGDs lead to a *smooth metric* in each chart, provided $G_\pm(x), H_\pm(x)$ are differentiable and invertible functions. In the rest of the chapter, we will only consider such functions. It can be verified that such a class of functions is sufficiently general to generate (through transformations such as (I.42)) any pair of physically sensible holographic stress tensors at both boundaries.

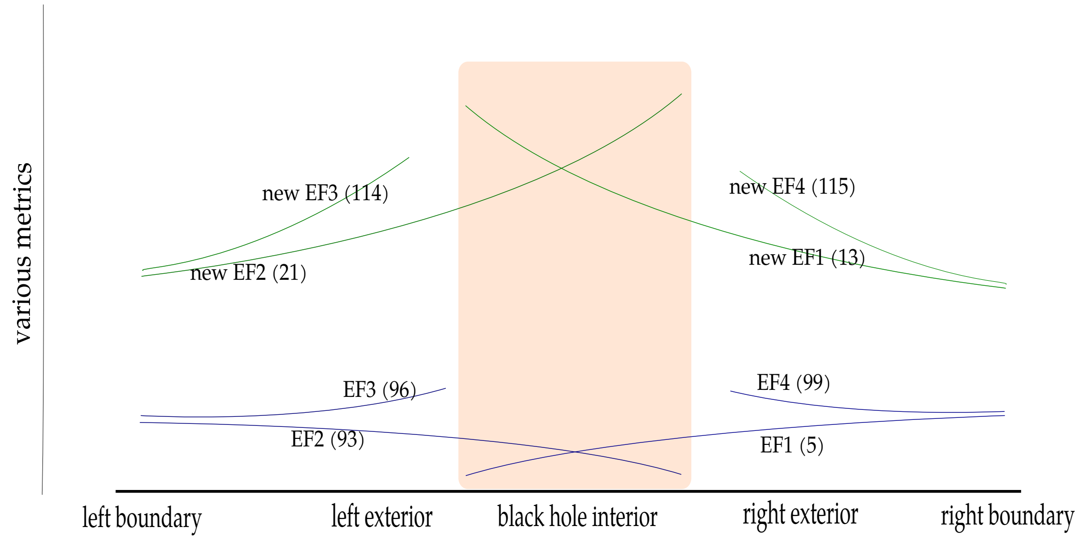

Figure I.3: A schematic illustration of the metrics related by trivial and nontrivial diffeomorphisms (see the definition 2.5). The metrics (I.5), (I.93), (I.96) and (I.99), represented by the blue lines, define the eternal BTZ geometry; they are all related by trivial diffeomorphisms, which either do not extend to the boundaries or when they do, they become identity asymptotically. The metrics (I.13), (I.21), (I.114) and (I.115), represented by the green lines, define our new solution characterized by the functions $G_\pm, H_\pm$. These are also all related by trivial diffeomorphisms, which satisfy the same criteria as above. The two sets however represent physically different metrics since they are related to each other by nontrivial diffeomorphisms; for instance, (I.5) and (I.13) are related by a diffeomorphism, schematically represented by their separation, which does not vanish (become identity) asymptotically.

Analogy with the Dirac monopole

It is important to note that our new solutions can only be specified in terms of a different metric in different coordinate charts which are equivalent to each other. This is analogous to case of the Dirac monopole: the gauge field A_μ for a static U(1) magnetic monopole of charge q_m at the origin needs to be specified separately on two separate coordinate charts:

$$F = q_m \sin\theta \; d\theta \; d\phi : \; A_N = q_m(1-\cos\theta) \; d\phi, \; A_S = q_m(-1-\cos\theta) \; d\phi \tag{I.24}$$

Here $\mathbb{R}^3 - \{0\}$ is viewed as $\mathbb{R} \times S^2$ where S^2 is described by two coordinate charts N_N and N_S (such as obtained by a stereographic projection on to the plane) which include all points of S^2 minus the south and north pole respectively. A^θ_N vanishes (and is hence regular) at the north pole $\theta = 0$, but develops a string singularity at the south pole $\theta = \pi$ (for each $r > 0$). Similarly, A_S is regular at the south pole, but has a string singularity at the north pole. The important point to note is that in spite of appearances, A_N and A_S describe the same gauge field in the region of overlap $N_N \cap N_S$. This is because in this region, $A_N = A_S + d\chi$ where $\chi = 2q_m d\phi$ represents a pure gauge transformation for appropriately quantized q_m (Dirac quantization condition).

In the present case the metric (I.13) written in EF1, although non-singular on the future horizon, is singular on the past horizon for general $G_\pm$. In order to describe the metric in a neighbourhood of the past horizon, we must switch to the metric in EF4. Similarly, in order to describe the diffeomorphism at the bifurcation surface, we must use the metric (I.104) in the K5 coordinate chart.

Summary of this subsection:

The metrics (I.13), (I.21), (I.114), (I.115) and (I.104), valid in the coordinate charts EF1, EF2, EF3, EF4 and K5 respectively, define a spacetime with a regular metric. The metrics are asymptotically AdS_3 at both the right and left boundaries; the subleading terms in the metric are determined by the solution generating diffeomorphisms $G_\pm, H_\pm$ and can be chosen to fit boundary data specified by arbitrary holographic stress tensors. A schematic representation of our solution is presented in Figure I.3.

2.4 Horizon

In Section 2.2 we viewed the SGDs as a coordinate transformation. Alternatively, however, we can also view the diffeomorphism as an active movement of points: $x^M \to \tilde{x}^M = x^M + \xi^M$. In this viewpoint, the future horizon $\lambda = \lambda_H = \lambda_0$ (see (I.6)) on the right moves to

$$\tilde{\lambda}_H = G'_+(\tilde{v})\ G'_-(\tilde{w})\lambda_0,\ \tilde{\lambda}_{1,H} = H'_+(\tilde{u})\ H'_-(\tilde{\omega})\lambda_0 \tag{I.25}$$

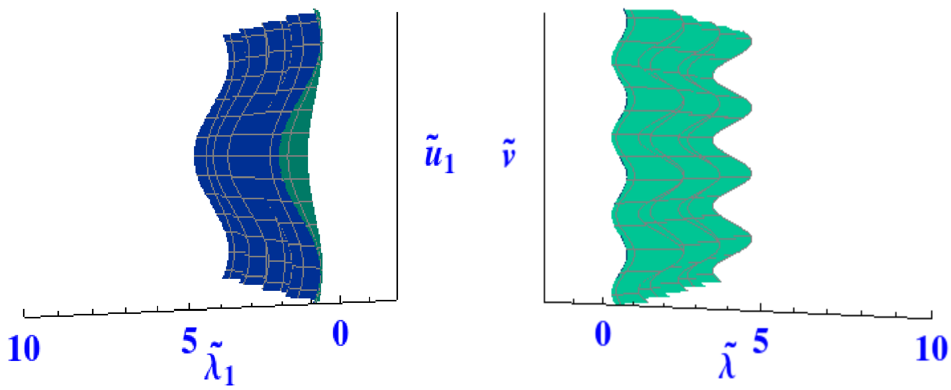

Figure I.4: The figure on the right shows the location of the horizon on the right in the $\tilde{\lambda}, \tilde{v}, \tilde{w}$ coordinates. The figure on the left shows the location of the horizon on the left in the $\tilde{\lambda}_1, \tilde{u}, \tilde{\omega}$ coordinates. These are described by (I.25). These surfaces are diffeomorphic to the undeformed horizon (I.6) depicted in Figure I.2. Although the horizon has an undulating shape in our coordinate system, the expansion parameter, measured by the divergence of the area-form, vanishes (see Eq. (I.74)).

Similar statements can be made in the other coordinate charts. The horizons represented this way are smooth but undulating (see figure I.4).

The geometry of warped horizons in [65, 64] was used to yield a holographic prescription for computing local entropy current of a fluid. In Section 7 we use a similar technology to compute a holographic entropy in our case.

2.5 On the nontriviality of solution generating diffeomorphisms

It is natural to wonder how a metric such as (I.13) provides a new solution since it is obtained by a diffeomorphism from (I.5); however, the fact that the diffeomorphism (I.12) is asymptotically nontrivial makes the new solution physically distinct. Thus, in (I.12) $\tilde{\lambda}$ remains different from λ in the asymptotic region. Indeed, as we will see, the first subleading term in the metric (I.13) carries nontrivial data about a holographic stress tensor (I.42) on the right boundary.

Asymptotically AdS_3 diffeomorphisms were first discussed by Brown and Henneaux [61] who showed that such transformation led to an additional surface contribution to conserved charges of the system. These observations were preceded by a general discussion of such surface charges in the context of gauge theories and gravity in [58, 59, 60]. These authors identified asymptotically non-vanishing pure gauge transformations as global charge rotations.

In the current AdS/CFT context, the surface charges are encapsulated by the holographic stress tensors on the two boundaries. As we will see shortly, they change nontrivially under the solution generating diffeomorphisms (SGD's). In fact, the SGD's reduce to conformal transformations on the boundary. As a result, the 'global charge rotations' mentioned above correspond to a *conformal* transformation of the stress tensor. The important point is that starting from a given constant stress tensor on each boundary, the two independent SGD's can generate two *independent* and *completely general* stress tensors by this method.

We should note that the diffeomorphisms define a new theory in which the appropriate choice of the IR cutoff surface is (I.16). In this description, the horizon becomes an undulating surface as in Fig I.4. An equivalent ('active') viewpoint is to describe the new geometry in terms of the old coordinates (I.5), but to change the IR-cutoff surface from (I.7) to (I.16). In either case, the holographic stress tensor changes.

We conclude this section with the following definition of a nontrivial diffeomorphism, which has been implicit in much of the above discussion.

Definition

A local diffeomorphism which does not extend to either boundary (left or right), or a diffeomorphism which extends to a boundary but asymptotically approaches the identity diffeomorphism there, is called a 'trivial' diffeomorphism. Contrarily, a diffeomorphism which extends to a boundary where it does not approach the identity diffeomorphism, is called 'nontrivial'. Quantitatively, a nontrivial diffeomorphism (f) is one under which the holographic stress tensor computed from the existing metric g at the boundary is different from that computed from the pulled back metric f^*g.

3 The Dual Conformal Field Theory

As we saw above, the SGD's reduce to conformal transformations at the boundary. We will construct the CFT-dual to the new solutions using the above idea.

Note that the eternal BTZ black hole geometry, described by (I.5) and (I.93), corresponds to the following thermofield double state [5, 7, 13, 14]

$$|\psi_0\rangle = Z(\beta_+, \beta_-)^{-1/2} \sum_n \exp[-\beta_+ E_{+,n}/2 - \beta_- E_{-,n}/2] |n\rangle |n\rangle \tag{I.26}$$

The states $|n\rangle \in \mathcal{H}$ denote all simultaneous eigenstates of $H_\pm = (H \pm J)/2$ with eigenvalues $E_{\pm,n}$. $|\psi_0\rangle$ here is a pure state in $\mathcal{H} \otimes \mathcal{H}$ obtained by the 'purification' of the thermal state (I.27). [13]

$$Z(\beta_+, \beta_-) = \mathrm{Tr}\rho_{\beta_+,\beta_-} \qquad \text{with} \qquad \rho_{\beta_+,\beta_-} = \exp[-\beta_+ H_+ - \beta_- H_-] = \exp[-\beta(H + \Omega J)] \tag{I.27}$$

represents the grand canonical ensemble in $\mathcal{H}$ with inverse temperature β and angular velocity Ω (which can be viewed as the thermodynamic conjugate to the angular momentum J). Also $\beta_\pm = \beta(1 \pm \Omega)$. [14]

Note that $|\psi_0\rangle$ is a pure state in $\mathcal{H} \otimes \mathcal{H}$, and is a 'purification' of the thermal state (I.27). The non-spinning BTZ: The CFT dual for the more familiar case of non-spinning eternal BTZ black hole ($\Omega = 0 = J$) is the standard thermofield double:

$$|\psi_{0,0}\rangle = Z(\beta)^{-1/2} \sum_n \exp[-\beta E_n/2] |n\rangle |n\rangle \tag{I.28}$$

where $|n\rangle$ now denotes all eigenstates of H. [15]

CFT duals of our solutions Following the arguments above (I.26), we claim that the CFT-duals to the new solutions described in Section 2.3 are described by the following pure states in $\mathcal{H} \otimes \mathcal{H}$:

$$|\psi\rangle = U_L U_R |\psi_0\rangle = Z(\beta_+, \beta_-)^{-1/2} \sum_n \exp[-\beta_+ E_{+,n}/2 - \beta_- E_{-,n}/2] U_L |n\rangle U_R |n\rangle \tag{I.29}$$

where U_R is the unitary transformation which implements the conformal transformations on the CFT on the right boundary (characterized by $G_\pm$), and U_L is the unitary transformation which implements the conformal transformations on the CFT on the left boundary (characterized by $H_\pm$). See Appendix I.E for an explicit construction of a unitary transformations U_R.

In the following sections, we will provide many checks for this proposal. However, first we shall discuss how to compute various correlators in the above state (I.29).

[13] For definiteness, we will sometimes call the two Hilbert spaces $\mathcal{H}_L$ and $\mathcal{H}_R$, where L, R represent 'left' and 'right', corresponding to the two exterior boundaries of the eternal BTZ. Indeed, L, R also have an alternative meaning. The left/right boundary of the eternal BTZ geometry maps to the left/right Rindler wedge of the boundary of Poincare coordinates, respectively.

[14] The thermal state ρ_{β_+,β_-} (see (I.27)) implies a field theory geometry where the light cone directions have periods $\beta_\pm$.

[15] An entanglement entropy for this state was calculated in [7] and matched with a bulk geodesic calculation. This was generalized to the spinning eternal BTZ black hole in [14].

3.1 Correlators

Let us first consider correlators in the standard thermofield double state (I.26). It is known that correlators of one-sided CFT observables, say O_R, satisfy an AdS/CFT relation of the form [16]

$$\langle\psi_0|O_R(P_1)O_R(P_2)...O_R(P_n)|\psi_0\rangle \equiv \mathrm{Tr}\left(\rho_{\beta_+,\beta_-}O_R(P_1)O_R(P_2)...O_R(P_n)\right) = G_{\text{bulk}}(\mathbf{P}_1,\mathbf{P}_2,...\mathbf{P}_n) \tag{I.30}$$

where the bulk correlator G_{bulk} is computed from the (right exterior region of) a dual black hole geometry with temperature $T = 1/\beta$ and angular velocity Ω. Two-sided correlators, similarly, satisfy a relation like

$$\langle\psi_0|O_R(P_1)O_R(P_2)...O_R(P_m)O_L(P_1')...O_L(P_n')|\psi_0\rangle = G_{\text{bulk}}(\mathbf{P}_1,\mathbf{P}_2,...\mathbf{P}_m;\mathbf{P}_1',...,\mathbf{P}_n') \tag{I.31}$$

where the bulk correlator on the RHS is computed from the two-sided geometry of the eternal BTZ black hole [5, 7, 13, 14], given in (I.5) and (I.93). The bold-faced label $\mathbf{P}$ above represents an image of the field theory point P on a cut-off surface in the bulk under the usual AdS/CFT map. E.g. in the coordinates of (I.5), the map is given by

$$P \mapsto \mathbf{P} \equiv (\lambda = \lambda_{ir} = 1/\epsilon^2, P) \tag{I.32}$$

where ϵ is the UV cut-off in the CFT, cf. (I.7)). There is a similar map for the *left* boundary. In particular, the holographic correspondence for the two point functions of scalar operators can be written simply as [16]:

$$\begin{aligned}\langle\psi_0|O_R(P)O_R(Q)|\psi_0\rangle &= \mathrm{Tr}(\rho_{\beta_+,\beta_-}O_R(P)O_R(Q)) = \exp[-2hL(\mathbf{P},\mathbf{Q})]\\ \langle\psi_0|O_R(P)O_L(Q')|\psi_0\rangle &= \exp[-2hL(\mathbf{P},\mathbf{Q}')]\end{aligned} \tag{I.33}$$

where $L(\mathbf{P},\mathbf{Q})$ is the length of the extremal geodesic connecting $\mathbf{P}$ and $\mathbf{Q}$ (similarly with $L(\mathbf{P},\mathbf{Q}')$).
It is easy to see that correlators in the new, transformed, state $|\psi\rangle$ (I.29) can be understood as correlators of transformed operators in the old state $|\psi_0\rangle$, i.e.

$$\langle\psi|O_R(P_1)...O_R(P_m)O_L(P_1')...O_L(P_n')|\psi\rangle = \langle\psi_0|\tilde{O}_R(P_1)...\tilde{O}_R(P_m)\tilde{O}_L(P_1')...\tilde{O}_L(P_n')|\psi_0\rangle \tag{I.34}$$

where

$$\tilde{O}_R(P) \equiv U_R^\dagger O_R(P)U_R, \qquad \tilde{O}_L(P') \equiv U_L^\dagger O_L(P')U_L \tag{I.35}$$

For a primary field O_R with conformal dimensions $(h,\bar{h})$, the conformally transformed operator satisfies the relation

$$\tilde{O}_R(\tilde{v},\tilde{w}) = O_R(v,w)\left(\frac{dv}{d\tilde{v}}\right)^h\left(\frac{dw}{d\tilde{w}}\right)^{\bar{h}} \tag{I.36}$$

[16]We will mostly use unprimed labels, $P_1, P_2, ...$ for points on the spacetime of the 'right' CFT, and primed labels, $P_1', P_2', ...$ for the space of the 'left' CFT.

3.2 Strategy for checking AdS/CFT

To check the claim that the states (I.29) are CFT-duals to the new bulk geometries found in Section 2.3, we need to show a relation of the form (cf. (I.31))

$$\langle\psi_0|\tilde{O}_R(P_1)...\tilde{O}_R(P_m)\tilde{O}_L(P'_1)...\tilde{O}_L(P'_n)|\psi_0\rangle = \tilde{G}_{\rm bulk}(\tilde{\mathbf{P}}_1, \tilde{\mathbf{P}}_2, ...\tilde{\mathbf{P}}_m; \tilde{\mathbf{P}}'_1, ..., \tilde{\mathbf{P}}'_n) \tag{I.37}$$

where the RHS is computed in the new geometries. Here $\tilde{\mathbf{P}}$ represents the image of the CFT point P, under AdS/CFT, on the cut-off surface (I.16) in the new geometry. In the language of (I.13), the map is

$$P \mapsto \tilde{\mathbf{P}} = (\tilde{\lambda} = \tilde{\lambda}_{ir} = 1/\epsilon^2, P) \tag{I.38}$$

<u>Two-point correlators:</u> In the particular case of two-point functions

$$\begin{aligned}\langle\psi_0|\tilde{O}_R(P)\tilde{O}_R(Q)|\psi_0\rangle &= \mathrm{Tr}(\rho_{\beta_+,\beta_-}\tilde{O}_R(P)\tilde{O}_R(Q)) = \exp[-2h\tilde{L}(\tilde{\mathbf{P}},\tilde{\mathbf{Q}})]\\ \langle\psi_0|\tilde{O}_R(P)\tilde{O}_L(Q')|\psi_0\rangle &= \exp[-2h\tilde{L}(\tilde{\mathbf{P}},\tilde{\mathbf{Q}}')]\end{aligned} \tag{I.39}$$

where $\tilde{L}(\tilde{\mathbf{P}},\tilde{\mathbf{Q}})$ is the length of the extremal geodesic connecting P and Q in the new geometry (similarly with $\tilde{L}(\tilde{\mathbf{P}},\tilde{\mathbf{Q}}')$). One may wonder how a geodesic length in the new geometry can be different from that in the original, eternal BTZ black hole geometry, since the former is obtained by a diffeomorphism from the latter; the point is that the bulk points $\tilde{\mathbf{P}}$, given by (I.38) are *not* the same as the bulk points $\mathbf{P}$ given by (I.32). For example, a geodesic with endpoints at a fixed IR cut-off $\tilde{\lambda} = 1/\epsilon^2$ (both on the right exterior) corresponds, in the eternal BTZ black hole, to a geodesic with two end-points at (I.18) $\lambda = 1/(\epsilon^2 G'_+(\tilde{v})G'_-(\tilde{w}))$. As we will see below, it is this shift which ensures the equality in (I.39). This is one more instance of how our geometries are nontrivially different from the original BTZ solution although they are obtained by diffeomorphisms (see Section 2.5 for more detail).

4 Holographic Stress Tensor

In this section we will discuss our first observable O: the stress tensor. We will first consider the stress tensor of the boundary theory on the right. The generalization to the stress tensor on the left is trivial. The equation (I.37) now implies that we should demand the following equality

$$\langle\psi|T_{vv}(P)|\psi\rangle \equiv \mathrm{Tr}\left(\rho_{\beta_+,\beta_-}U_R^\dagger T_{vv}(P)U_R\right) = \tilde{T}_{{\rm bulk},\tilde{v}\tilde{v}}(\tilde{\mathbf{P}}) \tag{I.40}$$

and a similar equation for the right-moving stress tensor $T_{ww}(w)$.

Bulk The RHS of this equation is simply the holographic stress tensor, computed in the new geometry (I.13). We use the definition of holographic stress tensor in [12, 15]:[17]

$$8\pi G_3 T_{\mu\nu} = \lim_{\epsilon\to 0}(K_{\mu\nu} - Kh_{\mu\nu} - h_{\mu\nu}) \tag{I.41}$$

[17]We drop the subscript bulk from the bulk stress tensor, as it should be obvious from the context whether we are talking about the CFT stress tensor or the holographic stress tensor.

where $h_{\mu\nu}$ is the induced metric on the cut-off surface $\Sigma : \tilde{\lambda} = \tilde{\lambda}_{ir} = 1/\epsilon^2$, chosen in accordance with (I.38) which is the natural one in the new geometry (note that it is different from the cut-off surface implied by (I.32)). $K_{\mu\nu}$ and K are respectively the extrinsic curvature and its trace on Σ. It is straightforward to do the explicit calculation; we find that

$$8\pi G_3 T_{\tilde{v}\tilde{v}} = \frac{L}{4} G'_+(\tilde{v})^2 + \frac{3G''_+(\tilde{v})^2 - 2G'_+(\tilde{v})G'''_+(\tilde{v})}{4G'_+(\tilde{v})^2},$$

$$8\pi G_3 T_{\tilde{w}\tilde{w}} = \frac{\bar{L}}{4} G'_-(\tilde{w})^2 + \frac{3G''_-(\tilde{w})^2 - 2G'_-(\tilde{w})G'''_-(\tilde{w})}{4G'_-(\tilde{w})^2} \tag{I.42}$$

This clearly looks like a conformal transformation of the original stress tensor (I.9). We will explicitly verify below that it agrees with the CFT calculation. The generalization to T_{ww} and to the stress tensors of the second CFT is straightforward. This clearly has the form of a conformal transformation of the original stress tensor (I.9). We will explicitly verify below in the CFT that it indeed is precisely a conformal transformation, as demanded by (I.40). The generalization of (I.42) to the stress tensors $T_{\tilde{u}\tilde{u}}, T_{\tilde{\omega}\tilde{\omega}}$ of the second CFT is straightforward.

We will sometimes use the notation $T_R, \bar{T}_R$ for $T_{\tilde{v}\tilde{v}}, T_{\tilde{w},\tilde{w}}$, and $T_L, \bar{T}_L$ [18] for $T_{\tilde{u}\tilde{u}}, T_{\tilde{\omega}\tilde{\omega}}$ respectively. It is clear that by appropriately choosing the functions $G_\pm$ and $H_\pm$, any set of boundary stress tensors $T_{R,L}, \bar{T}_{R,L}$ can be generated. This is how our solutions described in Section 2.3 solve the boundary value problem mentioned in the Introduction.

CFT The unitary transformation in the LHS of (I.40), implements, by definition, the following conformal transformation (see Appendix I.E for more details) on the quantum operator

$$U_R^\dagger T_{vv}(P) U_R = \left(\frac{\partial \tilde{v}}{\partial v}\right)^{-2} [T_{\tilde{v}\tilde{v}}(\tilde{v}) - \frac{c}{12} S(v, \tilde{v})] \tag{I.43}$$

From (I.12), the relevant conformal transformation here is $v = G_+(\tilde{v})$. Using this, the definition (I.122) of the Schwarzian derivative $S(v, \tilde{v})$, and the identification [61]

$$G_3 = 3/(2c), \tag{I.44}$$

we find that (I.43) exactly agrees with (I.42).

This *proves* the AdS-CFT equality (I.40) for the stress tensor.

5 General two-point correlators

In this section we will discuss general two-point correlators, both from the bulk and CFT viewpoints following the steps outlined in Section 3.1.

5.1 Boundary-to-Boundary Geodesics

As mentioned in (I.33), the holographic calculation of a two-point correlator reduces to computing the geodesic length between the corresponding boundary points. We will first calcu-

[18] $T_R, \bar{T}_R$ represent the left-moving and right-moving stress tensors on the Right CFT; similarly for $T_L, \bar{T}_L$.

late correlators in the thermofield double state (I.26), which involves computing geodesics in the eternal BTZ geometry (I.5).

In the eternal BTZ geometry

RL geodesic: Let us consider a geodesic running from a point $\mathbf{P}(1/\epsilon_R^2, v, w)$ on the right boundary to a point $\mathbf{Q}' = (1/\epsilon_L^2, u, \omega)$ on the left boundary.[19] As shown in Section I.A.3 (see [7]) both the right exterior ($\subset$ EF1) and the left exterior ($\subset$ EF2) can be mapped to a single coordinate chart in Poincare coordinates. Let the Poincare coordinates for $\mathbf{P}$ and $\mathbf{Q}'$, be $(X_{+R}, X_{-R}, \zeta_R)$ and $(X_{+L}, X_{-L}, \zeta_L)$ respectively. By using the coordinate transformations given in (I.112) and (I.113), we find, upto the first subleading order in ϵ_R and ϵ_L,

$$\begin{aligned} &X_{+R} = e^{\sqrt{L}v}, \quad X_{-R} = -e^{-\sqrt{L}w} + L\epsilon_R^2 e^{-\sqrt{L}w}, \quad \zeta_R^2 = L\epsilon_R^2\, e^{\sqrt{L}(v-w)} \\ &X_{+L} = -e^{\sqrt{L}u} + L\epsilon_L^2 e^{\sqrt{L}u}, \quad X_{-L} = e^{-\sqrt{L}\omega}, \quad \zeta_L^2 = L\epsilon_L^2\, e^{\sqrt{L}(u-\omega)} \end{aligned} \tag{I.45}$$

with $L = \bar{L}$.[20] The geodesic in Poincare coordinates is given by

$$X_+ = A\tanh\tau + C, \quad X_- = B\tanh\tau + D, \quad \zeta = \frac{\sqrt{-AB}}{\cosh\tau}$$

where τ is the affine parameter, which takes the values τ_R and τ_L at $\mathbf{P}$ and $\mathbf{Q}'$ respectively. The constants A, B, C, D, τ_L and τ_R are fixed by the endpoint coordinates given above. In the limit $\epsilon_R, \epsilon_L \to 0$, we obtain

$$\begin{aligned} \tau_R &= \log\Big[\frac{e^{-(\sqrt{L}v+\sqrt{L}\omega)/2}}{\sqrt{2}}\sqrt{\frac{(e^{\sqrt{L}v}+e^{\sqrt{L}u})(e^{\sqrt{L}w}+e^{\sqrt{L}\omega})}{\lambda_0\epsilon_R^2}}\Big] \\ \tau_L &= -\log\Big[\frac{e^{-\sqrt{L}(u+w)/2}}{\sqrt{2}}\sqrt{\frac{(e^{\sqrt{L}v}+e^{\sqrt{L}u})(e^{\sqrt{L}w}+e^{\sqrt{L}\omega})}{\lambda_0\epsilon_L^2}}\Big] \end{aligned}$$

where $\lambda_0 = L/2$ (see (I.6)). The geodesic length is now simply given by the affine parameter length

$$L(\mathbf{P}, \mathbf{Q}') = \tau_R - \tau_L = \log\left[\frac{4\cosh[\sqrt{L}(v-u)/2]\cosh[\sqrt{L}(w-\omega)/2]}{L\epsilon_R\epsilon_L}\right] \tag{I.46}$$

For comparison with CFT correlators in the thermofield double, we will put, in the above expression, $\epsilon_L = \epsilon_R = \epsilon$, where ϵ is the (real space) UV cut-off in the CFT.
RR geodesic: If we take the two boundary points on the same exterior region, say on the right, $\mathbf{P_1}(1/\epsilon_1^2, v_1, w_1)$ and $\mathbf{P_2}(1/\epsilon_2^2, v_2, w_2)$, then the corresponding Poincare coordinates are (using (I.112))

$$\begin{aligned} &X_{+1} = e^{\sqrt{L}v_1}, \qquad X_{-1} = -e^{-\sqrt{L}w_1} + L\epsilon_1^2 e^{-\sqrt{L}w_1}, \quad \zeta_1^2 = L\epsilon_1^2\, e^{\sqrt{L}(v_1-w_1)} \\ &X_{+2} = e^{\sqrt{L}v_2}, \qquad X_{-2} = -e^{-\sqrt{L}w_2} + L\epsilon_2^2 e^{-\sqrt{L}w_2}, \quad \zeta_2^2 = L\epsilon_2^2\, e^{\sqrt{L}(v_2-w_2)} \end{aligned} \tag{I.47}$$

[19]For the calculation at hand we need to put $\epsilon_L = \epsilon_R = \epsilon$; however, we keep the two cutoffs independent for later convenience.

[20]For simplicity, we present the calculation here for $L = \bar{L}$; the generalization to the spinning BTZ is straightforward.

Following steps similar to above, we have, in the $\epsilon_1, \epsilon_2 \to 0$ limit,

$$
\begin{aligned}
\tau_1 &= \log\Big[\frac{e^{-(v_1+w_2)/2}}{\sqrt{2}}\sqrt{\frac{(e^{v_1}-e^{v_2})(-e^{w_1}+e^{w_2})}{\lambda_0\epsilon_1^2}}\Big] \\
\tau_2 &= -\log\Big[\frac{e^{-(v_1+w_1)/2}}{\sqrt{2}}\sqrt{\frac{(-e^{v_1}+e^{v_2})(e^{w_1}-e^{w_2})}{\lambda_0\epsilon_2^2}}\Big]
\end{aligned}
$$

The geodesic length is then

$$
L(\mathbf{P_1},\mathbf{P_2}) = \tau_{+1} - \tau_{+2} = \log\left[\frac{4\,\sinh[(v_1-v_2)/2]\,\sinh[(w_1-w_2)/2]}{L\epsilon_1\epsilon_2}\right] \tag{I.48}
$$

For comparison with CFT, we will put $\epsilon_1 = \epsilon_2 = \epsilon$.

In the new geometries

As explained in Section 2, the IR boundary in the new solutions, obtained by the SGDs, is given by the equation (I.16) or equivalently by (I.18), and analogous equations on the left. This is encapsulated by the CFT-to-bulk map (I.38). In case of the *RL geodesic*, the CFT endpoints (P, Q') now translate to new boundary points $(\tilde{\mathbf{P}}, \tilde{\mathbf{Q}}')$ with the following new values of the old (λ, λ_1) coordinates:

$$
\lambda \equiv \frac{1}{\epsilon_R^2} = \frac{1}{\epsilon^2 G'_+(\tilde{v})G'_-(\tilde{w})}, \qquad \lambda_1 \equiv \frac{1}{\epsilon_L^2} = \frac{1}{\epsilon^2 H'_+(\tilde{u})H'_-(\tilde{\omega})} \tag{I.49}
$$

which just has the effect of conformally transforming the boundary coordinates// $\epsilon_R = \epsilon \to \epsilon_R = \epsilon\sqrt{G'_+(\tilde{v})G'_-(\tilde{w})}$, $\epsilon_L = \epsilon \to \epsilon_L = \epsilon\sqrt{H'_+(\tilde{u})H'_-(\tilde{\omega})}$. Using these new values of $\epsilon_{L,R}$, we get

$$
L(\tilde{\mathbf{P}}, \tilde{\mathbf{Q}}') = \log\left[\frac{4\cosh[\sqrt{L}(G_+(\tilde{v})-H_+(\tilde{u}))/2]}{\sqrt{L}\epsilon\sqrt{G'_+(\tilde{v})H'_+(\tilde{u})}}\frac{\cosh[\sqrt{L}(G_-(\tilde{w})-H_-(\tilde{\omega}))/2]}{\sqrt{L}\epsilon\sqrt{G'_-(\tilde{w})H'_-(\tilde{\omega})}}\right] \tag{I.50}
$$

Similarly,

$$
L(\tilde{\mathbf{P}}_1, \tilde{\mathbf{P}}_2) = \log\left[\frac{4\sinh[\sqrt{L}(G_+(\tilde{v}_1)-G_+(\tilde{v}_2))/2]}{\sqrt{L}\epsilon\sqrt{G'_+(\tilde{v}_1)G'_+(\tilde{v}_2)}}\frac{\sinh[\sqrt{L}(G_-(\tilde{w}_1)-G_-(\tilde{w}_2))/2]}{\sqrt{L}\epsilon\sqrt{G'_-(\tilde{w}_1)G'_-(\tilde{w}_2)}}\right] \tag{I.51}
$$

5.2 General two-point correlators from CFT

In the thermofield double state

RL correlator: For the eternal BTZ string, the coordinate transformations from the EF to Poincare (see Appendix I.A.3) reduce, at the boundary, to a conformal transformation from the Rindler to Minkowski coordinates, so that the boundary of the right (left) exterior maps to the right (left) Rindler wedge [7]. It is expedient to compute the CFT correlations first in the Minkowski plane, and then conformally transform the result to Rindler coordinates. Using this method of [7], we get the following result

$$\begin{aligned}\langle\psi_0|O(X_{+R},X_{-R})\,O(X_{+L},X_{-L})|\psi_0\rangle &= \frac{(\sqrt{L}e^{\sqrt{L}v})^h(\sqrt{L}e^{-\sqrt{L}w})^{\bar{h}}(-\sqrt{L}e^{\sqrt{L}u})^h(-\sqrt{L}e^{-\sqrt{L}\omega})^{\bar{h}}}{(\frac{e^{\sqrt{L}v}+e^{\sqrt{L}u}}{\epsilon})^{2h}(\frac{-e^{-\sqrt{L}w}-e^{-\sqrt{L}\omega}}{\epsilon})^{2\bar{h}}}\\ &= \Big(\frac{4\cosh[\sqrt{L}(v-u)/2]\,\cosh[\sqrt{L}(w-\omega)/2]}{L\epsilon^2}\Big)^{-2h}\end{aligned}$$

where the operator O is assumed to have dimensions $(h,\bar{h})$ and we have used a real space field theory cut-off ϵ. We have related the temperature of the CFT to $L(=\bar{L})$ by the equation $\sqrt{L}=2\pi/\beta$. // It is easy to see that this correlator satisfies the relation (I.33)

$$\langle\psi_0|O(X_{+R},X_{-R})\,O(X_{+L},X_{-L})|\psi_0\rangle = e^{-2hL(\mathbf{P},\mathbf{Q})} \tag{I.52}$$

where in the expression on the right hand side for the geodesic length (I.46), we use $\epsilon_R=\epsilon_L=\epsilon$ as explained before.

RR correlator: By following steps similar to the above, the two-point correlator between the points (I.47) is given by

$$\begin{aligned}\langle\psi_0|\mathcal{O}(X_{+1},X_{-1})\,\mathcal{O}(X_{+2},X_{-2})|\psi_0\rangle &= \frac{(\sqrt{L}e^{\sqrt{L}v_1})^h(\sqrt{L}e^{-\sqrt{L}w_1})^{\bar{h}}(\sqrt{L}e^{\sqrt{L}v_2})^h(\sqrt{L}e^{-\sqrt{L}w_2})^{\bar{h}}}{(\frac{(e^{\sqrt{L}v_1}-e^{\sqrt{L}v_2}}{\epsilon})^{2h}(\frac{-e^{-\sqrt{L}w_1}+e^{-\sqrt{L}w_2}}{\epsilon})^{2\bar{h}}}\\ &= \Big(\frac{4\sinh[\sqrt{L}(v_1-v_2)/2]\,\sinh[\sqrt{L}(w_1-w_2)/2]}{L\epsilon^2}\Big)^{-2h}\end{aligned}$$

It follows, therefore, that

$$\langle\psi_0|\mathcal{O}(X_{+1},X_{-1})\,\mathcal{O}(X_{+2},X_{-2})|\psi_0\rangle = e^{-2hL(\mathbf{P_1},\mathbf{P_2})} \tag{I.53}$$

where, again, the geodesic length on the right hand side is read off from (I.50) with $\epsilon_1=\epsilon_2=\epsilon$.

In the new states

As explained in (I.34), correlators in the state $|\psi\rangle$ (I.29) can be computed by using a conformal transformation (I.36) of the operators. The new correlator is, therefore, found from the old one (I.52) by a conformal transformation of the boundary coordinates and an inclusion of the Jacobian factors. The latter has, in fact, the effect of the replacement $\epsilon^2\to\epsilon^2\sqrt{G'_+(\tilde{v})G'_-(\tilde{w})H'_+(\tilde{u})H'_-(\tilde{\omega})}$. With these ingredients, it is straightforward to verify that (I.39) is satisfied. Similar arguments apply to RR and LL correlators.

6 Entanglement entropy

We define an entangling region $A=A_R\cup A_L$, where A_R is a half line $(v-w)/2>x_R$ on the right boundary at 'time' $(v+w)/2=t_R$ and A_L is a half line $(u-\omega)/2>x_L$ of the left boundary at 'time' $(u+\omega)/2=t_L$. The boundary of the region A consists of a point $P(v_{\partial A},w_{\partial A})$ on the right and a point $Q'(u_{\partial A},\omega_{\partial A})$ on the left, with coordinates

$$\begin{aligned}P:\quad v_{\partial A} &= t_R+x_R,\quad w_{\partial A}=t_R-x_R\\ Q':\quad u_{\partial A} &= t_L+x_L,\quad \omega_{\partial A}=t_L-x_L\end{aligned} \tag{I.54}$$

Bulk calculations

In the BTZ geometry

We calculate the entanglement entropy S_A of the region A using the holographic entanglement formula of [63, 13]. The HEE is given in terms of the geodesic length $L(\mathbf{P}, \mathbf{Q}')$. The geodesic length, as calculated in (I.46), is

$$L(\mathbf{P}, \mathbf{Q}') = \log \left[\frac{4 \cosh[\sqrt{L}(v_{\partial A} - u_{\partial A})/2] \cosh[\sqrt{L}(w_{\partial A} - \omega_{\partial A})/2]}{M\epsilon^2} \right] \tag{I.55}$$

The HEE is then given by $S_A = L(\mathbf{P}, \mathbf{Q}')/4G_3$. Using (I.44), we get

$$S_A = \frac{c}{6} \log \left[\frac{4 \cosh[\sqrt{L}((t_R + x_R) - (t_L + x_L))/2] \cosh[\sqrt{L}((t_R - x_R) - (t_L - x_L))/2]}{M\epsilon^2} \right] \tag{I.56}$$

Note that for $x_R = x_L = 0$ and $t = t_R = -t_L$ (which correspond to a non-trivial time evolution in the geometry) the HEE (I.56) reduces to

$$S_A = \frac{c}{3} \log \left[\cosh \frac{2\pi t}{\beta} \right] + \frac{c}{3} \log \left[\frac{\beta/\pi}{\epsilon} \right] \tag{I.57}$$

which reproduces the result for the HEE in [7].[21]

In the new geometries

The HEE corresponding to the conformally transformed state (I.29) is given by the length $L(\tilde{\mathbf{P}}, \tilde{\mathbf{Q}}')$ connecting the end-points P and Q' in the new geometries described in Section 2.3. Working on lines similar to the derivation of (I.48), the HEE is given by

$$\begin{aligned} S_A \;\; = \;\; & \frac{c}{6} \log \Bigg[\frac{4 \cosh[\sqrt{L}(G_+(\tilde{t}_R + \tilde{x}_R) - H_+(\tilde{t}_L + \tilde{x}_L))/2]}{\sqrt{L}\epsilon \sqrt{G'_+(\tilde{t}_R + \tilde{x}_R) H'_+(\tilde{t}_L + \tilde{x}_L)}} \\ & \qquad \frac{\cosh[\sqrt{L}(G_-(\tilde{t}_R - \tilde{x}_R) - H_-(\tilde{t}_L - \tilde{x}_L))/2]}{\sqrt{L}\epsilon \sqrt{G'_-(\tilde{t}_R - \tilde{x}_R) H'_-(\tilde{t}_L - \tilde{x}_L)}} \Bigg] \end{aligned} \tag{I.58}$$

CFT calculations

In the thermofield double state

The technique of calculating the entanglement entropy in the thermofield double state is well-known [66]. The Renyi entanglement entropy $S_A^{(n)}$ of the region A (I.54) is given by the trace of the n^{th} power of the reduced density matrix ρ_A^n. The latter can be shown to be a Euclidean path integral on an n-sheeted Riemann cylinder. This can then be calculated

[21] The UV cutoff in [7] is half of the cutoff, ϵ used here.

in terms of the two point correlator, on a complex plane, of certain twist fields $\mathcal{O}$, with conformal dimensions

$$h = \frac{c}{24}(n - 1/n), \quad \bar{h} = \frac{c}{24}(n - 1/n) \tag{I.59}$$

inserted at the end-points (P, Q') of A. The two-point correlator is given by a calculation similar to that in the previous section. Thus,

$$\begin{aligned} S_A^{(n)} &= \langle \mathcal{O}_R(v_{\partial A}, w_{\partial A})\, \mathcal{O}_L(u_{\partial A}, \omega_{\partial A}) \rangle \\ &= \frac{(\sqrt{L})^{2h+2\bar{h}}}{(4\cosh[\sqrt{L}((t_R + x_R) - (t_L + x_L))/2]/\epsilon)^{2h}(\cosh[\sqrt{L}((t_R - x_R) - (t_L - x_L))/2]/\epsilon)^{2\bar{h}}} \end{aligned}$$

The entanglement entropy $S_A = -\partial_n S_A^{(n)}|_{n=1}$ is

$$S_A = \frac{c}{6}\log\left[\frac{4\cosh[\sqrt{L}((t_R + x_R) - (t_L + x_L))/2]\cosh[\sqrt{L}((t_R - x_R) - (t_L - x_L))/2]}{L\epsilon^2}\right] \tag{I.60}$$

This proves that the CFT entanglement entropy and holographic entanglement entropy(I.56) are equal.

In the new states

The EE of the region A, computed in the new state (I.29), is given in terms of the conformally transformed two-point function described in (I.34). The conformally transformed points are given by

$$\begin{aligned} v_{\partial A} &= G_+(\tilde{v}_{\partial A}) = G_+(\tilde{t}_R + \tilde{x}_R), &\quad w &= G_-(\tilde{w}_{\partial A}) = G_-(\tilde{t}_R - \tilde{x}_R) \\ u_{\partial A} &= H_+(\tilde{u}_{\partial A}) = H_+(\tilde{t}_L + \tilde{x}_L), &\quad \omega &= H_-(\tilde{\omega}_{\partial A}) = H_-(\tilde{t}_L - \tilde{x}_L) \end{aligned}$$

It follows that the entanglement entropy is

$$\begin{aligned} S_{A,CFT} &= \frac{c}{6}\log\Big[\frac{4\cosh[\sqrt{L}(G_+(\tilde{t}_R + \tilde{x}_R) - H_+(\tilde{t}_L + \tilde{x}_L))/2]}{\epsilon\sqrt{L}\sqrt{G'_+(\tilde{t}_R + \tilde{x}_R)H'_+(\tilde{t}_L + \tilde{x}_L)}} \\ &\qquad \frac{\cosh[\sqrt{L}(G_-(\tilde{t}_R - \tilde{x}_R) - H_-(\tilde{t}_L - \tilde{x}_L))/2]}{\epsilon\sqrt{L}\sqrt{G'_-(\tilde{t}_R - \tilde{x}_R)H'_-(\tilde{t}_L - \tilde{x}_L)}}\Big] \end{aligned} \tag{I.61}$$

which matches with the HEE (I.58).

6.1 Dynamical entanglement entropy in a specific new geometry

We now compute the entanglement entropy in an illustrative geometry specified by a particular choice of the functions $G_\pm$ and $H_\pm$. In this example, we take

$$x_R = 0, \quad t_R = t, \quad x_L = 0, \quad t_L = -t$$

For simplicity, we consider $G_\pm$ and $H_\pm$ which satisfy

$$G_+(x) \equiv G_-(x) \equiv G(x), \quad H_+(x) \equiv H_-(x) \equiv H(x)$$

With the transformations given above, we have

$$\tilde{x}_R = 0, \quad \tilde{v}_{\partial A} = \tilde{w}_{\partial A} = \tilde{t}_R = \tilde{t}, \qquad \tilde{x}_L = 0, \quad \tilde{u}_{\partial A} = \tilde{\omega}_{\partial A} = \tilde{t}_L = -\tilde{t} \tag{I.62}$$

The expression for the HEE (I.58) then reduces to

$$S_A = \frac{c}{3} \log \left[\frac{2\cosh[\sqrt{L}(G(\tilde{t}) + H_1(\tilde{t}))/2]}{\epsilon\sqrt{L}\sqrt{G'(\tilde{t})H_1'(\tilde{t})}} \right] \tag{I.63}$$

where we have defined the notation $-H(-\tilde{t}) = H_1(\tilde{t})$.

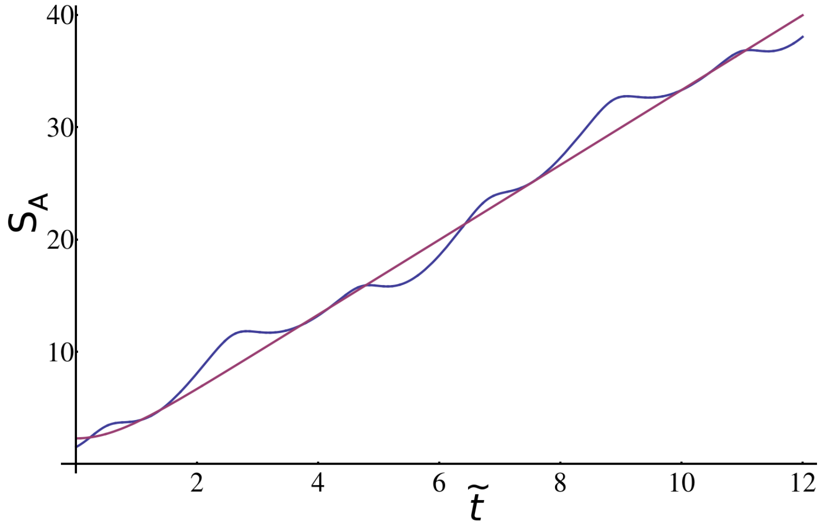

Figure I.5: Time evolution of HEE. The red-line represents the linear growth of HEE for a region consisting of spatial half-lines of both sides of a constant 2-sided BTZ geometry. The blue-line represents the HEE growth of the region consisting of half-lines of both sides of the SGD transformed geometry, for $G(\tilde{t}) = \tilde{t} + \frac{1}{6}\cos(3\tilde{t})$ and $H_1(\tilde{t}) = \tilde{t} + \frac{3}{5}\sin(\tilde{t})$. The undulating curve can be explained in terms of the quasiparticle picture of [20]; the entanglement entropy departs from its usual linear behaviour as the quasiparticle pairs locally go out and back in to the entangling region as the region is subjected to a conformal transformation.

7 Entropy

As discussed in previous sections, our solutions of Section 2.3 are characterized by a smooth, albeit undulating, horizon (see Figure I.4). This allows us, following [64], to define a holographic entropy current. We will first review the equilibrium situation (static black string), and then describe the calculation for the general, time-dependent solution. We will include a comparison with CFT calculations in both cases.

7.1 Equilibrium

Bulk calculation: In case $L = \bar{L} =$ constant, our solutions represent BTZ black strings (I.5) with a horizon at $\lambda = \lambda_0$. The horizon $\mathcal{H}$ is a two-dimensional null surface, described by the metric

$$ds^2|_{\mathcal{H}} \equiv H_{\mu\nu}dx^\mu dx^\nu = \left(\sqrt{L}dv/2 - \sqrt{\bar{L}}dw/2\right)^2 \tag{I.64}$$

Since the normal to $\mathcal{H}$ at any point, given by $n^M = \partial^M \lambda(M = \{\lambda, v, w\})$, also lies on $\mathcal{H}$, $\mathcal{H}$ possesses a natural coordinate system (τ, α) where α labels the one-parameter family of null geodesics, and τ measures the affine distance along the geodesics. In such a coordinate system, we get, by construction

$$ds^2|_{\mathcal{H}} = g d\alpha^2 \tag{I.65}$$

The area 1-form and the entropy current on the horizon are defined by the equations [64] [22],

$$a \equiv 4G_3 \epsilon_{\mu\nu} J_S^\mu dx^\nu = \sqrt{g} d\alpha, \tag{I.66}$$

By inspection, from (I.64) and (I.65), we find the following expressions for the area-form and the entropy current

$$\begin{aligned} a &= \sqrt{L}dv/2 - \sqrt{\bar{L}}dw/2 \\ J_s^v &= \frac{1}{8G_3}\sqrt{\bar{L}},\ J_S^w = \frac{1}{8G_3}\sqrt{L} \end{aligned} \tag{I.67}$$

The holographic entropy current on the boundary $\mathcal{B}$ is obtained by using a map $f : \mathcal{B} \to \mathcal{H}$ and pulling back the area-form (or alternatively the entropy current $J_{S,\mu}$) from the horizon to the boundary. It turns out [23] that the natural pull back retains the form of the area-form or entropy current, namely the expressions (I.67) still hold at the boundary.

To find the entropy density, we define the boundary coordinates $t = (v + w)/2, x = (v - w)/2$ (see Section 6), (so that (I.8) has the canonical form $-dt^2 + dx^2$). With this the entropy density becomes

$$s \equiv J_S^T = \frac{1}{8G_3}\left(\sqrt{L} + \sqrt{\bar{L}}\right) \tag{I.68}$$

CFT calculation: The entropy density from the Cardy formula is [24]

$$s = \sqrt{c\pi T_{vv}/3} + \sqrt{c\pi T_{ww}/3} \tag{I.69}$$

Using the identification (I.44) and (I.9), we can easily see that the two expressions (I.68) and (I.69) exactly match.

[22] Our convention for $\epsilon_{\mu\nu}$ is $\epsilon_{vw} = -1$.

[23] The map f is defined by shooting 'radial' null geodesics inwards from the boundary, and is found to be of the form $f : (\lambda_{ir}, v, w) \mapsto (\lambda_{ir}, v + C_1, w + C_2)$.

[24] Recall that both T_{vv}, T_{ww} are constant in this case. The more familiar form of (I.69), for a circular spatial direction of length 2π, is obtained by putting $S = 2\pi s$, $L_0 = 2\pi T_{vv}$, and $\bar{L}_0 = 2\pi T_{ww}$, which gives $S = 2\pi(\sqrt{cL_0/6} + \sqrt{c\bar{L}_0/6})$.

7.2 New metrics: non-equilibrium entropy

Bulk calculation: We will now follow a similar procedure as above, for the general solution in Section 2.3. We find that (in coordinate chart EF1)

$$ds^2|_{\mathcal{H}} = \frac{1}{4}d\alpha^2 = \frac{1}{4}(\sqrt{L}G'_+(\tilde{v})d\tilde{v} - \sqrt{\bar{L}}G'_-(\tilde{w})d\tilde{w})^2 \tag{I.70}$$

leading to the following area one form on the horizon

$$a = \frac{1}{2}\sqrt{L}G'_+(\tilde{v})d\tilde{v} - \frac{1}{2}\sqrt{\bar{L}}G'_-(\tilde{w})d\tilde{w} \tag{I.71}$$

Note that this could alternatively be obtained from the area form in (I.67) by a diffeomorphism. The resulting expression for the entropy current, following the steps above, is

$$\tilde{J}_s^{\tilde{v}} = \frac{1}{8G_3}\sqrt{\bar{L}}G'_-(\tilde{w}),\ \tilde{J}_S^{\tilde{w}} = \frac{1}{8G_3}\sqrt{L}G'_+(\tilde{v}) \tag{I.72}$$

Let us define, as before, the spacetime coordinates as $\tilde{x}, \tilde{t}$ with $(\tilde{v}, \tilde{w}) = \tilde{t} \pm \tilde{x}$. The entropy density is then given by

$$\tilde{s} = \tilde{J}_S^{\tilde{t}} = \frac{1}{4G_3}\left(\frac{1}{2}\sqrt{L}G'_+(\tilde{v}) + \frac{1}{2}\sqrt{\bar{L}}G'_-(\tilde{w})\right) \tag{I.73}$$

Note that the entropy current is divergenceless

$$\partial_\mu \tilde{J}_S^\mu = \partial_{\tilde{v}}\tilde{J}_S^{\tilde{v}} + \partial_{\tilde{w}}\tilde{J}_S^{\tilde{w}} = 0 \tag{I.74}$$

This has two implications:

1. No dissipation: We have entropy transfers between different regions with no net entropy loss or production (see Figure I.6).

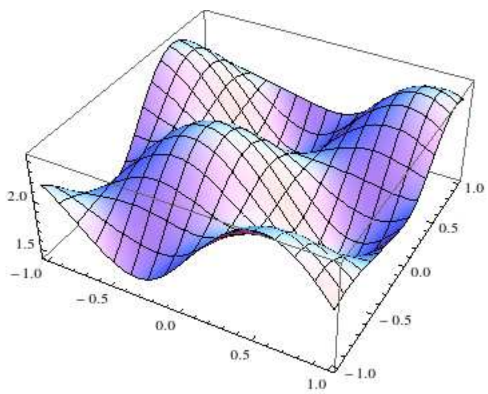

Figure I.6: The undulating horizon of Figure I.2 leads to the non-trivial entropy current (I.73). In this figure, we plot the entropy density $\tilde{s}$ as a function of $\tilde{v}, \tilde{w}$ for the right CFT. Note that although the entropy density fluctuates, the entropy flow here is such that there is no net entropy production (or destruction) (see Eq. (I.74)).

2. Total entropy is not changed by the conformal transformation: The other implication is that the integrated entropy over a space-like (or null) slice Σ

$$\tilde{S} = \int_{\Sigma} \epsilon_{\mu\nu} J_S^{\mu} d\sigma^{\nu} \tag{I.75}$$

is independent of the choice of the slice. In particular, choosing the slice to be $\Sigma_0 : t = v + w = 0$, we get

$$\tilde{S} = \frac{1}{8G_3} \int_{\Sigma_0} \left(\sqrt{L} G'_+(\tilde{v}) d\tilde{v} - \sqrt{\bar{L}} G'_-(\tilde{w}) d\tilde{w}\right) = \frac{1}{8G_3} \int_{\Sigma_0} \left(\sqrt{L} dv - \sqrt{\bar{L}} dw\right) \tag{I.76}$$

$$= \frac{1}{8G_3} \int dx \left(\sqrt{L} + \sqrt{\bar{L}}\right) = \int dx\; s = S \tag{I.77}$$

Hence although the entropy density is clearly transformed, the total entropy is not changed by the conformal transformation.

CFT calculation:

In a non-equilibrium situation, there is no natural notion of an entropy. However under the adiabatic approximation, the instantaneous eigenstates of a time-dependent Hamiltonian are a fair representation of the actual time-dependent wave functions. The consequent energy level density can thus be used to define an approximate time-dependent entropy. Generalizing this principle to slow time *and* space variations, and applying this to the stress tensor, one expects a space-time dependent version of (I.69), namely

$$\tilde{s} = \sqrt{\frac{\pi c}{3} \tilde{T}_{\tilde{v}\tilde{v}}} + \sqrt{\frac{\pi c}{3} \tilde{T}_{\tilde{w}\tilde{w}}} \tag{I.78}$$

where the stress tensors are given by (I.42). Since we have made the adiabatic approximation, we expect the above formula to be valid only up to the leading order of space and time derivatives. Under this approximation, we have

$$8\pi G_3 T_{\tilde{v}\tilde{v}} = \frac{L}{4} G'_+(\tilde{v})^2, \quad 8\pi G_3 T_{\tilde{w}\tilde{w}} = \frac{\bar{L}}{4} G'_-(\tilde{w})^2 \tag{I.79}$$

which exactly agrees with the holographic entropy density in (I.73). [25]

Total entropy for $\mathcal{H}_R$ is unchanged by the conformal transformation:

Under the conformal transformation (I.35), the reduced density matrix ρ_R is changed by a unitary transformation:

$$\rho_R = \mathrm{Tr}_{\mathcal{H}_L} |\psi\rangle\langle\psi| = U_R\, \rho_{0,R}\, U_R^{\dagger}, \quad \rho_{0,R} = \mathrm{Tr}_{\mathcal{H}_L} |\psi_0\rangle\langle\psi_0| \tag{I.80}$$

The total entropy of the system after the transformation is given by the von Neumann entropy $\tilde{S} = -\mathrm{Tr}\rho_R \ln \rho_R$ which, therefore, is equal to the entropy before; it is unchanged by the unitary transformation.

[25] Note that we have not used the adiabatic approximation anywhere in this chapter. Thus, it is unsatisfactory to use this approximation here. It is, in fact, tempting to believe that the entropy density in (I.73), and not that in (I.78), actually gives the CFT entropy in general; however, this requires more investigation.

8 Conclusion and open questions

We have solved the boundary value problem for 3D gravity (with $\Lambda < 0$) with independent boundary data on two asymptotically AdS_3 exterior geometries. The boundary data, specified in the form of arbitrary holographic stress tensors, yields spacetimes with wormholes, *i.e.* with exterior regions connected across smooth horizons. The explicit metrics are constructed by the technique of solution generating diffeomorphisms (SGD) from the eternal BTZ black string. By using the fact that the SGD's reduce to conformal transformations at both boundaries, we claim that the dual CFT states are specific time-dependent entangled states which are conformal transformations of the standard thermofield double. We compute various correlators and a dynamical entanglement entropy, in the bulk and in the CFT, to provide evidence for the duality. We also arrive at an expression for a non-equilibrium entropy function from the area-form on the horizon of these geometries.

Our work has implications for a number of other issues. We briefly discuss two of them below; a detailed study of these is left to future work.

8.1 ER=EPR

As mentioned above, our work constructs an infinite family of AdS-CFT dual pairs in which quantum states entangling two CFTs are holographically dual to spacetimes containing a wormhole region which connects the two exteriors. Both the quantum states and the wormhole geometries are explicitly constructed (see eqns. (I.29) and (I.13,I.21)). Our examples generalize the construction in [5, 7, 14][26] (for other remarks on unitary transformations of the thermofield double and related geometries see [49, 51, 54, 55, 56]) and provide an infinite family of examples of the relation ER=EPR, proposed in [4]. Since this relation has been extensively discussed and debated in the literature ([49, 54, 55, 56]), we would like to make some specific points pertaining to some of these discussions.

RR correlators vs RL correlators

It has been argued in [56],[49] and [54] that for typical entangled states connecting two CFTs, $\mathcal{H}_\mathcal{R}$ and $\mathcal{H}_\mathcal{L}$, correlators involving operators on the left and the right are suppressed relative to those involving operators all on the right. In particular, according to [56], correlators of the form $\langle O_R O_L \rangle$ are of the order $e^{-S}\langle O_R O_R \rangle$, where S is the entropy of the right sided Hilbert space.

In Section 5 we have computed general two-point functions, both of the kind $\langle O_R(P) O_R(Q)\rangle$ and $\langle O_R(P) O_L(Q')\rangle$.[27] In case of the eternal BTZ (dual to the standard thermofield double), an inspection of (I.46) and (I.48) suggests that as the boundary point $\mathbf{P}$ goes off to infinity, the cosh and sinh factors tend to be equal, thus $L(\mathbf{P}, \mathbf{Q}) \approx L(\mathbf{P}, \mathbf{Q}')$, thus there is no extra suppression in the two-sided correlator $\langle O_R\, O_L \rangle$. Of course, such a statement, regarding the standard thermofield double, has been regarded as somewhat of a special nature.

We are therefore naturally led to ask: what happens in case of the new solutions found here? The geodesic lengths $L(\mathbf{P}, \mathbf{Q})$ and $L(\mathbf{P}, \mathbf{Q}')$ are now given by (I.50) and (I.51). Once

[26] See [4, 49, 54]

[27] We use unprimed labels for operators on the right and primed labels for those on the left.

again, if the point P goes off towards the boundary of the Poincare plane, $\tilde{v} \to \infty$. Hence $G_+(\tilde{v}) \to \infty$ (since G_+ is a monotonically increasing function). Hence, both the geodesic lengths approach each other. Thus, we do not see any peculiar additional suppression, even for our general entangled state, arising when the second point of the correlation function is moved from the right to the left CFT.

On the genericity of our family of examples

We start with the following Lemma.
Lemma: Any state $\in \mathcal{H} \otimes \mathcal{H}$,

$$|\Psi\rangle = \sum_{i,j} C_{ij} |i\rangle |j\rangle, \;\; C_{ij} \in \mathbb{C}, \tag{I.81}$$

can be expressed in the form

$$|\Psi\rangle = \sum_{i,j,n} e^{-\lambda_n} U_{L,in} U_{R,jn} |n\rangle |n\rangle \tag{I.82}$$

where U_R, U_L are two unitary operators and $\lambda_n \geq 0$.

Proof: Using the canonical map $\mathcal{H} \otimes \mathcal{H} \to \mathcal{H} \otimes \mathcal{H}^*$, we can regard the above state $|\Psi\rangle$ as an operator $\mathbf{\Psi}$ in $\mathcal{H}$, with matrix elements C_{ij}. Using the singular value decomposition theorem on a general complex matrix, we can write $C = U_L D U_R^\dagger$ where D is a diagonal matrix with real, non-negative entries. By denoting D as diag$[e^{-\lambda_n}]$, we get (I.82).

The state (I.82) can be regarded as a thermofield double with Hamiltonian $H = \sum_n \lambda_n/\beta |n\rangle\langle n|$ transformed by unitary operators U_L on the left and by U_R on the right. Thus, the above Lemma suggests that the most general entangled state (I.81) can be written as a unitary transformation of *some* thermofield double state.

Now, note that the state (I.82) is of the same general form as that of (I.29) discussed above. However, while the unitary operators appearing in (I.82) are arbitrary, the $U_{L,R}$'s we use in (I.29) are made of Virasoro generators, [28] hence although the states (I.29) constitute a large class of states, they represent a subset of the most general entangled states (I.81).

Weakly entangled states

To assess the genericity of our states, we ask a different question now: do our set of states (I.29), which are *all* explicitly dual to wormholes, include those with a very small entanglement entropy S for a given energy E?[29] The answer to this question turns out to be yes. As we have noted in the remarks around (I.77) and (I.80), the entropy S, which is actually the entanglement entropy of the right Hilbert space, is the same for all our states. However, the same manipulations as in (I.77) shows that the energy of these states are *not*

[28] If a CFT dual to pure gravity were to exist, then our states (I.29) in such a theory would indeed be the most general state of the form (I.81). However, such a unitary theory is unlikely to exist [67, 68], although chiral gravity theories which are dual to CFTs with only the Virasoro operator have been suggested (see, e.g. [69]). We would like to thank Justin David for illuminating discussions on this point.

[29] This question was suggested to us by Sandip Trivedi.

the same; indeed by choosing the derivatives $G'_\pm$ to be large, we can make the energy of the transformed state to be much larger than that of the standard thermofield double. Stated in another way, for states of a given energy, our set of states includes states with entanglement entropy much less than that of the thermofield double. This is consistent with the proposal of [4] that even a small entanglement is described by a wormhole geometry.

8.2 Generalizations and open questions

It would be interesting to rephrase the results of this chapter in terms of the $SL(2,R) \times SL(2,R)$ Chern-Simons formulation [70] of three-dimensional gravity. By the arguments in [70], all diffeomorphisms (together with appropriate local Lorentz rotations) can be understood as gauge transformations of the Chern-Simons theory. The Chern-Simons formulation has been extended to the gauge group $SL(N,R) \times SL(N,R)$ to describe higher spin theories [9, 71]. It would be interesting to see whether our nontrivial gauge transformations generalize to these higher gauge groups, and hence to higher spin theories. A possible application of our methods in this case would be to compute HEE by the prescriptions in [72] and [73] in the nontrivial higher spin geometries[30]. We hope to come back to this issue shortly.

The solutions presented in this chapter are generated by SGDs which can be regarded as forming a group $(\widetilde{\text{Vir}} \times \widetilde{\text{Vir}})_L \times (\widetilde{\text{Vir}} \times \widetilde{\text{Vir}})_R$. Here the first $\widetilde{\text{Vir}}$ denotes a group of SGDs which is parametrized by the function G_+, and so on. As we emphasized in (I.80), the reduced density matrix on the right ρ_R undergoes a unitary transformation under this group of transformations, leaving the entropy unaltered. The family of pure states (I.29), therefore, be considered as an infinite family of purifications of the class of density matrices ρ_R; it would be interesting to see if these can be regarded as 'micro-states' which can 'explain' the entropy of ρ_R. We hope to return to this issue shortly.

It would also be interesting to use our work to explicitly study various types of holographic quantum quenches involving quantum states entangling two CFTs.[31] It would be of particular interest to study limiting cases of our solutions which correspond to shock-wave geometries.

[30] We thank Rajesh Gopakumar for a discussion on this issue.

[31] For a single CFT, a similar computation was done in, e.g., [62, 74].

I.A Coordinate systems for the eternal BTZ geometry

As we explained in the Introduction, the metric (I.1) describes only the region exterior to the black hole horizon (I.3). As is well-known, for constant $(L, \bar{L})$, (I.1) describes a standard BTZ black hole with mass M and angular momentum J given by

$$L = 8G_3(M + J),\ \bar{L} = 8G_3(M - J) \tag{I.83}$$

In this section we will describe various coordinate systems for this case. In particular, we will describe the five coordinate charts of Figure I.1 which cover our spacetime.

I.A.1 Eddington-Finkelstein coordinates

EF1 (Right Exterior + Black Hole Interior) For a black hole with constant mass and angular momentum, it is straightforward to find a coordinate transformation from the (z, x_+, x_-) coordinates to a set of Eddington Finkelstein coordinates which we denote by EF1 (λ, v, y)

$$x_+ = v - \frac{1}{2\sqrt{L}} \log\left(\frac{\lambda - \lambda_0}{\lambda + \lambda_0}\right),\ \ x_- = y + \sqrt{\frac{L}{\bar{L}}}v - \frac{1}{2\sqrt{\bar{L}}} \log\left(\frac{\lambda^2 - \lambda_0^2}{4\bar{L}}\right) \tag{I.84}$$

$$z = \sqrt{\frac{2}{\lambda_0^2}\left(\lambda - \sqrt{\lambda^2 - \lambda_0^2}\right)} \tag{I.85}$$

Under these transformations, we obtain the following metric

$$ds^2 = -\frac{2}{\bar{L}}\lambda_0(\lambda - \lambda_0)dv^2 + \frac{1}{\sqrt{\bar{L}}}dvd\lambda + \frac{\bar{L}}{4}dy^2 - (\lambda - \lambda_0)dvdy \tag{I.86}$$

The horizon (I.3) of the metric (I.1) is now located at $\lambda_0 = \sqrt{L\bar{L}}/2$. The metric is obviously smooth and describes the black hole interior.[32] To achieve a symmetry between the boundary coordinates, we find it convenient to make one further coordinate transformation from y to w

$$y = w - \sqrt{\frac{L}{\bar{L}}}v + \frac{1}{\sqrt{\bar{L}}} \log\left(\frac{\lambda + \lambda_0}{2\sqrt{\bar{L}}}\right) \tag{I.87}$$

In these new coordinates (λ, v, w), the metric becomes

$$ds^2 = \frac{d\lambda^2}{4(\lambda + \lambda_0)^2} + \frac{L}{4}dv^2 + \frac{\bar{L}}{4}dw^2 - \lambda dvdw + \frac{\sqrt{L}}{2(\lambda + \lambda_0)}dvd\lambda + \frac{\sqrt{\bar{L}}}{2(\lambda + \lambda_0)}dwd\lambda, \tag{I.88}$$

which is clearly symmetric between the 'boundary coordinates' v and w.

[32] It develops a coordinate singularity at the inner horizon $\lambda = -\lambda_0$; we do not discuss interpolation beyond the inner horizon here, although it can be easily done. In any case, there are strong reasons to believe that generically, the inner horizon and the associated exotic feature of infinitely repeating universes are unstable against even infinitesimal perturbations.

EF2 (Left Exterior + Black Hole Interior)

We can invent a second set of coordinate transformations starting from the metric in the (z, x_+, x_-) coordinates which would describe the left exterior region of the black hole along with the interior. This transformation is the following

$$x_+ = u + \frac{1}{2\sqrt{L}} \log\left(\frac{\lambda_1 - \lambda_0}{\lambda_1 + \lambda_0}\right), \quad x_- = y_1 + \sqrt{\frac{L}{\bar{L}}}u + \frac{1}{2\sqrt{\bar{L}}} \log\left(\frac{\lambda_1^2 - \lambda_0^2}{4\bar{L}}\right) \tag{I.89}$$

$$z = \sqrt{\frac{2}{\lambda_0^2}\left(\lambda_1 - \sqrt{\lambda_1^2 - \lambda_0^2}\right)} \tag{I.90}$$

The Eddington-Finkelstein metric obtained via this transformation is

$$ds^2 = -\frac{2}{\bar{L}}\lambda_0(\lambda_1 - \lambda_0)du^2 - \frac{1}{\sqrt{\bar{L}}}dud\lambda_1 + \frac{\bar{L}}{4}dy_1^2 - (\lambda_1 - \lambda_0)dudy_1 \tag{I.91}$$

As before, we make a further coordinate transformation y_1 to ω

$$y_1 = \omega - \sqrt{\frac{L}{\bar{L}}}u - \frac{1}{\sqrt{\bar{L}}} \log\left(\frac{\lambda_1 + \lambda_0}{2\sqrt{\bar{L}}}\right) \tag{I.92}$$

to obtain the following metric in the (λ_1, u, ω) coordinates

$$ds^2 = \frac{d\lambda_1^2}{4(\lambda_1 + \lambda_0)^2} + \frac{L}{4}du^2 + \frac{\bar{L}}{4}d\omega^2 - \lambda_1 dud\omega - \frac{\sqrt{\bar{L}}}{2(\lambda_1 + \lambda_0)}d\omega d\lambda_1 - \frac{\sqrt{L}}{2(\lambda_1 + \lambda_0)}dud\lambda_1 \tag{I.93}$$

EF3 (Left Exterior + White Hole Interior)

Starting from (z, x_+, x_-) coordinates, we do the following transformations

$$x_+ = v_1 - \frac{1}{2\sqrt{L}} \log\left(\frac{\lambda_1 - \lambda_0}{\lambda_1 + \lambda_0}\right), \quad x_- = w_1 - \frac{1}{2\sqrt{\bar{L}}} \log\left(\frac{\lambda_1 - \lambda_0}{\lambda_1 + \lambda_0}\right) \tag{I.94}$$

$$z = \sqrt{\frac{2}{\lambda_0^2}\left(\lambda_1 - \sqrt{\lambda_1^2 - \lambda_0^2}\right)} \tag{I.95}$$

The metric obtained is

$$ds^2 = \frac{d\lambda_1^2}{4(\lambda_1 + \lambda_0)^2} + \frac{L}{4}dv_1^2 + \frac{\bar{L}}{4}dw_1^2 - \lambda_1 dv_1 dw_1 + \frac{\sqrt{L}}{2(\lambda_1 + \lambda_0)}dv_1 d\lambda_1 + \frac{\sqrt{\bar{L}}}{2(\lambda_1 + \lambda_0)}dw_1 d\lambda_1 \tag{I.96}$$

This metric covers the left exterior and the white hole interior.

EF4(Right Exterior + White Hole Interior)

Starting from (z, x_+, x_-) coordinates, we do the following transformations

$$x_+ = u_1 + \frac{1}{2\sqrt{L}}\log\left(\frac{\lambda-\lambda_0}{\lambda+\lambda_0}\right), \quad x_- = \omega_1 + \frac{1}{2\sqrt{\bar{L}}}\log\left(\frac{\lambda-\lambda_0}{\lambda+\lambda_0}\right) \tag{I.97}$$

$$z = \sqrt{\frac{2}{\lambda_0^2}\left(\lambda - \sqrt{\lambda^2-\lambda_0^2}\right)} \tag{I.98}$$

The metric obtained is

$$ds^2 = \frac{d\lambda^2}{4(\lambda+\lambda_0)^2} + \frac{L}{4}du_1^2 + \frac{\bar{L}}{4}d\omega_1^2 - \lambda du_1 d\omega_1 - \frac{\sqrt{L}}{2(\lambda+\lambda_0)}du_1 d\lambda - \frac{\sqrt{\bar{L}}}{2(\lambda+\lambda_0)}d\omega_1 d\lambda \tag{I.99}$$

This metric covers the right exterior and the white hole interior.

Regions of Overlap

Right Exterior The 'Right Exterior' region is described by both the EF1 (λ, v, w) and EF4 (λ, u_1, ω_1) coordinates. These are related by the following smooth coordinate transformations

$$v = u_1 + \frac{1}{\sqrt{L}}\log\left(\frac{\lambda-\lambda_0}{\lambda+\lambda_0}\right) \qquad w = \omega_1 + \frac{1}{\sqrt{\bar{L}}}\log\left(\frac{\lambda-\lambda_0}{\lambda+\lambda_0}\right) \tag{I.100}$$

Black Hole Interior The 'Black Hole Interior' region is described by both the EF1 (λ, v, w) and EF2 (λ_1, u, ω) coordinates, which are related by the following smooth coordinate transformations

$$v = u + \frac{1}{\sqrt{L}}\log\left(\frac{\lambda_0-\lambda_1}{\lambda_0+\lambda_1}\right), \qquad w = \omega + \frac{1}{\sqrt{\bar{L}}}\log\left(\frac{\lambda_0-\lambda_1}{\lambda_0+\lambda_1}\right), \quad \lambda_1 = \lambda \tag{I.101}$$

Left Exterior The 'Left Exterior' region is described by both the EF2 (λ_1, u, ω) and EF3 $(\lambda_1, v_1, \omega_1)$ coordinates, which are related by the following smooth coordinate transformations:

$$v_1 = u + \frac{1}{\sqrt{L}}\log\left(\frac{\lambda_1-\lambda_0}{\lambda_1+\lambda_0}\right) \qquad w_1 = \omega + \frac{1}{\sqrt{\bar{L}}}\log\left(\frac{\lambda_1-\lambda_0}{\lambda_1+\lambda_0}\right) \tag{I.102}$$

White Hole Interior The 'White Hole Interior' finds a description in both the EF3 $(\lambda_1, v_1, \omega_1)$ and EF4 (λ, u_1, ω_1) coordinates, which are related by the following smooth coordinate transformations:

$$v_1 = u_1 + \frac{1}{\sqrt{L}}\log\left(\frac{\lambda_0-\lambda}{\lambda_0+\lambda}\right), \qquad w_1 = \omega_1 + \frac{1}{\sqrt{\bar{L}}}\log\left(\frac{\lambda_0-\lambda_1}{\lambda_0+\lambda_1}\right), \quad \lambda = \lambda_1 \tag{I.103}$$

I.A.2 Kruskal coordinates

The union of all the above coordinate patches, together with a neighbourhood (indicated by K5 in Fig I.1) of the bifurcation surface (the meeting point of the past and future horizons in the Penrose diagram) can be described by a set of Kruskal coordinates, in which the metric reads

$$ds^2 = -\frac{1}{2\lambda_0} dU dV + \frac{1}{\sqrt{\bar{L}}} U dV dy + \frac{\bar{L}}{4} dy^2 \qquad \text{(I.104)}$$

The coordinate transformation between various EF coordinates and the Kruskal coordinates are given below.

1. Right exterior + Black Hole Interior : EF1 to Kruskal

The transformation from EF1 to the (U, V, y) coordinates is

$$U = -\exp(-\sqrt{L}v)(\lambda - \lambda_0), \;\; V = \exp(\sqrt{L}v), \;\; y = w - \sqrt{\frac{L}{\bar{L}}} v + \frac{1}{\sqrt{\bar{L}}} \log\left(\frac{\lambda + \lambda_0}{2\sqrt{\bar{L}}}\right) \qquad \text{(I.105)}$$

In the 'Right Exterior' region, $\lambda > \lambda_0$, while in the 'Black Hole Interior', $\lambda < \lambda_0$. The above transformations give us the metric (I.104) in both the regions.

2. Left Exterior + Black Hole Interior : EF2 to Kruskal

The transformation from EF2 to (U, V, y) coordinates is

$$U = \exp(-\sqrt{L}u)(\lambda_1 + \lambda_0), \;\; V = -\exp(\sqrt{L}u)\frac{\lambda_1 - \lambda_0}{\lambda_1 + \lambda_0}, \;\; y = \omega - \sqrt{\frac{L}{\bar{L}}} u + \frac{1}{\sqrt{\bar{L}}} \log(\lambda_1 + \lambda_0) \qquad \text{(I.106)}$$

with,

$$y_1 = y - \frac{2}{\sqrt{\bar{L}}} \log\left(\frac{\lambda_1 + \lambda_0}{2\sqrt{\bar{L}}}\right) \qquad \text{(I.107)}$$

In the 'Black Hole Interior' $\lambda_1 < \lambda_0$, while in the 'Left Exterior' region $\lambda_1 > \lambda_0$. These coordinate transformations give us the metric (I.104) in both the regions.

3. Left Exterior + White Hole Interior : EF3 to Kruskal

The transformations from EF3 to the (U, V, y) coordinates is

$$U = \exp(-\sqrt{L}v_1)(\lambda_1 - \lambda_0), \;\; V = -\exp(\sqrt{L}v_1), \;\; y = w_1 - \sqrt{\frac{L}{\bar{L}}} v_1 + \frac{1}{\sqrt{\bar{L}}} \log\left(\frac{\lambda_1 + \lambda_0}{2\sqrt{\bar{L}}}\right) \qquad \text{(I.108)}$$

In the 'Left Exterior' region $\lambda_1 > \lambda_0$, while in the 'White Hole Interior', $\lambda_1 < \lambda_0$. These transformations give us the metric (I.104) in both the regions.

4. Right Exterior + White Hole Interior : EF4 to Kruskal

The transformation from EF4 to the (U, V, y) coordinates is

$$U = -\exp(-\sqrt{L}u_1)(\lambda + \lambda_0), \;\; V = \exp(\sqrt{L}u_1)\frac{\lambda - \lambda_0}{\lambda + \lambda_0}, \;\; y = \omega_1 - \sqrt{\frac{L}{\bar{L}}} u_1 + \frac{1}{\sqrt{\bar{L}}} \log(\lambda + \lambda_0) \qquad \text{(I.109)}$$

with,

$$y_1 = y - \frac{2}{\sqrt{\bar{L}}} \log\left(\frac{\lambda_1 + \lambda_0}{2\sqrt{\bar{L}}}\right) \tag{I.110}$$

In the 'White Hole Interior' $\lambda < \lambda_0$, while in the 'Right Exterior' region $\lambda > \lambda_0$. The above transformations give us the metric (I.104) in both the regions.

I.A.3 Poincare

In this section we show how the EF1, EF2 coordinates can, in fact, be obtained from Poincare coordinates $\zeta, X_\pm = X_0 \pm X_1$, in terms of which the metric is written as

$$ds^2 = \frac{1}{\zeta^2}(d\zeta^2 - dX_+ dX_-) \tag{I.111}$$

We will choose $L = \bar{L}$ for simplicity, so $\lambda_0 = L/2$.

The coordinate transformation from $X_\pm, \zeta$ to the EF1 coordinates is given by

$$v = \frac{\log(X_+)}{\sqrt{L}},\ w = -\frac{1}{\sqrt{L}} \log\left(\frac{-X_+X_- + \zeta^2}{X_+}\right),\ \frac{\lambda}{\lambda_0} = \frac{-2X_+X_- + \zeta^2}{\zeta^2} \tag{I.112}$$

whereas the coordinate transformation from $X_\pm, \zeta$ to the EF2 coordinates is given by

$$u = \frac{1}{\sqrt{L}} \log\left(\frac{-X_+X_- + \zeta^2}{X_-}\right),\ \omega = -\frac{\log(X_-)}{\sqrt{L}},\ \frac{\lambda_1}{\lambda_0} = \frac{-2X_+X_- + \zeta^2}{\zeta^2} \tag{I.113}$$

There are similar coordinate transformations between the other charts EF3/4 and Poincare.[33]

I.B The new metrics in the charts EF3 and EF4

$$\begin{aligned}\text{EF3:}\ ds^2 = \frac{1}{B^2}\Big[& d\tilde{\lambda}_1^2 + A_+^2 d\tilde{v}_1^2 + A_-^2 d\tilde{w}_1^2 + 2A_+ d\tilde{u}_1 d\tilde{\lambda}_1 + 2A_- d\tilde{w}_1 d\tilde{\lambda}_1 \\ & - \tilde{\lambda}_1\Big(B^2 + 2\Big(A_+\frac{H''_-(\tilde{w}_1)}{H'_-(\tilde{w}_1)} + A_-\frac{H''_+(\tilde{v}_1)}{H'_+(\tilde{v}_1)} + \tilde{\lambda}\frac{H''_+(\tilde{v}_1)H''_-(\tilde{w}_1)}{H'_+(\tilde{v}_1)H'_-(\tilde{w}_1)}\Big)\Big) d\tilde{w}_1 d\tilde{v}_1\Big]\end{aligned} \tag{I.114}$$

where

$$A_+ = \sqrt{L}H'_+(\tilde{v}_1)(\tilde{\lambda}_1 + \tilde{\lambda}_{10}) - \tilde{\lambda}_1\frac{H''_+(\tilde{v}_1)}{H'_+(\tilde{v}_1)},\ A_- = \sqrt{\bar{L}}H'_-(\tilde{w}_1)(\tilde{\lambda}_1 + \tilde{\lambda}_{10}) - \tilde{\lambda}_1\frac{H''_-(\tilde{w}_1)}{H'_-(\tilde{w}_1)},\ B = 2(\tilde{\lambda}_1 + \tilde{\lambda}_{10})$$

$$\begin{aligned}\text{EF4 :}\ \ ds^2 = \frac{1}{B^2}\Big[& d\tilde{\lambda}^2 + A_+^2 d\tilde{u}_1^2 + A_-^2 d\tilde{\omega}_1^2 - 2A_+ d\tilde{u}_1 d\tilde{\lambda} - 2A_- d\tilde{\omega}_1 d\tilde{\lambda} \\ & - \tilde{\lambda}\Big(B^2 - 2\Big(A_+\frac{G''_-(\tilde{\omega}_1)}{G'_-(\tilde{\omega}_1)} + A_-\frac{G''_+(\tilde{u}_1)}{G'_+(\tilde{u}_1)} - \tilde{\lambda}\frac{G''_+(\tilde{u}_1)G''_-(\tilde{\omega}_1)}{G'_+(\tilde{u}_1)G'_-(\tilde{\omega}_1)}\Big)\Big) d\tilde{\omega}_1 d\tilde{u}_1\Big]\end{aligned} \tag{I.115}$$

where

$$A_+ = \sqrt{L}G'_+(\tilde{u}_1)(\tilde{\lambda} + \tilde{\lambda}_0) + \tilde{\lambda}\frac{G''_+(\tilde{u}_1)}{G'_+(\tilde{u}_1)},\ A_- = \sqrt{\bar{L}}G'_-(\tilde{\omega}_1)(\tilde{\lambda} + \tilde{\lambda}_0) + \tilde{\lambda}\frac{G''_-(\tilde{\omega}_1)}{G'_-(\tilde{\omega}_1)},\ B = 2(\tilde{\lambda} + \tilde{\lambda}_0)$$

[33] As explained in [7] , it is possible to describe the BTZ black string in terms of a single Poincare chart. The BTZ black *hole* is a quotient of AdS_3, which in appropriate coordinates [75] corresponds to the periodic identification of the spatial direction; the BTZ string discussed in this chapter is obtained by decompactifying the spatial circle, which gives back AdS_3.

I.C UV/IR cutoffs in EF coordinates

From AdS/CFT it is well-known that in a Fefferman-Graham coordinate system such as in (I.1), an IR cutoff surface $z = \epsilon$ in the asymptotically AdS spacetime corresponds to a UV cutoff ϵ in the CFT. We wish to express the IR cutoff in the geometry in terms of the EF coordinates. By using the relation

$$z = \sqrt{\frac{2}{\lambda_0^2}\left(\lambda - \sqrt{\lambda^2 - \lambda_0^2}\right)} \tag{I.116}$$

we clearly see that $z = \epsilon$ for ϵ small, corresponds to $\lambda = 1/\epsilon^2$.

I.D An alternative to Banados' metric

In [62], Roberts showed that the Banados metric (I.1) can be obtained from the Poincare metric (I.111) by a Brown-Henneaux type diffeomorphism (an 'SGD' in the language we have used), given by

$$\begin{aligned}
X_\pm &= f_\pm(x_\pm) + \frac{2z^2 f'_\pm(x_\pm)^2 f''_\mp(x_\mp)}{8f'_\pm(x_\pm)f'_\mp(x_\mp) - z^2 f''_\pm(x_\pm)f''_\mp(x_\mp)} \\
\zeta &= z\,\frac{\left(4f'_+(x_+)f'_-(x_-)\right)^{\frac{3}{2}}}{8f'_+(x_+)f'_-(x_-) - z^2 f''_+(x_+)f''_-(x_-)}
\end{aligned} \tag{I.117}$$

It was shown in [62] that the above diffeomorphism reduces to a conformal transformation on the boundary, with the the following asymptotic form (as z→0)

$$\begin{aligned}
X_\pm &= f_\pm(x_\pm) + O(z^2) \\
\zeta &= z\sqrt{f'_+(x_+)f'_-(x_-)} + O(z^3)
\end{aligned} \tag{I.118}$$

It was also shown here that $L(x_+), \bar{L}(x_-)$ appearing in (I.1) can be obtained from the zero stress tensor through the conformal transformation $f_\pm$.

A different choice of gauge: The SGD (I.117) used by Roberts seems fairly involved compared to the ones we use here in this work, e.g. (I.12). Can we obtain the metric (I.1) by a simpler SGD similar to ours, which nevertheless has the same conformal asymptotic form (I.118)? The answer turns out to be yes. Indeed the simplest way of inventing such a transformation is to take the asymptotic form (I.118) and gauge fix all the higher order terms in z to 0. We then have a new, exact transformation of the form

$$X_\pm = f_\pm(x_\pm), \qquad \zeta = z\sqrt{f'_+(x_+)f'_-(x_-)} \tag{I.119}$$

Note the similarity with our SGDs, say (I.12) (recall that $z \sim 1/\sqrt{\lambda}$ near the boundary). (I.119) transforms the Poincare metric to

$$\begin{aligned}
ds^2 =& \frac{dz^2}{z^2} + \frac{f''_+(x_+)}{zf'_+(x_+)}dx_+dz + \frac{f''_-(x_-)}{zf'_-(x_-)}dx_-dz + \frac{1}{4}\left(\frac{f''_+(x_+)^2}{f'_+(x_+)^2}dx_+^2 + \frac{f''_-(x_-)^2}{f'_-(x_-)^2}dx_-^2\right) \\
&- \left(\frac{2}{z^2} - \frac{f''_+(x_+)f''_-(x_-)}{2f'_+(x_+)f'_-(x_-)}\right)dx_+dx_-
\end{aligned} \tag{I.120}$$

A priori this is a new metric different from (I.1). However, the holographic stress tensor [12] obtained from this metric is the same as obtained from (I.1) given by (I.42). As discussed in Section 2.5 and 2.5, the above metric and (I.1) differ only by a trivial diffeomorphism, and are hence essentially identical.[34] Note that this example shows the enormous gauge ambiguity in the choice of a metric in AdS_3 (whose physical content is manifested in the boundary behaviour). Indeed, by the same token even the SGD's are ambiguous; the solutions presented in Section 2 are one of a gauge equivalent class of metrics.

I.E Unitary realization of conformal transformation

Under a finite, non-trivial, holomorphic coordinate transformation, $w \to w' = f(w)$, the stress tensor of a 2D CFT transforms as

$$\tilde{T}(w') = \left(\frac{\partial w'}{\partial w}\right)^{-2} [T(w) - \frac{c}{12} S(w', w)] \tag{I.121}$$

with the Schwarzian derivative S(w', w) given by

$$S(w', w) = \left(\frac{\partial^3 w'}{\partial w^3}\right)\left(\frac{\partial w'}{\partial w}\right)^{-1} - \frac{3}{2}\left(\frac{\partial^2 w'}{\partial w^2}\right)^2 \left(\frac{\partial w'}{\partial w}\right)^{-2} \tag{I.122}$$

For an infinitesimal transformation $w \to w' = f(w) = w + \epsilon(w)$, the Schwarzian derivative turns out to be

$$S(w', w) = \epsilon'''(w) + \mathcal{O}(\epsilon^2) \tag{I.123}$$

The change in the stress tensor, under such a transformation, becomes

$$\delta T(w) \approx -\epsilon(w) T'(w) - 2\epsilon'(w) T(w) - \frac{c}{12}\epsilon'''(w) + \mathcal{O}(\epsilon^2) \tag{I.124}$$

Now, the Laurent expansion of $T(w)$ and $\epsilon(w)$ is

$$T(w) = \sum_{m=-\infty}^{\infty} \frac{L_m}{w^{m+2}} \qquad\qquad \epsilon(w) = \sum_{m=-\infty}^{\infty} \epsilon_m w^{-m+1} \tag{I.125}$$

where $L_n^\dagger = L_{-n}$, $\epsilon_n^\dagger = -\epsilon_{-n}$ and the L_n's satisfy the Virasoro algebra

$$[L_m, L_n] = (m-n) L_{m+n} + \frac{c}{12} m(m^2 - 1)\delta_{m+n,0} \tag{I.126}$$

Plugging (I.125) into (I.124), we get

$$\delta L_m = \sum_{n=-\infty}^{\infty} \left\{(m+n) L_{m-n}\epsilon_n + \frac{c}{12} n(n^2-1)\epsilon_n \delta_{m-n,0}\right\} \tag{I.127}$$

[34]Note that in this new metric (I.120), the position of the horizon is at $z = \infty$. Of course, it can be brought to a finite value by an additional coordinate transformation involving the radial coordinate.

We wish to construct a unitary operator $U = U(\epsilon)$ which implements the above conformal transformations, namely that it satisfies

$$U(\epsilon)^\dagger L_m U(\epsilon) - L_m = \delta L_m + O(\epsilon^2) \tag{I.128}$$

The required unitary operator, in fact, is

$$U(\epsilon) = \exp(\sum_{n=-\infty}^{\infty} \epsilon_n L_{-n}) \tag{I.129}$$

The proof is straightforward. Note that the LHS of (I.128) becomes

$$(1 - \sum_n \epsilon_{-n} L_n) L_m (1 + \sum_n \epsilon_n L_{-n}) - L_m = - \sum_{n=-\infty}^{\infty} \epsilon_{-n} (L_n L_m) + \sum_{n=-\infty}^{\infty} \epsilon_n (L_m L_{-n}) + \mathcal{O}(\epsilon^2)$$

After flipping the sign of n in the first sum, this becomes

$$\epsilon_n [L_m, L_{-n}]$$

which reduces to the expression (I.127) upon using the Virasoro algebra (I.126).

Thus, we have explicitly constructed a unitary operator U such that $U^\dagger T(w) U - T(w)$ is given by (I.124).

Chapter II

Thermalization with Chemical Potentials[1]

1 Introduction and Summary

The study of thermalization in closed interacting quantum systems has a long history (see, e.g. [17] for a review). It has been known ever since the celebrated work of Fermi, Pasta and Ulam (FPU) that interacting classical systems need not necessarily equilibrate. The question of finding sufficient conditions for thermalization in quantum systems is also an open one. Recently, the advent of holography has linked the issue of thermalization in strongly coupled quantum field theories to another important, classical, problem of black hole formation (see, e.g. [76, 77, 78, 79] and references therein). In the latter setting too, the issue of gravitational collapse of a given matter distribution is rather nontrivial; indeed there is an interesting debate in the current literature (see, e.g., [80, 81, 82, 83, 84, 85]) regarding the fate of perturbations in anti-de-Sitter spacetimes.

In this chapter, we will focus on two-dimensional conformal field theories (CFTs) on an infinite line $\sigma \in \mathbb{R}$. We will consider the system at $t = 0$ to be in a "quenched state"[2]

$$|\psi_0\rangle = \exp[-\epsilon_2 H - \sum_{n=3}^{\infty} \epsilon_n W_n]|Bd\rangle \tag{II.1}$$

Here $|Bd\rangle$ is a conformal boundary state; the exponential factors cut off the UV modes to make the state normalizable. W_n denote the additional conserved charges in the theory.[3]

[1]The contents of this chapter have partial overlap with the thesis work of Ritam Sinha. The conclusions arrived at are results of joint effort.

[2]In the original sense of the term, a quantum quench is defined as a sudden change from a hamiltonian H_0 to a hamiltonian H which governs further evolution for $t \geq 0$. The system is assumed to be in the ground state of H_0 at $t = 0$, which serves as an initial state for subsequent dynamics; the dynamics is nontrivial since the initial state prepared this way is not an eigenstate of H. In this work, as in [20], we will mean by a "quenched state" simply a pure state which is not an eigenstate of the Hamiltonian H. The kind of quenched state defined in (II.1) is sometimes said to describe a global quench or a homogeneous quench, as the state is translationally invariant. We will briefly mention inhomogeneous and local quenches in Section 6.

[3]For the purposes of this chapter, we will identify them with W_n-charges of 2D CFT, $n = 3, 4, ...$ (with

This choice of the quenched state is a generalization of that in [20] for which $\epsilon_n = 0$, for $n > 3$.

The wavefunction for $t > 0$ is given by

$$|\psi(t)\rangle = \exp[-iHt]|\psi_0\rangle \tag{II.2}$$

The questions we will explore, and answer, are: what is the long time behaviour of various observables in $|\psi(t)\rangle$? In particular, does the expectation value of an operator (or a string of operators) approach a constant? If so, (i) is the constant value characterized by a thermodynamic equilibrium, and (ii) what is the rate of approach to the constant value? More generally, we would also address, and partially answer, the questions: how does the existence and rate of thermalization depend on the initial state and the choice of observables?

Thermalization We find in this work that the expectation values of local observables (supported on a finite interval $A : \sigma \in [-l/2, l/2]$) asymptotically approach (see (II.12) for the precise statement) their values in an equilibrium ensemble,

$$\rho_{eqm} = \frac{1}{Z} \exp[-\beta H - \sum_n \mu_n W_n], \quad Z = \mathrm{Tr} \exp[-\beta H - \sum_n \mu_n W_n] \tag{II.3}$$

whose temperature and chemical potentials are related to the cutoff scales in (II.5) as follows

$$\beta = 4\epsilon_2, \quad \mu_n = 4\epsilon_n, \quad n = 3, 4, ... \tag{II.4}$$

The relations (II.4) are uniquely dictated by the requirement that the expectation values of the conserved charges $H, W_3, W_4, ...$ in the initial state match those in the mixed state (II.3) (see (II.52)). In the absence of the extra parameters $\epsilon_n, n = 3, 4, ...$ this result is derived by the elegant method of conformal transformations [20]. In the presence of these parameters, this method is not available; in this work, we deal with the extra exponential factors in terms of an infinite series and do a resummation.

We emphasize that the thermalization we found above persists even when we have an integrable model with an infinite number of conserved charges. Relaxation in integrable systems has been found in recent years in the context of, e.g., (a) one-dimensional hardcore bosons [21], (b) transverse field Ising model [22], and (c) matrix quantum mechanics models [23]. The equilibrium ensembles in this context have been called a generalized Gibbs ensemble (GGE). Our present result on integrable conformal field theories adds to the list of these examples. Interestingly, the thermalization we find works even for free conformal field theories, e.g. a free scalar field theory.[4]

With the above identification of parameters, we will rewrite the initial quenched state (II.1) henceforth as

$$|\psi_0\rangle = \exp[-(\beta H - \sum_{n=3}^{\infty} \mu_n W_n)/4]|Bd\rangle \tag{II.5}$$

$W_2 \equiv H$), although much of what we say will go through independent of this specific choice as long as these charges mutually commute and are defined from currents which are quasiprimary fields of the conformal algebra.

[4]This happens essentially due to the fact that we consider here thermalization of local observables and that local field modes are mutually coupled even in a free field theory. Thermalization happens at times greater than the scale of localization, as we will see below.

We find the following specific results:

1. Thermalization time scale for single local observables: We find that at large times

$$\langle\psi(t)|\phi_k(\sigma)|\psi(t)\rangle = \mathrm{Tr}\left(\phi_k(0)\rho_{eqm}(\beta,\mu_i)\right) + a_k\, e^{-\gamma_k t} + ... \tag{II.6}$$

where $\phi_k(\sigma)$ is an arbitrary quasiprimary field (labelled by an index k). Below we compute the thermalization exponent γ_k in a perturbation in the chemical potentials and to linear order it is given by

$$\gamma_k = \frac{2\pi}{\beta}\left[\Delta_k + \sum_n \tilde{\mu}_n Q_{n,k} + O(\tilde{\mu}^2)\right],\ \tilde{\mu}_n \equiv \frac{\mu_n}{\beta^{n-1}}, \tag{II.7}$$

Here $\Delta_k = h_k + \bar{h}_k$ is the scaling dimension and $Q_{n,k}$ are the (shifted) W_n-charges (see (II.37) for the full definition) of the field ϕ_k (in case of primary fields) or of the minimum-dimension field which appears in the conformal transformation of ϕ_k. To obtain this result, we perform the infinite resummation mentioned below (II.4). At large times, the perturbation series for the one-point function in the chemical potentials exponentiates (see (II.37)), to give the corrected exponent in the above equation. *In various related contexts, finite orders of perturbation terms in chemical potentials have been computed before [36, 37, 86]. Our finding in this work is that at large times, there is a regularity among the various orders leading to an exponential function as in (II.6) (see Section 2.2 for details).*
Universality: In the case of zero chemical potentials, it has been noted in [87], that although the relaxation time $\tau_k = \pi\epsilon_2/(2\Delta_k) = 2\pi\beta/(\Delta_k)$ is non-universal (in the sense that it depends on the specific initial state (II.1)), the ratio of relaxation times for two different fields, namely, $\tau_{k_1}/\tau_{k_2} = \Delta_{k_2}/\Delta_{k_1}$ is universal (it depends only on the CFT data and not on the initial state and is hence expected to be valid for a general class of initial states). In the presence of the additional cut-off parameters $\epsilon_i, i = 3, ...$ in the initial state (II.1), the ratio $\tau_{k_1}/\tau_{k_2} = \gamma_{k_2}/\gamma_{k_1}$= $(\Delta_{k_2} + \sum_n \tilde{\mu}_n Q_{n,k_2})/(\Delta_{k_1} + \sum_n \tilde{\mu}_n Q_{n,k_1})$ is, however, not independent of the initial state.

However, as we will briefly discuss in Section 6, for a large class of quench states (e.g. where the energy density is uniform outside of a domain of compact support) the β-dependence of τ_k, in the absence of chemical potentials, can be understood as the dependence on the uniform energy density (see a related discussion in [57]). The time scales τ_k, therefore, do have a limited form of universality in the sense that it depends on a rather robust feature of the initial state. Our calculations in this chapter leads us to believe that this feature will continue in the presence of chemical potentials, in the sense that the additional dependence of the time scales $1/\gamma_k$ on the μ_n is fixed by the charge densities corresponding to the additional conserved charges. We hope to address this in [88].

2. Multiple local observables, reduced density matrix: Besides the one-point functions discussed above, it turns our that we can demonstrate thermalization of *all operators in an interval A of length l*. It is convenient to define a 'thermalization function' $I_A(t)$ [28]

as

$$I_A(t) = \mathrm{Tr}(\hat\rho_{dyn,A}(t)\hat\rho_{eqm,A}(\beta,\mu_n)) = \frac{\mathrm{Tr}(\rho_{dyn,A}(t)\rho_{eqm,A}(\beta,\mu_n))}{[\mathrm{Tr}(\rho_{dyn,A}(t)^2)\mathrm{Tr}(\rho_{eqm,A}(\beta,\mu_i)^2)]^{1/2}}$$
$$\rho_{dyn,A}(t) = \mathrm{Tr}_{\bar A}\ |\psi(t)\rangle\langle\psi(t)|,\ \rho_{eqm,A}(\beta,\mu_n) = \mathrm{Tr}_{\bar A}\ \rho_{eqm}(\beta,\mu_i) \tag{II.8}$$

Here $\hat\rho = \rho/\sqrt{\mathrm{Tr}\rho^2}$ denotes a 'square-normalized' density matrix.[56] We show below that at large times the thermalization function has the form

$$I_A(t) = 1 - \alpha(\tilde l)\ e^{-2\gamma_m t} + ...,\ \tilde l \equiv l/\beta \tag{II.9}$$

where γ_m refers to the exponent (III.9) for the operator ϕ_m with minimum scaling dimension.[7] $\alpha(\tilde l)$ is computed as a power series in $\tilde l$ which we find using the short interval expansion, valid for $\tilde l \ll 1$, i.e. $l \ll \beta$.

Two immediate consequences of (II.9) are

(i) Thermalization of an arbitrary string of operators: Note, from (II.9), that

$$I_A(t) \xrightarrow{t\to\infty} 1, \tag{II.10}$$

Since the square-normalized density matrices can be regarded as unit vectors (in the sense of footnote 5), and $I_A(t)$ can be regarded as the scalar product $\hat\rho_{dyn,A}(t)\cdot\hat\rho_{eqm,A}$, (II.10) clearly implies

$$\hat\rho_{dyn,A}(t) \xrightarrow{t\to\infty} \hat\rho_{eqm,A} \tag{II.11}$$

This implies the following statement of thermalization for an arbitrary string of local operators (with $\sigma_1, \sigma_2, ... \in A$)

$$\langle\psi(t)|O(\sigma_1,t_1)O(\sigma_2,t_2)...|\psi(t)\rangle = \mathrm{Tr}(\hat\rho_{dyn,A}(t)O(\sigma_1,t_1)O(\sigma_2,t_2)...) \xrightarrow{t\to\infty} \mathrm{Tr}(\hat\rho_{eqm,A}O(\sigma_1,t_1)O(\sigma_2,t_2)...). \tag{II.12}$$

(ii) Long time behaviour of reduced density matrix:

Carrying on with the interpretation of $I_A(t)$ as a scalar product, we can infer following asymptotic behaviour of $\hat\rho_{dyn}(t)$ from (II.9):

$$\hat\rho_{dyn,A}(t) = \hat\rho_{eqm,A}(\beta,\mu_i)\left(1-\alpha\, e^{-2\gamma_m t}+...\right) + \hat Q\left(\sqrt{2\alpha}\, e^{-\gamma_m t}+...\right) \tag{II.13}$$

[5]Note that operators in a Hilbert space H can themselves be regarded as vectors in $\mathsf{H}\times\mathsf{H}^*$; under this interpretation $\mathrm{Tr}(A\ B)$ defines a positive definite scalar product. With this understanding, we will regard the hatted density matrices as unit vectors.

[6]Throughout this chapter, we will consider field theories with an infinite spatial extent. The entire Hilbert space is assumed to be of the form $\mathsf{H}_A \otimes \mathsf{H}_{\bar A}$. $\mathrm{Tr}_{\bar A}$ implies tracing over $\mathsf{H}_{\bar A}$.

[7]We will assume here that the spectrum of such Δ's is bounded below by a finite positive number. In case of a free scalar field theory, we can achieve this by considering a compactified target space.

where $\mathrm{Tr}(\hat{Q}^2) = 1, \quad \mathrm{Tr}(\hat{\rho}_{eqm,A}(\beta, \mu_i)\hat{Q}) = 0$. We will specify further properties of $\hat{Q}$ later on.

Importance of local observables: In case of a free massless scalar field, it is easy to show that quantities like $\langle\psi(t)|\alpha_1^2\alpha_1^\dagger|\psi(t)\rangle$ perpetually oscillate and never reach a constant (see a related calculation in [23]). The modes α_n represent Fourier modes and are non-local. Indeed, as [28, 44, 87] showed, in the absence of chemical potentials, the exponential term in (II.9) is $e^{-2\gamma_m(t-l/2)}$ and the thermalization sets in only after t exceeds $l/2$. Thus, for $l = \infty$, there is no thermalization, which is consistent with the above observation about perpetual oscillations. We expect the form $e^{-2\gamma_m(t-l/2)}$ to continue to hold in the presence of chemical potentials[8], since the effect of the chemical potentials on the exponent γ_k can be viewed as a shift of the anomalous dimension $\delta\Delta_k = \sum_n \tilde{\mu}_n Q_{n,k} + O(\tilde{\mu}^2)$ (see, e.g. (II.64)). This shows that, as in the case of zero chemical potentials, equilibration sets in only after t exceeds $l/2$. We will see a similar phenomena next in the context of a decay of perturbations to a thermal state.

3. Decay of perturbations to a thermal state: We compute (see Section 4 for details) the time-dependent two-point Green's function $G_+(t, l; \beta, \mu)$ for two points spatially separated by a distance l. We find that for $t, l, t - l \gg \beta$, the time-dependence is exponential, with the same exponent as in (II.6):

$$G_+(t, l; \beta, \mu) \equiv \frac{1}{Z}\mathrm{Tr}\left(\phi_k(l, t)\phi_k(0, 0)e^{-\beta H - \sum_n \mu_n W_n}\right) = \text{const } e^{-\gamma_k t} \qquad \text{(II.14)}$$

Note that the above thermalization sets in for $t > l$. For $t < l$, the two-point function has an exponential decay in the spatial separation (see Section 4 and Figure II.3).

The computation of the above relaxation times in the presence of an arbitrary number of chemical potentials uses the technique, described above, of summing over an infinite number of Feynman diagrams, and is one of the main results of our work.

4. Collapse to higher spin black holes: In [5, 7] the bulk dual to the time-dependent state (II.2) corresponding to initial condition (II.5), for large central charges, has been constructed in the case of zero chemical potentials. The dual geometry corresponds to one half of the eternal BTZ (black string) geometry, whose boundary represents an end-of-the-world brane. In [14] the result has been extended to the case of non-zero angular momentum and a Chern-Simons charge. In case of an infinite number of chemical potentials, a bulk dual to the equilibrium ensemble (II.3) has been identified, in the context of the Gaberdiel-Gopakumar hs(λ) theory [32], as a higher spin black hole with those chemical potentials [33, 34]. It is natural to conjecture [14, 23] that the time-development (II.2) should be dual to a collapse to this higher spin black hole. At late times, therefore, the thermalization exponent found above should correspond to the quasinormal frequency of the higher spin black hole. We find that (see Section 5 and [89]) this is indeed borne out in a specific example.

[8]Although, in the short-interval expansion employed in this chapter to derive (II.9), which uses $t\ gg\beta \gg l$, such an l-dependence in the exponent cannot be easily seen from the pre-factor $\alpha(\tilde{l})$ unless one sums over an infinite orders in $\tilde{l}$.

The plan of the chapter is as follows. The results 1, 2, 3 and 4 above are described in Sections 2, 3, 4 and 5, respectively. The resummation of an infinite number of Feynman diagrams (corresponding to insertions of arbitrary number of chemical potential terms) is discussed in Section 2.2, which uses results in Appendix II.A. The calculation of the overlap of reduced density matrices in Section 3 needs the use of the short-interval expansion, which is described in Appendix II.B. In Section 6 we present our conclusions and make some remarks on inhomogeneous quench [88].

2 One-point functions

In this section we will consider the behaviour of the following one-point functions of a quasiprimary field $\phi_k(\sigma)$

$$\begin{aligned}\langle\phi_k(\sigma,t)\rangle_{dyn} &\equiv \langle\psi(t)|\phi_k(\sigma)|\psi(t)\rangle,\\ \langle\phi_k(\sigma)\rangle_{eqm} &\equiv \mathrm{Tr}\left(\phi_k(\sigma)\rho_{eqm}(\beta,\mu_n)\right)\end{aligned} \tag{II.15}$$

We will briefly recall how these are computed in the absence of the chemical potentials [20, 24]. The first expectation value corresponds to the one-point function on a strip geometry, with complex coordinate $w=\sigma+i\tau$, $\sigma\in(-\infty,\infty)$, $\tau\in(-\beta/4,\beta/4)$ where τ is eventually to be analytically continued to $\tau=it$. This can be conformally transformed to an upper half plane by using the map

$$z = ie^{(2\pi/\beta)w} \tag{II.16}$$

For a primary field with $h_k=\bar h_k$ (of the form $\phi_k(w,\bar w)=\varphi_k(w)\varphi_k(\bar w)$), this procedure gives [9](for other primary fields, the one-point function vanishes)

$$\begin{aligned}\langle\phi_k(\sigma,t)\rangle_{dyn} &= \langle\phi_k(w,\bar w)\rangle_{str} = \left(\frac{\partial z}{\partial w}\right)^{h_k}\left(\frac{\partial \bar z}{\partial \bar w}\right)^{\bar h_k}\langle\phi_k(z,\bar z)\rangle_{UHP}\\ &= a_k\left(e^{2\pi t/\beta}+e^{-2\pi t/\beta}\right)^{-2h_k}\sim a_k e^{-\gamma_k^{(0)}t}+\ldots,\ \ \gamma_k^{(0)}=2\pi\Delta_k/\beta=4\pi h_k/\beta\end{aligned} \tag{II.17}$$

We have used the following result for the one-point function on the UHP:

$$\langle\phi_k(z,\bar z)\rangle_{UHP}=A_k\langle\varphi_k(z)\varphi_k^*(z')\rangle_{UHP}=A_k(z-z')^{-2h_k},\ \ h_k=\bar h_k,\ z'=\bar z \tag{II.18}$$

which follows by using the method of images where the antiholomorphic factor of $\phi_k(z,\bar z)$ on the upper half plane at the point $(z,\bar z)$ is mapped (up to a constant) to the holomorphic φ_k^* [10] on the lower half plane at the image point $(z',\bar z')$ with $z'=\bar z, \bar z'=z$ [25, 24]. In the above a_k, A_k are known numerical constants. Note that

$$z=ie^{2\pi(\sigma+i\tau)/\beta}=ie^{2\pi(\sigma-t)/\beta},\ \ z'=\bar z=-ie^{2\pi(\sigma-i\tau)/\beta}=-ie^{2\pi(\sigma+t)/\beta} \tag{II.19}$$

so that in the large time limit we have

$$t\to\infty\Rightarrow z\to 0, \bar z\to -i\infty. \tag{II.20}$$

[9]The subscripts *str, cyl* will denote a 'strip' and a 'cylinder', respectively.
[10]We distinguish φ_k^* from φ_k to allow for charge conjugation.

The second, thermal, expectation value in (II.15), for $\mu_n = 0$, corresponds to a cylindrical geometry in the w-plane, with $\tau = 0$ identified with $\tau = \beta$. By using the same conformal map (II.16) this can be transformed to a one-point function on the plane. For a primary field the latter vanishes. Hence (II.6) is trivially satisfied.

For a quasiprimary field ϕ_k, its conformal transformation generates additional terms, including possibly a c-number term c_k (e.g. the Schwarzian derivative term for $\phi_k = T_{ww}$) and generically lower order operators. The c-number term does not distinguish between a plane and an UHP. This leads to the following overall result (for $\mu_n = 0$):

$$\begin{aligned} &\langle \phi_k(\sigma) \rangle_{eqm} = \langle \phi_k(w, \bar{w}) \rangle_{cyl} = c_k, \\ &\langle \phi_k(\sigma, t) \rangle_{dyn} = \langle \phi_k(w, \bar{w}) \rangle_{str} = c_k + a_k e^{-\gamma_k^{(0)} t} + ..., \quad \gamma_k^{(0)} = 2\pi\Delta_k/\beta, \end{aligned} \tag{II.21}$$

where Δ_k now is the scaling dimension of the minimum-dimension operator in a $T(z_1)\phi_k(z)$ OPE. This is clearly of the general form (II.6) for $\mu_n = 0$.

We now turn to a discussion of these expectation values (II.15) in the presence of chemical potentials $\mu_n, n = 3, 4, ...$, as in (II.5) and (II.3). We will denote the new conserved currents as $\mathcal{W}_n(w)$ and $\bar{\mathcal{W}}_n(\bar{w})$, $n = 3, 4, ...$ The conserved charge, W_n, is defined as

$$W_n = \frac{1}{2\pi} \int_\Gamma W_{\tau\tau...\tau} d\sigma = \frac{1}{2\pi} \int_\Gamma \left(i^n dw_1 \, \mathcal{W}_n(w_1) + (-i)^n d\bar{w}_1 \, \bar{\mathcal{W}}_n(\bar{w}_1) \right) \tag{II.22}$$

Here the contour Γ is taken to be a $\tau =$ constant line along which $dw_1 = d\bar{w}_1 = d\sigma$. Under the conformal transformation (II.16) to the plane/UHP, the holomorphic part of the contour integral becomes

$$W_n|_{hol} = \frac{i^n}{2\pi} \left(\frac{2\pi}{\beta} \right)^{n-1} \int_{\Gamma_1} dz_1 \left[z_1^{n-1} \mathcal{W}_n(z_1) + \sum_{m=1}^{\lfloor n/2 \rfloor} a_{n,n-2m} z_1^{n-2m-1} \mathcal{W}_{n-2m}(z_1) \right] \tag{II.23}$$

where the $a_{n,n-2m}$ denote the mixing of $\mathcal{W}_n(z_1)$ with lower order W-currents under conformal transformations [26, 27]. The contour Γ_1 is an image of the contour Γ onto the plane. The expression for the antiholomorphic part $W_n|_{antihol}$ is similar.

As mentioned before, in this chapter we will regard the W_n as conserved charges of a W-algebra, although the results we derive will be equally valid as long as these charges, together with H, form a mutually commuting set, and the currents $(\mathcal{W}_n(w), \bar{\mathcal{W}}_n(\bar{w}))$ are quasiprimary fields.

2.1 One-point function on the cylinder with chemical potentials

For simplicity we first consider the equilibrium expectation value in (II.15). Unfortunately, unlike the thermal factor above, the factor $e^{-\sum_n \mu_n W_n}$ in (II.3) cannot be dealt with in terms of a conformal map. We will, therefore, treat this factor as an operator insertion, and write

$$\langle \phi_k(\sigma) \rangle_{eqm} \equiv \mathrm{Tr} \left(\phi_k(w, \bar{w}) \rho_{eqm}(\beta, \mu_n) \right) = \frac{\langle e^{-\sum_n \mu_n W_n} \phi_k(w, \bar{w}) \rangle_{cyl}}{\langle e^{-\sum_n \mu_n W_n} \rangle_{cyl}} \equiv \langle \phi_k(w, \bar{w}) \rangle_{cyl}^\mu \tag{II.24}$$

We will now illustrate how to compute this for a single chemical potential, say μ_3, using perturbation theory Feynman diagrams:[11]

$$\langle \phi_k(w,\bar{w})\rangle^{\mu}_{cyl} = \langle \phi_k(w,\bar{w})\rangle_{cyl} - \mu_3 \langle W_3 \phi_k(w,\bar{w})\rangle^{conn}_{cyl} + \frac{\mu_3^2}{2!}\langle\, W_3 W_3 \phi_k(w,\bar{w})\rangle^{conn}_{cyl} + \mathcal{O}(\mu_3^3) \tag{II.25}$$

The first term in the above expression is the constant c_k that we already encountered in (II.21). For a holomorphic primary field ϕ_k, the second, $O(\mu_3)$, term, transformed on to the plane, gives

$$\langle W_3 \phi_k(w)\rangle^{conn}_{cyl} = \frac{2\pi}{\beta^2} z^{h_k}\left[i^3 \int_{\Gamma_1} dz_1\; z_1^2 \langle \mathcal{W}_3(z_1)\phi_k(z)\rangle^{conn}_{\mathbb{C}} + (-i)^3 \int_{\Gamma_1} d\bar{z}_1\; \bar{z}_1^2 \langle \bar{\mathcal{W}}_3(\bar{z}_1)\phi_k(z)\rangle^{conn}_{\mathbb{C}}\right] \tag{II.26}$$

Here we have used the contour representations (II.22) and (II.23). The correlator inside the second integral obviously vanishes (it factorizes into a holomorphic and an antiholomorphic one-point functions, leading to a vanishing connected part). The first integral vanishes unless $\phi_k = \mathcal{W}_3$ (this uses the orthogonality of the basis of quasiprimary fields). In the latter case, using

$$\langle \mathcal{W}_3(z_1)\mathcal{W}_3(z)\rangle_{\mathbb{C}} = \frac{c/3}{(z_1 - z)^6}$$

the integral evaluates to $c/(90z^3)$; combining with the factor of z^3 outside ($h_k = 3$ in this case) we get a z-independent constant, as we must, because of translational invariance on the plane. With an antiholomorphic primary field ϕ_k, the calculation is isomorphic. For a primary field with nonvanishing $h_k, \bar{h}_k$ the result vanishes. For quasiprimary ϕ_k, as well as for other W_n charges, the conformal transformation to the plane additionally generates lower order operators (see, e.g. (II.23))), each of which can be dealt with as in (II.26). The result is a finite constant which we will denote as

$$\langle W_n \phi_k(w,\bar{w})\rangle = c_{n,k}$$

(this will be non-vanishing only for special choices of ϕ_k, e.g. $\phi_k = \mathcal{W}_n$). As explained above, for $n = 3$ and $\phi_k(w,\bar{w}) = \mathcal{W}_3(w)$, $c_{n,k} = -2\pi c/(90\beta^2)$.

In a similar fashion, the $O(\mu_3^2)$ term in (II.25) can be transformed to the plane. Again, we present the explicit expression for the simple case of a holomorphic primary field ϕ_k.

$$\begin{aligned}\langle W_3 W_3 \phi_k(w)\rangle^{conn}_{cyl} &= \left(\frac{2\pi}{\beta^2}\right)^2 z^{h_k}\Big[i^6 \int_{\Gamma_1} dz_1 \int_{\Gamma_2} dz_2 \langle \mathcal{W}_3(z_1)\mathcal{W}_3(z_2)\phi_k(z)\rangle^{conn}_{\mathbb{C}}\; z_1^2 z_2^2 \\ &+ (-i)^6 \int_{\Gamma_1} d\bar{z}_1 \int_{\Gamma_2} d\bar{z}_2 \langle \bar{\mathcal{W}}_3(\bar{z}_1)\bar{\mathcal{W}}_3(\bar{z}_2)\phi_k(z)\rangle^{conn}_{\mathbb{C}}\; \bar{z}_1^2 \bar{z}_2^2 + \int_{\Gamma_1} dz_1 \int_{\Gamma_2} d\bar{z}_2 \langle \mathcal{W}_3(z_1)\bar{\mathcal{W}}_3(\bar{z}_2)\phi_k(z)\rangle^{conn}_{\mathbb{C}}\; z_1^2 \bar{z}_2^2 \\ &+ \int_{\Gamma_1} d\bar{z}_1 \int_{\Gamma_2} dz_2 \langle \bar{\mathcal{W}}_3(\bar{z}_1)\mathcal{W}_3(z_2)\phi_k(z)\rangle^{conn}_{\mathbb{C}}\; \bar{z}_1^2 z_2^2 \Big]\end{aligned} \tag{II.27}$$

For holomorphic quasiprimary ϕ_k, additional, similar, terms appear due to the generation of lower order operators under conformal transformation to the plane. Only the holomorphic

[11] The superscript *conn* denotes 'connected'.

correlator survives (as in the O(μ_3) calculation). Thus, e.g. if $\phi_k = T(z)$, the stress tensor, we have

$$\langle \mathcal{W}_3(z_1)\mathcal{W}_3(z_2)T(z)\rangle_{\mathbb{C}} = \frac{c}{(z_1-z_2)^4(z_1-z)^2(z_2-z)^2}$$

Again, after performing the integration over z_1 and z_2, we obtain a z-independent constant, as we must. The analysis of more general fields ϕ_k and two arbitrary W-charges is straightforwardly generalizable. The result is a finite constant (can be zero for a particular ϕ_k) which we denote as

$$\langle W_m W_n \phi_k(w,\bar{w})\rangle = c_{mn,k}$$

Note that in (II.27) the result does not depend on the location of the contours Γ_1, Γ_2 on the plane, since the W-currents are conserved.

Summarizing, we get

$$\langle \phi_k(w,\bar{w})\rangle^{\mu}_{cyl} = c_k - \sum_n \mu_n\ c_{n,k} + \frac{1}{2!}\sum_{m,n}\mu_m\mu_n\ c_{mn,k} + O(\mu^3) \tag{II.28}$$

2.2 One-point function on the strip with chemical potentials

Similarly to the previous subsection, we will treat the μ-deformations in (II.5) as operator insertions:

$$\langle \phi_k(\sigma,t)\rangle_{dyn} \equiv \langle \psi(t)|\phi_k(\sigma)|\psi(t)\rangle = \frac{\langle e^{-\sum_n \mu_n W_n/4}\ \phi_k(w,\bar{w})\ e^{-\sum_n \mu_n W_n/4}\rangle_{str}}{\langle e^{-\sum_n \mu_n W_n/2}\rangle_{str}} \equiv \langle \phi_k(w,\bar{w})\rangle^{\mu}_{str} \tag{II.29}$$

As before, we begin by illustrating the calculation of this quantity with the simplest case of a single chemical potential μ_3, using perturbation theory Feynman diagrams:

$$\begin{aligned}\langle \phi_k(w,\bar{w})\rangle^{\mu}_{str} &= \langle \phi_k(w,\bar{w})\rangle_{str} - \frac{\mu_3}{4}\langle\{W_3, \phi_k(w,\bar{w})\}\rangle^{conn}_{str} \\ &+ \left(\frac{\mu_3}{4}\right)^2 \frac{1}{2!}(\langle\{W_3W_3, \phi_k(w,\bar{w})\}\rangle^{conn}_{str} + 2\langle W_3\phi_k(w,\bar{w})W_3\rangle^{conn}_{str}) + \mathcal{O}(\mu_n^3)\end{aligned} \tag{II.30}$$

The $\{\ ,\}$ denotes an anticommutator. The operator ordering implies the following: when W_3 appears on the left of $\phi_k(w,\bar{w})$, e.g., in $\langle W_3\phi_k(w,\bar{w})\rangle$, the integration contour (II.22) for W_3 on the strip lies above the point $(w,\bar{w})$; similarly when W_3 appears on the right of $\phi_k(w,\bar{w})$, e.g. in $\langle \phi_k(w,\bar{w})W_3\rangle$, the contour for W_3 is below the point $(w,\bar{w})$.

The first, μ-independent, term in the above expansion is already calculated in (II.21).

$\mathcal{O}(\mu_n)$ Calculation

As before, we find it convenient to use the conformal transformation (II.16). The correlator on the strip then reduces to that on the UHP, as in the $\mu=0$ case before. For a holomorphic primary field ϕ_k, this gives

$$\langle W_3\phi_k(w)\rangle^{conn}_{str} = \frac{2\pi}{\beta^2}z^{h_k}\left[i^3\int_{\Gamma_1} dz_1\ z_1^2\langle \mathcal{W}_3(z_1)\phi_k(z)\rangle^{conn}_{\mathrm{UHP}} + (-i)^3\int_{\Gamma_1} d\bar{z}_1\ \bar{z}_1^2\langle \bar{\mathcal{W}}_3(\bar{z}_1)\phi_k(z)\rangle^{conn}_{\mathrm{UHP}}\right] \tag{II.31}$$

where the operator ordering explained above implies that the contour Γ_1 lies to the left of the point $(z, \bar{z})$ on the UHP. Now, in the analogous calculation (II.26), the second connected correlator on the complex plane vanished because of factorization into one-point functions. Correlators on the UHP are, however, related to those on the plane by the method of images (an example of which we saw in (II.18)). In particular, $\bar{\mathcal{W}}_3$ at the point $(z_1, \bar{z}_1)$ on the UHP becomes the holomorphic operator $\mathcal{W}_3^* = -\mathcal{W}_3$ on the LHP at the point $(z_1', \bar{z}_1')$ with $z_1' = \bar{z}_1$ [25, 24]. The contour Γ_1 gets mapped to its mirror image Γ_1' on the lower half plane. With this, we get

$$\langle W_3 \phi_k(w) \rangle_{str}^{conn} = \frac{2\pi}{\beta^2} z^{h_k} \left[i^3 \int_{\Gamma_1 + \Gamma_1'} dz_1 \; z_1^2 \langle \mathcal{W}_3(z_1) \phi_k(z) \rangle_{\mathbb{C}}^{conn} \right] \tag{II.32}$$

On the complex plane, the contour Γ_1 on the UHP can be deformed to Γ_1' on the LHP, hence the two contours simply yield a factor of 2. In fact, combining with the other ordering, and applying a similar reasoning, we get an overall factor of 4. Thus, combining with results from Section 2.1, we get, for holomorphic primary fields

$$-\frac{\mu_3}{4} \langle \{ W_3, \phi_k(w) \} \rangle_{str}^{conn} = -\mu_3 \langle W_3 \phi_k(w) \rangle_{cyl}^{conn} \tag{II.33}$$

A similar statement is true for an antiholomorphic primary field.

Let us turn now to primary fields $\phi_k(w, \bar{w})$ with $h_k, \bar{h}_k \neq 0$ (of the form $\phi_k(w, \bar{w}) = \varphi_k(w) \varphi_k(\bar{w})$, as discussed before in the context of (II.18)). In the cylinder calculation in Section 2.1 the μ-corrections for these vanished. In the present case, they are non-zero for operators of the form $\phi_k(w, \bar{w}) = \varphi_k(w) \bar{\varphi}_k(\bar{w})$, with $h_k = \bar{h}_k$ (as in (II.17)). After conformally transforming to the UHP, we regard $\bar{\varphi}_k$ on the UHP as φ_k^* at the image point on the LHP (up to a constant). Combining with the arguments used for the holomorphic operators, we eventually get

$$\begin{aligned} \frac{\langle \{ W_3, \phi_k(w, \bar{w}) \} \rangle_{str}^{conn}}{\langle \phi_k(w, \bar{w}) \rangle_{str}} &= i^3 \frac{2\pi}{\beta^2} (z\bar{z})^h I_3(z, z'), \\ I_3(z, z') &\equiv \int_{\Gamma_1 + \Gamma_1' + \tilde{\Gamma}_1 + \tilde{\Gamma}_1'} dz_1 \; z_1^2 \langle \mathcal{W}_3(z_1) \varphi_k(z) \varphi_k^*(z') \rangle_{\mathbb{C}}^{conn} / \langle \varphi_k(z) \varphi_k^*(z') \rangle_{\mathbb{C}}^{conn} \end{aligned} \tag{II.34}$$

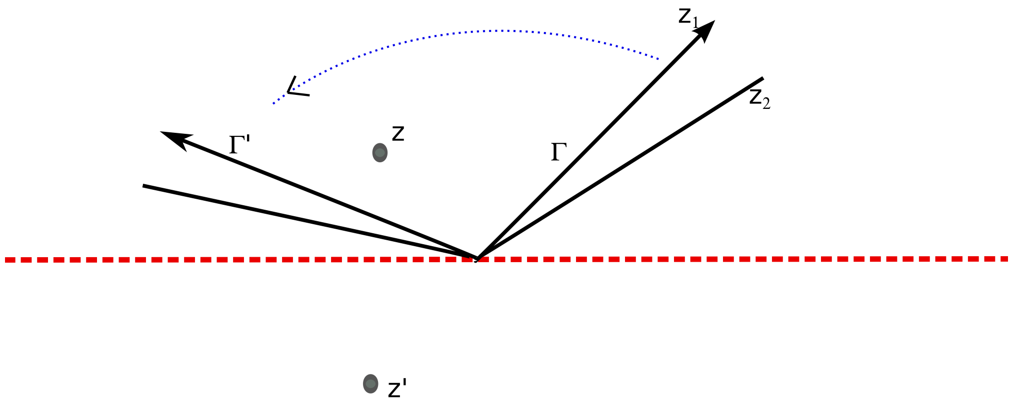

Figure II.1: Various contours needed to compute the W_n insertions in (II.30). At late times, the insertion of each contour, irrespective of the position of the contour, amounts to insertion of a given factor linear in t. This allows to resum arbitrary orders of arbitrary W_n-charge insertions, leading to the exponential time-dependence as in (II.6). See Figure II.2 for more.

The ratio of correlators inside the integral is given by

$$\langle \mathcal{W}_3(z_1)\varphi_k(z)\varphi_k^*(z')\rangle_{\mathbb{C}}^{conn}/\langle \varphi_k(z)\varphi_k^*(z')\rangle_{\mathbb{C}}^{conn} = q_3\frac{(z-z')^3}{(z_1-z)^3(z_1-z')^3} \tag{II.35}$$

where q_3 is the $\mathcal{W}_3$-charge of the field ϕ_k. Integrals of the kind (II.34) are discussed in detail in Appendix II.A.2. The final result (see (II.71)) is that the $O(\mu_3)$ correction, in the long time limit (II.20), is given by (using that all four contours $\Gamma_1, \tilde{\Gamma}_1, \Gamma_1', \tilde{\Gamma}_1'$ contribute equally, cancelling the 1/4 in $-\mu_3/4$)

$$\begin{aligned}&\langle \phi_k(\sigma,t)\rangle_{dyn} = a_k e^{-2\pi\Delta_k t/\beta}\left(1 - Q_{3,k}\tilde{\mu}_3\ (\frac{2\pi t}{\beta} + \text{constant}) + O(\mu_3^2)\right) + ...,\\ &Q_{3,k} = i^3 2q_{3,k}(2\pi),\ \tilde{\mu}_3 = \frac{\mu_3}{\beta^2},\ \Delta_k = 2h_k\end{aligned} \tag{II.36}$$

Up to $O(\mu_3)$, it agrees with (III.9).

In case of a quasiprimary field $\phi_k(w,\bar{w})$, it mixes, under conformal transformation to the plane, with lower dimension operators. The most relevant operator among these, which is of the form $\varphi_k(z)\varphi_k(\bar{z})$, is then to be used in (II.34) for obtaining the dominant time-dependence; in that case $\Delta_k, Q_{3,k}$ refer to this operator (rather than to the original ϕ_k).

For higher W_n charges, the currents $\mathcal{W}_n(w)$ are typically quasiprimary, and hence they mix with lower order $\mathcal{W}_m(z)$ under conformal transformation to the UHP. Thus the $O(\mu_n)$ correction to the dynamical one-point function $\langle\phi_k\rangle_{dyn}$ is a linear combination of terms of the form (II.68) (weighted by a set of coefficients $a_{n,m}$, as in (II.37) below). Collecting all this, the $O(\mu)$ correction with all chemical potentials is given by

$$\langle\phi_k(\sigma,t)\rangle_{dyn} = a_k e^{-2\pi\Delta_k t/\beta}\left(1-\sum_{n=3} Q_{n,k}\tilde{\mu}_n\;(\frac{2\pi t}{\beta}+\text{constant})+O(\mu^2)\right)+...,$$
$$\tilde{\mu}_n = \frac{\mu_n}{\beta^{n-1}},\;\Delta_k = h_k+\bar{h}_k = 2h_k$$
$$Q_{n,k} = 2\sum_{m=0}^{\lfloor n/2-1\rfloor} a_{n,m} i^{n-2m}(2\pi)^{n-2m-2}q_{n-2m,k}$$
$$= i^n(2\pi)^{n-2}2q_{n,k}+i^{n-2}(2\pi)^{n-4}a_{n,2}\,2q_{n-2,k}+..., \tag{II.37}$$

Note that for W_3 deformations, the expression for Q_3 as in (II.36) corresponds only to the first term in the above series expression for Q_n. This is because the $\mathcal{W}_3$ current is a primary field and does not mix with any lower $\mathcal{W}$ current under a conformal transformation. From $n=4$ onwards, the additional terms in $Q_{n,k}$'s represent the mixing of $\mathcal{W}_n$ currents with $\mathcal{W}_{n-2m}$ under conformal transformations.

Higher order μ-corrections

Let us first consider that $O(\mu_n^2)$ correction:

$$\langle\phi_k(w,\bar{w})\rangle_{str}^{conn}|_2^{\mu_n} \equiv \frac{(\mu_n/4)^2}{2!}(\langle\{W_nW_n,\phi_k(w,\bar{w})\}\rangle_{str}^{conn}+2\langle W_n\phi_k(w,\bar{w})W_n\rangle_{str}^{conn}) \tag{II.38}$$

Again, for holomorphic (or antiholomorphic) primary fields $\phi_k(w)$, it is straightforward to generalize (II.33) to this order.

$$\langle\phi_k(w)\rangle_{str}^{conn}|_2^{\mu_n} = \frac{\mu_n^2}{2!}\langle W_nW_n\phi_k(w)\rangle_{cyl}^{conn} \tag{II.39}$$

For a primary field of the form $\phi_k(w,\bar{w}) = \varphi_k(w)\varphi_k(\bar{w})$, proceeding as in the previous subsection, we get

$$\langle\phi_k(w)\rangle_{str}^{conn}|_2^{\mu_n} = \frac{1}{2!}\left(Q_{n,k}\tilde{\mu}_n t\,\frac{2\pi}{\beta}\right)^2+\mu_n^2(\text{constant}\times t+\text{constant})+... \tag{II.40}$$

The essential ingredient in this calculation is

$$I_{nm}(z,z'|\Gamma_1,\Gamma_2) \equiv \int_{\Gamma_1}dz_1\;z_1^{n-1}\int_{\Gamma_2}dz_2\;z_2^{m-1}f_{nm}(z_1,z_2,z,z'),$$
$$f_{nm}(z_1,z_2,z,z') = \frac{\langle\mathcal{W}_n(z_1)\mathcal{W}_m(z_2)\varphi_k(z)\varphi_k^*(z')\rangle_{\mathbb{C}}^{conn}}{\langle\varphi_k(z)\varphi_k^*(z')\rangle_{\mathbb{C}}^{conn}} \tag{II.41}$$

By repeating the strategy of (II.75), we get

$$\text{Coefficient of }[\log(-z')-\log(-z)]^2\text{ in }I_{nm}(z,z'|\Gamma_1,\Gamma_2)$$
$$=\text{Residue}_{z_1=z}\left[\text{Residue}_{z_2=z}\left(\frac{\langle\mathcal{W}_n(z_1)\mathcal{W}_m(z_2)\varphi_k(z)\varphi_k^*(z')\rangle_{\mathbb{C}}^{conn}}{\langle\varphi_k(z)\varphi_k^*(z')\rangle_{\mathbb{C}}^{conn}}\right)\right] = q_{n,k}\,q_{m,k} \tag{II.42}$$

where we have first used the $\mathcal{W}_m(z_2)\varphi_k(z)$ OPE, and then the $\mathcal{W}_n(z_1)\varphi_k(z)$ OPE. In a manner similar to that in Appendix II.A.2, we conclude the following structure of $I_{nm}(z,z')$:

$$I_{nm}(z,z'|\Gamma_1,\Gamma_2) = q_{n,k}\, q_{m,k}([\log(-z') - \log(-z)] + \text{constant}) \times ([\log(-z') - \log(-z)] + \text{constant}) \quad \text{(II.43)}$$

Note that at late times $t \gg \beta$, $([\log(-z') - \log(-z)] \to 2(2\pi t)/\beta$ and dominates over the constant term (the precise sense is that of (II.48)). Similar to Appendix II.A.2, the $4\times 4 = 16$ locations of the contour-pairs (Γ_1,Γ_2),(Γ_1,Γ_2'), $(\Gamma_1,\tilde{\Gamma}_2)$,$(\Gamma_1,\tilde{\Gamma}_2')$, ..., all contribute equally, therefore converting $(\mu_n/4)(\mu_m/4) \to \mu_n\mu_m$. Combining all these, we get (II.40). The charges q_n that are defined by the $\mathcal{W}_n\varphi$ OPE and appear in (II.42), get multiplied by some constants [12] and shifted by lower $\mathcal{W}_{n-2k}$ charges to give the Q_n in (II.42), as in (II.37).

Arbitrary orders and Exponentiation:

It is straightforward to generalize the above $O(\tilde{\mu}^2)$ calculation to higher orders in the perturbation in chemical potentials. Thus, at the order $\prod_{i=1}^r \mu_{n_i}$, there are r insertions of $\mathcal{W}$-currents, leading to integrals of the form

$$I_{n_1n_2...n_r}(z,z'|\Gamma_1,\Gamma_2,...,\Gamma_r) \equiv \int_{\Gamma_1} dz_1\ z_1^{n_1-1} \int_{\Gamma_2} dz_2\ z_2^{n_2-1} ... \int_{\Gamma_r} dz_2\ z_r^{n_r-1} f_{n_1n_2...n_r}(z_1,z_2,...,z_r;z,z'),$$
$$f_{n_1n_2...n_r}(z_1,z_2,...,z_r;z,z') = \frac{\langle \mathcal{W}_{n_1}(z_1)\mathcal{W}_{n_2}(z_2)...\mathcal{W}_{n_r}(z_r)\varphi_k(z)\varphi_k^*(z')\rangle_{\mathbb{C}}^{conn}}{\langle \varphi_k(z)\varphi_k^*(z')\rangle_{\mathbb{C}}^{conn}} \quad \text{(II.44)}$$

Again, repeating the strategy of (II.75), we get the following leading (*viz.* $(\log)^r$) contribution (see (II.48) for the definition of the leading-log contribution)

$$\begin{aligned}&\text{Coefficient of } [\log(-z') - \log(-z)]^r \text{ in } I_{n_1n_2...n_r}(z,z'|\Gamma_1,\Gamma_2,...,\Gamma_r)\\ &= \text{Residue}_{z_1=z}\left[...\text{Residue}_{z_{r-1}=z}\left\{\text{Residue}_{z_r=z}\left(\frac{\langle \mathcal{W}_{n_1}(z_1)...\mathcal{W}_{n_{r-1}}(z_{r-1})\mathcal{W}_{n_r}(z_r)\varphi_k(z)\varphi_k^*(z')\rangle_{\mathbb{C}}^{conn}}{\langle \varphi_k(z)\varphi_k^*(z')\rangle_{\mathbb{C}}^{conn}}\right)\right\}\right]\\ &= q_{n_1,k}...q_{n_{r-1},k}\, q_{n_r,k} \end{aligned} \quad \text{(II.45)}$$

where we have first used the $\mathcal{W}_{n_r}(z_r)\varphi_k(z)$ OPE, then $\mathcal{W}_{n_{r-1}}(z_{r-1})\varphi_k(z)$ OPE, etc. As in the $O(\mu^2)$ calculation above, we obtain the following behaviour at late times

$$\begin{aligned}&I_{n_1n_2...n_r}(z,z'|\Gamma_1,\Gamma_2,...,\Gamma_r)\\ &= q_{n_1,k}...q_{n_{r-1},k}\, q_{n_r,k}\ \underbrace{([\log(-z') - \log(-z)] + \text{constant}) \times ... \times ([\log(-z') - \log(-z)] + \text{constant})}_{r\text{ terms}}\end{aligned} \quad \text{(II.46)}$$

The two equations above show that the leading log contribution to (II.44) from every contour integral of the $\mathcal{W}_{n_i}$ current contributes the factor $q_{n_i}[\log(-z') - \log(-z)]$. This is the first basic ingredient for the exponentiation we are going to find. Furthermore, it is easy to see that the leading log contribution is the same irrespective of where each contour Γ_i is placed (out of 4 possible choices, e.g. $\Gamma_1,\Gamma_1',\tilde{\Gamma}_1,\tilde{\Gamma}_1'$ in Figure II.1). As before we must combine the contribution of all positions of the contours, which, therefore, amounts to multiplying the result for (II.44) by 4^r which converts the original coefficients coming from $\exp[-\sum_n \mu_n W_n/4]$ as follows

$$\frac{\prod_{i=1}^r \mu_i/4}{r!} \to \frac{\prod_{i=1}^r \mu_i}{r!}.$$

[12]Each $\mathcal{W}_n$ current comes with a factor of $\frac{i^n}{2\pi}\left(\frac{2\pi}{\beta}\right)^{n-1}$, as in (II.23).

This is the second basic factor leading to the exponentiation. Combining all these, and incorporating some additional constants (see footnote 12) we get the following, leading, order $(\mu_{n_1}...\mu_{n_r})$ contribution

$$\langle \phi_k(w) \rangle_{str}^{conn}|_r^{\mu_{n_1}...\mu_{n_r}} = \frac{1}{r!}\prod_{i=1}^{r}\left(Q_{n_i,k}\tilde{\mu}_{n_i}\ \frac{2\pi}{\beta}\right) + O(\mu^r t^{r-l}) \qquad \text{(II.47)}$$

Once again, the constants Q_n are related to the q_n as in (II.37)) in a manner similar to the $O(\tilde{\mu})$ and the $O(\tilde{\mu}^2)$ calculation above. We note that the leading log contribution used in this chapter can be isolated by considering a scaling

$$\tilde{\mu}_n \to 0, \tilde{t} \equiv \frac{t}{\beta} \to \infty, \text{ such that } \tilde{\mu}_n\tilde{t} = \text{constant}. \qquad \text{(II.48)}$$

The second term in (II.47), or for that matter, in (II.40), is subleading at large times in the sense of this scaling.

Using the above results, we now have, for primary fields of the form $\phi_k(w,\bar{w}) = \varphi_k(w)\varphi_k(\bar{w})$

$$\begin{aligned}\langle \phi_k(w,\bar{w}) \rangle_{str} = a_k e^{-\frac{2\pi\Delta_k t}{\beta}} \Bigg[1 &- \sum_n \tilde{\mu}_n\ Q_{n,k}(\frac{2\pi t}{\beta} + \text{const}) \\ &+ \frac{1}{2!}\sum_{n,m}\tilde{\mu}_n\tilde{\mu}_m\ Q_{n,k}(\frac{2\pi t}{\beta} + \text{const})\ Q_{m,k}(\frac{2\pi t}{\beta} + \text{const}) + ... \\ &+ \frac{1}{r!}\sum_{\{n_i\}}\prod_{i=1}^{r}\tilde{\mu}_{n_i}Q_{n_i,k}\left(\underbrace{(\frac{2\pi t}{\beta} + \text{const})...(\frac{2\pi t}{\beta} + \text{const})}_{r\text{ terms}}\right) + ... \Bigg] \\ &= a_k e^{-2\pi t/\beta\left(\Delta_k + \sum_n \tilde{\mu}_n Q_{n,k} + O(\tilde{\mu}^2)\right)} = a_k e^{-\gamma_k t} \end{aligned} \qquad \text{(II.49)}$$

where we have absorbed some constant factors in a_k. γ_k is given by (III.9); $Q_{n,k}$ are the shifted W_n charges of ϕ_k as defined in (II.37). The proof of the above equation for general quasiprimary operators $\phi_k(w,\bar{w})$ works out much the same way as in case of the $O(\mu)$ terms, as discussed in Section 2.2. *We emphasize that it is only the leading contributions at large times which we have proved here to exponentiate.* Thus, we do not claim that the constant terms marked "const" in the above equation are all the same. As we have remarked before, the leading contributions can be isolated using the scaling mentioned in (II.48).

The schematics of the above calculation is explained in the Figure II.2.

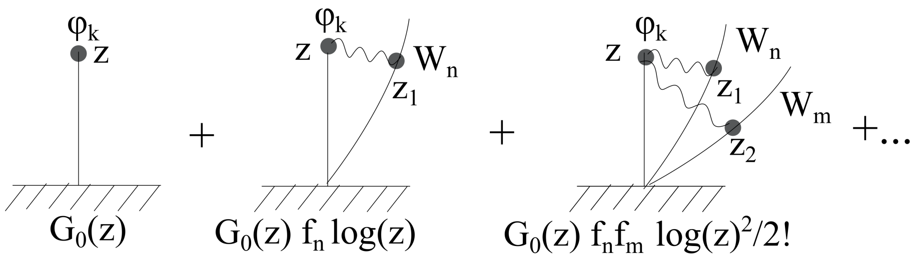

Figure II.2: The schematics of the calculation of the one-point function. The first term represents the zero-order boundary Green's function (II.17) without chemical potentials (the shading indicates the boundary of the upper half plane). The second term represents the $O(\mu_n)$ correction, which involves one insertion of a W_n-charge (which is an integral over the z_1-contour. As explained in the text, at long times, this insertion amounts to multiplying the zero order term by a term of the form $f_n \log(z)$, where f_n is described in (II.37). The third term represents insertion of two such W-charges; as we explained in the text (see (II.40) and below), each insertion again amounts to multiplying by the factor mentioned above, along with a factor of $\frac{1}{2!}$. The pattern continues, to ensure an exponentiation to $G_0(z)\, z^{\sum_n f_n}$, as in (II.49). Since at long times $G_0(z) \sim e^{-\gamma_k^{(0)} t}$ (see (II.17)), and $z \sim e^{-2\pi t/\beta}$, adding the chemical potentials amount to a shift of the exponent $\gamma_k^{(0)} \to \gamma_k$ as in (II.6).

3 Calculation of $I(t)$

Let us rewrite the expression for the thermalization function $I(t)$ (II.8) in the form

$$\begin{aligned}
&I(t) = Z_{sc}/\sqrt{Z_{ss}Z_{cc}} = \hat{Z}_{sc}/\sqrt{\hat{Z}_{ss}\hat{Z}_{cc}},\\
&Z_{sc} \equiv \mathrm{Tr}(\rho_{dyn,A}(t)\rho_{eqm,A}(\beta,\mu)),\ \hat{Z}_{sc} = Z_{sc}/(Z_s Z_c)\\
&Z_{ss} \equiv \mathrm{Tr}(\rho_{dyn,A}(t)\rho_{dyn,A}(t)),\ \hat{Z}_{ss} = Z_{ss}/Z_s^2,\\
&Z_{cc} \equiv \mathrm{Tr}(\rho_{eqm,A}(\beta,\mu)\rho_{eqm,A}(\beta,\mu)),\ \hat{Z}_{cc} = Z_{cc}/Z_c^2,\\
&Z_s = \mathrm{Tr}(\rho_{dyn}(t)) = \langle\psi_0|\psi_0\rangle,\ Z_c = \mathrm{Tr}(\rho_{\beta,\mu}) \qquad \text{(II.50)}
\end{aligned}$$

In Appendix II.B we explain how to compute $I(t)$ using the short interval expansion, valid when the length of the interval l is small compared with the other time scales β and t in the problem. We reproduce the main formula (II.79) for our purpose, where we explicitly denote the dependencies on the length l of the interval, the inverse temperature β and the chemical potentials μ (the dependence on β on the RHS is implicit; the one-point functions depend on both β and μ— see Section 2).

$$\begin{aligned}
\hat{Z}_{sc}(l,\beta,\mu) &= \sum_{k_1,k_2} C_{k_1,k_2}(l)\langle\phi_{k_1}(w_1,\bar{w}_1)\rangle^\mu_{str}\langle\phi_{k_2}(w_2,\bar{w}_2)\rangle^\mu_{cyl},\\
\hat{Z}_{ss}(l,\beta,\mu) &= \sum_{k_1,k_2} C_{k_1,k_2}(l)\langle\phi_{k_1}(w_1,\bar{w}_1)\rangle^\mu_{str}\langle\phi_{k_2}(w_2,\bar{w}_2)\rangle^\mu_{str},\\
\hat{Z}_{cc}(l,\beta,\mu) &= \sum_{k_1,k_2} C_{k_1,k_2}(l)\langle\phi_{k_1}(w_1,\bar{w}_1)\rangle^\mu_{cyl}\langle\phi_{k_2}(w_2,\bar{w}_2)\rangle^\mu_{cyl} \qquad \text{(II.51)}
\end{aligned}$$

It is understood, for the logic of the short interval expansion to go through, that all contours which represent insertion of the W-charges (see Fig II.1) are drawn outside of the small disc-like region of both sheets of Fig II.4.

3.1 Proof of thermalization

Using the short-interval expansion above, and the long time behaviour of one-point functions from Section 2), it is easy to prove that the system thermalizes in the sense of (II.10) or (II.11).

To prove this, note that it is only the holomorphic (or antiholomorphic) fields ϕ_k which possibly have non-zero expectation values in the long time limit (II.20). For these fields, the one-point functions on the cylinder and on the strip agree (see (II.21), (II.33), (II.39)). By virtue of (II.51), we therefore have in the long time limit $Z_{sc} = Z_{ss} = Z_{cc}$. Hence using the expression (II.50) for the thermalization function we get $I(t \to \infty) = 1$ which proves (II.10) and consequently (II.11).

The above-mentioned equality of one-point functions between the strip and cylinder geometries for holomorphic (or antiholomorphic) fields imply the same for the conserved $\mathcal{W}_n$- (or $\bar{\mathcal{W}}_n$)- currents. This, therefore, proves that

$$\langle\psi(t)|W_n|\psi(t)\rangle = \mathrm{Tr}(W_n \rho_{eqm}) \tag{II.52}$$

Note that in proving this, we have used the correspondence (II.4) between the parameters of the initial state and the putative equilibrium state. The above equation, therefore, proves the correspondence (II.4).

3.2 Thermalization rate

To evaluate the rate of approach of $I(t)$ to its asymptotic value 1, we organize the terms in $\hat{Z}_{sc}, \hat{Z}_{ss}, \hat{Z}_{cc}$ as follows

$$\begin{aligned}
&\hat{Z}_{sc} = C_{0,0}(1 + S_1^{sc}),\ S_1^{sc} = \sum_a \hat{C}_{a,0}(\langle\phi_a\rangle^\mu_{str} + \langle\phi_a\rangle^\mu_{cyl}) + \sum_{ab} \hat{C}_{a,b}\langle\phi_a\rangle^\mu_{str}\langle\phi_b\rangle^\mu_{cyl} \\
&\hat{Z}_{ss} = C_{0,0}(1 + S_1^{ss} + S_2^{ss}),\ S_1^{ss} = 2\sum_a \hat{C}_{a,0}\langle\phi_a\rangle^\mu_{str} + \sum_{ab} \hat{C}_{a,b}\langle\phi_a\rangle^\mu_{str}\langle\phi_b\rangle^\mu_{str},\ S_2^{ss} = \sum_k \hat{C}_{k,k}(\langle\phi_k\rangle^\mu_{str})^2 \\
&\hat{Z}_{cc} = C_{0,0}(1 + S_1^{cc}),\ S_1^{cc} = 2\sum_a \hat{C}_{a,0}\langle\phi_a\rangle^\mu_{cyl} + \sum_{ab} \hat{C}_{a,b}\langle\phi_a\rangle^\mu_{cyl}\langle\phi_b\rangle^\mu_{cyl}
\end{aligned} \tag{II.53}$$

where $a, b, ...$ denote descendents of the identity operator, k labels other primaries (than the identity) and their descendents. $\hat{C} \equiv C/C_{0,0}$.

$\mu = 0$

Let us first consider the case of zero chemical potentials. Using the results in Sections 2, and Appendices II.A and II.B.1, we get

$$\begin{aligned}
S_1^{sc} &= -a_T \tilde{l}^2 \left(1 + O(\tilde{l})^2\right) + a_{T\bar{T}} \tilde{l}^4 e^{-8\pi t/\beta} \left(1 + O(\tilde{l})^2\right) + O(e^{-8\pi\tilde{t}}) \\
S_1^{ss} &= -a_T \tilde{l}^2 \left(1 + O(\tilde{l})^2\right) + 2a_{T\bar{T}} \tilde{l}^4 e^{-8\pi\tilde{t}} \left(1 + O(\tilde{l})^2\right) + O(e^{-8\pi\tilde{t}}) \\
S_2^{ss} &= \sum_k \left[a_k \tilde{l}^{4h_k} e^{-8\pi h_k t/\beta} \left(1 + O(\tilde{l})^2\right) + O(e^{-12\pi h_k \tilde{t}})\right] \\
S_1^{cc} &= -a_T \tilde{l}^2 \left(1 + O(\tilde{l})^2\right) \\
a_T &= \frac{c\pi^2}{24},\ a_{T\bar{T}} = \frac{A_{T\bar{T}}\pi^4}{8c}\ a_k = \frac{A_k^2}{n_k}\left(\frac{\pi}{2}\right)^{4h_k}
\end{aligned} \tag{II.54}$$

To this order, it is easy to see that the contribution to $I(t)$ from descendents of identity, demarcated by $a_T, a_{T\bar{T}}$, vanishes. The leading contribution to $I(t)$, demarcated by a_k, occurs only in $\hat{Z}_{ss}$ and comes from $\left(\langle\phi_m(z,\bar{z})\rangle_{str}\right)^2$ for which h_k is the minimum ($= h_m$) (this could be a field which appears after a conformal transformation of the original quasiprimary field). The time-dependence shown of S_2^{ss} comes from (II.17). Using this, we get

$$I(t) = 1 - \alpha \exp[-2\gamma_m^{(0)} t] + ...,\ \gamma_m^{(0)} = 2\pi\Delta_m/\beta \tag{II.55}$$

This is of the form (II.9) for $\mu = 0$, with

$$\alpha \equiv \frac{A_m^2}{n_m}\left(\frac{\pi}{2}\right)^{4h_m} (\tilde{l})^{4h_m} \left(1 + O(\tilde{l})^2\right) \tag{II.56}$$

The discarded terms in (II.55) are faster transients. This proves (II.9) for zero chemical potential. This result has already appeared in [28].[13]

$\mu \neq 0$

The generalization of the above result to the case of non-zero chemical potentials is straightforward. Once again, the dominant time-dependence arises from $\left(\langle\phi_m(z,\bar{z})\rangle_{str}^{\mu}\right)^2$ in the S_2^{ss} or $\hat{Z}_{ss}$. The time-dependence (II.9) follows by using (II.49) in S_2^{ss}.

3.3 Properties of $\hat{Q}$

From the asymptotic behaviour (II.9) of the thermalization function we indicated the asymptotic behaviour (II.13) of the dynamical reduced density matrix $\hat{\rho}_{dyn}(t)$. By using the long time behaviour of the one-point functions (II.6), we can easily deduce the following dominant behaviour of overlaps of $\hat{Q}$ with various quasiprimary fields at late times

$$\mathrm{Tr}(\hat{Q}\phi_k(t)) \propto e^{-(\gamma_k - \gamma_m)t},\ \mathrm{Tr}(\hat{Q}\phi_m(t)) \to \text{constant}.$$

[13] Our exponent differs from Cardy's value by a factor of 2.

4 Decay of perturbations of a thermal state

We found in the previous sections that the long time behaviour of the reduced density matrix $\rho_{dyn,A}(t)$ resembles that of a thermal ensemble plus a small deformation which decays exponentially. We will find in the next section that the thermal ensemble (or more accurately the generalized Gibbs ensemble) corresponds to a (higher spin) black hole geometry in the bulk. The small perturbation of the equilibrium ensemble is thus expected to correspond to a small deformation of the black hole geometry. Consequently, the exponential decay of the deformation in the CFT should correspond to a 'ringing-down' or a quasinormal mode in the bulk.

We will address the above issue in the next section which deals with bulk geometry. However, in order to make the correspondence of the above paragraph more precise, in this section we will directly present a CFT computation of the decay of a perturbation to a thermal state. Note that this computation is, in principle, different from the exponential decay of the one-point function in the quenched state, (II.6). However, what we will find is that the long time behaviour (II.6) of an operator $\phi_k(0,t)$ in the quenched state is the same as that of its two-point function (II.57) in the thermal state (II.3) (with chemical potentials). The latter measures the thermal decay of a perturbation and is more directly related to a black hole quasinormal mode. Throughout this section, we will assume that the conformal dimensions of ϕ_k satisfy $h_k = \bar{h}_k$.

We define the thermal two-point function as [14]

$$G_+(t,0;\beta,\mu) \equiv \frac{1}{Z}\mathrm{Tr}(\phi_k(0,t)\phi_k(0,0)e^{-\beta H-\sum_n \mu_n W_n}) \tag{II.57}$$

By the techniques developed in the earlier sections, a computation of this quantity amounts to calculating the following correlator on the plane

$$\langle \phi_k(z,\bar{z})\phi_k(y,\bar{y})e^{-\sum_n \mu_n W_n}\rangle, \quad z = ie^{-2\pi t/\beta}, \bar{z} = -ie^{2\pi t/\beta}, y = i, \bar{y} = -i \tag{II.58}$$

where the μ_n-deformations are understood as an infinite series of contours as in the previous section.

For $\mu = 0$, the above two-point function is standard. Including the Jacobian of transformation, we get

$$G_+(t,0;\beta,0) = (\frac{2\pi}{\beta})^{4h_k}\left[(ie^{-2\pi t/\beta} - i)(-ie^{2\pi t/\beta} + i)\right]^{-2h_k} \xrightarrow{t\to\infty} \text{const } e^{-2\pi t\Delta_k/\beta}, \tag{II.59}$$

which clearly matches the long time behaviour of the one-point function (II.6) in the quenched state for $\mu = 0$. Here $\Delta_k = 2h_k$.

In the above, we considered the thermal Green's function for two points which are both at the same spatial point $\sigma = 0$. It is easy to compute the Green's function when the two points are spatially separated by a distance l, say with $\sigma_1 = l$ and $\sigma_2 = 0$. We get

$$G_+(t,l;\beta,0) \equiv \frac{1}{Z}\mathrm{Tr}(\phi_k(l,t)\phi_k(0,0)e^{-\beta H}) = \left[\frac{2\pi}{\beta}e^{\pi l/\beta}\right]^{4h_k}\left((ie^{2\pi(l-t)/\beta} - i)(-ie^{2\pi(l+t)/\beta} + i)\right)^{-2h_k}$$

$$\xrightarrow{t,l\gg\beta} \begin{cases} \text{const } e^{-2\pi t\Delta_k/\beta}, & (t-l) \gg \beta \\ \text{const } e^{-2\pi l\Delta_k/\beta}, & (l-t) \gg \beta \end{cases} \tag{II.60}$$

[14] We use the same notations as in [29].

The coordinates of the two points, in the notation of (II.58) are modified here to $z = ie^{2\pi(l-t)/\beta}$, $\bar{z} = -ie^{2\pi(l+t)/\beta}$, $y = i, \bar{y} = -i$. The prefactor with the square bracket comes from the Jacobian of the transformation from the cylinder to the plane. The behaviour of the Green's function is shown in Figure II.3. It is important to note that the exponential decay, found in (II.6) shows up only for time scales $t \gg l$.

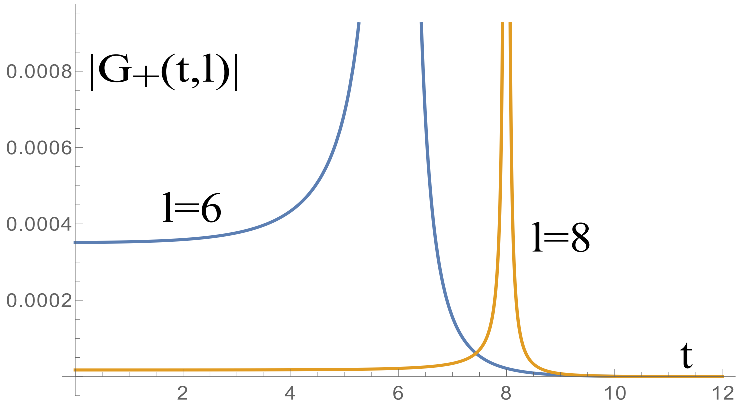

Figure II.3: Plots of the thermal Green's function $G_+(t, l; \beta, 0)$ for $\beta = 2\pi$, $\Delta_k = 1.5$. The curve on the left (blue) is for $l = 6$, and the curve on the right (orange) is for $l = 8$. Note that the exponential decay in time occurs for times larger than l.

The effect of turning on the chemical potentials can be dealt with as in the previous sections. At $O(\mu_n)$, we will have, as before, a holomorphic contribution and an antiholomorphic contribution. The former is proportional to

$$\langle \phi_k(\bar{z})\phi_k(\bar{y})\rangle \times \int_\Gamma dz_1 z_1^{n-1} \langle \mathcal{W}_n(z_1)\phi_k(z)\phi_k(y)\rangle \tag{II.61}$$

As we see, the structure of the integral is the same as in the previous section. As before, logarithmic terms appear in the above integrals which give the leading, linear, t-dependence. Similar remarks also apply to the antiholomorphic contour. Since the calculations are very similar to those in the previous two sections, we do not provide all details. By resumming the series over the infinite number of contours, we find in a straightforward fashion that

$$G_+(t, 0; \beta, \mu) \xrightarrow{t\to\infty} G_+(0, 0; \beta, 0) b(\mu) e^{-\gamma_k t} \tag{II.62}$$

where $b(\mu)$ is time-independent, and is of the form $b(\mu) = 1 + O(\mu)$. This long time decay is the same as that of the one-point function (II.6) in the quenched state, as claimed above. For points separated by a distance l, the above exponential decay shows up for $t \gg l$, as in (II.60).

In the above, we have discussed the two-point function in real space. It is straightforward to convert the result (II.60) without chemical potentials to Fourier space, which develops poles at

$$\omega_{k,m}|_{\mu=0} = -i\frac{2\pi}{\beta}(\Delta_k + 2m),\ m = 0, 1, 2, ... \tag{II.63}$$

Our results in (II.6) can be interpreted as a shift, caused by the presence of the chemical potentials μ_n, of the dominant pole $\omega_{k,0}|_{\mu=0}$ to

$$\omega_{k,0} = -i\frac{2\pi}{\beta}(\Delta_k + \sum_n \tilde{\mu}_n Q_{n,k}) = -i\gamma_k, \tag{II.64}$$

where the notation is the same as that of (II.6). In this chapter we will not address the question of the shift of the subdominant poles $\omega_{k,m}$ (for $m = 1, 2, ...$) due to chemical potentials (the current status of these can be found in [35, 36, 37]).

Two-point functions of the kind (II.57), for a single chemical potential μ_3, and up to order μ_3^2, have appeared earlier in [36] (calculations up to $O(\mu_3^5)$ have appeared in [37]). What we find in this work is that at large times, the perturbation series in μ_n, up to all orders in all chemical potentials, can be resummed, to yield the leading correction to the thermalization rate in the presence of chemical potentials.

At a technical level, the one-point function in the quenched state corresponds to a one-point function in a geometry with a boundary, and for operators considered here, these turn into a two-point function on the plane, by virtue of the method of images. The thermal decay naturally involves a two-point function on the plane [15] and agrees with the above two-point function at late times.

5 Holography and higher spin black holes

Zero chemical potential: As remarked in the Introduction, a global quantum quench described by an initial state of the form (II.5), for large central charges and zero chemical potentials, has been shown in [5, 7, 14] to be dual to one half of the eternal BTZ (black string) geometry, whose boundary represents an end-of-the-world brane.

In an independent development, it was found in [30] that the quasinormal mode of a scalar field $\Phi_k(\sigma, t, z)$ of mass m in a BTZ background (dual to a CFT operator ϕ_k of dimension $\Delta_k \equiv 1 + \sqrt{1 + m^2}$) is of the form $\exp[-2\pi\Delta t/\beta]$ at large times. This time-dependence agrees with the CFT exponent in (II.60) exactly. This shows that the exponential decay of a CFT perturbation to a thermal state corresponds to the decay of the corresponding scalar field in the bulk geometry. This result has been extended to higher spin fields in the BTZ background in [31].

Non-zero chemical potentials: In case the CFT has additional conserved charges, in particular if it has a representation of a W_∞ algebra (and consequently the hs(λ) algebra [32]), then the bulk dual corresponding to those conserved charges have been conjectured to be the conserved higher spin charges of higher spin gravity. In particular, [33, 34] have shown that if one interprets the grand canonical ensemble (II.4) (more generally, the GGE) in the framework of an hs(λ) representation, then the bulk dual corresponds to a higher spin black hole.

[15] Actually the thermal calculation involves a product of two such factors, one holomorphic and the other antiholomorphic, but one of the factors just gives an overall constant and only one factor leads to the important time-dependence.

Thus, we would like to conjecture that the bulk dual of the quantum quench with chemical potentials, would correspond to a gravitational collapse to a higher spin black hole.

As an important consistency check, by analogy with the case with zero potential, in the present case too, the leading quasinormal mode (QNM) of a scalar field $\Phi_k(\sigma, t, z)$ should have a time-dependence given by (II.62). Following the results in [35] (see also [36, 37, 89]) [16] we find that at late times $t \gg \beta$ the QNM for the hs(λ) scalar field Φ_+ behaves, up to $O(\mu_3)$, as $e^{-i\omega_{k,0}t}$, where

$$\omega_{k,0} = -i\frac{2\pi}{\beta}\left(1 + \lambda + \tilde{\mu}_3\frac{1}{3}(1+\lambda)(2+\lambda)\right) \tag{II.65}$$

where the index k here refers to the operator ϕ_k dual to the scalar field Φ_+. Noting that for this operator we have $\Delta_k = 1 + \lambda$, and $Q_{3,k} = \frac{1}{3}(1+\lambda)(2+\lambda)$ [36, 37], we see that the QNM frequency $\omega_{k,0}$ agrees, to the relevant order, with the pole (II.64) of the thermal 2-point function which, in turn, is related to the thermalization exponent by the relation $\omega_{k,0} = -i\gamma_k$, with γ_k given in (II.6).

6 Discussion

In this work, 2D conformal field theories were considered with additional conserved charges besides the energy. We probed non-equilibrium physics starting from global quenches described by conformal boundary states modified by multiple UV cut-off parameters (II.1). It was found that local observables in such a state thermalize to an equilibrium described by a grand canonical ensemble (II.4) with temperature and chemical potentials related to the cut-off parameters. We computed the thermalization rate for various observables, including the reduced density matrix for an interval. It was found that the same rate appears also in the long time decay of two-point functions in equilibrium (see (II.6) and (II.14)). In the context where the number of conserved charges is infinite, and they are identified with commuting W_∞ charges, the equilibrium ensemble (a generalized Gibbs ensemble, GGE) corresponds to a higher spin black hole [33, 34]. We found that the thermalization rate found above agrees with the leading quasinormal frequency of the higher spin black hole; this constitutes an additional, dynamical, evidence for the holographic correspondence between the global quenches in this work and the evolution into the higher spin black hole.

One of the main technical advances made in this chapter is the resummation of leading-log terms at large times, presented in Section 2.2, which leads to exponentiation of the perturbation series, leading to the thermalization rate, presented in (II.6), (II.49), as a function of chemical potentials. This allows us to also compute the effect of chemical potentials on the relaxation times of thermal Green's functions. Another technical advance consists of the computation of the long-time reduced density matrix (II.9), using a short-interval expansion, which allows us to prove thermalization of an arbitrary string of local observables.

One might wonder whether the results presented in this chapter are tied to the use of translationally invariant quenched states such as (II.1), whose energy density and various

[16] We wish to thank Alejandro Cabo-Bizet and Viktor Giraldo-Rivera for informing us that the difference between equation (II.65) above and the corresponding equation (4.2) in a previous version of their paper [35] was due to a typo, which has now been corrected in the new version of their paper.

charge densities are uniform. We will address the question of inhomogeneous quench in a forthcoming paper [88], both in the CFT and in the holographic dual, using the methods of [1] where we create an inhomogeneous energy density by applying conformal transformations. It turns out [88] that if the initial state has inhomogeneities in a compact domain and has uniform energy densities outside, local observables again thermalize asymptotically with exponents governed by the uniform densities. Other important issues involve local quenches (see, e.g. [90, 91]), and compact spatial dimensions. The issue of thermalization when space is compact is quite subtle. It has been shown in [28] that at large times one can have the phenomenon of revival (observables effectively returning to their initial values). The dynamical entanglement entropy for a quantum quench in a space with boundaries is an interesting, related, issue; we hope to come back to this in a forthcoming publication [92].

II.A Some details on one-point functions

Here we collect some additional helpful material on the one-point functions discussed in this chapter.

II.A.1 A few explicit one-point functions with zero chemical potentials

Case k = descendent of identity: In this case, $\phi_k(w,\bar{w})$ is of the form $T, \bar{T}$, or $:T\bar{T}:$ or some descendents thereof. Under a conformal transformation (II.16), these operators pick up a c-number term in addition to a term proportional to the corresponding operator on the plane/UHP. We will give some examples to illustrate the calculation

1. *cylinder:* In this case

$$\langle T(w)\rangle_{cyl} = \langle\Big(-\frac{c\pi^2}{6\beta^2} - \frac{4\pi^2}{\beta^2}z^2T(z)\Big)\rangle_{UHP} = -\frac{c\pi^2}{6\beta^2}$$
$$\langle :T\bar{T}:(w,\bar{w})\rangle_{cyl} = \langle\Big([-\frac{c\pi^2}{6\beta^2} - \frac{4\pi^2}{\beta^2}z^2T(z)][-\frac{c\pi^2}{6\beta^2} - \frac{4\pi^2}{\beta^2}\bar{z}^2\bar{T}(\bar{z})]\Big)\rangle_{UHP} = (\frac{c\pi^2}{6\beta^2})^2 \tag{II.66}$$

2. *strip:* In this case

$$\langle T(w)\rangle_{str} = \langle\Big(-\frac{c\pi^2}{6\beta^2} - \frac{4\pi^2}{\beta^2}z^2T(z)\Big)\rangle_{UHP} = -\frac{c\pi^2}{6\beta^2} = \langle T(w)\rangle_{cyl}$$
$$\begin{aligned}\langle :T\bar{T}:(w,\bar{w})\rangle_{str} &= \langle\Big([-\frac{c\pi^2}{6\beta^2} - \frac{4\pi^2}{\beta^2}z^2T(z)][-\frac{c\pi^2}{6\beta^2} - \frac{4\pi^2}{\beta^2}\bar{z}^2\bar{T}(\bar{z})]\Big)\rangle_{UHP} \\ &= (\frac{c\pi^2}{6\beta^2})^2 + A_{T\bar{T}}(z-\bar{z})^{-4} = (\frac{c\pi^2}{6\beta^2})^2 + a_{T\bar{T}}e^{-8\pi t/\beta} + \ldots\end{aligned} \tag{II.67}$$

where $A_{T\bar{T}}$, $a_{T\bar{T}}$ are constants as in (II.17) and (II.18).

Case k = descendent of other primaries: In this case,

1. *cylinder:* The one-point function vanishes as in the case of primaries.
2. *strip:* The one-point function can be related to one-point function of primaries which is dealt with above.

II.A.2 Some details on $O(\mu_n)$ correction to the one-point function

In this section we will consider the following integrals which arise in connection with $O(\mu_n)$ correction to the one-point function $\langle\phi(\sigma,t)\rangle_{dyn}$:

$$I_n(z,z'|\Gamma_1) \equiv \int_{\Gamma_1} dz_1\; z_1^{n-1} f_n(z_1,z,z'), \quad g_n(z_1,z,z') \equiv \int dz_1\; z_1^{n-1} f_n(z_1,z,z')$$
$$f_n(z_1,z,z') = \frac{\langle \mathcal{W}_n(z_1)\varphi_k(z)\varphi_k^*(z')\rangle_{\mathbb{C}}^{conn}}{\langle\varphi_k(z)\varphi_k^*(z')\rangle_{\mathbb{C}}^{conn}} = q_{n,k}\frac{(z-z')^n}{(z_1-z)^n(z_1-z')^n} \tag{II.68}$$

The second integral on the first line is an indefinite integral. The integrals above can be explicitly computed. E.g.

$$\begin{aligned}
g_3(z_1, z, z') &= q_{3,k}[R_3(z, z')(\log(z_1 - z) - \log(z_1 - z')) - \frac{z^2}{2(z_1 - z)^2} + \frac{z'^2}{2(z_1 - z')^2} \\
&\qquad + \frac{z'(2z + z')}{(z - z')(z_1 - z')} + \frac{z(2z' + z)}{(z - z')(z_1 - z)}] \\
I_3(z, z'|\Gamma_1) &= q_{3,k}[R_3(z, z')(-\log(-z) + \log(-z')) + 3\frac{(z + z')}{(z - z')}] \\
R_3(z, z') &\equiv \frac{(z^2 + 4zz' + z'^2)}{(z - z')^2}
\end{aligned} \tag{II.69}$$

Note that I_3 is essentially obtained from the lower limit of the integral, i.e. from $-g(0, z, z')$. The contour Γ_1 in I_3 specifies which branch of the log is to be taken. In particular

$$I_3(z, z'|\Gamma_1) - I_3(z, z'|\tilde{\Gamma}_1) = -2\pi i q_{3,k}\ R_3(z, z') \tag{II.70}$$

In the long time limit (II.20), we get

$$I_3(z, z'|\Gamma_1) = I_3(z, z'|\tilde{\Gamma}_1) = 2q_{3,k}t(2\pi/\beta) + q_{3,k} \times \text{const} + O(e^{-2\pi t/\beta}) \tag{II.71}$$

In this equation we have displayed the principal value of the relevant integrals (the discontinuity (II.70) tells us the coefficient of the log term or the linear t term).

However, we would like to understand the above results more simply, by using the $\mathcal{W}_n(z_1)\varphi_k(z)$ OPE which is of the form:

$$\mathcal{W}_n(z_1)\varphi_k(z) = q_{n,k}\frac{\varphi_k(z)}{(z_1 - z)^n} + \sum_{i=1}^{n-1} \alpha_{n,i}\frac{\varphi_{k,i}(z)}{(z_1 - z)^{n-i}} + \text{regular terms} \tag{II.72}$$

where $\varphi_{k,i}(z)$ is of dimension $h_k + i$.[17] Using this, we get an expansion for the connected 3-point function of the form:

$$\frac{\langle \mathcal{W}_n(z_1)\varphi_k(z)\varphi_k^*(z')\rangle_{\mathbb{C}}^{conn}}{\langle \varphi_k(z)\varphi_k^*(z')\rangle_{\mathbb{C}}^{conn}} = \frac{q_{n,k}}{(z_1 - z)^n} + \frac{C_{n,1}}{(z_1 - z)^{n-1}(z - z')} + O(z - z')^{-2} \tag{II.73}$$

Performing the integral in (II.68),

$$\begin{aligned}
g_n(z_1, z, z') = q_{n,k}&\left(\log[z_1 - z] - (n - 1)\frac{z}{z_1 - z} + ...\right) \\
&+ \frac{C_{n,1}}{z - z'}\left(z_1 - z + (n - 1)z\log[z_1 - z] + ...\right) + ...
\end{aligned}$$

The ellipsis in each round bracket represents terms with higher powers of $1/(z_1 - z)$ (up to a maximum of $(z_1 - z)^{-n}$); successive round brackets themselves are arranged in higher inverse

[17]This is the general form; some of the $\alpha_{n,i}$ coefficients may, of course, vanish.

powers of $z - z'$. Using the $\mathcal{W}_n(z_1)\varphi_k^*(z')$ OPE in a similar fashion and using the symmetry property $g_n(z_1, z, z') = (-1)^n g_n(z_1, z', z)$ we can arrive at a general structure

$$g_n(0, z, z') = q_{n,k}(\log[-z] - \log[-z'])R_n(z, z') + ...$$

where $R_n(z, z') = (-1)^{n-1}R_n(z', z)$ is of the form $P_{n-1}(z, z')/(z - z')^{n-1}$ ($P_{n-1}(z, z')$ is a homogeneous symmetric polynomial of degree zero). See the explicit form of R_n for $n = 3$ in (II.69). The omitted terms are all ratios of homogeneous polynomials in (z, z') of the same degree in the numerator and in the denominator. This implies that we have, in the long time limit (II.20)

$$I_n(z, z'|\Gamma_1) = I_3(z, z'|\tilde{\Gamma}_1) = 2q_{n,k}(2\pi/\beta)t + q_{n,k} \times \text{const} + O(e^{-2\pi t/\beta}) \tag{II.74}$$

which, of course, agrees with (II.71).

Note that the dominant time-dependence $2q_{n,k}t(2\pi/\beta)$ comes from the long-time limit of the coefficient $R_n(z, z')$ of the log terms, which can be read off from the discontinuity $I_n(z, z'|\Gamma_1) - I_n(z, z'|\tilde{\Gamma}_1)$ (see (II.70)). Now, the contour $\int_{\Gamma_1 - \tilde{\Gamma}_1} dz_1$ can be deformed to a very small circle $\oint \Gamma_z dz_1$ around the point z; therefore the leading long-time behaviour $R_n^{(0)}(z, z')$ can be derived by using the leading OPE singularity in (II.72) and computing the residue at $z_1 = z$:

$$\begin{aligned}&\text{Coefficient of } [\log(-z') - \log(-z)] \text{ in } I_n(z, z') \\ &= \text{Residue}_{z_1=z}\left(\frac{\langle \mathcal{W}_n(z_1)\varphi_k(z)\varphi_k^*(z')\rangle_{\mathbb{C}}^{conn}}{\langle \varphi_k(z)\varphi_k^*(z')\rangle_{\mathbb{C}}^{conn}}\right) \equiv q_{n,k}R_n^{(0)}(z, z') = q_{n,k}\end{aligned} \tag{II.75}$$

II.B Short interval expansion

In this section we will explain a formalism suitable for computing partition functions of the kind that appear in (II.50). For convenience we will first compute these quantities in Euclidean time $\tau = it$ and later analytically continue back to Lorentzian time. With this, each of the expressions Z_{sc}, Z_{ss}, Z_{cc} is of the form

$$\text{Tr}(\rho_{A,1}\rho_{A,2}) = \int_{\text{geometry 1}} \mathbf{D}\varphi_1 \int_{\text{geometry 2}} \mathbf{D}\varphi_2 \ \delta(F[\varphi_1, \varphi_2]) \exp\left(-S[\varphi_1] - S[\varphi_2]\right) \tag{II.76}$$

where $S[\varphi]$ represents the action for the CFT (with fields φ) and the delta-functional in the measure represents a gluing condition between a geometry '1' and a geometry '2' along a 'cut' which is the location, at a particular time τ, of the spatial interval $A : \sigma \in (-l/2, l/2)$ [18] For Z_{ss}, both geometries are that of a strip of the Euclidean plane described by complex coordinates $(w, \bar{w}) = \sigma \pm i\tau$ defined by boundaries at $\tau = \pm\beta/4$ with boundary conditions determined by the boundary state $|Bd\rangle$ introduced in (II.5). For Z_{cc}, both geometries are that of a cylinder cut of the Euclidean plane with identified boundaries at $\tau = -\beta/4, 3\beta/4$. The geometries for both Z_{ss} and Z_{cc} are familiar from calculations of Entanglement Renyi

[18] To be precise, $\delta[F] = \delta(\varphi_1(A_<) - \varphi_2(A_>))\ \delta(\varphi_1(A_>) - \varphi_2(A_<))$, where $A_<$ ($A_>$) represents the limiting value from below (above) the cut.

entropy (of order 2) and can be calculated from appropriate correlation functions of twist fields [93] which exchange two identical geometries. For Z_{sc}, the two glued geometries are different (that of a strip and a cylinder), hence the method of twist operators do not apply in a straightforward fashion. (See Figure II.4). In this work, we will therefore, employ the method of the short interval expansion.

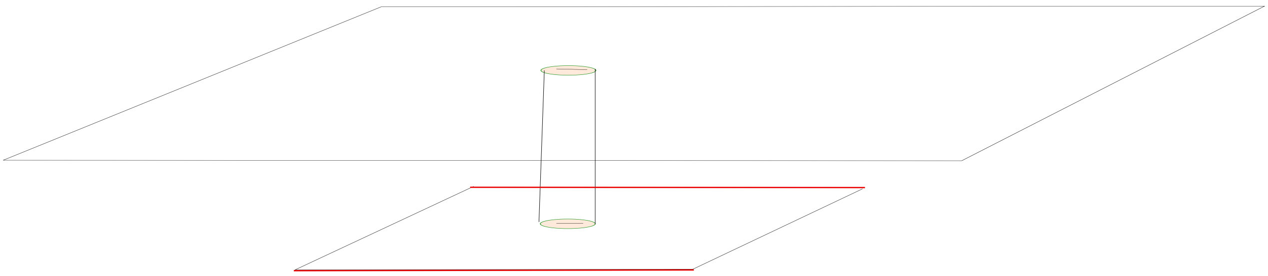

Figure II.4: Two different geometries, the strip and the cylinder, glued along the cut as described in the text. The method of the short interval expansion allows us to compute the functional integral over this geometry by replacing a small tube enclosing the two glued cuts by a complete basis of operators $\phi_{k_1} \otimes \phi_{k_2}$ where the operators live in the two Hilbert spaces.

The idea of the short interval expansion [94] is as follows. To begin, we express the functional integral (II.76) as an overlap of two wavefunctions in $\mathsf{H}_1 \otimes \mathsf{H}_2$, as follows

$$\begin{aligned}
Z_{12} = \mathrm{Tr}(\rho_{A,1}\rho_{A,2}) = \langle \psi_{out}|\psi_{in}\rangle = \int_{w_1\in\mathcal{D}_1}\!\mathbf{D}\overline{\varphi}_1(w_1)\int_{w_2\in\mathcal{D}_2}\!\mathbf{D}\overline{\varphi}_2(w_2)\ \ \psi_{in}[\overline{\varphi_1},\overline{\varphi_2}]\ \psi^*_{out}[\overline{\varphi_1},\overline{\varphi_2}] \\
\psi_{in}[\overline{\varphi_1},\overline{\varphi_2}] \equiv \int_{w_1\in\mathcal{D}_1}\!\mathbf{D}\varphi_1(w_1)\int_{w_2\in\mathcal{D}_2}\!\mathbf{D}\varphi_2(w_2)\delta(\varphi_1|_{\partial\mathcal{D}_1}-\overline{\varphi_1})\delta(\varphi_2|_{\partial\mathcal{D}_2}-\overline{\varphi_2})\delta(F[\varphi_1,\varphi_2])\exp\left(-S[\varphi_1]-S[\varphi_2]\right) \\
\psi_{out}[\overline{\varphi_1},\overline{\varphi_2}] \equiv \int_{w_1\notin\mathcal{D}_1}\!\mathbf{D}\varphi_1(w_1)\int_{w_2\notin\mathcal{D}_2}\!\mathbf{D}\varphi_2(w_2)\delta(\varphi_1|_{\partial\mathcal{D}_1}-\overline{\varphi_1})\delta(\varphi_2|_{\partial\mathcal{D}_2}-\overline{\varphi_2})\exp\left(-S[\varphi_1]-S[\varphi_2]\right)
\end{aligned} \tag{II.77}$$

Here $\mathcal{D}_1$ (respectively, $\mathcal{D}_2$) is a small disc drawn around the cut in geometry 1 (respectively, geometry 2).

Note that only $|\psi_{in}\rangle$ depends on the gluing condition since the delta functional in the measure does not affect $|\psi_{out}\rangle$. The basic point of the short interval is that in the limit when the length l of the cut is small compared with the characterizing length scale of the geometries (in our case, when $l \ll \beta$), the wavefunction $\psi_{in}[\varphi_1,\varphi_2]$ becomes jointly localized at the centre $(w_1,\bar{w}_1)$ of the disc $\mathcal{D}_1$ *and* at the centre $(w_2,\bar{w}_2)$ of the disc $\mathcal{D}_2$ [19], and hence can be expanded in terms of local operators, as follows

$$|\psi_{in}\rangle = \sum_{k_1,k_2} C_{k_1,k_2}\ \phi_{k_1}(w_1,\bar{w}_1)\,\phi_{k_2}(w_2,\bar{w}_2)|0\rangle_1\otimes|0\rangle_2 \tag{II.78}$$

Here k_1, k_2 label a complete basis of quasiprimary operators of the CFT Hilbert space. Each term in the sum represents a factorized wavefunction (between geometries 1 and 2), which,

[19]We will take the centre of the disc in each geometry to coincide with the centre of the cut, which has coordinates $w = i\tau, \bar{w} = -i\tau$.

therefore, gives [20]

$$
\begin{aligned}
\hat{Z}_{sc} &= \sum_{k_1,k_2} C_{k_1,k_2} \langle \phi_{k_1}(w_1, \bar{w}_1) \rangle_{str} \langle \phi_{k_2}(w_2, \bar{w}_2) \rangle_{cyl}, \\
\hat{Z}_{ss} &= \sum_{k_1,k_2} C_{k_1,k_2} \langle \phi_{k_1}(w_1, \bar{w}_1) \rangle_{str} \langle \phi_{k_2}(w_2, \bar{w}_2) \rangle_{str}, \\
\hat{Z}_{cc} &= \sum_{k_1,k_2} C_{k_1,k_2} \langle \phi_{k_1}(w_1, \bar{w}_1) \rangle_{cyl} \langle \phi_{k_2}(w_2, \bar{w}_2) \rangle_{cyl}
\end{aligned}
\tag{II.79}
$$

Here the subscripts *str* and *cyl* refer to "strip", and "cylinder" respectively. The one-point functions are evaluated on the respective geometries without any cut (see Section 2 for more details). The glued functional integral (II.76), (II.77) is recovered by summing over k_1, k_2 with the coefficients C_{k_1,k_2}; , as clear from (II.79) these are determined by the gluing condition and depend on the size of the cut [94] (see Section II.B.1 for more details).

II.B.1 The coefficients C_{k_1,k_2}

As explained in [94] (see also Section II.B), the coefficients C_{k_1,k_2} are determined by the equation

$$
C_{k_1,k_2} = \frac{Z_2}{Z_1^2} (n_{k_1} n_{k_2})^{-\frac{1}{2}} \lim_{z_1 \to \infty_1, z_2 \to \infty_2} (z_1 z_2)^{2(h_{k_1}+h_{k_2})} (\bar{z}_1 \bar{z}_2)^{2(\bar{h}_{k_1}+\bar{h}_{k_2})} \langle \phi_{k_1}(z_1, \bar{z}_1) \phi_{k_2}(z_2, \bar{z}_2) \rangle_{\mathbb{C}_2}
\tag{II.80}
$$

where $\mathbb{C}_2$ represents two infinite planes glued along a cut A, Z_2 is the functional integral such a glued geometry and Z_1 is the functional integral over a single plane. This equation can be easily proved by inserting quasiprimary a operator at infinity in each plane in an equation like (II.76) or (II.77). The two point function in the glued geometry is to be determined by using the uniformizing map:

$$
y = \sqrt{(z + l/2)/(z - l/2)}
\tag{II.81}
$$

The normalization constants n_k are determined by the following orthogonality condition of the quasiprimary operators

$$
\langle \phi_{k_1}(z_1, \bar{z}_1) \phi_{k_2}(z_2, \bar{z}_2) \rangle_{\mathbb{C}} = \frac{n_{k_1} \delta_{k_1,k_2}}{z_{12}^{h_{k_1}+h_{k_2}} \bar{z}_{12}^{\bar{h}_{k_1}+\bar{h}_{k_2}}}
\tag{II.82}
$$

where n_{k_1} is a normalization constant. Note that $C_{k_1,k_2} = C_{k_2,k_1}$. Below we will use the notation

$$
\hat{C}_{k_1,k_2} = C_{k_1,k_2}/C_{0,0}
\tag{II.83}
$$

<u>Case $(k_1, k_2) = (0, 0)$</u>: We will denote the identity operator as $\phi_0 = 1$. It is obvious that

$$
C_{0,0} = Z_2/Z_1^2
\tag{II.84}
$$

[20] In case geometries 1 and 2 are identical, the superscripts in $w_i, \bar{w}_i, i = 1, 2$ indicate which sheet we are considering.

Case $(k_1, k_2) = (k, 0)$: The only case where $C_{k,0} \neq 0$ is when $\phi_k(z, \bar{z})$ is a descendent of the identity operator, e.g. $T(z)$, $\bar{T}(\bar{z})$, $:T(z)\bar{T}(\bar{z}):$, $\Lambda(z)$, $\Lambda(\bar{z})$ etc.[21] E.g.

$$\hat{C}_{T,0} = C_{T,0}/C_{0,0} = \hat{C}_{\bar{T},0} = \frac{l^2}{16}; \hat{C}_{T\bar{T},0} = \frac{l^4}{256}; ... \tag{II.85}$$

All other $C_{k,0}$ vanish as they are proportional to a one-point function of a primary operator on the Riemann surface (and hence to that on the complex plane).

Case $(k_1, k_2) =$ (primary, primary): In case ϕ_{k_1}, ϕ_{k_2} are primary operators, (II.80) gives

$$\hat{C}_{k_1,k_2} = \frac{1}{n_{k_1}} \delta_{k_1,k_2} \left(\frac{l e^{i\pi/2}}{4} \right)^{2(h_{k_1} + \bar{h}_{k_1})} \tag{II.86}$$

Case $(k_1, k_2) =$ (descendent, descendent): In case ϕ_{k_1} is of the form $L_{-n_1} L_{-n_2} ... \bar{L}_{-m_1} \bar{L}_{-m_2} ... \phi_{l_1}$ and ϕ_{k_2} is of the form $L_{-r_1} L_{-r_2} ... \bar{L}_{-s_1} \bar{L}_{-s_2} ... \phi_{l_2}$, we can show that

$$\begin{aligned} &\hat{C}_{k_1,k_2} = \delta_{l_1,l_2}\, \delta_{\sum n, \sum r}\, \delta_{\sum m, \sum s}\, A(n_1, n_2, ..., m_1, m_2, ...; r_1, r_2, ..., s_1, s_2, ...)\, l^{2(h_{k_1} + \bar{h}_{k_1})}, \\ &h_{k_1} = h_{l_1} + \sum n, \;\; h_{k_2} = h_{l_2} + \sum m \end{aligned} \tag{II.87}$$

where $A(...)$ is a numerical coefficient.

[21] Here $\Lambda(z) = \; :TT:(z) - \frac{3}{10} \partial_z^2 T$ is the level 4 quasiprimary descendent of the identity.

Chapter III

Free Scalar and Fermion Quenches

1 Introduction and Summary

The dynamics of systems undergoing a quantum quench has been extensively studied in recent years [17]. In a quantum quench, some parameter of the Hamiltonian changes over a brief period of time. The initial wavefunction in the pre-quench phase, whether it is a ground state or otherwise, typically evolves to a non-stationary state, which then evolves by the post-quench Hamiltonian which is time-independent. An important question in such a dynamics is whether correlators equilibrate at long times, and if so, whether the equilibrium is described by a thermal ensemble or otherwise [17, 18, 19]. With the advent of AdS/CFT, the issue of thermalization has assumed additional significance as it maps to the subject of gravitational collapse to a black hole [78, 95]. This has given rise to an extensive literature on holographic thermalization (see, e.g. [76, 96, 97], for some of the early papers on the subject). This correspondence has a direct bearing on the issue of universality of thermalization since a collapse to a black hole state is also typically associated with loss of most memory of the collapsing matter. In this chapter, we will find that the final equilibrium state is characterized by an infinite number of thermodynamic paramaters (chemical potentials) which retain a partial memory of the quench protocol[1]; in the holographic dual, this corresponds to retention of memory by the final black hole of the collapsing matter.

A significant step in proving thermalization in a closed 2D system was taken in a recent paper (MSS) [2] (similar results have subsequently appeared in [8]). MSS considered 1+1 dimensional quenches[2], ending with a critical post-quench Hamiltonian and made the following assumptions:
(a) the post-quench wavefunction is of the generalized Calabrese-Cardy (gCC) form[3]

$$|\psi\rangle_{gCC} = \exp[-\kappa_2 H - \sum_{n>2} \kappa_n W_n]|Bd\rangle \tag{III.1}$$

[1]For a quench from a ground state, the final chemical potentials retain a full memory of the quench process. When the initial state is different, the final chemical potentials retain partial information about the initial state and the quench protocol.

[2]Unless otherwise stated, the spatial direction will be regarded as non-compact.

[3]In an obvious notation, we will define the boundary state with an energy cut-off, $\exp[-\kappa_2 H]|Bd\rangle$ as the Calabrese-Cardy state $|\psi\rangle_{CC}$. These states were introduced in [44] to describe 2D critical quenches.

where W_n are additional conserved charges in the system (the results are valid even without the additional charges present in the system). It was assumed that the charges are obtained from local currents. Below, for specificity, we will assume that the system is integrable, with a $\mathbb{W}_\infty$ algebra[4] and the W_n, $n = 2, 3, ...$ ($W_2 = H$) are $\mathbb{W}_\infty$ charges.
(b) The spectrum of conformal dimensions in the post-quench critical theory has a gap.
(c) The dimensionless parameters $\tilde{\kappa}_n = \kappa_n/\kappa_2^{n-1}, n > 2$ are small and can be treated perturbatively.
(d) The size l of the interval is small compared to κ_2.[5]

With these assumptions in place, MSS proved that the reduced density matrix of an interval of size l in the state (III.1) asymptotes to that in a GGE [6], defined by

$$\rho_{\text{GGE}} = \frac{e^{-\beta H - \sum_{n=3}^{\infty} \mu_n W_n}}{Z}, \; \beta = 4\kappa_2, \; \mu_n = 4\kappa_n, n > 2 \tag{III.2}$$

with a relaxation rate given by[7]

$$\gamma = \frac{2\pi}{\beta}\left[\Delta + \sum_{n=3}^{\infty} \tilde{\mu}_n Q_n + O(\tilde{\mu}^2)\right], \; \tilde{\mu}_n \equiv \frac{\mu_n}{\beta^{n-1}}, \tag{III.3}$$

where Δ, Q_n are given by the conformal dimension and other $\mathbb{W}_\infty$ charges of the most relevant operator of the CFT (by assumption (b) above, $\Delta > 0$). A consequence of this result is that the expectation value of an arbitrary string of local operators, which can be enclosed in an interval of length l, exponentially thermalizes to its expectation value in the GGE.

One of the motivations of the present work is to extend the proof of thermlization, without making the assumptions made in MSS, in theories of free scalars or fermions with a time-dependent mass $m(t)$ quenched to $m = 0$. We allow for nontrivial pre-quench states.

We proceed in two ways:

- We consider arbitrary quench protocols $m(t)$ and arbitrary squeezed states as pre-quench states (including the ground state) and show, by mapping the quench problem to an auxiliary one-dimensional scattering problem, that the quench leads to a wave-function of the gCC form. This proves the main ansatz of MSS (assumption (a) above). We also show that by judiciously choosing the pre-quench states one can satisfy the perturbative assumption (c). Thus, for theories satisfying (b) and, for intervals satisfying (d), thermalization follows from first principles.

[4]This clearly holds for the theory of free scalars and fermions discussed in this work.

[5]The assumptions (c) and (d) were made for technical reasons, which can, in principle, be obviated in other methods, e.g. if the higher spin deformations $\kappa_{n>2}$ can be represented geometrically (like κ_2 which is treated as an imaginary time). Assumption (b) appears to be more essential. In case of the scalar field model discussed in the present work, this condition implies compactifying the range of ϕ on a circle.

[6]GGE refers to a generalized Gibbs ensemble; see, e.g. [98] for a review. Thermalization to a GGE in the context of an integrable CFT was anticipated earlier in [99, 14], and, for more general general integrable models, in [100, 101, 21, 102, 103, 104, 22, 105, 99, 23, 106].

[7]To be precise the overlap of the square-normalized reduced density matrix in the pure state (III.1) with that in the mixed state (III.2), behaves like $1 - (\text{const})e^{-2\gamma t}$. See MSS for more details.

- For specific quench protocols, but with arbitrary pre-quench states as above, we compute exact time-dependent correlators, and explicitly show thermalization of one- and two-point functions, without making any of the assumptions of MSS.[8]

One of the technical advances in this work is the use of non-trivial pre-quench states, which we take to be squeezed states. The motivation for considering this class of states is that besides being technically accessible, these states are experimentally realizable (see, e.g. [38, 39]) and carry non-trivial quantum entanglement encoded by the squeezing function.

We list below some salient features of our analysis:

1. **Memory retention by the equilibrum ensemble:** By using inverse scattering methods applied to the above-mentioned auxiliary potential scattering, we are able to relate the post-quench wavefunction, in particular κ_n-parameters of the gCC state, to the quench protocol $m(t)$. In fact, if we start with the ground state of the pre-quench Hamiltonian, the κ_n parameters completely encode $m(t)$, implying that *the equilibrium ensemble specified by $\mu_n = 4\kappa_n$, carries a precise memory of the quench protocol!* In case we start with a squeezed state, the equilibrium ensemble remembers a combination of the quench protocol and the knowledge of the initial state.

2. **UV/IR mixing (IR sensitivity to irrelevant operators):** As already found in MSS, the relaxation rate of various operators (III.3), which govern late time dynamics, depends on all the chemical potentials μ_n, equivalently on the κ_n. Now from (III.1) it is clear that the κ_n represent perturbing a given initial state by higher dimensional (irrelevant) operators. Indeed, our computation of the exact correlators, shows that for a large class of operators, these correlators at long times and large distances, are affected by all these chemical potentials, in apparent contradiction to IR universality (this is elaborated in Section 6). This phenomenon is actually related to the memory retention mentioned above.

3. **Holographic correspondence:** Our results show that for a given quench protocol, a GGE with a finite number of specified chemical potentials can be obtained by taking the pre-quench state to be a suitably chosen squeezed state. By using this result and the correspondence shown in MSS between thermalization to GGE and quasinormal decay to a higher spin black hole, we infer that higher spin black holes with an arbitrary set of chemical potentials get related to thermalization of *squeezed states* in the field theory.

Outline: The outline and organization of the chapter is as follows:

In Section 2 we consider mass quenches in a free scalar in two dimensions. We relate the dynamics to an equivalent potential scattering problem, discussed further in Appendix III.A. We find that the exact time-dependent wavefunction can be related to a Bogoliubov transform of the 'out' vacuum (the post-quench ground state). Using this fact we write

[8] Of course, as we mentioned above, the assumption (a) about the gCC form of the wavefunction is in any case true.

down the exact form of the scalar propagator. These results hold for a general mass quench, including quenches from a massless to a massless theory. We find that the quenched state is always describable in terms of a gCC state (using an application of the BCH formula, as described in Apendix III.B). In Section 2.4 we work out all this for a specific quench protocol (i.e. specific time dependence of the mass parameter). In Section 2.6 we consider cases where the pre-quench state is a squeezed state. We show that this gives us a large class of initial conditions, by tuning which we can prepare a quench state in the exact form $\exp[-\sum_n \kappa_n W_n]|D\rangle$ which has a finite number of given κ_n coefficients.

In Section 3 we show how to generalize the above results to fermions.

In Section 4 we work out the scalar propagator for the specific quench protocol of Section 2.4. This allows us to compute various exact correlators, starting either from a ground state or from specific quench states leading to a gCC state with a finite number of κ_n parameters. We show that these correlators thermalize exponentially to a GGE; the relaxation rate is found non-perturbatively, which agrees with (III.3) in the perturbative regime.

In Section 5 real time Wightman correlators in a GGE are computed.

In Section 6 we show that the IR behaviour of exact correlators is sensitive to all the chemical potentials even though these represent perturbation by irrelevant operators. We also show that the equilibrium ensemble remembers the quench protocol.

In Section 7 we make concluding remarks and mention some open problems. In Appendices III.C and III.D we discuss some notations and general results about bosonic and fermionic theories.

2 Critical quench of a scalar field: general strategy

An important example of quantum quench is provided by free scalar field theories with time-dependent mass (our notations will closely follow [107, 40], which also contain an extensive reference to the relevant literature).

$$\begin{aligned} S &= -\frac{1}{2}\int d^2x(\partial_\mu\phi\,\partial^\mu\phi - m^2(t)\phi^2) \\ &= \frac{1}{2}\int \frac{dkdt}{2\pi}\left(|\dot\phi(k,t)|^2 - (k^2+m^2(t))|\phi(k,t)|^2\right),\ \ \phi(-k,t) = \phi^*(k,t) \end{aligned} \tag{III.4}$$

In this section we will consider a mass function $m(t)$ (this is referred to as a 'quench protocol') which decreases from an asymptotic value m_0 in the past to the asymptotic value $m = 0$ in the future. This is called a critical quench since mass gap vanishes following the quench.

The equations of motion of various Fourier modes in (III.4) get decoupled, where each mode satisfies a Schrödinger-type equation with $-m^2(t)$ playing the role of a potential:

$$-\frac{d^2\phi(k,t)}{dt^2} + V(t)\phi(k,t) = E\phi(k,t), \quad V(t) = -m^2(t),\ E = k^2. \tag{III.5}$$

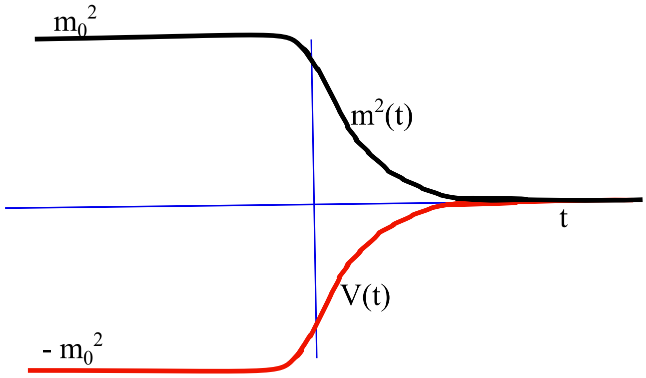

Figure III.1: The equivalent Scrhödinger problem. We have assumed a quench of the mass parameter from m_0 to 0, so that $m^2(t) \xrightarrow{t\to-\infty} m_0^2$, $m^2(t) \xrightarrow{t\to\infty} 0$.

As explained in Appendix III.A (see, e.g. [108], Chapter 3 for details), the solution for the field $\phi(k,t)$ can be expressed in two distinct ways, as (*cf.* (III.98))

$$\begin{aligned} &\phi(k,t) = a_{in}(k)u_{in}(k,t) + a_{in}^\dagger(-k)u_{in}^*(-k,t) = a_{out}(k)u_{out}(k,t) + a_{out}^\dagger(-k)u_{out}^*(-k,t), \\ &\phi(x,t) = \int \frac{dk}{2\pi}\, \phi(k,t)\, e^{ikx} \end{aligned} \tag{III.6}$$

where the 'in' and 'out' wavefunctions $u_{in,out}(k,t)$ are defined as in (III.99). The in- and out-oscillators are related to each other through the Bogoliubov coefficients $\alpha(k), \beta(k)$

$$\begin{aligned} a_{in}(k) &= \alpha^*(k)a_{out}(k) - \beta^*(k)a_{out}^\dagger(-k), \\ a_{out}(k) &= \alpha(k)a_{in}(k) + \beta^*(k)a_{in}^\dagger(-k), \end{aligned} \tag{III.7}$$

which are related to the potential scattering data as explained in Appendix III.A. The Bogoliubov coefficients are actually functions of $|k|$, as explained in Appendix III.A.2.

2.1 General proof of the gCC ansatz [2] for the ground state

The two sets of oscillators define two distinct vacua $|0,in\rangle$ and $|0,out\rangle$, defined by $a_{in}(k)|0,in\rangle = 0$ and $a_{out}(k)|0,out\rangle = 0$. Using the first line of (III.7), we can express the in-vacuum in terms of the out-vacua as follows[9]

$$|0,in\rangle = \exp[\frac{1}{2}\sum_k \gamma(k)a_{out}^\dagger(k)a_{out}^\dagger(-k)]|0,out\rangle, \tag{III.8}$$

where

$$\gamma(k) = \beta^*(k)/\alpha^*(k) = r^*(k). \tag{III.9}$$

In the last step we have used the expression for the reflection amplitude in (III.101). Equation (III.9) establishes the relation between the quantum quench problem in the QFT and the auxiliary potential scattering problem discussed in Appendix III.A.

[9] This is proved by simply checking that the right hand side is annihilated by $\alpha^*(k)a_{out}(k) - \beta^*(k)a_{out}^\dagger(-k)$. Here $\sum_k$ is defined as the sum over discretized values of k, as elaborated in Appendix III.C.

In the above expression (III.8) we represent the states in the Heisenberg picture, as is customary in QFT in curved spacetime.

With the above ingredients in place, it's a simple exercise, using the Baker-Campbell-Hausdorff formula (see Appendix III.B), to show that the in-vacuum can be written in the following form[10]

$$|0,in\rangle = \exp[\frac{1}{2}\sum_k \gamma(k)a^\dagger_{out}|(k)a^\dagger_{out}(-k)]0,out\rangle = \exp[-\sum_k \kappa(k)a^\dagger_{out}(k)a_{out}(k)]|D\rangle,$$
$$\kappa(k) = -\frac{1}{2}\log(-\gamma(k)) \tag{III.10}$$

where $|D\rangle$ is a Dirichlet boundary state (III.113), defined in terms of the 'out' Fock space:

$$|D\rangle = \exp[-\frac{1}{2}\sum_k a^\dagger_{out}(k)a^\dagger_{out}(-k)]|0,out\rangle. \tag{III.11}$$

Using the relation with the scattering problem (as described in Appendix III.A), especially (III.9) and (III.104) we find that $\gamma(k)$ admits a small-momentum expansion of the form

$$\gamma(k) = -1 + \gamma_1|k| + \gamma_2|k|^2 + \gamma_3|k|^3 + ...,\ \gamma_n = r_n^*,\ Re(\gamma_1) \geq 0 \tag{III.12}$$

Using this power series expansion, and the expression for $\kappa(k)$ in (III.10), we can expand $\kappa(k)$ also in a power series, as follows:

$$\kappa(k) = \kappa_2|k| + \kappa_3|k|^2 + \kappa_4|k|^3 - ...,$$
$$\kappa_2 = \frac{\gamma_1}{2}, \kappa_3 = \frac{1}{4}\left(\gamma_1^2 + 2\gamma_2\right), \kappa_4 = \frac{1}{6}\left(\gamma_1^3 + 3\gamma_1\gamma_2 + 3\gamma_3\right), ... \tag{III.13}$$

Note that it follows that Re $\kappa_2 \geq 0$. Below we will find explicit examples of this power series for specific quench protocols $m(t)$ which interpolate from m_0 to $m = 0$. For quenches involving a single real scalar field, we will find that the above expansion (III.13) has only odd powers of $|k|$,[11] and, explicitly $\kappa_2 > 0$.[12] Putting everything together, we find the following expression for the ground state $|0,in\rangle$, in a gCC form (III.1) with the boundary state identified as a Dirichlet state (III.11):

$$|0,in\rangle = \exp[-\kappa_2 H - \sum_{n=2}^{\infty} \kappa_{2n}W_{2n}]|D\rangle \tag{III.14}$$

where $W_{2n}, n = 1,2,...,(W_2 = H)$ are the even W_∞ charges [41] of the final massless scalar field theory, which we define here as follows[13,14]

$$H \equiv W_2 = \sum_k |k|a^\dagger_{out}(k)a_{out}(k),\ W_{2n} = \sum_k |k|^{2n-1}a^\dagger_{out}(k)a_{out}(k),\ n = 2,3,... \tag{III.15}$$

[10] This result was independently found some time ago, for the quench protocol discussed in Section 2.4, in [109]. We thank Sumit Das for sharing these results with us.

[11] This is consistent with the fact that a real scalar field provides a representation of the W_∞ algebra [41] where the odd W_n's vanish. See below.

[12] For massless→massless quench, κ_2 turns out to be purely imaginary (see Section 2.5).

[13] The normalization convention here for the W-charges differs from that of [41].

[14] If the time-dependence of the Hamiltonian stops after a finite time, the post-quench Hamiltonian coincides with the W_2 charge, and the other W_{2n} charges also represent conserved charges of the post-quench evolution.

The values of these charges are given by

$$\langle W_{2l}\rangle = \sum_k |k|^{2l-1}\langle N(k)\rangle,\ l = 1, 2, 3, ...,$$
$$\text{where}\ \ \langle N(k)\rangle \equiv \langle 0_{in}|a^\dagger_{out}(k)a_{out}(k)|0_{in}\rangle = |\beta(k)|^2 \tag{III.16}$$

The last step famously follows by expressing the out-oscillators in terms of the in-oscillators using (III.7).

Note that (III.14) is a relation between Heisenberg states, that is, the LHS, evolved to any time t, equals the RHS evolved to the same time t. Thus, if the time-dependence of the Hamiltonian stops at time $t = t_0$, then we have[15]

$$T\left(e^{i\int_{-\infty}^{t} H(t')dt'}\right)|0, in\rangle = e^{-\kappa_2 H - \sum_{n=2}^{\infty}\kappa_{2n}W_{2n}}|D\rangle,\ t \geq t_0 \tag{III.17}$$

Conclusion: *Thus, we find that the ground state, under a quantum quench to zero mass, is exactly represented in the generalized Calabrese-Cardy (gCC) form, as predicted in [2].*

We will indeed, find below that the above conclusion holds even when we start from more general states in the initial massive theory.

2.2 Thermalization to GGE

As proved for general initial gCC-type initial states (III.1) in MSS [2], for a perturbative domain in the κ_n parameters, and as we will show below explicitly for a large number of specific cases, the post-quench state, which is of the form (III.1) shows subsystem thermalization to the GGE (III.2):

$$|\psi(\kappa_2, \{\kappa_n\})\rangle_{\text{gCC}} \xrightarrow[\text{thermalization}]{\text{subsystem}} \rho_{\text{GGE}}(\beta, \{\mu_n\}), \quad \beta = 4\kappa_2, \mu_n = 4\kappa_n \tag{III.18}$$

Note the alternative form of this equation:

$$\exp[-\sum_k \kappa(k)\hat{N}(k)]|D\rangle \xrightarrow[\text{thermalization}]{\text{subsystem}} \frac{1}{Z}\exp[-\sum_k \mu(k)\hat{N}(k)], \quad \mu(k) = 4\kappa(k) \tag{III.19}$$

Both equations are to be interpreted as the statement that a reduced density matrix on the LHS asymptotically approaches that in the RHS. We will compute explicit correlators below which satisfy the same property.

The energy and W-charges (as well as the number operator) are conserved in the post-quench CFT dynamics, we have

$$\langle H\rangle_{\text{gCC}} = \langle H\rangle_{\text{GGE}},\ \langle W_n\rangle_{\text{gCC}} = \langle W_n\rangle_{\text{GGE}},\ \langle N(k)\rangle_{\text{gCC}} = \langle N(k)\rangle_{\text{GGE}} \tag{III.20}$$

[15]In case the time-development continues asymptotically, but as e^{-t/t_0} as in (III.24), then (III.17) is again true for $t \gg t_0$, up to terms of magnitude e^{-t/t_0}.

Thus, the charges (III.16) measured for the post-quench state also refer to those of the GGE. In particular, note that

$$\langle N(k)\rangle = |\beta(k)|^2 = \frac{|\gamma(k)|^2}{1-|\gamma(k)|^2} = \frac{1}{e^{4\kappa(k)}-1} \tag{III.21}$$

This relation can be identified with a similar relation in [21]. To prove the above equation, we have used (III.9), (III.10) and (III.102).

2.3 The propagator

Using the defining property of the in-vacuum $|0, in\rangle$, and the mode expansion of $\phi(x,t)$ in terms of the in-modes, it is easy to derive the following basic two-point function

$$\begin{aligned}
\langle 0, in|\phi(x_1,t_1)\phi(x_2,t_2)|0, in\rangle &= \int \frac{dk}{2\pi}\, u_{in}(k,t_1)u_{in}^*(k,t_2)\; e^{ik(x_1-x_2)} \\
= \int \frac{dk}{2\pi}\; \big[&|\alpha(k)|^2 u_{out}(k,t_1)u_{out}^*(k,t_2) + \alpha(k)\beta^*(k)u_{out}(k,t_1)u_{out}(-k,t_2) \\
&+\alpha^*(k)\beta(k)u_{out}^*(-k,t_1)u_{out}^*(k,t_2) + |\beta(k)|^2 u_{out}^*(-k,t_1)u_{out}(-k,t_2)\big]\, e^{ik(x_1-x_2)}
\end{aligned} \tag{III.22}$$

In the second step we have used the relation (III.103) between the ‘in’ and ‘out’ modes. Using (III.9) and (III.102), we can find

$$\begin{aligned}
|\alpha(k)|^2 &= \frac{1}{1-|\gamma(k)|^2},\; |\beta(k)|^2 = \frac{|\gamma(k)|^2}{1-|\gamma(k)|^2}, \\
\alpha(k)\beta^*(k) &= \frac{\gamma(k)}{1-|\gamma(k)|^2},\; \alpha^*(k)\beta(k) = \frac{\gamma^*(k)}{1-|\gamma(k)|^2}
\end{aligned} \tag{III.23}$$

The propagator (III.22) has recently appeared in [110] who used it to study the relation between smooth fast quenches and instantaneous quenches. Related expressions, in a somewhat different form, have appeared in [111].
Using the relation (III.9) to relate $\gamma(k)$ to the reflection coefficient $r^*(k)$ (see Appendix III.A), we find that the above propagator can be expressed in terms of the solution of the auxiliary potential scattering problem. In Section 4 we will determine this propagator exactly for a specific quench protocol.

2.4 A specific quench protocol

We will now work out some of the above ideas for the specific mass function

$$m^2(t) = m_0^2(1-\tanh(\rho t))/2 \tag{III.24}$$

The Schrödinger problem with a *tanh* potential can be exactly solved (see, e.g. [108], Chapter 3, where this model appears in a simple model of cosmological particle creation). Using this fact, we can find the following explicit solutions for $u_{in}(k,t)$ and $u_{out}(k,t)$:

$$u_{in}(k,t) = \frac{e^{-i\omega_{in}t}}{\sqrt{2\omega_{in}}}\, {}_2F_1\left(\frac{i\omega_-}{\rho}, -\frac{i\omega_+}{\rho}; 1-\frac{i\omega_{in}}{\rho}; -e^{2\rho t}\right) \tag{III.25}$$

$$u_{out}(k,t) = \frac{e^{-i\omega_{out}t}}{\sqrt{2\omega_{out}}}\, {}_2F_1\left(\frac{i\omega_-}{\rho}, \frac{i\omega_+}{\rho}; \frac{i\omega_{out}}{\rho}+1; -e^{-2\rho t}\right) \tag{III.26}$$

where ${}_2F_1$ is a hypergeometric function and

$$\omega_{in} = \sqrt{k^2 + m_0^2}, \quad \omega_{out} = |k|, \quad \omega_\pm = \frac{1}{2}(\omega_{out} \pm \omega_{in})$$

Using (III.103) (see Appendix III.A for details) and properties of hypergeometric functions [112] for large arguments, we find the following Bogoliubov coefficients

$$\alpha(k) = \sqrt{\frac{\omega_{out}}{\omega_{in}}} \frac{\Gamma\left(-\frac{i\omega_{out}}{\rho}\right)\Gamma\left(1-\frac{i\omega_{in}}{\rho}\right)}{\Gamma\left(-\frac{i\omega_+}{2\rho}\right)\Gamma\left(1-\frac{i\omega_+}{2\rho}\right)}, \quad \beta(k) = \sqrt{\frac{\omega_{out}}{\omega_{in}}} \frac{\Gamma\left(\frac{i\omega_{out}}{\rho}\right)\Gamma\left(1-\frac{i\omega_{in}}{\rho}\right)}{\Gamma\left(\frac{i\omega_-}{2\rho}\right)\Gamma\left(1+\frac{i\omega_-}{2\rho}\right)}$$

Using these values, and the general method of Section 2, we find that the ground state is of the gCC form (III.14),

$$|0, in\rangle = \exp[-\kappa_2 H - \sum_{n=2}^{\infty} \kappa_{2n} W_{2n}]|D\rangle$$

where the κ_n's are found by using (III.10), as follows:

$$\kappa_2 = \frac{i\left(\gamma + \psi^{(0)}\left(-\frac{im_0}{\rho}\right)\right)}{\rho}, \; \kappa_4 = \frac{-im_0\psi^{(2)}\left(-\frac{im_0}{\rho}\right) + 6\rho\psi^{(1)}\left(-\frac{im_0}{\rho}\right) + 7im_0\psi^{(2)}(1) + \pi^2\rho}{24m_0\rho^3} \tag{III.27}$$

where $\psi^{(n)}(z)$ is the n-th derivative of the digamma function $\psi(z) = \Gamma'(z)/\Gamma(z)$. In an expansion in $1/m_0, m_0/\rho$ (to be interpreted in the sense of Appendix III.E), these coefficients read as follows

$$\kappa_2 = \frac{1}{m_0}\left(1 + \frac{\pi^2}{12}\frac{m_0^2}{\rho^2} - i\frac{\zeta(3)}{4}\frac{m_0^3}{\rho^3} + ...\right), \; \kappa_4 = \frac{1}{m_0^3}\left(-\frac{5}{160} + \frac{\pi^2}{288}\frac{m_0^2}{\rho^2} + ...\right), \; ... \tag{III.28}$$

Note that these are functions of both the scales m_0, ρ characterizing the quench protocol. The coefficient of odd powers of (m_0/ρ) in this expansion turns out to be purely imaginary. Note that the κ_n's (in this case the first two, κ_2 and κ_4) encode the quench protocol (III.24) completely; since the κ_n's are related in a one-to-one fashion to equilibrium chemical potentials $\mu_n = 4\kappa_n$ (III.2), it follows that from the equilibrium state one can retrieve the quench history (see Section 6.2 for more details).
For later reference, the "out"-number operator (III.16) turns out to be

$$\langle N(k)\rangle = \text{csch}\left(\frac{\pi k}{\rho}\right)\sinh^2\left(\frac{\pi\left(k - \sqrt{k^2+m_0^2}\right)}{2\rho}\right)\text{csch}\left(\frac{\pi\sqrt{k^2+m_0^2}}{\rho}\right) \tag{III.29}$$

Once again, we verify, as in (III.17), that the time-evolved ground state can be exactly described by a gCC state, of the form (III.1).[16]

[16] We should note the distinction of this statement with the exact form in (III.17). Since for the "tanh" protocol, there is no finite time t_0 beyond which the Hamiltonian is time-dependent, one should use (III.17) here as an asymptotic statement, for $t \gg 1/\rho$, with exponentially small corrections $O(e^{-\rho t})$.

Sudden limit

We will be especially interested in the sudden limit ($\rho \to \infty$) of the above quench protocol

$$m^2(t) = m_0^2 \Theta(-t) \tag{III.30}$$

For later use, we note that in the sudden limit

$$\rho \to \infty, \tag{III.31}$$

the Bogoliubov coefficients become

$$\alpha(k) = \frac{1}{2} \frac{|k| + \omega_{in}}{\sqrt{|k|\omega_{in}}}, \ \beta(k) = \frac{1}{2} \frac{|k| - \omega_{in}}{\sqrt{|k|\omega_{in}}} \tag{III.32}$$

whereas the in- and out- waves become

$$u_{in}(k,t) = \frac{e^{-i\omega_{in}t}}{\sqrt{2\omega_{in}}}, \ u_{out}(k,t) = \frac{e^{-i\omega_{out}t}}{\sqrt{2\omega_{out}}} \tag{III.33}$$

The κ_n coefficients in this limit are given by taking the $\rho \to \infty$ limit of (III.28):

$$\kappa_2 = \frac{1}{m_0}, \ \kappa_4 = \frac{1}{m_0^3}\left(-\frac{5}{160}\right), \ ... \tag{III.34}$$

Thus,

$$|0, in\rangle = \exp[-\frac{H}{m_0} + \frac{5W_4}{160m_0^3} + ...]|D\rangle \tag{III.35}$$

which is a gCC state.[17] In the sudden limit, the number operator (III.29) becomes

$$\langle N(k)\rangle = \frac{\left(\sqrt{k^2 + m_0^2} - |k|\right)^2}{4\sqrt{k^2 + m_0^2}|k|} \tag{III.36}$$

A more precise and careful version of the sudden limit, than (III.31) is described in Appendix III.E.

2.5 Quenching from critical to critical

We will consider a quantum quench for the scalar field where both the initial and final masses vanish (i.e. a quench from a critical Hamiltonian to a critical Hamiltonian).

[17]One might be alarmed by the positive sign of the W_4-coefficient in this state. This would mean that if all the higher $\kappa_{n>3}$ were absent, $\kappa(k)$ would have grown as $+k^3$, hence implying a divergent norm of the gCC state $e^{-\sum_k \kappa(k)N(k)}|D\rangle$. However, such catastrophies are avoided by higher κ_n coefficients, as they must, since the gCC state is equal, as a Heisenberg state, to the initial ground state, which has a finite norm. We will have more to say in Appendix III.E on other possible divergences associated with the sudden limit.

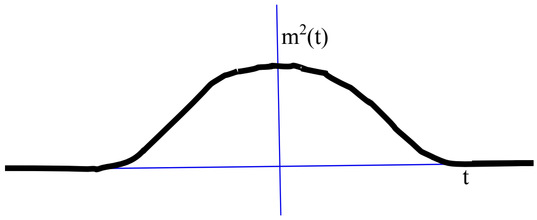

Figure III.2: A mass-profile describe quantum quench from a critical Hamiltonian back to the critical Hamiltonian. Here $m^2(t) \xrightarrow{t\to\pm\infty} 0$.

A typical mass function which follows this property is [40]:

$$m^2(t) = m_0^2 \,\text{sech}^2(\rho t). \tag{III.37}$$

Using the coordinate transformation $y = e^{2\rho t}$. The equation of motion, analogous to (III.5), becomes

$$\phi''(k,y) + \frac{\phi'(k,y)}{y} + \left(\frac{k^2}{4\rho^2 y} + \frac{m_0^2}{\rho^2(1+y)^2}\right)\phi(k,y) = 0 \tag{III.38}$$

With $\alpha = 1/2 + \frac{1}{\rho}\sqrt{4m_0^2+\rho^2}$, this equation can be solved to give

$$\begin{aligned} u(k,t) = e^{-ikt}(1+e^{2\rho t})^{\alpha}\Bigg[C_1\, e^{2ikt}\ {}_2F_1\left(\alpha, \frac{ik}{\rho}+\alpha, 1+\frac{ik}{\rho}, -e^{2\rho t}\right) \\ + C_2\, {}_2F_1\left(\alpha, -\frac{ik}{\rho}+\alpha, 1-\frac{ik}{\rho}, -e^{2\rho t}\right)\Bigg] \end{aligned} \tag{III.39}$$

$C_1 = 1$ and $C_2 = 0$ gives the incoming solution $u_{in}(k)$ which satisfies the property (III.99). On taking the $t \to +\infty$ limit of $u_{in}(k)$ we can express $u_{in}(k)$ in the form $\alpha(k)u_{out}(k)+\beta(k)u^*_{out}(k)$ (see Appendix III.A for more details), where

$$\alpha(k) = \frac{\Gamma\left(\frac{ik}{\rho}+1\right)\Gamma\left(\frac{ik}{\rho}\right)}{\Gamma\left(\frac{ik}{\rho}-\alpha+1\right)\Gamma\left(\frac{ik}{\rho}+\alpha\right)} \tag{III.40}$$

$$\beta(k) = i\sin(\pi\alpha)\text{cosech}\left(\frac{\pi k}{\rho}\right) \tag{III.41}$$

Using (III.9) and (III.10), we can express the in-vacuum in a gCC form (III.1) with

$$\kappa(k) = \frac{ik\rho}{2m_0^2} - \frac{k^2\rho^2}{4m_0^4} - \frac{ik^3\rho^3}{6m_0^6} + \frac{k^4\rho^4}{8m_0^8} + \frac{ik^5\rho^5}{10m_0^{10}} + \ldots, \tag{III.42}$$

which leads to

$$\kappa_2 = \frac{i\rho}{2m_0^2}, \kappa_3 = \frac{-\rho^2}{4m_0^4}.$$

Note that κ_2 is imaginary. By contrast, κ_2 in a massive quench, is real and positive (see e.g. (III.34)), and is identified with $\beta/4$ where β is the inverse temperature of the associated thermal state. With imaginary κ_2, such an identification is clearly problematic. We will find in the next section that starting with an appropriate squeezed state, one can manufacture a CC state with positive κ_2.

2.6 Quenching squeezed states

Suppose, instead of the ground state we start with a squeezed state[18] of the pre-quench Hamiltonian:[19]

$$|\psi, in\rangle = |f\rangle \equiv \exp\left[\frac{1}{2}\sum_k f(k) a_{in}^\dagger(k) a_{in}^\dagger(-k)\right] |0, in\rangle \tag{III.43}$$

This is clearly a Bogoliubov transformation of $|0, in\rangle$. To see this, note that $|f\rangle$ is annihilated by $a_{in}(k) - f(k)a_{in}(-k)$,

$$\begin{aligned} 0 &= \left[a_{in}(k) - f(k)a_{in}^\dagger(-k)\right] |f(k), in\rangle \\ &= \left[\alpha^*(k)a_{out}(k) - \beta^*(k)a_{out}^\dagger(-k) - f(k)\left\{\alpha(k)a_{out}^\dagger(-k) - \beta(k)a_{out}(k)\right\}\right] |f(k), out\rangle \\ &= \left[\left\{\alpha^*(k) + f(k)\beta(k)\right\} a_{out}(k) - \left\{\beta^*(k) + f(k)\alpha(k)\right\} a_{out}^\dagger(-k)\right] |f(k), out\rangle \end{aligned} \tag{III.44}$$

Thus, it follows that the squeezed pre-quench state is also expressible as a generalized CC state

$$|\psi, in\rangle = |f\rangle = \exp\left[\frac{1}{2}\sum_k \gamma_{\text{eff}}(k) a_{out}^\dagger(k) a_{out}^\dagger(-k)\right] |0, out\rangle \tag{III.45}$$

where the effective $\gamma_{\text{eff}}(k)$ is

$$\gamma_{\text{eff}}(k) = \frac{\beta^*(k) + f(k)\alpha(k)}{\alpha^*(k) + f(k)\beta(k)} \tag{III.46}$$

Using the result (III.45) and the method leading to (III.10), we can again show

$$\begin{aligned} |f\rangle &= \exp[\sum_k -\kappa_{\text{eff}}(k) a_{out}^\dagger(k) a_{out}(-k)] |D\rangle, \\ \kappa_{\text{eff}}(k) &\equiv -\frac{1}{2}\log\left(-\gamma_{\text{eff}}(k)\right) \end{aligned} \tag{III.47}$$

where $\kappa_{eff}(k)$ has an expansion of the form (III.13) as argued below.

General arguments from scattering theory: Using elements of scattering theory described in Appendix III.A, we can rewrite (III.46) as follows

$$\gamma_{\text{eff}}(k) = \left(\frac{f(k) - r'(k)}{1 - r'^*(k) f(k)}\right)\left(\frac{\alpha^*(k)}{\alpha(k)}\right) \tag{III.48}$$

[18] These states have importance in diverse contexts [38, 43] including quantum entanglement [39]. Time-development of these states can address the issue of dynamical evolution of quantum entanglement, among other things.

[19] We assume that the norm of the squeezed state is finite, which is ensured by the finiteness of the integral $\int dk/(2\pi)\log(1 - |f(k)|^2)$.

Here we have used $\beta^*(k) = -r'(k)\alpha(k)$, where $r'(k)$ is the dual reflection coefficient (III.97), which has a small momentum expansion (III.105) $r'(k) = 1 + O(k)$. Assuming $f(k)$ to be regular at $k = 0$ so that it admits an expansion $f(k) = f(0) + O(k)$, we find that the first factor in the RHS has an expansion $-1 + O(k)$. Using (III.106), the RHS has an expansion $-1+O(k)$, which ensures an expansion of κ_{eff} in (III.47) of the form (III.13).[20] We will list a number of examples below to find such an expansion of $\kappa(k)$.

Explicit Examples: In the first two examples, we fix the quench protocol to be given by the 'tanh' function (III.24), in the sudden limit $\rho \to \infty$. We will determine the κ_{eff} explicitly by using (III.47) and the expressions for the Bogoliubov coefficients (III.32). In the

- **Gaussian:** For a Gaussian squeezing function with variance proportional to m_0^2, ie. $f = \exp[-k^2/(a^2 m_0^2)]$, we get

$$\kappa_{eff}(k) = \frac{|k|}{a^2 m_0} + \frac{(6a^4+1)\,|k|^3}{12a^6 {m_0}^3} - \frac{(30a^8 - 10a^4 - 3)\,|k|^5}{240a^{10}{m_0}^5} + O(|k|^7) \qquad \text{(III.49)}$$

- **Preparing CC states and gCC states with specified parameters:** It is clear from (III.47) that given specific Bogoliubov coefficients, e.g. (III.32), we can obtain any desired expression for $\kappa_{eff}(k)$ by tailoring the choice of the squeezing function $f(k)$. Thus, e.g.

$$f(k) = 1 - \frac{2|k|}{\sqrt{k^2 + {m_0}^2}\tanh\left(\kappa_{2,0}|k| + \kappa_{4,0}|k|^3\right) + |k|} \qquad \text{(III.50)}$$

yields a function $\kappa_{eff}(k) = \kappa_{2,0}|k| + \kappa_{4,0}|k|^3$ with specified parameters $\kappa_2 = \kappa_{2,0}$, $\kappa_4 = \kappa_{4,0}$. This identifies the squeezed state with a gCC state with these κ-parameters:[21]

$$|\psi, in\rangle = |f\rangle = \exp[-\left(\kappa_{2,0}H + \kappa_{4,0}W_4\right)|D\rangle \qquad \text{(III.51)}$$

Specializing even more, we can manufacture $\kappa_{2,0} = 1/m_0, \kappa_4 = 0$, i.e. $\kappa_{eff} = \kappa_{2,0}k$, (cf. (III.34)) by choosing

$$f(k) = 1 - \frac{2|k|}{\sqrt{k^2 + {m_0}^2}\tanh\left(|k|/m_0\right) + |k|} \qquad \text{(III.52)}$$

which yields a CC state of the form

$$|\psi, in\rangle = |f\rangle = \exp\left[-\frac{1}{m_0}\sum_k |k| a_k^\dagger a_k\right]|D\rangle \qquad \text{(III.53)}$$

We note that these squeezing functions are localised functions which vanish at both $k \to 0$ and $k \to \infty$ limits and hence the resultant squeezed state is normalisable. Note that the functions $f(k)$ are even functions, and hence are actually functions of $|k|$.

---

[20] This does not ensure $\mathrm{Re}(\kappa_2) > 0$ by itself. We have to tailor the choice of $f(k)$'s to ensure it, as done in the examples below.

[21] Note that we choose here $\kappa_{2,0}$, $\kappa_{4,0}$ to be positive to ensure that the gCC state is of finite norm; see footnote 19.

- **Critical to critical:** Applying the above method to the quench protocol discussed in Section 2.5, we find that the following choice of the squeezing function

$$f(k) = \frac{a\left(-e^{2|k|\left(\kappa_{2,0}+\kappa_{4,0}k^2\right)}\right)+a-i|k|}{-a+(a+i|k|)e^{2|k|(\kappa_{2,0}+\kappa_{4,0}k^2)}}$$

leads to a gCC state $e^{-\kappa_{2,0}H-\kappa_{4,0}W_4}|D\rangle$. Specializing to

$$f(k) = \frac{a\left(-e^{2\kappa_{2,0}|k|}\right)+a-i|k|}{-a+(a+i|k|)e^{2\kappa_{2,0}|k|}}$$

leads to a CC state $e^{-\kappa_{2,0}H}|D\rangle$.

The propagator in a squeezed state

The propagator in a squeezed state $|\psi, in\rangle = |f\rangle$ is obtained by replacing $\alpha \to \alpha_{eff}$, $\beta \to \beta_{eff}$ in (III.22):

$$\begin{aligned}
&\langle\psi, in|\phi(x_1,t_1)\phi(x_2,t_2)|\psi, in\rangle \\
&= \int \frac{dk}{2\pi}\ \left[|\alpha_{eff}(k)|^2 u_{out}(k,t_1)u^*_{out}(k,t_2) + \alpha_{eff}(k)\beta^*_{eff}(k)u_{out}(k,t_1)u_{out}(-k,t_2)\right. \\
&\left. +\alpha^*_{eff}(k)\beta_{eff}(k)u^*_{out}(-k,t_1)u^*_{out}(k,t_2) + |\beta_{eff}(k)|^2 u^*_{out}(-k,t_1)u_{out}(-k,t_2)\right] e^{ik(x_1-x_2)}
\end{aligned} \tag{III.54}$$

3 Fermion theories with time-dependent mass

We will now consider fermion field theories with a time-dependent mass:

$$S = -\int d^2x(i\bar{\Psi}\gamma^\mu\partial_\mu\Psi - m(t)\bar{\Psi}\Psi)$$

Once again, a general analysis of an auxiliary Schrödinger problem can be performed [42], to infer the emergence of the general Calabrese-Cardy (gCC) state. However, we present below the analysis for a mass quench specific quench protocol, involving a *tanh* function, which describes quantum quench from a non-critical to a critical Hamiltonian.

We start with the Dirac equation with the following time-dependent mass:[42, 40]

$$m(t) = \frac{m_0}{2}\left(1-\tanh\left(\rho t\right)\right)$$

The Dirac equation is

$$\left(i\gamma^\mu\partial_\mu - m(t)\right)\Psi = 0 \tag{III.55}$$

The ansatz for a solution of this equation is

$$\Psi(k;x,t) = \left(\gamma^0\partial_t - \gamma^1\partial_x - im(t)\right)e^{\pm ikx}\Phi(k,t) \tag{III.56}$$

where $\Phi(k,t)$ is a two-component spinor that satisfies the following equation

$$\left(\partial_t^2 + k^2 + m^2(t) - i\gamma^0 \dot{m}(t)\right)\Phi(k,t) = 0 \tag{III.57}$$

Defining $\Phi = (\phi_+, \phi_-)^T$, the equations decouple in the eigenbasis of γ^0 in Dirac basis,

$$\left(\partial_t^2 + k^2 + m^2(t) \mp i\dot{m}(t)\right)\phi_\pm(k,t) = 0 \tag{III.58}$$

where $\phi_+(t)$ is the solution corresponding to γ^0 eigenvalue 1 and its part with asymptotic positive energy eigenvalues appears with the spinor $u(0)$ in the mode expansion of $\Psi(x,t)$. Similarly, $\phi_-(t)$ is the solution corresponding to γ^0 eigenvalue -1 and its part with asymptotic negative energy eigenvalues appears with the spinor $v(0)$ in the mode expansion of $\Psi(x,t)$. The conventions and the explicit solutions are described in Appendix III.D. The explicit solutions lead to the following expressions of Bogoluibov coefficients $\alpha_\pm(k)$ and $\beta_\pm(k)$

$$\alpha_\pm(k) = \frac{\Gamma\left(-\frac{i|k|}{\rho}\right)\Gamma\left(1-\frac{i\omega_{in}}{\rho}\right)}{\Gamma\left(1-\frac{i(|k|\mp m_0+\omega_{in})}{2\rho}\right)\Gamma\left(-\frac{i(|k|\pm m_0+\omega_{in})}{2\rho}\right)} \tag{III.59}$$

$$\beta_\pm(k) = \frac{\Gamma\left(\frac{i|k|}{\rho}\right)\Gamma\left(1-\frac{i\omega_{in}}{\rho}\right)}{\Gamma\left(-\frac{i(-|k|\pm m_0+\omega_{in})}{2\rho}\right)\Gamma\left(1-\frac{i(-|k|\mp m_0+\omega_{in})}{2\rho}\right)} \tag{III.60}$$

In terms of the 'out' oscillators, the 'in' ground state is

$$|\psi\rangle = \exp\left[\sum_{k=-\infty}^{\infty}\gamma(k)a^\dagger_{k,out}b^\dagger_{-k,out}\right]|0,in\rangle$$

where $\gamma(k) = \chi(k)\frac{\beta_+(k)^*}{\alpha_+(k)^*}$ (III.122). Using a similar BCH formula to (III.10) for fermionic creation and annihilation operators, we get

$$|\Psi\rangle = e^{-\kappa_2 H + \kappa_4 W_4 - \kappa_6 W_6 - \dots}|D\rangle \tag{III.61}$$

$$\text{where} \qquad \kappa_2 = \frac{1}{2m} + \frac{\pi^2 m}{12\rho^2} + \frac{1}{m}\,\mathcal{O}(m/\rho)^3,\ \kappa_4 = \frac{1}{12m^3} - \frac{\pi^2}{24m\rho^2} + \frac{1}{m^3}\,\mathcal{O}(m/\rho)^3,$$

$$\kappa_6 = \frac{3}{80m^5} - \frac{\pi^2}{96m^3\rho^2} + \frac{1}{m^5}\,\mathcal{O}(m/\rho)^3$$

and $|D\rangle$ is the Dirichlet state of the fermionic theory. Using the chiral mode expansion (IV.116) and (IV.117),

$$|D\rangle = e^{\sum_k \mathrm{sign}(k) a_k^\dagger b_{-k}^\dagger}|0\rangle \tag{III.62}$$

In writing the $\mathbb{W}_\infty$ charges for the fermions, we have used the currents mentioned in the Appendix III.D.[22]

[22] We choose the overall normalization of the $W_{2n}(z)$-currents so that the W_{2n} charges are given by $W_{2n} = \sum_k |k|^{2n-1}\left[a^\dagger(k)a(k) + b^\dagger(k)b(k)\right]$.

4 Exact time-dependent correlators

4.1 Ground state

In this section, we will consider the specific quench protocol discussed in Section 2.4.[23] Using the general computation (III.22) of the propagator and the specific values (III.32) and (III.33), we find

$$\begin{aligned}
G_{q,0}(x_1,t_1;x_2,t_2) \;\equiv\; & \langle 0,in|\phi(x_1,t_1)\phi(x_2,t_2)|0,in\rangle = \\
\int \frac{dk}{2\pi} G_{q,0}(k) \Bigg[& \left(2|k|\left(|k|+\sqrt{k^2+m_0^2}\right)+m_0^2\right)\left(\Theta(k)e^{-ik(x_2^- - x_1^-)}+\Theta(-k)e^{ik(x_2^+ - x_1^-)}\right) \\
& +\left(2|k|\left(|k|-\sqrt{k^2+m_0^2}\right)+m_0^2\right)\left(\Theta(k)e^{-ik(x_2^+ - x_1^+)}+\Theta(-k)e^{ik(x_2^- - x_1^-)}\right) \\
& -m_0^2\left(\Theta(k)e^{-ik(x_2^+ - x_1^-)}+\Theta(-k)e^{-ik(x_2^- - x_1^+)}\right) \\
& -m_0^2\left(\Theta(k)e^{-ik(x_2^- - x_1^+)}+\Theta(-k)e^{-ik(x_2^+ - x_1^-)}\right)\Bigg]
\end{aligned} \tag{III.63}$$

where we have defined $x_i^\pm = x_i \pm t_i$, $i=1,2$. Note that the last two lines involve the combinations t_1+t_2, which reflect the fact that time-translation invariance is lost due to the time-dependent perturbation. In the above expression

$$G_{q,0}(k) = \frac{1}{8|k|^2\sqrt{k^2+m_0^2}} \tag{III.64}$$

is the significant part of the above propagator. Singularities of this quantity in the k-plane are explained Figure III.3: these are a double pole at $k=0$ and two branch points on the imaginary axis, at $k=\pm i m_0$.

After performing the Fourier transforms, the propagator is given by:

$$\begin{aligned}
& G_{q,0}(x_1,t_1;x_2,t_2) \\
& = \frac{1}{8\pi}\Bigg(-G_{1,3}^{2,1}\left(\frac{m_0^2}{4}\left(x_2^- - x_1^+\right)^2 \,\middle|\, \begin{matrix}\frac{3}{2}\\ 0,1,\frac{1}{2}\end{matrix}\right)+G_{1,3}^{2,1}\left(\frac{m_0^2}{4}\left(x_2^- - x_1^-\right)^2 \,\middle|\, \begin{matrix}\frac{3}{2}\\ 0,1,\frac{1}{2}\end{matrix}\right) \\
& + G_{1,3}^{2,1}\left(\frac{m_0^2}{4}\left(x_2^+ - x_1^+\right)^2 \,\middle|\, \begin{matrix}\frac{3}{2}\\ 0,1,\frac{1}{2}\end{matrix}\right)-G_{1,3}^{2,1}\left(\frac{1}{4}m_0^2\left(x_2^+ - x_1^-\right)^2 \,\middle|\, \begin{matrix}\frac{3}{2}\\ 0,1,\frac{1}{2}\end{matrix}\right) \\
& + 4K_0\left(m_0\left|x_2^- - x_1^-\right|\right)+4K_0\left(m_0\left|x_2^+ - x_1^+\right|\right) \\
& +2i\pi\,\mathrm{sgn}\left(x_2^- - x_1^-\right)-2i\pi\,\mathrm{sgn}\left(x_2^+ - x_1^+\right)\Bigg)
\end{aligned} \tag{III.65}$$

For $x_2 - x_1 = r$ and $t_1 = t_2 = t$, in the asymptotic limit this becomes

$$\begin{aligned}
G_{q,0}(0,t;r,t) &= \frac{1}{8}\left(m_0(2t-r)\right)+\frac{1}{8\sqrt{2\pi m_0}}\left(\frac{e^{-m_0(2t-r)}}{\sqrt{2t-r}}+\frac{e^{-m_0(r+2t)}}{\sqrt{r+2t}}+\frac{2e^{-m_0 r}}{\sqrt{r}}\right)+\ldots \quad r<2t \\
&= \frac{1}{8\sqrt{2\pi m_0}}\left(\frac{e^{-m_0(r-2t)}}{\sqrt{r-2t}}+\frac{e^{-m_0(r+2t)}}{\sqrt{r+2t}}+\frac{2e^{-m_0 r}}{\sqrt{r}}\right)+\ldots \quad r>2t
\end{aligned}$$

[23]Note that the quantities defined in Section 2.4 are obtained by a naive definition of the sudden limit (III.31). As explained in Appendix III.E, although for W_4 and higher charges, this definition has be refined as in (III.123), for correlator calculations we can continue to use the naive definition.

The linear terms are dictated by the double pole at the origin of the k-plane. These agree with the expressions obtained by [111] in the so-called deep quench limit (see Section 6 for more details). The ellipsis represent higher transients.

Correlators:

- Two-point functions of vertex operators $O_q = e^{iq\phi}$: The dominant behaviour in the IR limit is given by exponentiaing the linear part in the above $\langle\phi\phi\rangle$ propagator (after subtracting the coincident part). We get

$$\langle 0, in|e^{iq\phi(0,t)}e^{-iq\phi(r,t)}|0, in\rangle = e^{-\frac{q^2}{8}m_0 r}, \quad t > r/2 \tag{III.66}$$

  This result agrees with that in [111]. The dominant exponential is, again, given by the double pole at the origin of the k-plane. As remarked in Figure III.3, the thermal correlator is also dominated by this double pole at the origin. It is no surprise therefore that the above result (III.66) exactly agrees with the thermal result (III.87), with the identification $\beta = 4\kappa_2 = 4/m_0$.

- Two-point functions of the holomorphic operator: $O = \partial\phi$,[24]

$$\begin{aligned}
&\langle 0, \text{in}|\partial\phi(x_1,t_1)\partial\phi(x_2,t_2)|0,\text{in}\rangle \\
&= \int \frac{dk\, e^{ikr}}{2\pi\sqrt{k^2+m_0^2}} \left[\Theta(-k)(2|k|(k^2+m_0^2)^{1/2}+2k^2+m_0^2) + \Theta(k)(-2|k|(k^2+m_0^2)^{1/2}+2k^2+m_0^2)\right] \\
&= -\frac{m_0^2}{8\pi} K_2(m_0 r) \xrightarrow{r\to\infty} -e^{-m_0 r}\left(+\frac{m_0^{3/2}\sqrt{\frac{1}{r}}}{8\sqrt{2\pi}} + \frac{15\sqrt{m_0}\left(\frac{1}{r}\right)^{3/2}}{64\sqrt{2\pi}} + O\left[\frac{1}{r}\right]^{5/2}\right)
\end{aligned} \tag{III.67}$$

  where we have chosen $r = x_1 - x_2, t_1 = t_2$ (note that there is no time-dependence for equal times in this case, as we expect for holomorphic operators since these do not 'see' the boundary that represents the quench).

  Note that the derivatives annihilate the double pole at the origin of the k-plane, hence the two-point function is dictated solely by the distant singularity. Consequently, the rate of fall-off is NOT universal (see Section 6 for further details).

- Two-point functions $\langle\partial\phi\,\bar\partial\phi\rangle$:

$$\begin{aligned}
&\langle 0, \text{in}|\partial\phi(x_1,t)\bar\partial\phi(x_2,t)|0,\text{in}\rangle \\
&= -\int \frac{dk}{2\pi}\frac{m_0^2\, e^{ik(r+2t)}}{8(k^2+m_0^2)^{1/2}} = -\frac{m_0^2}{8\pi} K_0(m_0(r+2t))
\end{aligned} \tag{III.68}$$

[24] We define $\partial = \frac{1}{2}(\partial_x + \partial_t)$, $\bar\partial = \frac{1}{2}(\partial_x - \partial_t)$.

- One-point function $\langle \partial\phi\bar{\partial}\phi \rangle$:

$$
\begin{aligned}
&\langle 0,\mathrm{in}|\partial\phi\bar{\partial}\phi(x,t)|0,\mathrm{in}\rangle \\
&= -\int \frac{dk}{2\pi}\,\frac{m_0^2\, e^{i2kt}}{8(k^2+m_0^2)^{1/2}} = -\frac{m_0^2}{8\pi}\,K_0(2m_0t) \\
&\xrightarrow{t\to\infty} -e^{-2m_0t}\left[\frac{m_0^{3/2}\sqrt{\frac{1}{t}}}{16\sqrt{\pi}} - \frac{\sqrt{m_0}\left(\frac{1}{t}\right)^{3/2}}{256\sqrt{\pi}} + O\left(\frac{1}{t}\right)^{5/2}\right]
\end{aligned}
\tag{III.69}
$$

We also present a calculation of the energy density. In the $t\to\infty$ limit,

$$
\frac{E}{L} = m_0^2/(8\pi) \tag{III.70}
$$

Note that it does not agree with (III.88) with $\beta = 4/m_0$. In other words, the higher chemical potentials affect the asymptotic energy density.

4.2 Correlators in Squeezed States

The expression for the $\langle f|\phi\phi|f\rangle$ propagator in a squeezed is given in (III.54). In this section we will compute these in the squeezed states (III.50) which are tailored to produce a given real value of $\kappa_2 > 0$ and κ_4 (with all other $\kappa_n = 0$). We find

$$
\begin{aligned}
\langle \phi\phi \rangle &= \int \frac{dk}{4\pi}\frac{e^{ikr}}{|k|}\left(\coth\left(2|k|\left(\kappa_2+\kappa_4k^2\right)\right) - \cos(2|k|t)\mathrm{cosech}\left(2|k|\left(\kappa_2+\kappa_4k^2\right)\right)\right) \\
&= \int \frac{dk}{2\pi}\frac{e^{ikr}}{|k|}\left(\frac{1}{e^{4|k|(\kappa_2+\kappa_4k^2)}-1} - \frac{1}{2}\cos(2|k|t)\mathrm{cosech}\left(2|k|\left(\kappa_2+\kappa_4k^2\right)\right)+\frac{1}{2}\right) \\
\langle \partial\phi\partial\phi \rangle &= \int_0^\infty \frac{dk}{8\pi}e^{ikr}k\left(\coth\left(2k\kappa_2+2k^3\kappa_4\right)-1\right) \\
\langle \partial\phi\bar{\partial}\phi \rangle &= \int \frac{dk}{8\pi}e^{-2ikt}k\ \mathrm{cosech}\left(2\kappa_2k+2k^3\kappa_4\right)
\end{aligned}
\tag{III.71}
$$

The first two equations describe two-point functions with $(x_1,t_1) = (0,t)$, $(x_2,t_2) = (r,t)$, whereas the third equation is a one-point function at a point (x,t) (which is independent of x by translational invariance). In the propagator, the last term in the second line gives the usual $-log(r)$ term of free scalar in 2D spacetime.

With $\kappa_4 = 0$, i.e., for the CC state $e^{-\kappa_2 H}|D\rangle$, the integrals can be done exactly and energy density can also be calculated exactly,

$$
\langle \phi\phi \rangle = \frac{\log\left(\frac{1}{2}\mathrm{csch}^2\left(\frac{\pi r}{4\kappa_2}\right)\left(\cosh\left(\frac{\pi r}{2\kappa_2}\right)+\cosh\left(\frac{\pi t}{\kappa_2}\right)\right)\right)}{8\pi} \tag{III.72}
$$

$$
\langle \partial\phi\partial\phi \rangle_{CC} = -\frac{\pi\mathrm{cosech}^2\left(\frac{\pi r}{4\kappa_2}\right)}{64\kappa_2^2} \tag{III.73}
$$

$$
\langle \partial\phi\bar{\partial}\phi \rangle_{CC} = -\frac{\pi}{64\kappa_2^2}\,\mathrm{sech}^2\left(\frac{2\pi t}{4\kappa_2}\right) \tag{III.74}
$$

These results have also been obtained using BCFT in [44]. The energy density is

$$\frac{E}{L} = \frac{\pi}{96\kappa_2^2} \tag{III.75}$$

This agrees with the thermal energy density in (III.88) with $\beta = 4\kappa_2$.

With non-zero κ_4, let us first consider $\langle \partial\phi\bar{\partial}\phi\rangle$. The associated Fourier transform can be computed by contour integration. Note that the cosech function has simple poles in the k-plane at $2\kappa_4 k^3 + 2\kappa_2 k = i\pi n$. Thus, there are three simple poles for each n (see Figure III.3), given by

$$\begin{aligned}
k_1 &= \frac{-2\ 6^{2/3}\kappa_2 + \sqrt[3]{6}\left(\sqrt{48\kappa_2^3 - 81\pi^2\kappa_4 n^2} + 9i\pi\sqrt{\kappa_4}n\right)^{2/3}}{6\sqrt[3]{\sqrt{3}\sqrt{\kappa_4^3\left(16\kappa_2^3 - 27\pi^2\kappa_4 n^2\right)} + 9i\pi\kappa_4^2 n}} \\
k_2 &= \frac{4\sqrt[3]{-6}\kappa_2 + i\left(\sqrt{3}+i\right)\left(\sqrt{48\kappa_2^3 - 81\pi^2\kappa_4 n^2} + 9i\pi\sqrt{\kappa_4}n\right)^{2/3}}{2\ 6^{2/3}\sqrt[3]{\sqrt{3}\sqrt{\kappa_4^3\left(16\kappa_2^3 - 27\pi^2\kappa_4 n^2\right)} + 9i\pi\kappa_4^2 n}} \\
k_3 &= -\frac{\sqrt[3]{-1}\left(2\sqrt[3]{-6}\kappa_2 + \left(\sqrt{48\kappa_2^3 - 81\pi^2\kappa_4 n^2} + 9i\pi\sqrt{\kappa_4}n\right)^{2/3}\right)}{6^{2/3}\sqrt{\kappa_4}\sqrt[3]{\sqrt{48\kappa_2^3 - 81\pi^2\kappa_4 n^2} + 9i\pi\sqrt{\kappa_4}n}}
\end{aligned} \tag{III.76}$$

In an expansion in small κ_4, we get

$$k_1 = \frac{i\pi n}{2\kappa_2} + \frac{i\pi^3\kappa_4 n^3}{8\kappa_2^4} + \frac{3i\pi^5\kappa_4^2 n^5}{32\kappa_2^7} + \frac{3i\pi^7\kappa_4^3 n^7}{32\kappa_2^{10}} \tag{III.77}$$

$$k_2 = \frac{i\sqrt{\kappa_2}}{\sqrt{\kappa_4}} - \frac{i\pi n}{4\kappa_2} - \frac{3i\pi^2\sqrt{\kappa_4}n^2}{32\kappa_2^{5/2}} - \frac{i\pi^3\kappa_4 n^3}{16\kappa_2^4} \tag{III.78}$$

$$k_3 = -\frac{i\sqrt{\kappa_2}}{\sqrt{\kappa_4}} - \frac{i\pi n}{4\kappa_2} + \frac{3i\pi^2\sqrt{\kappa_4}n^2}{32\kappa_2^{5/2}} - \frac{i\pi^3\kappa_4 n^3}{16\kappa_2^4} \tag{III.79}$$

Out of these poles, it is clear that in the perturbative regime ($\kappa_4 \ll \kappa_2^3$), only k_1 will contribute. This is because a pole at $k = -ik_0$ will turn up in $e^{-2k_0 t}$ and so large values of k_2 and k_3 will contribute highly damped solutions (note that poles in the upper half plane do not contribute for $t > 0$). Thus, k_1 is the pole whose residue we are interested in for comparison with perturbative results. In practice, to get non-perturbative results, we would have to take into account the residues at the other two poles as well. Note that the pole at the origin (for $n = 0$) is cancelled by the k multiplying the cosech.

From the expansion of $\operatorname{cosech}\left(2\kappa_4\left(k-k_1\right)\left(k-k_2\right)\left(k-k_3\right)+i\pi n\right)$ around k_1, we find the residue of cosech to be

$$\frac{(-1)^n}{2\kappa_4\left(k_1-k_2\right)\left(k_1-k_3\right)} \tag{III.80}$$

Taking the leading order of the cosech residue which is given by the $n = \pm 1$ poles, we find the total residue

$$= -\frac{\pi}{16\kappa_2^2}\left(1 + 4\pi^2\tilde{\kappa}_4 + 48\pi^4\tilde{\kappa}_4^2\right)\exp\left(-\frac{4\left(\pi + 4\pi^3\tilde{\kappa}_4 + 48\pi^5\tilde{\kappa}_4^2\right)t}{4\kappa_2}\right) \tag{III.81}$$

where $\tilde{\kappa}_4 = \frac{\kappa_4}{4^2\kappa_2^3}$.

Comparison with MSS: Using the charge under the μ_4 current $q_4 = 3$, $\beta = 4\kappa_2$ and $\tilde{\kappa}_4 = \tilde{\mu}_4$, we match the results of MSS exactly. Note that above, $\tilde{\mu}_4^2 t$ also exponentiates, so this gives the behaviour expected by MSS and higher orders.

The computation of $\langle \partial\phi\partial\phi \rangle$ follows along similar lines. Here, the poles are the same. The only difference is the residue of coth at k_1 which is

$$\frac{1}{2\kappa_4\left(k_1 - k_2\right)\left(k_1 - k_3\right)} \tag{III.82}$$

Thus the total residue is similar to the earlier case.

$$= \frac{\pi}{16\kappa_2^2}\left(1 + 4\pi^2\tilde{\kappa}_4 + 48\pi^4\tilde{\kappa}_4^2\right)\exp\left(-\frac{2\left(\pi + 4\pi^3\tilde{\kappa}_4 + 48\pi^5\tilde{\kappa}_4^2\right)r}{4\kappa_2}\right) \tag{III.83}$$

which shows twice the relaxation rate as before (as expected from MSS).

5 Real time propagator in a GGE

We first review the purely thermal case briefly.

Real time propagator in a thermal ensemble Consider the real time, thermal Wightman propagator (see, e.g. [29] for the various definitions of propagators)

$$\begin{aligned} G_+(x_1, t_1; x_2, t_2; \beta) &\equiv \frac{1}{Z}\mathrm{Tr}\left(e^{-\beta H}\phi(x_2, t_2)\phi(x_1, t_1)\right) \\ &= \frac{1}{Z}\sum_{\{N_n\}}\langle\{N_n\}|\phi(x_1)e^{-itH}\phi(x_2)e^{-itH}e^{-\beta H}|\{N_n\}\rangle \end{aligned} \tag{III.84}$$

By using the occupation number representation of the Hamiltonian, it is easy to derive the following result ($x = x_2 - x_1, t = t_2 - t_1$):

$$\begin{aligned} G_+(x_1, t_1; x_2, t_2; \beta) = \frac{1}{2}\int\frac{dk}{2\pi}\left[G_+(k;\beta)e^{ikx - i|k|t} + G_-(k;\beta)e^{-ikx + i|k|t}\right], \\ G_\pm(k, \beta) = \frac{1}{|k|(\pm e^{\pm\beta|k|} \mp 1)} \end{aligned} \tag{III.85}$$

The two-point function of $\partial\phi$ is, therefore,

$$\frac{1}{Z}\mathrm{Tr}\left(e^{-\beta H}\partial\phi(x_2, t_2)\partial\phi(x_1, t_1)\right) = \frac{1}{2}\int\frac{dk}{2\pi}\frac{k\ e^{-ik(x+t)}}{e^{\beta|k|} - 1} = -\frac{\pi}{4\beta^2}\frac{1}{\sinh^2(\pi(x+t)/\beta)} \tag{III.86}$$

which is the well-known result obtained from CFT techniques [44].

It is also easy to compute from the above the thermal two-point function of exponential vertex operators

$$\langle \exp[iq\phi(0,t)] \exp[-iq\phi(r,t)]\rangle_\beta = \exp[-q^2 r/2\beta] \tag{III.87}$$

Note that this result agrees with the expected result [44] from conformal field theory $\exp[-2\pi\Delta r/\beta]$, using $\Delta = q^2/4\pi$ (see Appendix III.C).

The energy density in a thermal ensemble is

$$\frac{E}{L} = \frac{\pi}{6\beta^2} \tag{III.88}$$

We will now define the Wightman function in a GGE in an analogous fashion (for simplicity we consider only one chemical potential μ_4 here; the generalization to arbitrary number of chemical potentials is obvious):

$$\begin{aligned} G_+(x_1,t_1;x_2,t_2;\beta,\mu_4) &\equiv \frac{1}{Z}\mathrm{Tr}\left(e^{-\beta H-\mu_4 W_4}\phi(x_2,t_2)\phi(x_1,t_1)\right) \\ &\equiv \frac{1}{Z}\sum_{\{N_n\}}\langle\{N_n\}|\phi(x_1)e^{-itH}\phi(x_2)e^{-itH}e^{-\beta H-\mu_4 W_4}|\{N_n\}\rangle \end{aligned} \tag{III.89}$$

By a simple evaluation, this turns out to be

$$\begin{aligned} G_+(x_1,t_1;x_2,t_2;\beta,\mu_4) = \frac{1}{2}\int\frac{dk}{2\pi}&\left[G_+(k;\beta,\mu_4)e^{ikx-i|k|t} + G_-(k;\beta,\mu_4)e^{-ikx+i|k|t}\right], \\ G_\pm(k;\beta,\mu_4) &= \frac{1}{|k|(\pm e^{\pm(\beta|k|+\mu_4|k|^3)}\mp 1)} \end{aligned} \tag{III.90}$$

The holomorphic two-point function is now given by

$$\begin{aligned} \frac{1}{Z}\mathrm{Tr}\left(e^{-\beta H}\partial\phi(x_2,t_2)\partial\phi(x_1,t_1)\right) &= \frac{1}{2}\int_0^\infty \frac{dk}{2\pi}\frac{k\ e^{-ik(x+t)}}{e^{\beta|k|+\mu_4|k|^3}-1} \\ &= \frac{1}{4}\int_0^\infty\frac{dk}{2\pi}k\ e^{-ik(x+t)}\left(\coth(\beta|k|/2+\mu_4|k|^3/2)-1\right) \end{aligned} \tag{III.91}$$

which exactly matches (III.71) provided we define, in keeping with (III.2)

$$\beta = 4\kappa_2,\ \mu_4 = 4\kappa_4 \tag{III.92}$$

The explicit evaluation of this Fourier transform is carried out below (III.71).

6 Thermalization

In the previous two sections, we found that the exact correlators show thermalization at late times. Here's a brief summary for some specific correlators

	Ground state $\|0, in\rangle$	CC state $e^{-H_0/m_0}\|D\rangle$	Thermal state
$\langle\partial\phi(0,t)\partial\phi(r,t)\rangle$	$\sim e^{-m_0 r}/\sqrt{r}$	$\sim e^{-\pi m_0 r/2}$	$\sim e^{-\pi m_0 r/2}$
$\langle e^{iq\phi(0,t)}e^{-iq\phi(r,t)}\rangle$	$\sim e^{-q^2 m_0 r/8}$	$\sim e^{-q^2 m_0 r/8}$	$\sim e^{-q^2 m_0 r/8}$
energy density $\langle H\rangle$	$m_0^2/(16\pi)$	$\pi m_0^2/96$	$\pi m_0^2/96$
$\langle\partial\phi\bar{\partial}\phi(0,t)\rangle$	$\sim e^{-2m_0 t}/\sqrt{t}$	$\sim e^{-\pi m_0 t}$	0

Table III.1: The 2nd and 3rd columns give equal time correlators at late times for a mass quench (III.30); the 4th column gives the same correlator (time-independent) in a thermal state with $\beta = 4/m_0$. In the 2nd-column the initial state is the ground state $|0, in\rangle$; in the 3rd column, the initial state is a special squeezed state (III.53) which is of the Calabrese-Cardy form $e^{-H/m_0}|D\rangle$. In the first two rows, we list two-point functions at seperated points. In the 3rd row we list the asymptotic energy density. In the 4th row, we list the late time behaviour of a one-point function; the vanishing asymptotic value agrees with the thermal state— but we compare here the exponential decay in time between the second and third columns. Note that the asymptotic values always agree between the CC state and the thermal state, but barring the case of the exponential vertex operator, the late time behaviour differs from the CC state, signifying nontrivial modification of the behaviour by the higher chemical potentials.

Besides this, we also find an exact agreement between $t \to \infty$ correlators in the gCC state (III.50) and in the corresponding GGE (*cf.* equations (III.71) and (III.91)) with chemical potentials $\mu_n = 4\kappa_2$. The relaxation rate of one-point functions is seen to exactly exponentiate (see (III.81)), and its perturbation expansion in the higher κ_n coefficients agrees with the MSS value (III.3). We also found in the previous two sections that generically GGE correlators (equivalently, late time correlators in a gCC state) and thermal correlators (equivalently late time correlators in a CC state), characterized by the same temperature (equivalently same κ_2) are different, even at large distances (e.g. κ_4 appears in the correlation length in (III.83)).

It is clear from the above discussion and Table III.1 that while the fact of thermalization is true, the late time exponents depend nontrivially on the higher chemical potentials (or higher κ_n's), even though these correspond to perturbation by irrelevant operators in an RG sense. In the next subsection we address this issue of sensitivity to irrelevant operators in some detail. In the following subsection we will discuss a second (related) issue of memory retention by the equilibrium ensemble through the higher chemical potentials.

6.1 UV/IR mixing

In this section we will discuss the issue of large distance/time universality (or the lack thereof) in a critical quench. A useful guide in this turns out to be the pole structure of the propagator $\langle\phi(k)\phi(-k)\rangle$, which is explained in Figure III.3.

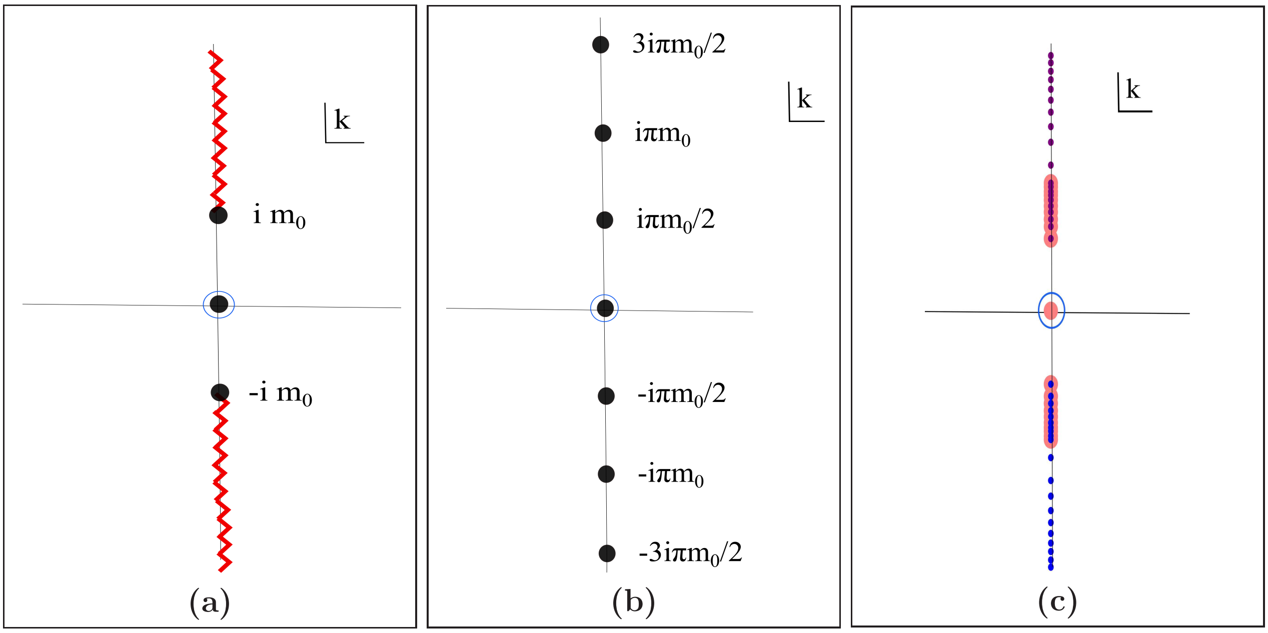

Figure III.3: Singularities governing the two-point function in the complex k-plane: **(a)** of the quantity $G_{q,0}(k)$ for the ground state quench propagator (III.63), **(b)** of the quantity $G_{\pm}(k;\beta)$ in the thermal propagator (III.86), **(c)** of the quantity $G_{\pm}(k;\beta,\mu_4)$ in the GGE propagator (III.90) with $\beta = 2, \mu_4 = 0.2$; we have shown 30 leading poles. In each case the pole at the origin is a double pole, and yields the universal linear large distance behaviour of $\langle\phi\phi\rangle$. Due to the equivalence between the quenched state and the gCC state (III.14), the branch cut in (a) can be seen as a limiting case of an accumulation of single poles in a generalized version of (c) with an infinite number of chemical potentials determined by (III.34),(III.92). *In two-point functions such as $\langle\partial\phi\partial\phi\rangle$, the double poles disappear and the large distance behaviour is sensitive to the sub-leading singularities, which are clearly different. This shows different types of large distance behaviour which are sensitive to the presence of higher dimensional operators.*

Universality: Let us first discuss the naive argument for universality in the present context. Note that in case of the sudden quench we found (III.35)

$$|0, in\rangle = \exp[-\frac{H}{m_0} - \frac{5W_4}{160m_0^3} + ...]|D\rangle$$

which would appear to imply that, in the limit when the scale of the quench is very high: $m_0 \to \infty$, the contribution of the Hamiltonian is the most dominant and those of the higher dimensional operators W_{2n}, $n > 1$, are subdominant. This argument, of course, is flawed, since m_0 is dimensionful, and we have to specify m_0 is large compared to what.

There are, of course, more refined arguments for universality which define an IR limit in terms of dimensionless distances and times

$$m_0 r, m_0 t \gg 1 \tag{III.93}$$

which is called the deep quench limit in [111]. Ref. [111] argues that in this limit, the propagator in (III.63) is dominated by the leading expansion of the integrand in $|k|/m_0$, which is given by a double pole. From (III.65), we find that the leading behaviour of this propagator is indeed given by the linear term which is solely determined by this double pole. We find that this double pole and the consequent leading behaviour exactly coincides with that of the thermal propagator (III.86). Indeed, all the three propagators, the quenched one (III.63), the thermal one (III.86) and the GGE one (III.90), coincide in the leading behaviour. Thus, the higher order chemical potentials do not modify the leading behaviour. Note, however, that the subleading behaviours are rather different in the three cases: the exponents are different, as well as in the quenched propagator there is a prefactor involving a square root.

Lack of Universality: The long-distance/time leading behaviour of the $\langle\phi\phi\rangle$ propagator is, of course, a rather limited part of the story. Does the above universality hold for correlators involving other operators, in particular, primary fields (recall that ϕ is not a primary field)?

To address this issue for one-point functions of primary fields of the kind $O(z,\bar{z}) = \varphi(z)\varphi^*(\bar{z})$ which has a decay rate given by (III.2), (III.3). For the sudden quench discussed in Section 2.4, using (III.34), we find that the fractional contribution of W_{2n} to the relaxation rate (III.3) is determined by the dimensionless quantity

$$\tilde{\mu}_n = \mu_n/\beta^{n-1} \sim \frac{1}{m_0^{n-1}} / \left(\frac{1}{m_0}\right)^{n-1}$$

which is of order one! What has happened is that, since the quench is characterized by a single scale, the chemical potentials due to the higher dimensional operators are determined by the same mass scale as the temperature, thus the dimensionless contribution due to $W_{n>2}$ is necessarily of order one. We would expect this kind of behaviour in any single-scale quench.

Indeed, we find in (III.68) that the leading behaviour of the one-point function of $\partial\phi\bar{\partial}\phi$ is not given by the thermal value (nor with any finite number of chemical potentials). This is best understood by looking at the Figure III.3. The derivatives $\partial, \bar{\partial}$ kill off the double pole at the origin in all three diagrams, leaving singularities away from the origin. These in Figure (a) differ from those in Figure (b) or in Figure (c). Figure (c), if redone with infinite number of chemical potentials as given by (III.34), reproduce the singularities of Figure (a).

Thus, we find that ALL higher dimensional operators are equally important in determining the long time behaviour of this operator. This is what we anticipated also from the MSS expression for the relaxation rate, as explained above.

The same story holds for two-point functions $\langle O(x_1,t_1)O(x_2,t_2)\rangle$. The exact quench computation, even in the deep quench limit (III.93) is not reproduced by the thermal result or any finite number of chemical potentials. This can be explicitly seen for $O = \partial\phi$ in the previous two sections. We have also verified this lack of universality for operators which are a composite of 'derivative' operators and exponential vertex operators, e.g. $O = \partial\phi e^{iq\phi}$. Once again, the reason is the annihilation of the double pole at the origin by these generic operators.

It is only the pure exponential vertex operators $O = e^{iq\phi}$ whose two-point functions (III.66) respect universality in the deep quench limit, that is it is reproduced by the thermal behaviour (these operators do not annihilate the pole at the origin).

Conclusion Generically universality, as defined above, is violated. Long time/distance behaviour is affected by perturbing the initial state by higher dimensional operators.

6.2 Memory retention

In this section we will discuss the issue of non-standard thermalization in the models studied where the equilibrium chemical potentials allow a reconstruction of the quench protocol (completely or partially depending on the situation).

Let us first consider the case of quenches from a ground state. As is clear from (III.10) and (III.9), the κ_n-coefficients of the gCC state (III.14) have a one-to-one relation to the reflection amplitude $r(k)$ of the potential scattering problem discussed in Appendix III.A. Now, it is well-known that the potential of a one-dimensional Schrodinger problem [45][25] can be reconstructed from the reflection amplitude $r(k)$. This implies, through the above correspondence between the quench problem and the scattering problem, that $m(t)$ can be reconstructed from $\kappa(k)$. This, in turn, means that the μ_n's carry complete knowledge of the quench protocol $m(t)$. Thus, the equilibrium ensemble remembers the quench protocol! As an example, the coefficients κ_n in (III.28) can be used to determine the parameters m_0 and ρ which specify the quench protocol $m(t)$ completely.

In case we consider a squeezed pre-quench state, the GGE is characterized by the function $\kappa_{eff}(k)$ (III.47) which is given by a combination of the knowledge of the squeezing function $f(k)$ and the quench protocol $m(t)$ (see (III.48)). For a given quench protocol, the initial state, characterized by $f(k)$ can be completely determined by the κ_n-parameters (see, e.g. (III.50)).

Thus, in case the pre-quench initial state as well as the quench protocol are unknown, the equilibrium ensemble has an imperfect recollection of the history.

7 Discussion

In this work, we explicitly verify for actual critical quenches the ansatz made in MSS for the generalized Calabrese-Cardy form (gCC) (III.1) of the initial state. We show that for an *arbitrary* mass quench in a theory of free scalars as well as in a theory of free fermions, a large choice of pre-quench initial states (ground state or squeezed states) leads to a gCC state. We find that our results hold even when the quantum quench begins and ends in a massless theory, although in this case, the putative temperature sometimes turns out to be imaginary and the issue of thermalization in these cases is subtle.

We find that while the ground state and generic squeezed states lead to gCC states with all infinite number of κ_n parameters present, one can choose special squeezed states to prepare gCC states with specific values of any given number of the κ_n-parameters; in particular we can prepare a CC state of the form $e^{-\kappa_2 H}|D\rangle$ from special squeezed states.

We compute the exact propagator in these quenches and hence the exact time-dependence of correlators. We find that the correlators thermalize at long times and the results verify those of MSS wherever a comparison is possible. We have a simple understanding of the identification (III.2) of the κ_n's with the chemical potentials μ_n in terms of poles of the propagator. In specially prepared gCC states with non-zero values of κ_2 and κ_4, we show that the exponential decay given by the relaxation rate (III.3) persists non-perturbatively in κ_4.

[25] We thank Basudeb Dasgupta for pointing out this reference to us.

We point out that the presence of the extra charges in the gCC state, which are higher dimensional operators, non-trivially modify the long distance and long time behaviour of correlators, in apparent contradiction to Wilsonian universality. This is an example of a UV/IR mixing; operators which are expected to be relevant in the UV by usual RG arguments are found here to affect the IR behaviour of various correlators. We present an understanding of this in terms of poles of the propagator in the complex momentum plane. We find that while exponential vertex operators do not suffer from these 'non-universal' corrections, all other operators (derivatives and composites of derivatives and exponentials) do show this non-universal behaviour.

We also find another atypical behaviour, related to the above: the equilibrium ensemble remembers about the quench protocol. In case we start from the ground state of the pre-quench Hamiltonian, the chemical potentials of the GGE encode a complete knowledge of the quench protocol $m(t)$. With pre-quench squeezed state, the chemical potentials encode a combination of information about the initial state and the quench protocol.

7.1 Higher spin black holes

In MSS we have established a relation between thermalization to a GGE and, in the holographic dual, quasinormal decay to a higher spin(hs) black hole. In particular, we have found that relaxation rate in the former process is equal to the imaginary part of the quasinormal frequency involved in the latter process.

The demonstration above depended on an ansatz about the initial state being given by a gCC state. In this work (see, e.g. (III.51)) we have shown explicitly that by choosing to start with a squeezed state with an appropriate squeezing function, one can explicitly generate such gCC states. In Section 4.2 we have shown explicitly (see (III.81)) that the exact formula for relaxation rate supports the perturbative formula (III.3). This, therefore, explicitly proves the relation between the quench dynamics and the quasinormal decay to higher spin black holes. Note that we now have the relaxation rate non-perturbatively, including the two non-perturbative branches (III.76). It would be interesting to compare these two branches with the corresponding non-perturbative branches of the hs black hole quasinormal frequency [35].

Although we have not computed an explicit collapse process to a higher spin black hole, it is natural to speculate that the memory retention by the thermal state in the field theory, discussed above, would imply that the higher spin black hole obtained from such a collapse starting from a pure AdS vacuum would remember the dynamics of the collapse which is governed by the dynamics of the quench.

We note that a massive to massless quench does not have a direct holographic dual since the theory in the past is not conformal. In this work we have included a discussion of quenches from a critical Hamiltonian to a critical Hamiltonian, starting from ground states/excited states. This can potentially describe a collapse geometry. We hope to return to this issue at a later point.

Other open problems: Some of the obviously important extensions of the above work are to the case of (i) massive to massive quenches, (ii) higher dimensions, (iii) interacting theories. In particular, it would be interesting if the phenomena of IR non-universality persists in higher dimensions. The calculation of Bogoliubov coefficients and exact propagator for the *tanh* protocol appears to go through [40] in higher dimensions in a straightforward manner. However, the analysis of the poles requires more care. We hope to come back to this issue shortly.

III.A Potential scattering and Bogoliubov transformation

In the text (see (III.5)) it has been shown that the scalar mass quench is equivalent to the following Schrödinger problem:

$$-\frac{d^2\psi(E,\mathtt{x})}{d\mathtt{x}^2}+V(\mathtt{x})\psi(E,\mathtt{x})=E\psi(E,\mathtt{x})$$

with the mapping (for a given fixed k)

$\mathtt{x}$	t
E	k^2
$V(\mathtt{x})$	$-m^2(t)$
$\psi(E,\mathtt{x})$	$\phi(k,t)$
$\psi^*(E,\mathtt{x})$	$\phi^*(k,t)=\phi(-k,t)$

We will focus on the potentials of the form depicted in Figure III.1. The generalization to the case of Figure III.2 is straightforward.

The wavefunctions in such a potential, which asymptotes to a constant at both ends (see Figure III.1) are of the general form[26]

$$\phi(k,t)=\begin{cases} A_1(k)e^{i\omega_{in}t}+B_1(k)e^{-i\omega_{in}t}, & t\to-\infty \quad \omega_{in}=\sqrt{k^2+m_0^2} \\ A_2(k)e^{i\omega_{out}t}+B_2(k)e^{-i\omega_{out}t}, & t\to\infty \quad \omega_{out}=|k| \end{cases} \tag{III.94}$$

where

$$A_2(k)=\alpha^*_{LL}(k)A_1(k)+\beta_{LL}(k)B_1(k),\ B_2(k)=\alpha_{LL}(k)B_1(k)+\beta^*_{LL}(k)A_1(k). \tag{III.95}$$

The coefficients $\alpha_{LL}(k),\beta_{LL}(k)$ are determined by the shape of the potential $V=-m^2(t)$[27] The reflection coefficient from the right is given in our conventions, by

$$r(k)=A_2(k)/B_2(k)|_{A_1=0}=\beta_{LL}(k)/\alpha_{LL}(k) \tag{III.96}$$

For later reference we note the reflection coefficient from the left is

$$r'(k)=B_1(k)/A_1(k)|_{B_2=0}=-\beta^*_{LL}(k)/\alpha_{LL}(k) \tag{III.97}$$

To make connections with QFT later, let us write[28]

$$\phi(k,t)=a_{in}(k)u_{in}(k,t)+a^*_{in}(-k)u^*_{in}(-k,t)=a_{out}(k)u_{out}(k,t)+a^*_{out}(-k)u^*_{out}(-k,t) \tag{III.98}$$

[26]We will closely follow the treatment in Landau and Lifshitz [113], Section 25.

[27]The suffix LL indicates the Landau-Lifshitz convention ([113], Section 25). Our α,β's (III.101) will differ from these by a normalization factor.

[28]Note that our conventions ensure $\phi(-k,t)=\phi^*(k,t)$ which is the reality condition for $\phi(x,t)=\int(dk/2\pi)\phi(k,t)\exp[ikx]$.

in terms of two separate sets of linearly independent solutions: (see, e.g. [108], Chapter 3) with the defining properties:

$$t \to -\infty : \; u_{in} \to \frac{e^{-i\omega_{in}t}}{\sqrt{2\omega_{in}}}, \qquad t \to \infty : \; u_{out} \to \frac{e^{-i\omega_{out}t}}{\sqrt{2\omega_{out}}} \tag{III.99}$$

Thus, u_{in} does not have a negative energy wave component $\propto e^{i\omega_{in}t}$ in the past),[29], similarly u_{out} does not have a negative energy wave component $\propto e^{i\omega_{out}t}$ in the future.

These expressions for ϕ agree with the earlier ones (III.94), if we identify

$$A_1(k) = \frac{1}{\sqrt{2\omega_{in}}} a^*_{in}(k), B_1(k) = \frac{1}{\sqrt{2\omega_{in}}} a_{in}(-k), A_2(k) = \frac{1}{\sqrt{2\omega_{out}}} a^*_{out}(k), B_2(k) = \frac{1}{\sqrt{2\omega_{out}}} a_{out}(-k)$$

This implies

$$a_{in}(k) = \alpha^*(k) a_{out}(k) - \beta^*(k) a^*_{out}(-k) \tag{III.100}$$

where the new scattering data $\{\alpha, \beta\}$, to be identified with Bogoliubov coefficients in the quantum theory, are related to old one (III.95) by some normalization factors

$$\alpha(k) = \sqrt{\frac{\omega_{out}}{\omega_{in}}} \alpha_{LL}(k), \; \beta(k) = \sqrt{\frac{\omega_{out}}{\omega_{in}}} \beta_{LL}(k), \tag{III.101}$$
$$r(k) = \beta_{LL}(k)/\alpha_{LL}(k) = \beta(k)/\alpha(k)$$

Note that the reflection amplitudes $r(k)$ remain unaltered. The new scattering data satisfy the normalization conditions

$$|\alpha(k)|^2 - |\beta(k)|^2 = 1 \tag{III.102}$$

which follows from probability conservation in the scattering problem. Upon quantization, the coefficients $a_{in,out}(k)$ are treated as operators in the Fock space (with $a^*_{in,out}(k)$ rewritten as $a^\dagger_{in,out}(k)$), as in the text (see (III.6)).

Note that the in- and out- wavefunctions are related to each other as follows:

$$u_{in}(k) = \alpha(k) u_{out}(k) + \beta(k) u^*_{out}(-k) \tag{III.103}$$

One of the important points of this analysis is that under some broad conditions on the potential (see [113], Section 25, also [114]), the reflection amplitude has a Taylor expansion[30]

$$r(k) = -1 + r_1|k| + r_2|k|^2 + r_3|k|^3 + ..., \; Re(r_1) \geq 0 \tag{III.104}$$

It is also of interest to note that the other reflection amplitude $r'(k)$ has an expansion

$$r'(k) = 1 + r'_1|k| + r'_2|k|^2 + r'_3|k|^3 + ... \tag{III.105}$$

Note that

$$-r^*(k)/r'(k) = \alpha(k)/\alpha^*(k) = 1 + o(|k|). \tag{III.106}$$

[29] We consider $\exp(\mp i\omega t)$ to be future/past directed, with energy defined by $i\partial/\partial t$. This is to be contrasted with $p = -i\partial/\partial x$ with $\exp[\pm ikx]$ identified as right/left directed.

[30] Roughly speaking, $r(0) = -1$ is due to a hard-wall reflection, and $Re(r_1) \geq 0$ follows from $1 - |r(k)|^2 \geq 0$ which, in turn, follows from (III.102).

III.A.1 Examples of potentials

Below we describe a few examples of potential scattering (see [113], Section 25) to test the validity of the power series expansions (III.104) and (III.105).

1. Consider a step potential $U_0\Theta(x)$. Let us choose a wavefunction in the past to come from the left, with energy slightly above the barrier U_0. We will denote the transmitted wave as $\sim e^{ikx}$; this plays the role of the 'out' wave. It is easy to find the left[31] reflection coefficient $r(k) = (|k| - \sqrt{k^2+U_0^2})/(|k| + \sqrt{k^2+U_0^2})$. This admits the following expansion in the right momentum $|k|$:

$$r(k) = -1 + \frac{2|k|}{U_0} - \frac{2k^2}{U_0^2} + \frac{|k|^3}{U_0^3} - \cdots$$

   which is consistent with the nature of the power series expansion (III.104) which was inferred from general arguments.

   It is easy to show that the right reflection coefficient is $r'(k) = -r(k)$. This clearly satisfies an expansion of the form (III.105).

2. For a rectangular barrier potential $U_0\Theta(x) - U_0\Theta(x-a)$ with width a, for $E > U_0$ the left reflection coefficient $r(k) = -\sqrt{(U_0^4 \sin^2\left(a\sqrt{k^2+U_0^2}\right))/(U_0^4 \sin^2\left(a\sqrt{k^2+U_0^2}\right) + 4|k|^2(k^+U_0^2))}$ admits the following expansion in the left momentum $|k|$:

$$r(k) = -1 + \frac{2k^2 \mathrm{cosec}^2\,(aU_0)}{U_0^2} + \cdots$$

3. For a smooth barrier potential $U_0\,(1+e^{-ax})^{-1}$, the left reflection coefficient $r(k) = \sinh\left(\frac{\pi\left(|k|-\sqrt{k^2+U_0^2}\right)}{a}\right) \mathrm{cosech}\left(\frac{\pi\left(|k|+\sqrt{k^2+U_0^2}\right)}{a}\right)$ admits the following expansion in the left momentum $|k|$:

$$r(k) = -1 + \frac{2\pi|k|\coth\left(\frac{\pi U_0}{a}\right)}{a} - \frac{2\pi^2k^2\coth^2\left(\frac{\pi U_0}{a}\right)}{a^2} + \cdots$$

III.A.2 Even parity of the Bogoliubov coefficients

It is clear from the correspondence between the QFT problem and the potential scattering problem that the A_i, B_i are actually functions of the energy E, implying that $\alpha(k), \beta(k)$ are all actually functions of k^2. In particular, for real k, the Bogoliubov coefficients have even parity

$$\alpha(k) = \alpha(-k) = \alpha(|k|),\ \beta(k) = \beta(-k) = \beta(|k|),\ r(k) = r(-k) = r(|k|),\ r'(k) = r'(-k) = r'(|k|) \tag{III.107}$$

[31] Note the left-right flip due to the mapping $-x \to t$, as explained in footnote 29.

III.B Baker-Campbell-Hausdorff Calculation

We will show that

$$|\psi\rangle \equiv \exp\left(\frac{1}{2}\sum_k \gamma(k)a^\dagger(k)a^\dagger(-k)\right)|0\rangle = \exp\left(-\sum_k \kappa(k)a^\dagger(k)a(k)\right)|Bd\rangle \qquad \text{(III.108)}$$

where[32]

$$\kappa(k) = -\frac{1}{2}\log(\gamma(k)/\gamma_0) \qquad \text{(III.109)}$$

and

$$|Bd\rangle \equiv \exp\left(\frac{1}{2}\sum_k \gamma_0 a^\dagger(k)a^\dagger(-k)\right)|0\rangle, \qquad \text{(III.110)}$$

The choice $\gamma_0 = -1$ corresponds to the Dirichlet state (III.113) (similarly, $\gamma_0 = 1$ corresponds to Neumann boundary condition). To derive (III.108), we note that the right hand side can be written as

$$\exp\left[\sum_k B(k)\right]\exp\left[\sum_k A(k)\right]|0\rangle = \exp\left[\sum_k B(k)\right]\exp\left[\sum_k A(k)\right]\exp\left[-\sum_k B(k)\right]|0\rangle$$

where we have defined $B(k) = -\kappa(k)a^\dagger(k)a(k)$ and $A(k) = \gamma_0 a^\dagger(k)a^\dagger(-k)$. The identity (III.108) follows by noting that $[B(l), A(k)] = -\kappa(k)A(k)\,(\delta_{k,l} + \delta_{k,-l})$, and by using the following form of the Baker-Campbell-Hausdorff (BCH) formula

$$e^X e^Y e^{-X} = e^{\exp(s)Y} \qquad \text{(III.111)}$$

where $[X, Y] = sY$.

In the context of this chapter, we will be interested in evaluating $\kappa(k)$ from (III.109) in a power series in k, using (III.12). Since the leading term in $\gamma(k)$ is -1, with the choice of the Dirichlet boundary state $\gamma_0 = -1$, we get the equation (III.10) in the text.

III.C Bosons

The action for a free massless scalar is

$$S = \frac{1}{2}\int dxdt\left[(\partial_t\phi)^2 - (\partial_x\phi)^2\right] = -\frac{1}{2}\int dxdt\;\partial_\mu\phi\partial^\mu\phi$$

[32] We thank Samir Mathur for drawing our attention to [115] where a relation of the form (III.109) was derived earlier in a somewhat different context for a single oscillator.

The normal mode expansion is (we use "box normalization" $k = 2\pi n/L$, $\int \frac{dk}{2\pi} = \frac{1}{L}\sum\limits_n$)[33]

$$\begin{aligned}\phi(x,t) &= \int \frac{dk}{2\pi}\left[\frac{a(k)}{\sqrt{2|k|}}\exp\left(ikx - i|k|t\right) + \frac{a^\dagger(k)}{\sqrt{2|k|}}\exp\left(-ikx + i|k|t\right)\right] \\ &= \sum_{n\neq 0}\frac{1}{\sqrt{4\pi L|n|}}a_n \exp\left(\frac{2\pi}{L}(inx - i|n|t)\right) + \text{h.c} \\ &\equiv \sum_{k\neq 0}\left[\frac{a(k)}{\sqrt{2|k|}}\exp\left(ikx - i|k|t\right) + \frac{a^\dagger(k)}{\sqrt{2|k|}}\exp\left(-ikx + i|k|t\right)\right] \qquad \text{(III.112)}\end{aligned}$$

We will often use $a_n \equiv a(k)$, with a slight abuse of notation. The commutation relations are $[a(k), a^\dagger(l)] = \delta_{kl}$.

Boundary states In terms of standard CFT oscillators $\alpha_n, \tilde{\alpha}_n$, the Dirichlet boundary state is given by (see, e.g. [116] Eq. 4.1.13)

$$|D\rangle = \exp[\sum_{n=1}^{\infty}\frac{1}{n}\alpha_{-n}\tilde{\alpha}_{-n}]|0\rangle$$

In terms of our oscillators $a_n \equiv a_k$

$$\begin{aligned}&\alpha_{-n} = i\sqrt{n}a^\dagger_{-n},\ \tilde{\alpha}_{-n} = i\sqrt{n}a^\dagger_n \\ &|D\rangle = \exp[-\sum_{n>0}a^\dagger_n a^\dagger_{-n}]|0\rangle = \exp[-\frac{1}{2}\sum_{n\neq 0}a^\dagger_n a^\dagger_{-n}]|0\rangle = \exp[-\frac{1}{2}\sum_{k\neq 0}a^\dagger(k)a^\dagger(-k)]|0\rangle \qquad \text{(III.113)}\end{aligned}$$

In the first step we used the relation between our oscillators here and the standard CFT conventions (see [24], Chap. 6).

Euclidean CFT We define $w = x + i\tau$, $\bar{w} = x - i\tau$, $\tau = it$. The Euclidean Propagator is

$$\langle\phi(0,0)\phi(x,\tau)\rangle = \langle\phi(0,0)\phi(w,\bar{w})\rangle = -\frac{1}{4\pi}(\ln w + \ln\bar{w})$$

Vertex operators Consider the exponential vertex operator $O(w,\bar{w}) = \exp[iq\phi(w,\bar{w})]$.

$$\langle\exp[iq\phi(0,0)]\exp[-iq\phi(w,\bar{w})]\rangle = w^{-q^2/4\pi}\bar{w}^{-q^2/4\pi}$$

Hence $h = \bar{h} = q^2/8\pi$, $\Delta = q^2/4\pi$.

Boson W-currents We have used the following definitions of the $\mathbb{W}_\infty$ currents [41] (normal ordering is implicit),

$$T(z) = \partial\phi(z)\partial\phi(z) \qquad \text{(III.114)}$$

$$W_4(z) = 2\partial^3\phi\partial\phi - 3\partial^2\phi\partial^2\phi \qquad \text{(III.115)}$$

[33] We use the conventions of [24].

III.D Fermions

We have used the following conventions in the text.

$$\eta_{\mu\nu} = \begin{bmatrix} 1 & 0 \\ 0 & -1 \end{bmatrix}, \quad \partial_\mu = (\partial_t, \partial_x), \quad \gamma^\mu \partial_\mu = \gamma^0 \partial_t - \gamma^1 \partial_x,$$

$$\gamma_d^0 = \begin{bmatrix} 1 & 0 \\ 0 & -1 \end{bmatrix}, \quad \gamma_d^1 = \begin{bmatrix} 0 & 1 \\ -1 & 0 \end{bmatrix}, \quad \text{in Dirac basis.}$$

$$S = \frac{1}{\sqrt{2}} \begin{bmatrix} 1 & -1 \\ 1 & 1 \end{bmatrix}, \gamma_c^0 = S\gamma_d^0 S^{-1} = \begin{bmatrix} 0 & 1 \\ 1 & 0 \end{bmatrix}, \quad \gamma_c^1 = S\gamma_d^1 S^{-1} = \begin{bmatrix} 0 & 1 \\ -1 & 0 \end{bmatrix}, \quad \text{in chiral basis.}$$

$$u(0) = \begin{pmatrix} 1 \\ 0 \end{pmatrix}, \qquad v(0) = \begin{pmatrix} 0 \\ 1 \end{pmatrix} \qquad \text{are the spinors in the rest frame.}$$

The spinors in a general frame are

$$\begin{aligned}
u(k,m) &= \frac{1}{\sqrt{(\omega+m)}} \begin{bmatrix} (\omega+m) \\ -k \end{bmatrix}, & v(k,m) &= \frac{1}{\sqrt{(\omega+m)}} \begin{bmatrix} k \\ -(\omega+m) \end{bmatrix} \\
\bar{u}(k,m) &= \frac{1}{\sqrt{(\omega+m)}} \begin{bmatrix} (\omega+m) & k \end{bmatrix}, & \bar{v}(k,m) &= \frac{1}{\sqrt{(\omega+m)}} \begin{bmatrix} k & (\omega+m) \end{bmatrix}
\end{aligned} \tag{III.116}$$

where we have used the normalization $\bar{u}(k,m)u(k,m) = -\bar{v}(k,m)v(k,m) = 2m$. In the chiral basis, the mode expansion in the massless limit is

$$\begin{aligned}
\Psi_c(x,t) &= S \cdot \Psi(x,t) = \frac{1}{\sqrt{2}} \begin{bmatrix} 1 & -1 \\ 1 & 1 \end{bmatrix} \cdot \int \frac{dk}{2\pi} \frac{1}{\sqrt{2}} \begin{bmatrix} a_k e^{-ik\cdot x} + \mathrm{sgn}(k) b_k^\dagger e^{ik\cdot x} \\ -\mathrm{sgn}(k) a_k e^{-ik\cdot x} - b_k^\dagger e^{ik\cdot x} \end{bmatrix} \\
&= \int_{-\infty}^{\infty} \frac{dk}{2\pi} \frac{1}{2} \begin{bmatrix} (1+\mathrm{sgn}(k))(a_k e^{-ik\cdot x} + b_k^\dagger e^{ik\cdot x}) \\ (1-\mathrm{sgn}(k))(a_k e^{-ik\cdot x} - b_k^\dagger e^{ik\cdot x}) \end{bmatrix}
\end{aligned} \tag{III.117}$$

Writing as $\psi(x,t)$ and $\bar{\psi}(x,t)$,

$$\psi(x,t) = \int_0^\infty \frac{dk}{2\pi} (a_k e^{-ik\cdot x} + b_k^\dagger e^{ik\cdot x}) \tag{III.118}$$

$$\bar{\psi}(x,t) = \int_{-\infty}^0 \frac{dk}{2\pi} (a_k e^{-ik\cdot x} - b_k^\dagger e^{ik\cdot x}) \tag{III.119}$$

Solution of Dirac equation and Bogoliubov coefficients Using the coordinate transformation $y = e^{-\rho t}$ and the ansatz, we get the following equation:

$$\phi_\pm''(y) + \frac{\phi_\pm'(y)}{y} + \phi_\pm(y) \left(\frac{k^2}{\rho^2 y^2} + \frac{m_0^2 y^2 \pm 2im_0\rho}{\rho^2 (y^2+1)^2} \right) = 0 \tag{III.120}$$

The 'in' solutions are solutions which become plane waves in far past and the 'out' solutions are solutions which become plane waves in far future. Due to the explicit i in the equation of $\phi_\pm$, the positive energy solutions $\phi_{\pm,in/out,p}(k,t)$ and the negative energy solutions $e^{-i\omega_{in/out}t}$ are related as

$$\phi_{+,in/out,m}(k,t) = \phi_{-,in/out,p}(k,t)^*, \qquad \phi_{-,in/out,m}(k,t) = \phi_{+,in/out,p}(k,t)^*$$

So, the solutions can be written as

$$\begin{aligned} \phi_{+,in/out}(k,t) &= \phi_{+,in/out,p}(k,t) + \phi_{-,in/out,p}(k,t)^* \\ \phi_{-,in/out}(k,t) &= \phi_{-,in/out,p}(k,t) + \phi_{+,in/out,p}(k,t)^* \end{aligned}$$

The explicit solutions are

$$\begin{aligned} \phi_{+,in}(k,t) &= \left(e^{-2\rho t}+1\right)^{-\frac{im_0}{2\rho}} e^{it(\omega_{in}+m_0)} \, {}_2F_1\left(\frac{i\,(k-m_0-\omega_{in})}{2\rho}, \frac{i\,(-k-m_0-\omega_{in})}{2\rho}; 1-\frac{i\omega_{in}}{\rho}; e^{2\rho t}\right) \\ \phi_{-,in}(k,t) &= \left(e^{-2\rho t}+1\right)^{\frac{im_0}{2\rho}} e^{-it(\omega_{in}-m_0)} \, {}_2F_1\left(\frac{i\,(k+m_0-\omega_{in})}{2\rho}, \frac{i\,(-k+m_0-\omega_{in})}{2\rho}; 1-\frac{i\omega_{in}}{\rho}; e^{2\rho t}\right) \\ \phi_{+,out}(k,t) &= e^{-ikt}\left(e^{-2\rho t}+1\right)^{-\frac{im_0}{2\rho}} \, {}_2F_1\left(\frac{i\,(k-m_0+\omega_{in})}{2\rho}, \frac{i\,(k-m_0-\omega_{in})}{2\rho}; 1+\frac{ik}{\rho}; -e^{-2\rho t}\right) \\ \phi_{-,out}(k,t) &= e^{-ikt}\left(e^{-2\rho t}+1\right)^{\frac{im_0}{2\rho}} \, {}_2F_1\left(\frac{i\,(k+m_0-\omega_{in})}{2\rho}, \frac{i\,(k+m_0+\omega_{in})}{2\rho}; 1+\frac{ik}{\rho}; -e^{-2\rho t}\right) \end{aligned} \tag{III.121}$$

Defining the Dirac spinors as

$$\begin{aligned} U_{in/out}(k,x,t) &= K_{in/out}\left(\gamma^0\partial_t - ik\gamma^1 - im(t)\right) e^{ikx}\phi_{+,in/out,p}(k,t)u(0) \\ V_{in/out}(k,x,t) &= -K_{in/out}\left(\gamma^0\partial_t + ik\gamma^1 - im(t)\right) e^{-ikx}\phi_{+,in/out,p}(k,t)^* v(0) \end{aligned}$$

where $K_{in/out} = i\left(\frac{1}{\omega_{in/out}+m_{in/out}}\right)^{1/2}$. For constant mass, $U(k,x,t) = u(k,m)e^{-ik\cdot x}$ and $V(k,x,t) = v(k,m)e^{ik\cdot x}$ where $u(k,m)$ and $v(k,m)$ have been defined in (IV.114). The mode expansion of $\Psi(x,t)$ in terms of in/out modes are

$$\Psi(x,t) = \int_{-\infty}^{\infty} \frac{dk}{\sqrt{2\omega_{in/out}}}\left[a_{k,in/out}U_{in/out}(k,x,t) + b^\dagger_{k,in/out}V_{in/out}(k,x,t)\right]$$

Using properties of hypergeometric functions [112], the Bogoliubov transformations between 'in' and 'out' solutions are

$$\begin{aligned} \phi_{+,in,p}(k,t) &= \alpha_+(k)\phi_{+,out,p}(k,t) + \beta_+(k)\phi_{-,out,p}(k,t)^* \\ \phi_{-,in,p}(k,t) &= \alpha_-(k)\phi_{-,out,p}(k,t) + \beta_+(k)\phi_{+,out,p}(k,t)^* \end{aligned}$$

Hence, the Bogoliubov transformations between the 'in' and 'out' operators are

$$\begin{aligned} a_{k,in} &= \left(\frac{\omega_{in}}{\omega_{out}}\right)^{1/2}\frac{K_{out}}{K_{in}}\left(\alpha_+(k)^* a_{k,out} - \chi(k)\beta_+(k)^* b^\dagger_{-k,out}\right) \\ b_{k,in} &= \left(\frac{\omega_{in}}{\omega_{out}}\right)^{1/2}\frac{K_{out}}{K_{in}}\left(\alpha_+(k)^* b_{k,out} + \tilde{\chi}(k)\beta_-(k)^* a^\dagger_{-k,out}\right) \end{aligned} \tag{III.122}$$

where $\chi(k) = \tilde{\chi}(k) = \mathrm{sgn}(k)$. It is straightforward now to find the expressions for the Bogoliubov coefficients which are reproduced in the text (III.60).

Fermion W-currents We have used the following definitions of the super-$\mathbb{W}_\infty$ currents [117] (normal ordering is implicit),

$$\begin{aligned}
T(z) &= -\frac{i}{2}\left(\psi^*\partial\psi(z) - \partial\psi^*\psi(z)\right) \\
W_4(z) &= \frac{4}{5}q^2\left(\partial^3\psi^*\psi(z) - 9\partial^2\psi^*\partial\psi(z) + 9\partial\psi^*\partial^2\psi(z) - \psi^*\partial^3\psi(z)\right) \\
&\qquad\qquad + 25\partial\psi^*\partial^4\psi - \psi^*\partial^5\psi(z))
\end{aligned}$$

III.E Subtleties of the sudden limit

In Section 2.4 we analyzed the behaviour of the quench under the "tanh" protocol for large ρ in a power series in m_0/ρ. In particular, in Section 2.4, we defined the sudden limit as the limit (III.31). In this section we will give a more precise definition of this limit. In certain quantities, like the number operator (III.29) in Section 2.4 and the propagator in Section 4.1 etc. the distinction is not essential, but in general the naive limit entails UV divergences. E.g. all W-charges, including the energy density, under a naive m_0/ρ expansion introduced in Section 2.4 appear to have progressively higher UV divergences as one goes down the order. To treat these divergences properly, let us first analyze these. Later on, we will find that terms in this expansion can be resummed to yield finite expressions, provided we define the sudden limit by the equation (III.123).

Energy density

$$\begin{aligned}
E/L = \frac{1}{2\pi}\int_{-\Lambda}^{\Lambda} dk|k|N_k = m_0^2\Bigg(&\frac{1}{8\pi} - \frac{m_0^2}{32\pi\Lambda^2} + O\left(\frac{m_0}{\Lambda}\right)^4 - \frac{m_0^2}{\rho^2}\left[\frac{1}{48}\pi\log\left(\frac{\Lambda}{m_0}\right)\right. \\
&\left. + \frac{1}{96}\pi\log(4) + \frac{\pi m_0^2}{192\Lambda^2} + O\left(\frac{m_0}{\Lambda}\right)^4\right] + O\left(\frac{m_0}{\rho}\right)^4\Bigg)
\end{aligned}$$

where we have used the asymptotic number density (III.29), in an m_0/ρ expansion:

$$N_k = \frac{\left(k - \sqrt{k^2+m_0^2}\right)^2}{4k\sqrt{k^2+m_0^2}} - \left(\frac{m_0}{\rho}\right)^2 \frac{\pi^2 m_0^2}{48\left(k\sqrt{k^2+m^2}\right)} + O\left(\frac{m_0}{\rho}\right)^4$$

W4 density

$$\begin{aligned}
W_4/L = \int_{-\Lambda}^{\Lambda}\frac{dk}{2\pi}|k|^3 N_k = m_0^4\Bigg[&\frac{4\log(\Lambda/m_0) - 3 + \log(16)}{64\pi} + \frac{m_0^2}{32\pi\Lambda^2} + O\left(\frac{m_0}{\Lambda}\right)^4 \\
+ \left(\frac{m_0}{\rho}\right)^2\left(-\frac{\pi\Lambda^2}{96m_0^2} + \frac{1}{192}\pi(2\log(\Lambda/m_0) - 1 + \log(4)) + \frac{\pi m_0^2}{256\Lambda^2} + O\left(\frac{m_0}{\Lambda}\right)^4\right) &+ O\left(\frac{m_0}{\rho}\right)^4\Bigg]
\end{aligned}$$

W_6 density

$$W_6/L = \int_{-\Lambda}^{\Lambda} \frac{dk}{2\pi} |k|^5 N_k = m_0^6 \Bigg[\left(\frac{\Lambda^2}{32\pi m_0^2} + \left(\frac{\log\left(\frac{m_0}{\Lambda}\right)}{16\pi} + \frac{1}{24\pi} - \frac{\log(4)}{32\pi} \right) - \frac{15 m_0^2}{512\pi\Lambda^2} + O\left(\frac{m_0}{\Lambda}\right)^4 \right) +$$
$$+ \frac{m_0^2}{\rho^2} \Bigg(- \frac{\pi\Lambda^4}{192 m_0^4} + \frac{\pi\Lambda^2}{192 m_0^2} + \frac{1}{128}\pi \log\left(\frac{m_0}{\Lambda}\right)$$
$$- \frac{1}{256}\pi\log(4) + \frac{7\pi}{1536} - \frac{5\pi m_0^2}{1536\Lambda^2} + O\left(\frac{m_0}{\Lambda}\right)^4 \Bigg) + O\left(\frac{m_0}{\rho}\right)^4 \Bigg]$$

III.E.1 Resumming the divergences

It turns out that the terms with growing UV-divergences with growing powers of m_0/ρ can be resummed to the following form.
Introduce the scaling functions

$$E/L = m_0^2 \mathcal{E}(x,y), \quad W_4/L = m_0^4 F(x,y), \quad W_6/L = m_0^6 G(x,y), \quad x = m_0^2/\rho^2,\ y = m_0^2/\Lambda^2$$

The leading singularities in the above expressions for the charges are captured by

$$\mathcal{E}(x,y) = \frac{1}{8\pi} + \frac{\left(\frac{5\pi^2 x}{8} + y\right)\log\left(\pi^2 x + y\right)}{60\pi} + \cdots = \frac{1}{8\pi} + \cdots$$
$$F(x,y) = -\frac{\left(\log\left(\frac{2\pi^4 x^2}{5} + y^2\right) + \log\left(\pi^2 x + y\right)\right)\left(40\left(5y+3\right) + \pi^4 x^2 + 20\pi^2 x\right)}{11520\pi} + \cdots$$
$$G(x,y) = \frac{1}{1536\pi}\left(\frac{\pi^4 x^2}{120} + \frac{1}{32}\pi^2 x(9y+4) + y^2 + y + 1\right)\Bigg[8\left(\frac{25}{\sqrt{\frac{26\pi^4 x^2}{3} + 25y^2}} + \frac{1}{\pi^2 x + y}\right)$$
$$+19\log\left(\frac{74\pi^4 x^2}{285} + y^2\right) + 10\log\left(\pi^2 x + y\right)\Bigg] + \cdots$$

The correct version of the "sudden" limit, therefore, is to take the limit $\Lambda \to \infty$ first, for finite, large ρ/m_0 (see Figure III.4). , i.e.

$$y = \frac{m_0^2}{\Lambda^2} \to 0,\ x = \frac{m_0^2}{\rho^2} = \text{small, fixed} \qquad \text{(III.123)}$$

In this limit, as we can see from the above expressions:

$$\mathcal{E}(x,0) = \frac{1}{8\pi} + \frac{\pi}{96} x\log(x) + \cdots = \frac{1}{8\pi} + \cdots, \quad F(x,0) \propto \log(x) + \cdots,\ G(x,0) \propto \log(x)/x + \cdots,$$

which implies

$$E/L = m_0^2\left(\frac{1}{8\pi} - \frac{\pi}{48}\frac{m_0^2}{\rho^2}\log(\frac{\rho}{m_0})\right) + \cdots = m_0^2 \frac{1}{8\pi} + \cdots$$
$$W_4/L \propto m_0^4 \ \log(\frac{\rho}{m_0}) + \cdots$$
$$W_6/L \propto m_0^6 \ \frac{\rho^2}{m_0^2}\log(\frac{\rho}{m_0}) + \cdots \qquad \text{(III.124)}$$

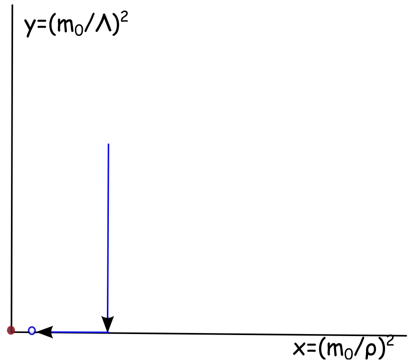

Figure III.4: The sudden limit.

III.E.2 Summary

In those quantities, which are UV-convergent in the limit $\Lambda/m_0 \to \infty$ (irrespective of the value of m_0/ρ), e.g. the energy density and the correlators discussed in the text, it is okay to use the naive definition of the sudden limit (III.31). However, for W_4 and the higher charges which have $\log(\Lambda/m_0)$ and higher UV divergences, the only uniformly sensible way to define this limit is (III.123), as in figure III.4.

Chapter IV

Exact Growth of Entanglement in Fermionic Quenches[1]

1 Introduction and Summary

Thermalization in unitary quantum field theories has been a topic of great significance. Using AdS/CFT correspondence, it has also been linked to black hole formation [78, 95]. One of the current views of thermalization is that of the thermalization of a finite subsystem, in which the conjugate subsystem is considered the heat bath. In other words, it is the thermalization observed by an observer who has access to only a subsystem of the full system. It can also be considered as if the 'fine-grained' observables[2] are spatially widely separated bilocal or higher point observables. Starting from a pure state, in the high energy (high effective temperature) limit, the final thermal entropy observed by such an observer is actually the entanglement entropy of the subsystem with its conjugate. Obviously, the pure state has to be a time-dependent state. Closely related to thermalization(equilibration in general), the study of time-dependent states after a quantum quench has also been of great interest[17, 19]. Quantum quench is the process in which the parameters of the Hamiltonian of a system in a certain state are changed with time. After the quantum quench, in the long time limit, if the subsystem of our interest looks like a thermal ensemble, in the sense that the expectation values of observables in the finite subsystem have the same expectation values as in a thermal ensemble, then we say that the system has thermalized. In this work, we will be mainly considering quantum quench as the preparation of the time-dependent states of our interest.

We will also restrict ourself to critical quantum quenches, in which the final Hamiltonian is a critical Hamiltonian, i.e., the corresponding theory is a conformal field theory (CFT). More specifically, we will be considering free fermions in which starting from a certain state in the massive theory, the mass is set to zero gradually or suddenly. In more general theories, starting from the ground state of a gapped theory, it has been proposed [20, 6] that the state obtained after the critical quench is a Calabrese-Cardy(CC) state which has the form

[1]The contents of this chapter have partial overlap with the M.Sc. thesis of Shruti Paranjape. The author made leading contributions in all the sections below.

[2]Observables which show the non-thermal behaviour of the pure state, in contrast to 'coarse-grained' observables which cannot distinguish between the pure state and the thermal ensemble.

$e^{-\kappa_2 H}|B\rangle$, where κ_2 is a scale given by the initial gap and the other scales of the quench process, H is the Hamiltonian of the CFT and $|B\rangle$ is a conformally invariant boundary state. It has been shown that such a state thermalizes to a thermal ensemble with temperature $T = 1/\beta = 1/(4\kappa_2)$. This result has also been generalised to the case in which the final theory has other conserved charges of local currents [2]. The corresponding ansatz for the state after quench from ground state is a generalized Calabrese-Cardy(gCC) states which have the form $e^{-\kappa_2 H - \kappa_4 W_4 - \kappa_6 W_6 - \cdots}|D\rangle$ where again the parameters $\kappa_2, \kappa_4, \kappa_6, \cdots$ are given by the initial gap and other scales in the quench process, e.g. $\delta t = 1/\rho$ the time taken to set the mass to zero, and $W_4, W_6, \cdots$ are the conserved charges of local currents. In this case also, it has been shown that the state thermalizes into a generalized Gibb's Ensemble(GGE) with the density matrix $e^{-\beta H - \mu_4 W_4 - \mu_6 W_6 - \cdots}$ where the corresponding temperature and chemical potentials are $T = 1/\beta = 1/(4\kappa_2)$, $\mu_4 = 4\kappa_4$, $\mu_6 = 4\kappa_6, \cdots$.

The gCC state ansatz has been shown to be true for mass quenches in free scalar and free fermion theories in a recent paper(MPS) [3]. Starting from the ground state of the massive theories, the quenched states obtained are of the gCC form with infinite number of charges W_{2n} with $n \in \mathbb{N}$ ($W_2 = H$). For the scalar theory, it was also found that naively taking the sudden limit when the mass profile is taken to be a step function, the final state is non-normalizable. For massless free scalar theory, $W_{2n} = \sum |k|^{2n-1} d_k^\dagger d_k$, where $d_k^\dagger$ and d_k are the bosonic annihilation and creation operators.[3] It was also shown that starting from specially prepared squeezed states of the massive scalar theory, CC state and gCC state with finite number of charges can also be created. By calculating correlators, thermalization of these states were explicitly shown.

In this work, we find similar results for the fermionic mass quench. In the sudden limit, starting from the ground state, we observe that the final state has divergent energy density, $W_4, W_6, \cdots$. Again, as in the case of scalar fields in MPS, starting from specially prepared squeezed states using the sudden quench limit, we can prepare CC state and gCC state with a finite number of charges of our choice. For the CC state and the gCC state with finite number of charges, we calculate correlators and explicitly show thermalization to thermal ensemble and GGE respectively.

Among the other calculable quantities, entanglement entropy(EE) is the most interesting one. The EE growth has been calculated(mostly numerically) in many dynamical systems, see for e.g. [20, 90, 118, 119, 120, 121, 122]. It has also been extensively examined in holographic systems [123, 7, 14, 77, 124]. Recently, non-monotonic EE growth consisting of an initial dip around the quench time has also been observed in a holographic set-up in [125].

Since our final theory consists of only massless Dirac fermions, so using bosonization, we could calculate EE in some of our time-dependent states. We are interested in EE of a single interval only. For CC states, we find that EE grows monotonically. The asymptotic time limit is given by the well-known expression from CFT in a thermal ensemble, $S_A = \frac{c}{3}\log(\sinh(\frac{\pi r}{\beta}))$, where for Dirac fermions $c = 1$ and the effective temperature $1/\beta = 1/4\kappa$. In case of gCC states, we are not able to calculate EE with the charges of the usual fermionic bilinear $\mathcal{W}_{1+\infty}$ currents. But we are able to calculate the EE with the fermionic charge corresponding to the bosonic charges $W_{2n} = \sum |k|^{2n-1} d_k^\dagger d_k$. These are the charges of bosonic bilinear $\mathcal{W}_{2n}$ currents for $n > 1$. For such gCC states with the W_4 charge, we found a dynamical phase

[3] The normalization of the charges differ from the normalization in [41, 26].

transition in which EE grows non-monotonically when the effective chemical potential μ_4 is greater than a critical value. Below this critical value, the EE growth is strictly monotonic.

In summary, the key results of the present work are:

1. For ground state quench, similar to the scalar quench, a naive sudden quench limit gives divergent conserved charges. Calculation of the correlators show equilibration explicitly. But the long distance and time and ultimately the stationary limit is significantly different from thermalization to a thermal ensemble. This is the same manifestation of the UV/IR mixing found in MPS.

2. Starting from appropriately prepared squeezed states of the massive theory, we can prepare CC and gCC states with specific W_{2n} charges using quench. Calculation of correlators in CC state and gCC states explicitly show thermalization to thermal ensemble and GGE respectively. Here again, for gCC state, the long time and long distance limit of the correlators have significant dependence on the chemical potentials. This is again another avatar of the UV/IR mixing.

3. For CC state, we are able to calculate the growth of entanglement entropy of a single interval explicitly in analytic form. The EE growth is strictly monotonically increasing for CC state. The stationary limit is, as expected, the entanglement entropy of a single interval in thermal ensemble.

4. We also calculate the EE growth of a single interval in gCC state with W_4 charge of the $\mathcal{W}_{2n}$ representation of fermion corresponding to the $\mathcal{W}_{2n}$ bilinear bosonic representation. We find dynamical phase transition in which the EE growth is monotonically increasing upto a critical value of κ_4. Beyond the critical value, the EE growth is non-monotonic.

The outline of the chapter is as follows:
In section 2, we solve the Dirac equation with time-dependent mass and from explicit solutions for a specific mass profile, we calculate the Bogoliubov coefficients for the transformation between the massive and massless modes. In section 3, we find the final state after the quench starting from the ground state and a few squeezed states of our interest. In sections 4 and 5, we calculate energy density and some correlators in the different quenched states that we obtained. The EE growth of a single subsystem in CC state is explicitly calculated in section 6. In section 7, we show the dynamical phase transition in the EE growth of a subsystem in a particular gCC state. Section 8 contains some discussions. The appendix contains details that we have omitted in the main sections.

2 Free Dirac fermions with time-dependent mass

The action for Dirac fermions with time-dependent mass is

$$S = -\int dx^2 \left[i\bar{\Psi}\gamma^\mu\partial_\mu\Psi - m(t)\bar{\Psi}\Psi \right] \tag{IV.1}$$

The equation of motion (EOM) is

$$\left[i\gamma^0\partial_t - i\gamma^1\partial_x - m(t)\right]\Psi(x,t) = 0 \tag{IV.2}$$

and we are interested in the solvable mass profile[42, 40]

$$m(t) = m[1 - \tanh(\rho t)]/2 \tag{IV.3}$$

m is the initial mass and ρ is the only scale of the quench process. $\rho \to \infty$ is the sudden limit in which the mass is set to zero suddenly - much faster than any other length scale in the theory. It is easier to solve (IV.2) in the Dirac basis in which γ_0 is diagonal. Since the system is translation invariant in the spatial x-direction, the solution ansatz is

$$\Psi(x,t) = \left[\gamma^0\partial_t - \gamma^1\partial_x - im(t)\right]e^{\pm ikx}\Phi(t) \tag{IV.4}$$

Substitution in the EOM gives,

$$\left[\partial_t^2 + k^2 + m(t)^2 - i\gamma^0\dot{m}(t)\right]e^{\pm ikx}\Phi(t) = 0$$

where $\dot{m}(t) = \partial_t m(t)$.

$\Phi(t)$ is solved in the eigenbasis of γ^0. For the two eigenvalues of γ^0 (1 and -1), the two solutions $\phi_+(t)$ and $\phi_-(t)$ are given by,

$$\begin{aligned}\left[\partial_t^2 + k^2 + m(t)^2 - i\dot{m}(t)\right]\phi_+(t) = 0\\ \left[\partial_t^2 + k^2 + m(t)^2 + i\dot{m}(t)\right]\phi_-(t) = 0\end{aligned} \tag{IV.5}$$

where $\Phi(t) = \begin{bmatrix}\phi_+(t) & \phi_-(t)\end{bmatrix}^{\mathrm{T}}$. The eigenstates of γ^0 are $u_0 = \begin{bmatrix}1\\0\end{bmatrix}$ and $v_0 = \begin{bmatrix}0\\1\end{bmatrix}$, they are the spinors in the rest frame.

For the mass profile (IV.3), there are two important bases of solutions in which we are interested in. The first one is the 'in' basis in which the two independent solutions of the second order linear differential equations become different single frequency modes in the $t \to -\infty$ limit. In other words, one solution becomes the negative energy mode and the other solution becomes the positive energy mode. Similarly, there is also an 'out' basis of solutions in which one solution becomes the negative energy mode and the other becomes the positive energy mode in the $t \to \infty$ limit. Accordingly, we will also have different 'in' and 'out' creation and annihilation operators. Consider the solutions of (IV.5) in the two bases to be

$$\phi_\pm(t,k) = \phi_{in,\pm p}(t,k) + \phi_{in,\pm m}(t,k) \tag{IV.6}$$
$$\phi_\pm(t,k) = \phi_{out,\pm p}(t,k) + \phi_{out,\pm m}(t,k) \tag{IV.7}$$

where the limits are

$$\lim_{t\to-\infty}\phi_{in,\pm p}(t,k) = e^{-i\omega_{in}t}, \quad \lim_{t\to-\infty}\phi_{in,\pm m}(t,k) = e^{i\omega_{in}t}$$
$$\lim_{t\to\infty}\phi_{out,\pm p}(t,k) = e^{-i\omega_{out}t}, \quad \lim_{t\to\infty}\phi_{out,\pm m}(t,k) = e^{i\omega_{out}t}$$

where 'p' means *positive energy* and 'm' means *negative energy.* The above solutions are the same but written in two different bases for simplicity in the appropriate time limits, they are related by Bogoliubov transformations.
But from (IV.5), we see that the equations of ϕ_+ and ϕ_- are the complex conjugates of each other, so

$$\phi_{in,+p}(t,k) = \phi^*_{in,-m}(t,k), \quad \phi_{in,+m}(t,k) = \phi^*_{in,-p}(t,k) \tag{IV.8}$$
$$\phi_{out,+p}(t,k) = \phi^*_{out,-m}(t,k), \quad \phi_{out,+m}(t,k) = \phi^*_{out,-p}(t,k) \tag{IV.9}$$

The Bogoliubov transformations are

$$\begin{aligned}\phi_{in,+p}(t,k) &= \alpha'_+(k)\phi_{out,+p}(t,k) + \beta'_+(k)\phi_{out,+m}(t,k) \\ &= \alpha'_+(k)\phi_{out,+p}(t,k) + \beta'_+(k)\phi^*_{out,-p}(t,k) \qquad \text{(IV.10)} \\ \phi_{in,-p}(t,k) &= \alpha'_-(k)\phi_{out,-p}(t,k) + \beta'_-(k)\phi_{out,-m}(t,k) \\ &= \alpha'_-(k)\phi_{out,-p}(t,k) + \beta'_-(k)\phi^*_{out,+p}(t,k) \qquad \text{(IV.11)}\end{aligned}$$

where $\alpha'_\pm(k)$ an $\beta'_\pm(k)$ are actually functions of $|k|$, since the equations of motion have only k^2 terms.

Now, suppressing the basis labels 'in' and 'out' since they apply to both bases, we write the u_0 part of $\Psi(x,t)$ as (upto normalization)

$$\tilde{U}(x,t;k) = \left[\gamma^0\partial_t + \gamma^1\partial_x - im(t)\right] e^{ikx}\phi_{+p}(t) \begin{bmatrix}1\\0\end{bmatrix} \tag{IV.12}$$

And the v_0 part of $\Psi(x,t)$ as

$$\begin{aligned}\tilde{V}(x,t;k) &= \left[\gamma^0\partial_t + \gamma^1\partial_x - im(t)\right] e^{-ikx}\phi_{-m}(t) \begin{bmatrix}0\\1\end{bmatrix} \\ &= \left[\gamma^0\partial_t + \gamma^1\partial_x - im(t)\right] e^{-ikx}\phi^*_{+p}(t) \begin{bmatrix}0\\1\end{bmatrix} \qquad \text{(IV.13)}\end{aligned}$$

We can define the spinors as (upto normalization)

$$\begin{aligned}\tilde{u}(t,k) &= \frac{1}{e^{ikx}\phi_{+p}(t)}\tilde{U}(x,t;k) \\ \tilde{v}(t,k) &= \frac{1}{e^{-ikx}\phi_{-m}(t)}\tilde{V}(x,t;k)\end{aligned}$$

With proper normalization, the final Dirac fermion mode expansion is

$$\begin{aligned}\Psi(x,t) &= \int \frac{dk}{2\pi}\frac{1}{\sqrt{2\omega}}\left[a_k U(x,t;k) + b^\dagger_k V(x,t;k)\right] \\ &= \int \frac{dk}{2\pi}\frac{1}{\sqrt{2\omega}}\left[a_k u(t;k)e^{ikx}\phi_{+p}(t) + b^\dagger_k v(t;k)e^{-ikx}\phi_{-m}(t)\right] \qquad \text{(IV.14)}\end{aligned}$$

2.1 Bogoliubov transformation of oscillators

The initial mass is taken to be $\lim_{t\to-\infty} m(t) = m$. It is convenient to take the final mass $\lim_{t\to\infty} m(t)$ to be some m_{out}, because of the spinor convention (in P&S), although we are interested in $m_{out} = 0$.

With time-dependent mass, as mentioned above, the spinors are functionals of $m(t)$, but their normalizations are constants or else they will not solve the Dirac equations. So, we have to differentiate between 'in' spinors and 'out' spinors. Taking this into account, the mode expansion of $\Psi(x,t)$ starting from 'in' basis to 'out' basis is

$$\begin{aligned}
\Psi(x,t) &= \int \frac{dk}{2\pi}\frac{1}{\sqrt{2\omega_{in}}}\left[a_{in,k}u_{in}(k,m)\phi_{in,+p}(t,k)e^{ikx} + b^\dagger_{in,k}v_{in}(k,m)\phi^*_{in,+p}(t,k)e^{-ikx}\right] \\
&= \int \frac{dk}{2\pi}\frac{1}{\sqrt{2\omega_{in}}}[\{\alpha'_+(k)a_{in,k}u_{in}(k,m)\phi_{out,+p}(t,k) + b^\dagger_{in,-k}v_{in}(-k,m)\beta'^*_+(k)\phi_{out,-p}(t,k)\}e^{ikx} \\
&\quad +\{\alpha'^*_+(k)b^\dagger_{in,k}v_{in}(k,m)\phi^*_{out,+p}(t,k) + a_{in,-k}u_{in}(-k,m)\beta'_+(k)\phi^*_{out,-p}(t,k)\}e^{-ikx}]
\end{aligned} \tag{IV.15}$$

where we have used the facts that the k integral is from $-\infty$ to ∞ and $\alpha'_\pm$, $\beta'_\pm$ and $\phi_{\pm p}$ are functions of $|k|$. In $t\to\infty$ limit, $m(t)\to m_{out}$, so,

$$\begin{aligned}
\lim_{t\to\infty}\Psi(x,t) &= \int \frac{dk}{2\pi}\frac{1}{\sqrt{2\omega_{out}}}\sqrt{\frac{\omega_{out}}{\omega_{in}}}[\{\alpha'_+(k)a_{in,k}u_{in}(k,m_{out}) + b^\dagger_{in,-k}v_{in}(-k,m_{out})\beta'^*_+(k)\}e^{-ik\cdot x} \\
&\quad +\{\alpha'^*_+(k)b^\dagger_{in,k}v_{in}(k,m_{out}) + a_{in,-k}u_{in}(-k,m_{out})\beta'_+(k)\}e^{ik\cdot x}]
\end{aligned}$$

Comparing with the mode expansion in the 'out' solution basis in the same limit $t\to\infty$,

$$\lim_{t\to\infty}\Psi(x,t) = \int \frac{dk}{2\pi}\frac{1}{\sqrt{2\omega_{out}}}\left[a_{out,k}u_{out}(k,m_{out})\phi_{out,+p}(t,k)e^{ikx} + b^\dagger_{out,k}v_{out}(k,m_{out})\phi^*_{out,+p}(t,k)e^{-ikx}\right]$$

we get the Bogoliubov transformations of the creation and annihilation operators.

$$a_{out,k} = \alpha_+(k)a_{in,k} + b^\dagger_{in,-k}\,\chi(k,m_{out})\beta^*_+(k) \tag{IV.16}$$
$$b^\dagger_{out,k} = \alpha^*_+(k)b^\dagger_{in,k} + a_{in,-k}\,\tilde\chi(k,m_{out})\beta_+(k) \tag{IV.17}$$

where $\alpha_+(k) = \sqrt{\frac{\omega_{out}(\omega_{out}+m_{out})}{\omega_{in}(\omega_{in}+m_{in})}}\,\alpha'_+$ and $\beta_+(k) = \sqrt{\frac{\omega_{out}(\omega_{out}+m_{out})}{\omega_{in}(\omega_{in}+m_{in})}}\,\beta'_+(k)$. Using (IV.114)

$$\begin{aligned}
\chi(k,m_{out}) &= \frac{1}{2m_{out}}\sqrt{\frac{\omega_{in}+m_{in}}{\omega_{out}+m_{out}}}\,\bar u_{out}(k,m_{out},\omega_{out})v_{in}(-k,m_{out},-\omega_{out}) \\
&= \mathrm{sgn}(k) \qquad \text{when} \quad m_{out}\to 0
\end{aligned} \tag{IV.18}$$

where we have to be careful that $v_{in}(k,m_{out})$ is a functional of the accompanying mode, which is $\sim e^{-i\omega_{out}t}$ in the above case. Similarly, with $m_{out}\to 0$,

$$\tilde\chi(k) = -\frac{1}{2m_{out}}\sqrt{\frac{\omega_{in}+m_{in}}{\omega_{out}+m_{out}}}\,\bar v(k,m_{out},\omega_{out})u(-k,m_{out},\omega_{out}) = \mathrm{sgn}(k) \tag{IV.19}$$

taking into account the normalization of $\bar{v}_{out}v_{out} = -2m_{out}$. Inverting (IV.16) and (IV.17), we get

$$a_{in,k} = \alpha_+^*(k)a_{out,k} - \text{sgn}(k)\beta_+^*(k)b^\dagger_{out,-k} \tag{IV.20}$$
$$b^\dagger_{in,-k} = \alpha_+(k)b^\dagger_{out,-k} + \text{sgn}(k)\beta_+(k)a_{out,k} \tag{IV.21}$$

From here on, we will suppress the subscript 'out' on creation and annihilation operators, so $a_{out,k} = a_k$, similarly for $b_{out,k}$ and their Hermitian conjugates. Also, since $\chi(k)$ and $\tilde{\chi}(k)$ are simple sign functions, with a slight abuse of the nomenclature, we will call $\alpha_+(k)$ and $\beta_+(k)$ as the Bogoluibov coefficients. Moreover, $\chi(k)^2$ and $\tilde{\chi}(k)^2$ are identically equal to 1. So, the fermionic anti-commutation relations of the 'in' and 'out' operators constraint the Bogoluibov coefficients as

$$|\alpha_+(k)|^2 + |\beta_+(k)|^2 = 1 \tag{IV.22}$$

2.2 Explicit solutions

In the 'in' basis, for our choice of mass profile, the solutions are

$$\phi_{in,+p} = e^{-it(\omega+m)}\left(e^{-2\rho t}+1\right)^{-\frac{im}{2\rho}}\ {}_2F_1\left(\frac{i\left(|k|-m-\omega\right)}{2\rho}, -\frac{i\left(|k|+m+\omega\right)}{2\rho}; 1-\frac{i\omega}{\rho}; -e^{2t\rho}\right)$$
$$\phi_{in,-m} = e^{it(\omega-m)}\left(e^{-2\rho t}+1\right)^{-\frac{im}{2\rho}}\ {}_2F_1\left(\frac{i\left(-|k|-m+\omega\right)}{2\rho}, \frac{i\left(|k|-m+\omega\right)}{2\rho}; \frac{i\omega}{\rho}+1; -e^{2t\rho}\right)$$

where $\omega = \sqrt{k^2+m^2}$. While in the 'out' basis, the solutions are

$$\phi_{out,+p} = e^{-i|k|t}\left(e^{-2\rho t}+1\right)^{-\frac{im}{2\rho}}\ {}_2F_1\left(\frac{i|k|-im+i\omega}{2\rho}, \frac{i|k|-im-i\omega}{2\rho}; 1+\frac{i|k|}{\rho}; -e^{-2\rho t}\right)$$
$$\phi_{out,-m} = e^{i|k|t}\left(e^{-2\rho t}+1\right)^{-\frac{im}{2\rho}}\ {}_2F_1\left(\frac{-i|k|-im+i\omega}{2\rho}, \frac{-i|k|-im-i\omega}{2\rho}; 1-\frac{i|k|}{\rho}; -e^{-2\rho t}\right)$$

Using the properties of confluent hypergeometric functions ${}_2F_1$ given in [112], the Bogoliubov coefficients of the frequency modes as defined in (IV.10) are

$$\alpha'_+ = \frac{\Gamma\left(-\frac{i|k|}{\rho}\right)\Gamma\left(1-\frac{i\omega}{\rho}\right)}{\Gamma\left(-\frac{i(|k|+m+\omega)}{2\rho}\right)\Gamma\left(1+\frac{-i|k|+im-i\omega}{2\rho}\right)} \tag{IV.23}$$
$$\beta'_+ = \frac{\Gamma\left(\frac{i|k|}{\rho}\right)\Gamma\left(1-\frac{i\omega}{\rho}\right)}{\Gamma\left(1-\frac{i(-|k|-m+\omega)}{2\rho}\right)\Gamma\left(-\frac{i(-|k|+m+\omega)}{2\rho}\right)} \tag{IV.24}$$

In the sudden limit($\rho \to \infty$). the Bogoliubov coefficients of the frequency modes are

$$\alpha'_+(k) = \frac{|k| + m_{in} + \sqrt{k^2+m^2}}{2|k|} \tag{IV.25}$$
$$\beta'_+(k) = \frac{|k| - m_{in} - \sqrt{k^2+m^2}}{2|k|} \tag{IV.26}$$

As mentioned above, for a quench starting from the ground state of the massive theory, the naive sudden limit gives a non-normalizable state in the massless theory [3]. The problem arises only for a quench starting from the ground state. In case the quench is starting from squeezed states of our interest, the naive sudden limit given above works well. As defined in (IV.16) and (IV.17), the Bogoluibov coefficients of the oscillator modes differ from $\alpha'_+(k)$ and $\beta'_+(k)$ by an overall factor.

$$\alpha_+ = \sqrt{1-\frac{m}{\sqrt{k^2+m^2}}}\frac{\Gamma\left(-\frac{i|k|}{\rho}\right)\Gamma\left(1-\frac{i\omega}{\rho}\right)}{\Gamma\left(-\frac{i(|k|+m+\omega)}{2\rho}\right)\Gamma\left(1+\frac{-i|k|+im-i\omega}{2\rho}\right)} \tag{IV.27}$$

$$\beta_+ = \sqrt{1-\frac{m}{\sqrt{k^2+m^2}}}\frac{\Gamma\left(\frac{i|k|}{\rho}\right)\Gamma\left(1-\frac{i\omega}{\rho}\right)}{\Gamma\left(1-\frac{i(-|k|-m+\omega)}{2\rho}\right)\Gamma\left(-\frac{i(-|k|+m+\omega)}{2\rho}\right)} \tag{IV.28}$$

In the sudden limit, they are

$$\alpha_+(k) = \sqrt{1-\frac{m}{\sqrt{k^2+m^2}}}\frac{|k|+m+\sqrt{k^2+m^2}}{2|k|} \tag{IV.29}$$

$$\beta_+(k) = \sqrt{1-\frac{m}{\sqrt{k^2+m^2}}}\frac{|k|-m-\sqrt{k^2+m^2}}{2|k|} \tag{IV.30}$$

For completeness, the expressions of α'_- and β'_- in (IV.11) for our particular quench protocol are

$$\alpha'_- = \frac{\Gamma\left(-\frac{i|k|}{\rho}\right)\Gamma\left(1-\frac{i\omega}{\rho}\right)}{\Gamma\left(-\frac{i(|k|-m+\omega)}{2\rho}\right)\Gamma\left(1-\frac{i(|k|+m+\omega)}{2\rho}\right)} \tag{IV.31}$$

$$\beta'_- = \frac{\Gamma\left(\frac{i|k|}{\rho}\right)\Gamma\left(1-\frac{i\omega}{\rho}\right)}{\Gamma\left(\frac{i(|k|+m-\omega)}{2\rho}\right)\Gamma\left(1-\frac{i(-|k|+m+\omega)}{2\rho}\right)} \tag{IV.32}$$

3 Quenched states

3.1 From ground state

Starting from the ground state of the massive theory $|\Psi\rangle = |0, in\rangle$, using Eq (IV.20), the state in terms of 'out' operators is given by

$$\begin{aligned} a_{in,k}|\Psi\rangle = 0 \quad &\Rightarrow \left[\alpha_+^*(k)a_k - \text{sgn}(k)\beta_+^*(k)b_{-k}^\dagger\right]|\Psi\rangle = 0 \\ &\Rightarrow |\Psi\rangle = e^{\sum_k \text{sgn(k)}\gamma(k)a_k^\dagger b_{-k}^\dagger}|0\rangle \end{aligned} \tag{IV.33}$$

$$\text{where} \quad \gamma(k) = \frac{\alpha_+^*(k)}{\beta_+^*(k)} \tag{IV.34}$$

where we have taken $|0\rangle$ to be the ground state of 'out' oscillators. Using the Baker-Campbell-Hausdorff(BCH) formula derived in appendix (IV.E), the above state can be written in gCC form. For the particular mass profile (IV.3), $\alpha_+(k)$ and $\beta_+(k)$ are given in (IV.27) and (IV.28). The gCC form which was first obtained in MPS is

$$|\Psi\rangle = e^{-\kappa_2 H - \kappa_4 W_4 - \kappa_6 W_6 - \dots}|D\rangle \tag{IV.35}$$

where

$$\kappa_2 = \frac{1}{2m} + \frac{\pi^2 m}{12\rho^2} + \frac{1}{m}\mathcal{O}\left(\frac{m}{\rho}\right)^3, \quad \kappa_4 = -\frac{1}{12m^3} + \frac{\pi^2}{24m\rho^2} + \frac{1}{m^3}\mathcal{O}\left(\frac{m}{\rho}\right)^3,$$
$$\kappa_6 = \frac{3}{80m^5} - \frac{\pi^2}{96m^3\rho^2} + \frac{1}{m^5}\mathcal{O}\left(\frac{m}{\rho}\right)^3, \dots \tag{IV.36}$$

and $|D\rangle$ is the Dirichelet state and the explicit expression is in Appendix IV.C. It should be noted that since the mass does not go to zero at any finite time, the above state should is only valid in sufficiently long time limit and the correction due to the non-vanishing mass is $\mathcal{O}(e^{-\rho t})$.

3.2 From squeezed states: CC state and gCC states

We could start with specially prepared squeezed states so that after the quench, the states become CC states or gCC states. Here, we will consider only the simple case of sudden quench ($\rho \to \infty$). For our aim of creating a CC state or a gCC state, finite 'ρ' quenches are an unnecessary complication.

We start with a squeezed state of 'in' modes

$$|S\rangle = \exp\left(\sum_{k=-\infty}^{\infty} f(k) a^\dagger_{in,k} b^\dagger_{in,-k}\right)|0, in\rangle \tag{IV.37}$$

where unlike $\gamma(k)$, $f(k)$ need not be an even function of k, but $|f(k)|^2$ is an even function of k.

It is easier to work with $|S\rangle$ as an operator relation. $|S\rangle$ can also be defined as

$$\tilde{a}_k|S\rangle = \tilde{b}_k|S\rangle = 0 \text{ and } \quad \left\{\tilde{a}_k, \tilde{a}^\dagger_{k'}\right\} = \left\{\tilde{b}_{-k}, \tilde{b}^\dagger_{-k'}\right\} = \delta(k-k') \tag{IV.38}$$

where the new operators in terms of the out modes using (IV.20) and (IV.21) are

$$\begin{aligned}
\tilde{a}_k &= \frac{1}{\sqrt{(1+|f(k)|^2)}} a_{in,k} - \frac{f(k)}{\sqrt{(1+|f(k)|^2)}} b^\dagger_{in,-k} \\
&= A^*(k) a_{out,k} - \text{sgn}(k) B^*(k) b_{out,-k} \\
\tilde{b}_{-k} &= \frac{1}{\sqrt{(1+|f(k)|^2)}} b_{in,-k} + \frac{f(k)}{\sqrt{(1+|f(k)|^2)}} a^\dagger_{in,k} \\
&= A^*(k) b_{out,-k} + \text{sgn}(k) B^*(k) a^\dagger_{out,k}
\end{aligned} \tag{IV.39}$$

where $A(k)$ and $B(k)$ are the Bogoliubov coefficients for the transformation from '*tilde*' operators to 'out' operators and are given by

$$A(k) = \frac{\alpha_+(k) - \text{sgn}(k)\beta_+^*(k)f^*(k)}{\sqrt{(1+|f(k)|^2)}}, \quad B(k) = \frac{\beta_+(k) + \text{sgn}(k)\alpha_+^*(k)f^*(k)}{\sqrt{(1+|f(k)|^2)}} \tag{IV.40}$$

$$|A(k)|^2 + |B(k)|^2 = 1 \tag{IV.41}$$

Now using the BCH formula (IV.133) from appendix (IV.E),

$$|S\rangle = \exp\left\{ -\sum_k \tilde{\kappa}(k) \left(a^\dagger_{out,k} a_{out,k} + b^\dagger_{out,k} b_{out,k} \right) \right\} |D\rangle \tag{IV.42}$$

$$\text{where} \quad \tilde{\gamma}(k) = \frac{B^*(k)}{A^*(k)}, \quad \text{and} \quad \tilde{\kappa}(k) = -\frac{1}{2}\log(\tilde{\gamma}(k))$$

For a CC state, i.e., so that $|S\rangle$ in eqn (IV.42) is $e^{-\kappa_2 H}|D\rangle$, $f(k)$ should be tuned as

$$f(k) = \frac{\left(\sqrt{k^2+m^2}+m\right)\cosh(\kappa_2 k) - k\sinh(\kappa_2 k)}{\left(\sqrt{k^2+m^2}+m\right)\sinh(\kappa_2 k) + k\cosh(\kappa_2 k)} \tag{IV.43}$$

Starting with

$$f(k) = \frac{k - k\, e^{2|k|\left(\kappa_2+\kappa_4 k^2\right)} + \text{sgn}(k)\left(\sqrt{k^2+m^2}+m\right)\left(e^{2|k|\left(\kappa_2+\kappa_4 k^2\right)}+1\right)}{|k|\left(e^{2|k|(\kappa_2+\kappa_4 k^2)}+1\right) + \left(\sqrt{k^2+m^2}+m\right)\left(e^{2|k|(\kappa_2+\kappa_4 k^2)}-1\right)} \tag{IV.44}$$

we get a gCC state of the form $e^{-\kappa_2 H - \kappa_4 W_4}|D\rangle$, where as mentioned earlier, W_4 is the conserved charge of the $\mathcal{W}_4$ current of free Dirac fermions[4]. Note that $f(k)$ are odd functions of k. For future reference, we can invert Eq (IV.39) and we write down the 'in' and 'out' operators in terms of the '*tilde*' operators.

$$a_{in,k} = \frac{1}{\sqrt{(1+|f(k)|^2)}}\tilde{a}_k + \frac{f(k)}{\sqrt{(1+|f(k)|^2)}}\tilde{b}^\dagger_{-k} \tag{IV.45}$$

$$b^\dagger_{in,-k} = \frac{1}{\sqrt{(1+|f(k)|^2)}}\tilde{b}^\dagger_{-k} - \frac{f^*(k)}{\sqrt{(1+|f(k)|^2)}}\tilde{a}_k \tag{IV.46}$$

$$a_{out,k} = A(k)\tilde{a}_k + \text{sgn}(k)B^*(k)\tilde{b}^\dagger_{-k} \tag{IV.47}$$

$$b^\dagger_{out,-k} = A^*(k)\tilde{b}^\dagger_{-k} - \text{sgn}(k)B(k)\,\tilde{a}_k \tag{IV.48}$$

4 Energy density

In the post-quench theory, the occupation number is given by

$$\hat{N}_k = a^\dagger_k a_k + b^\dagger_k b_k \tag{IV.49}$$

[4]For the action (IV.1), $H = \sum_k |k|(a^\dagger_k a_k + b^\dagger_k b_k)$ or $H = \int \frac{dk}{2\pi}|k|(a^\dagger_k a_k + b^\dagger_k b_k)$. $\mathcal{W}_4$ has been normalized so that $W_4 = \sum_k |k|^3(a^\dagger_k a_k + b^\dagger_k b_k)$ or $W_4 = \int \frac{dk}{(2\pi)^3}|k|^3(a^\dagger_k a_k + b^\dagger_k b_k)$ in the continuum limit.

using the Bogoliubov transformations (IV.47) and (IV.48) and definition of $|\tilde{0}\rangle$ in (IV.38), the expectation value of the occupation number is given by

$$\begin{aligned} N_k &= \lim_{t\to\infty}\langle\tilde{0}|a_k^\dagger a_k + b_k^\dagger b_k|\tilde{0}\rangle \\ &= B^*(k)B(k)\langle\tilde{0}|\tilde{b}_{-k}^\dagger\tilde{b}_{-k}|\tilde{0}\rangle + B^*(-k)B(-k)\langle\tilde{0}|\tilde{a}_{-k}^\dagger\tilde{a}_{-k}|\tilde{0}\rangle + ... \\ &= B^*(k)B(k) + B^*(-k)B(-k) \end{aligned} \tag{IV.50}$$

The expression of $B(k)$ is given in (IV.40). For ground state, we have to use $f(k) = 0$ in the expression of $B(k)$. So, energy density of the post-quench state is given by

$$E = \int_{-\infty}^{\infty}\frac{dk}{2\pi}|k|\left[B^*(k)B(k) + B^*(-k)B(-k)\right] \tag{IV.51}$$

Ground state quench

For ground state quench, the occupation number is given by

$$N_k = \lim_{t\to\infty}\langle 0, in|\hat{N}_k|0, in\rangle = |\beta_+(k)|^2 + |\beta_+(-k)|^2$$

Since $\alpha_+(k)$ and $\beta_+(k)$ are even functions of k. Using (IV.22), (IV.34) and (IV.134), we have

$$|\beta_+(k)|^2 = \frac{|\gamma(k)|^2}{1+|\gamma(k)|^2}, \qquad |\gamma(k)|^2 = e^{-4\kappa(k)} \tag{IV.52}$$

Hence, the occupation number in the ground state in the asymptotically long time limit is given by

$$N_k = \frac{2}{e^{4\kappa(k)}+1} \tag{IV.53}$$

This is the occupation number in a GGE defined as

$$\mathrm{Tr}\, e^{-\sum_k 4\kappa(k)\hat{N}_k} = \mathrm{Tr} e^{-4\kappa_2 H - 4\kappa_4 W_4 - \kappa_6 W_6 - \cdots} \tag{IV.54}$$

where the κ's are given in (IV.36). Using the expressions of $\beta_+(k)$ from (IV.28), the explicit expression of the occupation number is

$$\begin{aligned} N_k &= \operatorname{csch}\left(\frac{\pi k}{\rho}\right)\left(\cosh\left(\frac{\pi m}{\rho}\right) - \cosh\left(\frac{\pi\left(k-\sqrt{k^2+m^2}\right)}{\rho}\right)\right)\operatorname{csch}\left(\frac{\pi\sqrt{k^2+m^2}}{\rho}\right) \\ &\xrightarrow{\rho\to\infty} 1 - \frac{k}{\sqrt{k^2+m^2}} \end{aligned}$$

It is interesting that in $m \to \infty$ limit, $N_k \to 1$, not 2. This is because $\lim_{\rho\to\infty}|\alpha_+(k)|^2 = 1/2$ and we have the constraint $|\alpha_+(k)|^2 + |\beta_+(k)|^2 = 1$.
For arbitrary ρ, the energy density cannot be calculated in closed form. In the sudden limit $\rho \to \infty$, the energy density diverges as $\log(\Lambda)$ where Λ is the UV cutoff. Hence, all other W charges also diverge in the sudden limit. Hence, naively taking $\rho \to \infty$ produce a non-renormalizable state. So, the sudden limit has to be taken as in MPS where $m/\Lambda \to 0$ while $m/\rho \to \epsilon^+$. Simply put, the quench rate parameter ρ should be much small than the UV cut-off.

Squeezed state quench: CC and gCC states

For CC state given by (IV.43), the expectation value of occupation number is given by

$$N_k = \frac{2}{1 + e^{4\kappa_2 |k|}} \tag{IV.55}$$

This is the occupation number of fermions in a thermal ensemble of temperature $1/\beta = 1/4\kappa_2$. The enengy density is

$$E = \int_{-\infty}^{\infty} \frac{dk}{2\pi} N_k = \frac{\pi}{96\kappa_2^2} \tag{IV.56}$$

Similarly, for gCC state given by (IV.44), the expectation value of occupation number is given by

$$N_k = \langle gCC|\hat{N}_k|gCC\rangle = \frac{2}{1 + e^{4\kappa_2|k| + 4\kappa_4|k|^3}} \tag{IV.57}$$

This is same as the occupation number of fermions in a generalised Gibbs ensemble of temperature $1/\beta = 4\kappa_2$ and chemical potential $\mu_4 = 4\kappa_4$ of W_4 charge. The enengy density cannot be calculated in closed form.

5 Correlation functions

Since our theory is a free theory, all the observables can be explicitly calculated. In the following subsections we calculate $\langle \psi^\dagger(r,t)\psi(0,t)\rangle$ correlation functions for the three different states obtained above. The quench process cannot differentiate between holomorphic dof('left-movers') and anti-holomorphic dof('right-movers'), so $\langle \bar{\psi}^\dagger(0,t)\bar{\psi}(r,t)\rangle$ is equal to $\langle \psi^\dagger(r,t)\psi(0,t)\rangle$ and they are time independent quantities.[5] We also calculated $\langle \bar{\psi}^\dagger(r,t)\psi(0,t)\rangle$ which has non-trivial time-dependence. Also as expected, $-\langle \psi^\dagger(0,t)\bar{\psi}(r,t)\rangle$ is the complex conjugate of $\langle \bar{\psi}^\dagger(r,t)\psi(0,t)\rangle$. Since, we are calculating equal-time correllation functions, so for example for $\langle \psi^\dagger(r,t)\psi(0,t)\rangle$, we would rather be calculating $\frac{1}{2}\langle \psi^\dagger(r,t)\psi(0,t) - \psi(0,t)\psi^\dagger(r,t)\rangle$.

Using the Bogoluibov transformations (IV.47) and (IV.48) in the chiral mode expansions (IV.116) and (IV.117) we get

$$\psi(w) = \int_0^\infty \frac{dk}{2\pi}\Big[A(k)\tilde{a}_k e^{-ikw} + \mathrm{sgn}(k)B^*(k)\tilde{b}^\dagger_{-k}e^{-ikw} + A^*(-k)\tilde{b}^\dagger_k e^{ikw} + \mathrm{sgn}(k)B(-k)\tilde{a}_{-k}e^{ikw}\Big] \tag{IV.58}$$

$$\bar{\psi}(\bar{w}) = \int_0^\infty \frac{dk}{2\pi}\Big[A(-k)\tilde{a}_{-k}e^{-ik\bar{w}} - \mathrm{sgn}(k)B^*(-k)\tilde{b}^\dagger_k e^{-ik\bar{w}} - A^*(k)\tilde{b}^\dagger_{-k}e^{ik\bar{w}} + \mathrm{sgn}(k)B(k)\tilde{a}_k e^{ik\bar{w}}\Big] \tag{IV.59}$$

[5]A simple reason why these quantities are time independent is the fact that they are holomorphic-holomorphic and antiholomorphic-antiholomorphic quantities and they cannot 'see' the presence of the boundary state $|D\rangle$. They are already thermalized/equilibrated.

where $w = t - x$ and $\bar{w} = t + x$. For the ground state quench, $f(k) = 0$, $\tilde{a}_k = a_{in,k}$, $\tilde{b} = b_{in,k}$ and $|\tilde{0}\rangle = |0, in\rangle$.
For a general $f(k)$ corresponding to some $|\tilde{0}\rangle$, the correlation functions are

$$\langle\tilde{0}|\psi^\dagger(0,t)\psi(r,t)|\tilde{0}\rangle = \frac{1}{2}\int_0^\infty \frac{dk}{2\pi}\left[(2|B(k)|^2-1)e^{ikr} - (2|B(-k)|^2-1)e^{-ikr}\right] \tag{IV.60}$$

$$\langle\tilde{0}|\bar{\psi}^\dagger(0,t)\psi(r,t)|\tilde{0}\rangle = -\int_0^\infty \frac{dk}{2\pi}\left[\mathrm{sgn}(k)A^*(-k)B(-k)e^{ik(2t-r)} + \mathrm{sgn}(k)A(k)B^*(k)e^{-ik(2t-r)}\right] \tag{IV.61}$$

where we have used (IV.41) to write $A(k)$ in terms of $B(k)$ in the first equation.

Ground state quench:

Taking careful limit, for ground state quench, we have

$$\begin{aligned}
\langle 0, in|\psi^\dagger(0,t)\psi(r,t)|0, in\rangle &= -\frac{1}{2}\int_{-\infty}^\infty \frac{dk}{2\pi}\frac{|k|}{\sqrt{k^2+m^2}} \\
&= \frac{1}{4}m\left[\boldsymbol{L}_{-1}(mr) - I_1(mr)\right] \\
&\xrightarrow{m\to\infty} \frac{1}{2\pi m r^2} + \frac{3}{2\pi m^3 r^4} + O\left(\frac{1}{m^4}\right) \qquad \text{(IV.62)} \\
\langle\tilde{0}|\bar{\psi}^\dagger(0,t)\psi(r,t)|\tilde{0}\rangle &= \int_0^\infty \frac{dk}{2\pi}\frac{i\,\mathrm{sgn}(k)\,m\sin(k(2t-r))}{\sqrt{k^2+m^2}} \\
&= -\frac{im}{4}\left[\mathrm{sgn}(r-2t)I_0(m(r-2t)) - \boldsymbol{L}_0(m(r-2t))\right] \\
&\xrightarrow[t>r/2]{m\to\infty} \frac{i}{2\pi(2t-r)} + \frac{i}{2\pi m^2(2t-r)^3} + O\left(\frac{1}{m^4}\right) \qquad \text{(IV.63)}
\end{aligned}$$

where $I_\nu(x)$ is Modified Bessel Function of the First Kind and $\boldsymbol{L}_\nu(x)$ is Modified Struve Function.

Quenched squeezed state - CC state:

For CC state, all the calculations are done in $|S_{CC}\rangle$ defined as the state (IV.37) with the expression of $f(k)$ given in (IV.43).

$$\begin{aligned}
\langle CC|\psi^\dagger(0,t)\psi(r,t)|CC\rangle &= -i\int_0^\infty \frac{dk}{2\pi}\tanh(2\kappa_2|k|)\sin(kr) && \text{(IV.64)}\\
&= -i\int_0^\infty \frac{dk}{2\pi}\sin(kr)\left[\frac{1}{e^{4\kappa_2|k|}+1}-\frac{1}{2}\right] && \text{(IV.65)}\\
&= -\frac{i\,\mathrm{csch}\left(\frac{\pi r}{4\kappa_2}\right)}{8\kappa_2} && \text{(IV.66)}\\
\langle CC|\bar{\psi}^\dagger(0,t)\psi(r,t)|CC\rangle &= -i\int_0^\infty \frac{dk}{2\pi}\mathrm{sech}(2k\kappa_2)\cos(k(2t-r)) && \text{(IV.67)}\\
&= -\frac{i\,\mathrm{sech}\left(\frac{\pi(2t-r)}{4\kappa_2}\right)}{8\kappa_2} && \text{(IV.68)}
\end{aligned}$$

These are exactly what have been calculated using BCFT techniques [44]. It is evident from (IV.65) that $\psi^\dagger\psi$ expectation value is already the thermal expectation value at temperature $T = 1/\beta = 1/(4\kappa_2)$, i.e., it is already thermalized.

Quenched squeezed state - gCC state with W_4:

Similarly, for gCC state, all the calculations are done in $|S_{fCC}\rangle$ defined as the state (IV.37) with the expression of $f(k)$ given in (IV.44).

$$\begin{aligned}
\langle\psi^\dagger(0,t)\psi(r,t)\rangle_{gCC} &= -i\int_0^\infty \frac{dk}{2\pi}\tanh\left(2\kappa_2|k|+2\kappa_4|k|^3\right)\sin(kr) && \text{(IV.69)}\\
&= -i\int_0^\infty \frac{dk}{2\pi}\sin(kr)\left[\frac{1}{e^{4\kappa_2|k|+4\kappa_4|k|^3}+1}-\frac{1}{2}\right] && \text{(IV.70)}\\
\langle\bar{\psi}^\dagger(r,t)\psi(0,t)\rangle_{gCC} &= -i\int_0^\infty \frac{dk}{2\pi}\mathrm{sech}(2\kappa_2 k+2\kappa_4 k^3)\cos(k(2t-r)) && \text{(IV.71)}
\end{aligned}$$

Again, it is evident from (IV.70) that $\psi^\dagger\psi$ expectation value is already thermalized into the expectation value in a GGE with $T = 1/\beta = 1/4\kappa_2$ and $\mu = 4\kappa_4$. A possible way of evaluating these integrals (which yield no closed form answer) is via the residue theorem. The integrands in both cases, have poles at the solutions of $2\kappa_2 k + 2\kappa_4 k^3 = \frac{2n+1}{2}i\pi$, where $n \in \mathbb{Z}$. These poles and their residues have been treated in detail in [3]. The sum of residues is still an infinite sum which cannot be performed. In the perturbative regime ($\kappa_4/\kappa_2^3 << 1$), we see that our correlators match the general form presented in [2] with $h = 1/2$ as expected.

As expected form MPS, here in the fermionic theory also we see the UV/IR mixing. For the ground state quench, all the charges affect the long distance and long time limit of the correlators. This is explicit seen in the case of gCC state with W_4 charge only. The long time and large distance limit or the correlators are very much dependent upon k_4, although a naive Wilsonian RG argument would show that k_4 is an irrelevant coupling.

6 Exact Growth of Entanglement in CC state

We will consider only a finite single interval or subsystem A, with its endpoints at $(w_1, \bar{w}_1)$ and $(w_2, \bar{w}_2)$ in light-cone coordinates, or $(0, t)$ and (r, t) in space and time coordinates. Using the replica trick ([126], [93]), the n^{th} Rényi entropy $S_n(A)$ of the interval is given by the logarithm of the expectation value of twist and antitwist operators inserted at the end-points.

$$S_n(A) = \frac{1}{1-n} \log\langle\Psi(t)|\mathcal{T}_n(w_1, \bar{w}_1)\tilde{\mathcal{T}}_n(w_2, \bar{w}_2)|\Psi(t)\rangle \tag{IV.72}$$

The entanglement entropy(EE) S_A is given by $\lim_{n\to 1} S_n(A)$. We can diagonalize the twist operators and write them as products of twist fields. Hence,

$$\mathcal{T}_n(w, \bar{w}) = \prod_{k=-(n-1)/2}^{k=(n-1)/2} \mathcal{T}_{k,n}(w, \bar{w}), \quad \tilde{\mathcal{T}}_n(w, \bar{w}) = \prod_{k=-(n-1)/2}^{k=(n-1)/2} \tilde{\mathcal{T}}_{k,n}(w, \bar{w}) \tag{IV.73}$$

In CC state, in Heisenberg picture, the quantity of our interest is

$$Z_k = \langle D_f|e^{-\kappa_2 H_f}\mathcal{T}_{k,n}(0, t)\tilde{\mathcal{T}}_{k,n}(r, t)e^{-\kappa_2 H_f}|D_f\rangle \tag{IV.74}$$

The subscript 'f' means we are working in the fermionic theory and the subscript 'b' would mean we are working in the bosonic theory. To find the exact expression of the entanglement entropy of a spatial region in our free fermionic CFT, we will use the method using bosonization described in [127]. Moreover, as shown in Appendix(IV.D), Dirichlet state $|D_f\rangle$ in fermionic theory corresponds to a Dirichlet state in the bosonic theory $|D_b\rangle$ and H_f corresponds to H_b. So, we get

$$Z_k = \langle D_b|e^{-\kappa_2 H_b}e^{i\sqrt{4\pi}\frac{k}{n}(\phi(0,t)-\phi(r,t))}e^{-\kappa_2 H_b}|D_b\rangle \tag{IV.75}$$

This is a free scalar theory in a strip geometry with Dirichlet boundary conditions and operator insertions at $(0, t)$ and (r, t). It can be calculated explicitly

$$\log[Z_k] = -4\pi \frac{2k^2}{n^2} \left(\langle\phi(0, t)\phi(0, t)\rangle - \langle\phi(0, t)\phi(r, t)\rangle\right) \tag{IV.76}$$

The n^{th} Rényi entropy of interval A is given by

$$\begin{aligned} S_n(A) &= -4\pi\frac{1}{1-n}\sum_{k=-(n-1)/2}^{k=(n-1)/2} \frac{2k^2}{n^2} \left(\langle\phi(0, t)\phi(0, t)\rangle - \langle\phi(0, t)\phi(r, t)\rangle\right) \\ &= 4\pi \frac{n+1}{6n} \left(\langle\phi(0, t)\phi(0, t)\rangle - \langle\phi(0, t)\phi(r, t)\rangle\right) \end{aligned} \tag{IV.77}$$

Taking $n \to 1$ limit, we get the entanglement entropy,

$$S_A = 4\pi \frac{1}{3} \left(\langle\phi(0, t)\phi(0, t)\rangle - \langle\phi(0, t)\phi(r, t)\rangle\right) \tag{IV.78}$$

Remark on winding number: While the free boson considered in MPS [3] is the uncompactified free boson, the boson in (IV.75) is a compactified free boson. So, Hamiltonian of the compactifed boson has zero mode terms but the winding number is not important for our analysis. In the large system size limit($L \to \infty$), the zero modes vanished. Even if we are taking the limiting case of a finite size system, the zero momentum modes do not play any role in our calculation. Using the mode expansion of the boson $\phi(w, \bar{w}) = \varphi(w) + \bar{\varphi}(\bar{w})$ in [128],

$$\varphi(w) = Q + \frac{P}{2L} w + \sum_{n>0} \frac{1}{\sqrt{4\pi n}} \left(d_n e^{-inw} + d_n^\dagger e^{inw} \right) \tag{IV.79}$$

$$\bar{\varphi}(\bar{w}) = \bar{Q} + \frac{\bar{P}}{2L} \bar{w} + \sum_{n>0} \frac{1}{\sqrt{4\pi n}} \left(d_{-n} e^{-in\bar{w}} + d_{-n}^\dagger e^{in\bar{w}} \right) \tag{IV.80}$$

First, Q and $\bar{Q}$ are cancelled identically in (IV.75). Moreover, by bosonization formulae [128, 129],

$$P = \sqrt{4\pi} N_f \qquad \bar{P} = \sqrt{4\pi} \bar{N}_f \tag{IV.81}$$

$$N_f = J_0 = -\sum_{k=0}^{\infty} \left[a_k^\dagger a_k - b_k^\dagger b_k \right] \qquad \bar{N}_f = \bar{J}_0 = -\sum_{k=0}^{\infty} \left[a_{-k}^\dagger a_{-k} - b_{-k}^\dagger b_{-k} \right] \tag{IV.82}$$

But for our particular CC state, from (IV.131), $N_f|CC_f\rangle = 0$ and $\bar{N}_f|CC_f\rangle = 0$. Now, P and $\bar{P}$ commute with all the other bosonic creation and annihilation operators of non-zero momentum, hence they don't play any role in the calculation of (IV.75). If we still keep the system size finite, the winding number would be important to interpret the stationary limit as a thermal ensemble. But we must take the $L \to \infty$ limit, if we want to examine the stationary limit. In other words, L is the largest length scale in our theory and time $t << L$.

The bosonic propagator in CC state has been calculated in [3]. It is given by

$$\langle CC|\phi(0,t)\phi(r,t)|CC\rangle = -\frac{1}{8\pi} \log \left(\frac{2\sinh^2\left(\frac{\pi r}{4\kappa_2}\right)}{\cosh\left(\frac{\pi r}{2\kappa_2}\right) + \cosh\left(\frac{\pi t}{\kappa_2}\right)} \right) \tag{IV.83}$$

$r \to 0$ gives the UV divergence of scalar field theory in 2D spacetime. The n^{th} Rényi entropy and entanglement entropy of interval A in CC state is given by

$$S_n(A) = \frac{n+1}{12n} \left[\log \left(\frac{\sinh^2\left(\frac{\pi r}{4\kappa_2}\right)\left(1 + \cosh\left(\frac{\pi t}{\kappa_2}\right)\right)}{\cosh\left(\frac{\pi r}{2\kappa_2}\right) + \cosh\left(\frac{\pi t}{\kappa_2}\right)} \right) - \lim_{\epsilon \to 0+} 2\log(\epsilon) - \log\left(\frac{\pi^2}{16\kappa_2^2}\right) \right] \tag{IV.84}$$

$$S_A = \frac{1}{3} \left[\frac{1}{2} \log \left(\frac{\sinh^2\left(\frac{\pi r}{4\kappa_2}\right)\left(1 + \cosh\left(\frac{\pi t}{\kappa_2}\right)\right)}{\cosh\left(\frac{\pi r}{2\kappa_2}\right) + \cosh\left(\frac{\pi t}{\kappa_2}\right)} \right) - \lim_{\epsilon \to 0+} \log(\epsilon) - \frac{1}{2}\log\left(\frac{\pi^2}{16\kappa_2^2}\right) \right] \tag{IV.85}$$

Taking the stationary limit $t \to \infty$ gives the entanglement entropy of A in a thermal ensemble at temperature $T = 1/\beta = 1/(4\kappa_2)$.

$$S_A = \frac{1}{3} \left[\log \left(\sinh\left(\frac{\pi r}{4\kappa_2}\right) \right) - \lim_{\epsilon \to 0+} \log(\epsilon) - \frac{1}{2}\log\left(\frac{\pi^2}{16\kappa_2^2}\right) \right] \tag{IV.86}$$

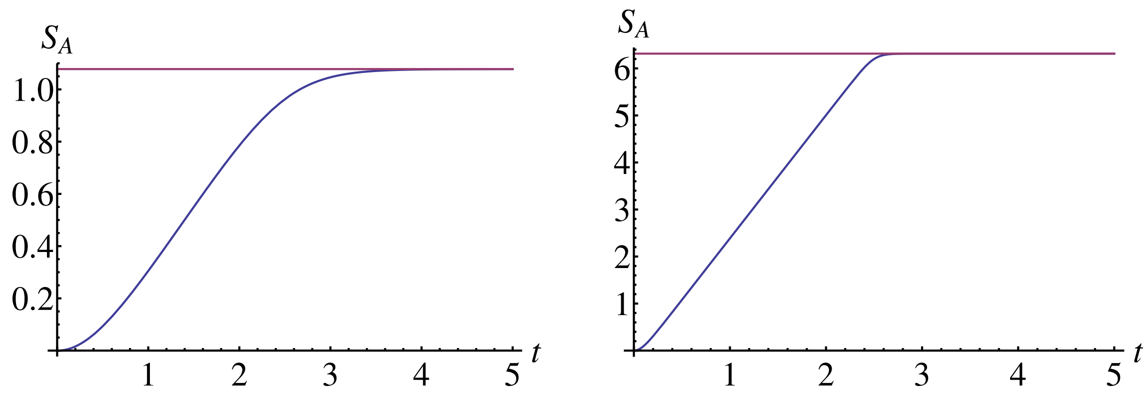

(a) Low effective temperature, $\kappa_2 = 1$ (b) High effective temperature, $\kappa_2 = 0.2$

Figure IV.1: Entanglement entropy growth of an interval(r=5) in CC state.

This exactly matches the thermal value which has been calculated using CFT techniques [93]. It is fixed only by the temperature, the central charge of the CFT($c = 1$ for dirac fermion), and 'r' the length of the interval. Taking the high temperature limit $\kappa_2 \to 0$, we get the extensive thermal entropy formula $S_{therm} = \frac{1}{3}\frac{\pi r}{\beta}$.

Besides the thermalization, the most interesting aspect of figure (IV.1) is that the entanglement entropy grows monotonically. The first derivative of S_A w.r.t. time is

$$\left\langle \frac{\partial S_A}{\partial t} \right\rangle_{CC} = \frac{\pi \sinh^2\left(\frac{\pi r}{4\kappa_2}\right) \tanh\left(\frac{\pi t}{2\kappa_2}\right)}{3\kappa_2 \left[\cosh\left(\frac{\pi r}{2\kappa_2}\right) + \cosh\left(\frac{\pi t}{\kappa_2}\right)\right]} \tag{IV.87}$$

$$= \frac{\pi}{12\kappa_2}\left[2\tanh\left(\frac{\pi t}{2\kappa_2}\right) - \tanh\left(\frac{\pi(r+2t)}{4\kappa_2}\right) + \tanh\left(\frac{\pi(r-2t)}{4\kappa_2}\right)\right] \tag{IV.88}$$

From the first expression, as a function of time $t > 0$, it is clear that there are no finite zero. Hence, the EE growth of CC state is always monotonically increasing. Also note that in the high effective temperature limit $\kappa_2 \to 0$, the approach to thermal value is sharper. In the limiting case, from the second expression, it is clear that the thermalization time is

$$t = \frac{r}{2} \tag{IV.89}$$

which has also been calculated using BCFT techniques in [20].

It would be interesting to check the monotonicity of EE growth in gCC states. Unfortunately, even for the free fermions with explicit twist operators, the entanglement entropy in gCC state with W_4 charge cannot be explicitly calculated. The bilinear fermionic $\mathcal{W}_4(w)$ current when bosonized gives ϕ^4 terms[26], so the bosonized theory is an intereacting theory.

7 Non-Monotonic EE Growth and Dynamical Phase Transition

Although we could not calculate EE in gCC state with W_4 charge of the fermionic bilinear $\mathcal{W}_4$ current, we can still calculate entanglement entropy explicitly with the fermionic

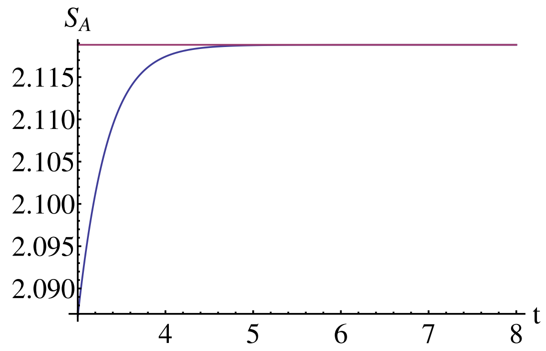

(a) Monotonic behavior, $\kappa_4 = 0.01$

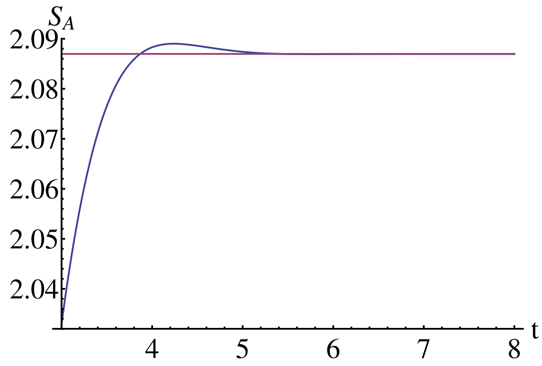

(b) Non-monotonic behaviour, $\kappa_4 = 0.30$

Figure IV.2: Entanglement entropy growth of an interval(r=5) for different choice of κ_4 and $\kappa_2 = 1$.

charge corresponding to the bosonic charge $W_4(w) = \sum_k |k|^3 d_k^\dagger d_k$, where $d_k^\dagger$ and d_k are the bosonic annihilation and creation operators. As mentioned above, the zero modes do not play any role. Refermionization of the bosonic bilinear $\mathcal{W}_4$ is done in Appendix IV.F.[6] So, the fermionic state that we are considering is

$$|\Psi\rangle = \mathrm{e}^{-\kappa_2 H_f - \kappa_4 \tilde{W}_4} |D_f\rangle \tag{IV.90}$$

where the expression for $\tilde{W}_4$ is given in (IV.137).

Again, the Rényi and entanglement entropies are given by the expression (IV.77) and (IV.78). The scalar propagator with the bosonic W_4 charge has also been calculated in MPS.

$$\langle \phi(0,t)\phi(r,t)\rangle = \int_{-\infty}^{\infty} \frac{dk}{8\pi}\frac{e^{ikr}}{k}\left[\coth\left(2k\left(\kappa_2+\kappa_4 k^2\right)\right) - \cos(2kt)\mathrm{cosech}\left(2k\left(\kappa_2+\kappa_4 k^2\right)\right)\right] \tag{IV.91}$$

The momentum integral cannot be done explicitly. But we still can plot the entanglement entropy numerically. Figure (IV.2) are the plots of EE growth with 'small' and 'large' values of κ_4. As expected, the entanglement entropy reaches an equilibrium quickly.

The most interesting aspect of Figure (IV.2) is the non-monotonic growth of EE in the gCC state with 'large' κ_4. As in case of CC state, to study the monotonic or non-monotonic behaviour of S_A, the more appropriate quantity is not S_A but rather $\frac{\partial S_A}{\partial t}$, the expression also simplifies tremendously.

$$\begin{aligned}\left\langle \frac{\partial S_A}{\partial t}\right\rangle_{gCC} &= \frac{1}{3}\int_{-\infty}^{\infty} dk\,(1-e^{ikr})\mathrm{cosech}(2\kappa_2 k + 2\kappa_4 k^3)\sin(2kt) \\ &= \frac{1}{3}\int_{-\infty}^{\infty} dk\,(1-\cos(kr))\mathrm{cosech}(2\kappa_2 k + 2\kappa_4 k^3)\sin(2kt)\end{aligned} \tag{IV.92}$$

Unfortunately, the above integral still cannot be done in closed form. The objective is to find finite positive real zeroes of the above expression as a function of time t. But, calculating

[6] We would like to thank Justin David for informing us that this refermionization could be done in principle using U(1) currents and it has not been done anywhere.

zeroes of Fourier transforms, unless it can be done in closed form, is notoriously hard, the most famous example being the Riemann hypothesis.

The most interesting question that can be asked in Figure (IV.2) is whether even a small infinitesimal κ_4, although not visible in the numerical plot, gives rise to the non-monotonic EE growth or whether the non-monotonic behaviour starts from a sharp finite value of κ_4. If it is the second case, then it is a dynamical phase transition. In other words, the question is whether (IV.92) has finite zeroes as a function of time even for an infinitesimal κ_4 or do the finite zeroes appear for κ_4 greater than a critical value.

We found that the non-monotonic behaviour starts abruptly at a critical value of $\kappa_4 = 16\kappa_2^3/27\pi^2$, *i.e., it is a dynamical phase transition. In terms of the effective temperature and chemical potential in the stationary limit,* $\beta = 4\kappa_2$ *and* $\mu_4 = 4\kappa_4$, *the critical value is* $\mu_4 = \beta^3/27\pi^2$.

Althought the integral (IV.92) cannot be done in closed form, we can take advantage of the fact that for our question we do not need to know the precise zeroes. Using contour integration, the integral is given by the sum of residues of the poles given by $2\kappa_2 k + 2\kappa_4 k^3 = in\pi$ where $n \in \mathbb{Z} - \{0\}$. $n = 0$ is not a pole of (IV.92). The expressions of the poles(from MPS)[7] are

$$k_1 = \frac{-2\,6^{2/3}\kappa_2 + \sqrt[3]{6}\left(\sqrt{48\kappa_2^3 - 81\pi^2\kappa_4 n^2} + 9i\pi\sqrt{\kappa_4}n\right)^{2/3}}{6\sqrt[3]{\sqrt{3}\sqrt{\kappa_4^3\left(16\kappa_2^3 - 27\pi^2\kappa_4 n^2\right)} + 9i\pi\kappa_4^2 n}} \tag{IV.93}$$

$$k_2 = \frac{4\sqrt[3]{-6}\kappa_2 + i\left(\sqrt{3}+i\right)\left(\sqrt{48\kappa_2^3 - 81\pi^2\kappa_4 n^2} + 9i\pi\sqrt{\kappa_4}n\right)^{2/3}}{2\,6^{2/3}\sqrt[3]{\sqrt{3}\sqrt{\kappa_4^3\left(16\kappa_2^3 - 27\pi^2\kappa_4 n^2\right)} + 9i\pi\kappa_4^2 n}} \tag{IV.94}$$

$$k_3 = -\frac{\sqrt[3]{-1}\left(2\sqrt[3]{-6}\kappa_2 + \left(\sqrt{48\kappa_2^3 - 81\pi^2\kappa_4 n^2} + 9i\pi\sqrt{\kappa_4}n\right)^{2/3}\right)}{6^{2/3}\sqrt{\kappa_4}\sqrt[3]{\sqrt{48\kappa_2^3 - 81\pi^2\kappa_4 n^2} + 9i\pi\sqrt{\kappa_4}n}} \tag{IV.95}$$

Out of the three poles, only one is perturbative. In $\kappa_4 \to 0$ series expansion, the other two start with $\mathcal{O}(\frac{1}{\sqrt{\kappa_4}})$. One of the three poles is always imaginary for arbitrary n and arbitrary positive κ_4.

There are three important ingredients for the proof of the dynamical phase transition:

1. All three n^{th} poles become purely imaginary when $16\kappa_2^3 - 27\pi^2\kappa_4 n^2$ is negative, or κ_4 is greater than $16\kappa_2^3/27\pi^2 n^2$, we will call this the n^{th} critical value $\kappa_{4c,n}$,

$$\kappa_{4c,n} = \frac{16\kappa_2^3}{27\pi^2 n^2} \tag{IV.96}$$

[7]The numerical values of the poles may get interchanged for specific values of the parameters but the result will always be the same set of roots. This arises from the particular method used for solving the cubic equation.

Below this value, the residues of the n^{th} poles are exponential decaying functions of time t, with no oscillatory factor. Obviously, $(n = \pm 1)$ critical[8] value κ_{4c} is larger than $\kappa_{4c,n}$ for $|n| > 1$. With κ scaled to 1, κ_{4c} is $16\kappa_2^3/27\pi^2 \sim 0.0600422$.

2. With κ_4 less than $(n = \pm 1)$ critical value, the sum of the residues of $(n = \pm 1)$ poles is larger than the sum of the residues of all the other $(|n| > 1)$ poles. Hence, the behaviour of the first poles of $n = \pm 1$ dictate the behaviour of the integral (IV.92) when $\kappa_4 < 16\kappa_2^3/27\pi^2$.

3. Above this critical value, for each n, two of the poles have real parts while one of them, say k_1, is imaginary. The poles are

$$k_1 = -2i\,\mathrm{sgn}(n)\,b, \qquad k_2 = a + i\,\mathrm{sgn}(n)\,b, \qquad k_3 = -a + i\,\mathrm{sgn}(n)\,b \tag{IV.97}$$
$$a = \frac{B^{2/3} - 2\sqrt[3]{6}\kappa_2}{2\;2^{2/3}\sqrt[6]{3}\sqrt[3]{B}\sqrt{\kappa_4}}, \qquad b = \frac{B^{2/3} + 2\sqrt[3]{6}\kappa_2}{2\;6^{2/3}\sqrt[3]{B}\sqrt{\kappa_4}}$$
$$B = \sqrt{81\pi^2\kappa_4 n^2 - 48\kappa_2^3} + 9\pi|n|\sqrt{\kappa_4}$$

where we have to take the real roots of the radicals. k_1's have the largest imaginary parts and the exponential decay of their residues as a function of time are faster while the other poles k_2 and k_3 have comparatively large magnitudes and ocsillations.[9] In the total integral, the contributions of the imaginary poles k_1's cannot compete with the contributions of the oscillating poles. Lastly, it would be a very special arrangment if all ocsillating terms conspire to give a non-oscillatory sum. Hence, the total integral is oscillatory as a function of time and the EE growth is non-monotonic.

For future reference, we also note that the expansion of the real part 'a' in (IV.97) around the n^{th} critical value $\kappa_{4c,n}$ is

$$a = \frac{\sqrt[3]{\pi}\sqrt[3]{|n|}\sqrt{\kappa_4 - \kappa_{4c,n}}}{2^{2/3}\sqrt{3}\kappa_{4c,n}^{5/6}} - \frac{35\left(\sqrt[3]{\pi}\sqrt[3]{|n|}\right)(\kappa_4 - \kappa_{4c,n})^{3/2}}{54\left(2^{2/3}\sqrt{3}\kappa_{4c,n}^{11/6}\right)} + \frac{1001\sqrt[3]{\pi}\sqrt[3]{|n|}(\kappa_4 - \kappa_{4c,n})^{5/2}}{1944\;2^{2/3}\sqrt{3}\kappa_{4c,n}^{17/6}} + \mathcal{O}(\kappa_4 - \kappa_{4c,n})^{7/2} \tag{IV.98}$$

For all our calculations below, we have scaled κ_2 to be 1. The first point is clear from figure (IV.3). The real parts of $(n = \pm 1)$ poles vanish at $\kappa_4 \sim 0.060$, which is the critical value found above. The critical value of $(n = \pm 2)$ poles is $\kappa_4 \sim 0.015$.

[8] We will call this value just 'critical value' without the 'n^{th}' specification because, as shown below, this is the critical value of κ_4 where the dynamical phase transition happens.

[9] This competition between poles of each n might be important, if we have turned on W_6 chemical potential instead of W_4, in which case there will be five poles, or W_8 in which case there will be seven poles and so on.

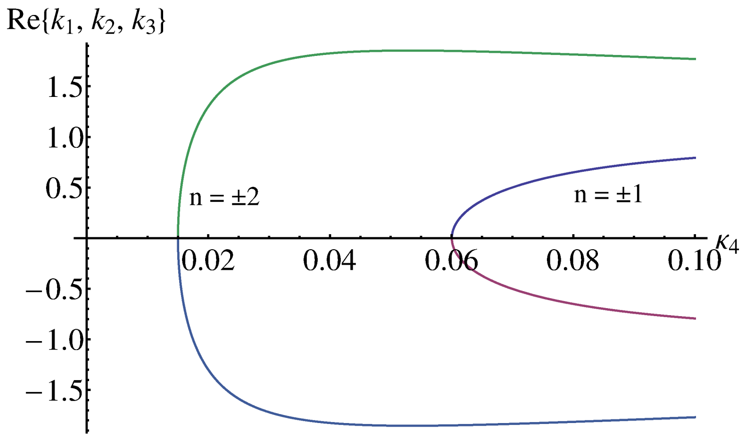

Figure IV.3: Real parts of poles of $n \in \{\pm 1, \pm 2\}$ as a function of κ_4 with κ_2 scaled to 1.

Below the critical value, we will show that the total contributions from $n = \pm 1$ poles is larger than the sum of all residues of $|n| > 1$ poles. We will concentrate on the late time period, $t > r/2$. For e^{i2kt} of $\sin(2kt)$ factor in (IV.92), the contour is closed upward encircling the upper half plane, and for e^{-i2kt}, the contour is closed downward encircling the lower half plane. From the expansion of cosech $(2\kappa_4 (k - k_1)(k - k_2)(k - k_3) + i\pi n)$ around k_1, the contribution from k_1 poles for arbitrary n are the real parts of

$$P_n(k_1) = 2\pi i R_1(k_1) = \frac{(-1)^n}{6\kappa_4(k_1 - k_2)(k_1 - k_3)} \left(e^{i2k_1 t} - \frac{e^{ik_1(r+2t)} + e^{ik_1(-r+2t)}}{2} \right) \qquad \text{if } \mathrm{Im}[k_1] > 0 \tag{IV.99}$$

$$Q_n(k_1) = -2\pi i R_2(k_1) = \frac{(-1)^n}{6\kappa_4(k_1 - k_2)(k_1 - k_3)} \left(e^{-i2k_1 t} - \frac{e^{ik_1(r-2t)} + e^{-ik_1(r+2t)}}{2} \right) \qquad \text{if } \mathrm{Im}[k_1] < 0 \tag{IV.100}$$

where R_1 and R_2 denote the residues. Similarly, cyclic replacements of k_1 with k_2 and k_3 give the contributions of k_2 and k_3 poles. For the poles in the lower half of the complex plane, since the contour is anticlockwise, Q_n have an extra minus sign in the residue. We will call the contributions to the integral form $n = \pm 1$ poles as $I_0(t)$ and the contributions of the $|n| > 1$ poles as $I_1(t)$. The other parameters (κ_4, r and κ which is already scaled to 1) are suppressed.

As a first visual evidence, Figure (IV.4) is the comparison of numerical integration of (IV.92) and $I_0(t)$. It is evident that the residues of ($n = \pm 1$) poles dominate the contour integration. We have chosen $\kappa_4 = 0.0600420$ which is very close to the critical value. As mentioned above, with this choice, all the poles except the $n = \pm 1$ poles give ocsillating residues as a function of time. Although it is not very conspicuous, it is also evident from the graph that $I_1(t)$ is oscillating around $I_0(t)$, the value of the numerical integration is above the $I_0(t)$ curve in some regions and below in other regions of time t.

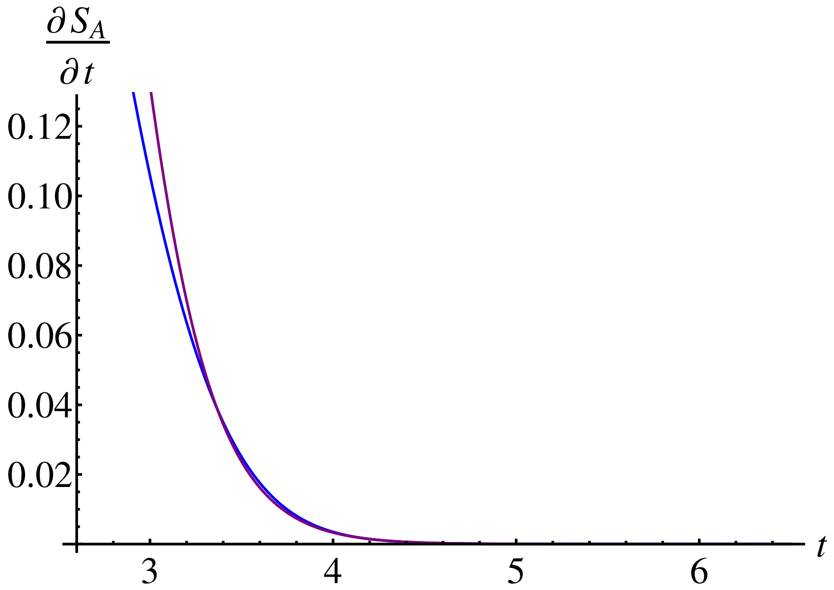

Figure IV.4: Comparison of numerical integration of $\langle \partial S_A/\partial t\rangle_{gCC}$ (blue curve) and $I_0(t)$ (purple curve) as a function of time t. The parameters are $\kappa_4 = 0.0600420$, $r = 5$.

The numerical integration is unreliable in the long time limit. So, to complete our argument, we will calculate an upper bound of $I_1(t)$ and compare it with $I_0(t)$ for a specific time t. The choice of the parameters are

$$\kappa = 1,\ \kappa_4 = 0.0600420,\ r = 5,\ t = 4r = 20, \tag{IV.101}$$

With these parameters, the $n = 1$ and $n = -1$ poles are

$$k_1 = 2.3538234i \qquad k_2 = 2.3585719i \qquad k_3 = -4.7123954i \qquad ;\ n = 1 \tag{IV.102}$$
$$k_1 = 4.7123954i \qquad k_2 = -2.3538234i \qquad k_3 = -2.3585719i \qquad ;\ n = -1 \tag{IV.103}$$

and $I_0(t)$ is given by

$$\begin{aligned} I_0(t)|_{t=20} &= P(k_1)|_{n=1} + P(k_2)|_{n=1} + Q(k_3)|_{n=1} + P(k_1)|_{n=-1} + Q(k_2)|_{n=-1} + Q(k_3)|_{n=-1} \\ &= 6.646589 \times 10^{-35} \end{aligned} \tag{IV.104}$$

We can show that $I_1(t)|_{t=20}$ is less than $I_0(t)|_{t=20}$. The first few poles are

$$k_1 = 5.5495551i \qquad k_2 = 2.5383386 - 2.7747775i \qquad k_3 = -2.5383386 - 2.7747775i \quad ;\ n = -3$$
$$k_1 = 5.1737935i, \qquad k_2 = 1.8496206 - 2.5868967i \qquad k_3 = -1.8496206 - 2.5868967i \quad ;\ n = -2$$
$$k_1 = -5.1737935i \qquad k_2 = -1.8496206 + 2.5868967i \qquad k_3 = 1.8496206 + 2.5868967i \quad ;\ n = 2$$
$$k_1 = -5.54955505i \qquad k_2 = -2.5383386 + 2.7747775i \qquad k_3 = 2.5383386 + 2.7747775i \quad ;\ n = 3$$

The residues of these ($|n| > 1$) poles cannot be summed up into a closed form, as that would amount to doing the integral in closed form. We are interested in an upper bound. The residues of two of the three poles of every ($|n| > 1$) have an oscillation factor. As we saw, even each residue has a separate 3-6 real oscillating terms as a function of time. So, we can represent the sum of the modulus (absolute value of the amplitude) of the oscillating terms of the three residues for each n, by a bigger function which has the analytic sum from $|n| > 1$ to infinity. And if the sum is less $I_0(t)$, then $I_0(t)$ dominates the contribution from all the other poles.[10]

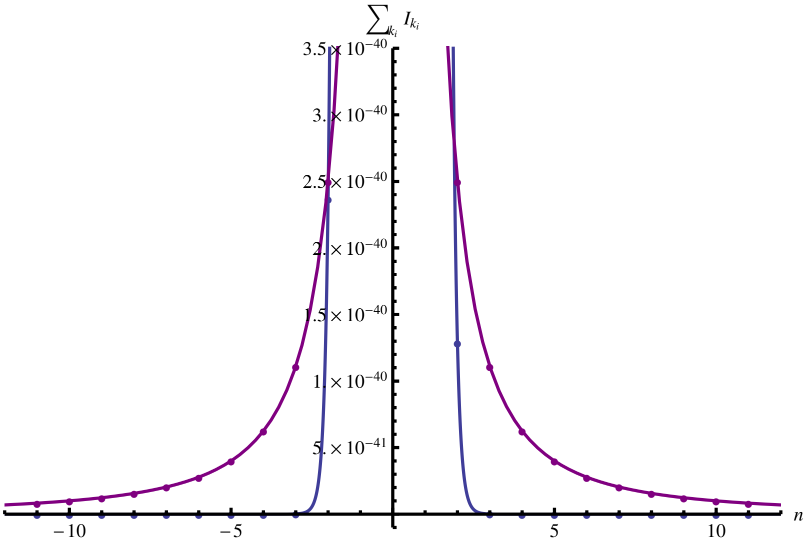

Figure IV.5: Comparison of sum of modulus of residues of ($|n| > 1$) poles with the approximating function $f(n) = 10^{-39}/n^2$. The dots are the discrete n values of the corresponding functions.

Figure (IV.5) are the plots of the sum of the moduli separately for the oscillating terms of the three residues as a function of n and the approximating function $f(n) = 10^{-39}/n^2$. Now, we have

$$\sum_{-\infty}^{n=-2} \frac{10^{-39}}{n^2} + \sum_{n=2}^{\infty} \frac{10^{-39}}{n^2} = 1.289868 \times 10^{-39} \tag{IV.105}$$

This is much less than $I_0(t)|_{t=20}$ in (IV.104) and is of the order of 10^{-5} of $I_0(t)|_{t=20}$. So, the non-oscillating $I_0(t)$ dominates $I_1(t)$, the contribution from the other poles. Hence, below $\kappa_4 = 16\kappa_2^3/27\pi^2$, the EE growth is monotonic.

Visually from figure (IV.4), $t = 3.7$ is a time-slice where the difference between $I_0(t)$ and the numerical integration has a local maxima. At this time slice, repeating the above exercise, $I_0(t)|_{t=3.7} = 0.109727$ and repeating the same exercise of estimating the upper bound of $I_1(t)|_{t=3.7}$ with the same parameters as (IV.101) except the change in t, we get a good upper bound to be 0.0064493 which is less than $I_0(t)|_{t=3.7}$ and is of the order of 60% of $I_0(t)|_{t=3.7}$. So, the approximation of the full integral by $I_0(t)$ gets better with increasing time. In the long time limit, we can effectively take the only time-dependence to be the

[10] A simplified example of our strategy is the comparison between say X and $a\sin(x) + b\cos(y)$ where $\{X, a, b, x, y\} \in \mathcal{R}$, while $A > |a|$ and $B > |b|$ and $\{A, B\} \in \mathcal{R}^+$, then $A + B > |a| + |b| > a\sin(x) + b\cos(y)$ and if $X > A + B$ then $X > a\sin(x) + b\cos(y)$.

time-dependence of $I_0(t)$. *It is worth mentioning here that even* $(n = \pm 1)$ *pole calculations take into account* κ_4 *non-perturbatively, since two of the poles of each* n *are non-perturbative in* κ_4.

As listed above as one of the main points, above the critcal value, each n has an imaginary pole but the other two poles have real parts and also have larger magnitudes so the total residue of the three poles of each n is oscillatory. It would also be a very special arrangement if all the oscillatory contributions of each n conspire to give a non-oscillatory $\partial S_A/\partial t$. Hence, we conclude that the EE growth is non-monotonic above the critical value.

Near the critical point $(\kappa_4 - \kappa_{4c}) \to 0^+$, we can try to estimate an upper bound of the time upto which the EE growth is monotonic. The upper bound is half of the longest time period. Using the leading term in expansion of 'a' from (IV.98) and the expressions of the residues (IV.99) and (IV.100), the lowest frequency($|n| = 1$) gives the upper bound as

$$\frac{\sqrt[3]{\pi}\sqrt{\kappa_4 - \kappa_{4c}}}{2^{2/3}\sqrt{3}\kappa_{4c}^{5/6}}(2t - r) = \pi \quad \Rightarrow \quad t = \frac{(2\pi)^{2/3}\sqrt{3}\kappa_{4c}^{5/6}}{2\sqrt{\kappa_4 - \kappa_{4c}}} + \frac{r}{2} \sim \frac{2.95\,\kappa_{4c}^{5/6}}{\sqrt{\kappa_4 - \kappa_{4c}}} \tag{IV.106}$$

where finite 'r' can be neglected in the limit $(\kappa_4 - \kappa_{4c}) \to 0^+$.

The critical value in terms the effective temperature $\beta = 4\kappa_2$ and chemical potential $\mu_4 = 4\kappa^4$ in the stationary limit is

$$\mu_4 = \frac{\beta^3}{27\pi^2} \tag{IV.107}$$

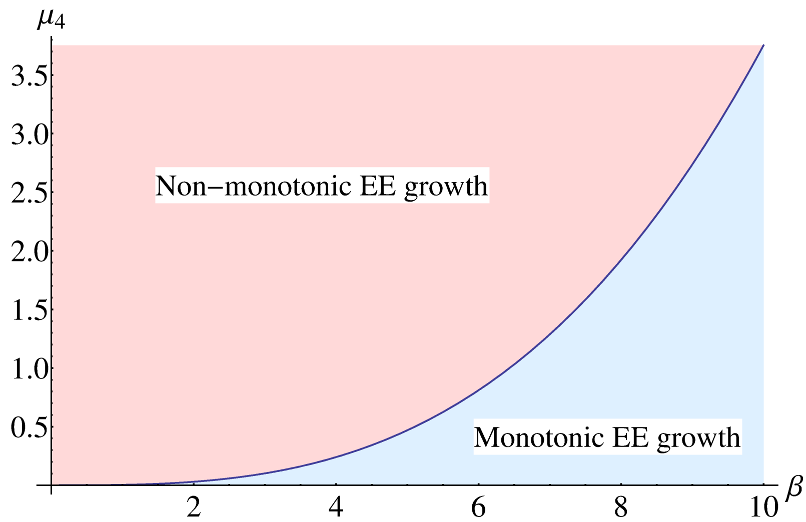

Figure IV.6: The critical curve $\mu_4 = \beta^3/27\pi^2$ in terms of the effective temperature and chemical potential in the stationary limit and the phase diagram.

For the early times $t < r/2$, in the residue calculations (IV.99) and (IV.100), we have to replace the sign of the exponents with $r - 2t$ so the magnitudes of the exponentials decreases as time increases. Upto the critical value of κ_4, the EE growth is always monotonic for this time period.

7.1 Turning on other charges

We could also calculate the EE growth of gCC states with other charges of the fermionic theory corresponding to bosonic bilinear $W_{2n} = \sum |k|^{2n-1} d_k^\dagger d_k$ where $n = 3, 4, 5, ...$ Repeating the exercise of quenching tuned squeezed states of scalar field theory in MPS, the propagator with these charges are simply given by

$$\langle \phi(0,t)\phi(r,t)\rangle = \int \frac{dk}{4\pi}\frac{e^{ikr}}{k}\left(\coth\left(2\kappa_2 k + \sum_{n=2}^{\infty}\kappa_{2n}k^{2n-1}\right)\right.$$
$$\left. - \cos(2kt)\text{cosech}\left(2\kappa_2 k + \sum_{n=2}^{\infty}\kappa_{2n}k^{2n-1}\right) - 1\right) \quad \text{(IV.108)}$$

Substituting this propagator in the general formula (IV.77) and (IV.78) give the Rényi entropy and entanglement entropy. The first derivative of EE w.r.t. time is

$$\left\langle \frac{\partial S_A}{\partial t}\right\rangle_{gCC} = \frac{1}{3}\int_{-\infty}^{\infty} dk\,(1-\cos(kr))\text{cosech}\left(2\kappa k + \sum_{n=2}^{\infty}\kappa_{2n}k^{2n-1}\right)\sin(2kt) \quad \text{(IV.109)}$$

We believe the dynamics will be much richer with these other charges, with much more complex phase diagrams which can be in a $n-1$ dimensional space. But the general poles analysis cannot be done in these cases because the poles will be given by quintic and higher order equations. Considering gCC states with W_4 and W_6 charges, the numerical plots of EE growth looks the same as (IV.2) where by trial and error method, some parameter subspace gives monotonic growth and some subspaces do not give monotonic growth. Considering $n = \pm 1$, the poles are given by $2\kappa_2 k + 2\kappa_4 k^3 + 2\kappa_6 k^5 = i\pi$. For $\kappa_2 = 1$ and $\kappa_4 = 0.06$, numerically we find two interesting parameter subspaces of κ_6. The first one is when all the poles become imaginary when κ_4 is decreased.

$$\begin{aligned}&k_1 = 2.0887597\,\text{sgn}(n)\,i, \quad k_2 = 2.9527785\,\text{sgn}(n)\,i, \quad k_3 = -6.5425830\,\text{sgn}(n)\,i,\\ &k_4 = -6.6158300\,\text{sgn}(n)\,i, \quad k_5 = 8.1168748\,\text{sgn}(n)\,i \qquad \text{for} \qquad \kappa_6 = 0.0007249\end{aligned} \quad \text{(IV.110)}$$

$$\begin{aligned}&k_1 = -0.0076887 - 6.5788763\,\text{sgn}(n)\,i, \quad k_2 = 2.0887456\,\text{sgn}(n)\,i, \quad k_3 = 2.9528549\,\text{sgn}(n)\,i,\\ &k_4 = 8.1161520\,\text{sgn}(n)\,i, \quad k_5 = 0.0076887 - 6.5788763\,\text{sgn}(n)\,i \qquad \text{for} \qquad \kappa_6 = 0.0007250\end{aligned} \quad \text{(IV.111)}$$

This looks like the same transition if $n = \pm 1$ dominates, but the poles with real parts have large imaginary part also, so they would be highly damped. The other case is

$$\begin{aligned}&k_1 = -0.8215058 + 1.9681831\,\text{sgn}(n)\,i, \quad k_2 = -5.2389645\,\text{sgn}(n)\,i, \quad k_3 = -5.2472000\,\text{sgn}(n)\,i,\\ &k_4 = 6.5497983\,\text{sgn}(n)\,i, \quad k_5 = 0.8215058 + 1.9681831\,\text{sgn}(n)\,i \qquad \text{for} \qquad \kappa_6 = 0.0019179\end{aligned} \quad \text{(IV.112)}$$

$$\begin{aligned}&k_1 = -0.8215060 + 1.9681836\,\text{sgn}(n)\,i, \quad k_2 = -0.0040372 - 5.2430724\,\text{sgn}(n)\,i,\\ &k_3 = 6.5497775\,\text{sgn}(n)\,i, \quad k_4 = 0.0040372 - 5.2430724\,\text{sgn}(n)\,i,\\ &k_5 = 0.8215060 + 1.9681836\,\text{sgn}(n)\,i \qquad \text{for} \qquad \kappa_6 = 0.0019180\end{aligned} \quad \text{(IV.113)}$$

for the smaller κ_4, although two of the poles have real parts, they have to compete with the three imaginary poles. So, this could also be phase transition.

8 Discussion

In this work, we have examined free fermionic mass quench. We find that the ground state quench equilibrates but not to a thermal ensemble. Starting from specially prepared squeezed states, we get CC and gCC states with fermionic bilinear W_{2n} charges. Calculation of correlators in CC and gCC states explicitly shows thermalization to thermal emsemble and GGE respectively.

For CC state, we calculate EE growth exactly. The EE growth is strictly monotonically increasing. For gCC state with a particular charge, we find dynamical phase transition in which the EE growth is monotonic upto a critical value of the effective chemical potential. In the pure state, the effective chemical potential is the coupling constant of the current corresponding to the charge. Above the critical value, the EE growth is non-monotonic. It would be interesting to reproduce our result in large c holographic CFTs and examine what it would mean for Black hole physics.

IV.A Conventions

$$\eta_{\mu\nu} = \begin{bmatrix} 1 & 0 \\ 0 & -1 \end{bmatrix}, \quad \partial_\mu = (\partial_t, \partial_x), \quad \gamma^\mu \partial_\mu = \gamma^0 \partial_t - \gamma^1 \partial_x,$$

$$w = t - x, \quad \bar{w} = t + x, \quad \partial = \frac{\partial}{\partial w} = \frac{1}{2}\left(\frac{\partial}{\partial t} - \frac{\partial}{\partial x}\right), \quad \bar{\partial} = \frac{\partial}{\partial \bar{w}} = \frac{1}{2}\left(\frac{\partial}{\partial t} + \frac{\partial}{\partial x}\right)$$

$$\gamma^0_d = \begin{bmatrix} 1 & 0 \\ 0 & -1 \end{bmatrix}, \quad \gamma^1_d = \begin{bmatrix} 0 & 1 \\ -1 & 0 \end{bmatrix}, \quad \text{in Dirac basis.}$$

$$S = \frac{1}{\sqrt{2}}\begin{bmatrix} 1 & -1 \\ 1 & 1 \end{bmatrix}, \gamma^0_c = S\gamma^0_d S^{-1} = \begin{bmatrix} 0 & 1 \\ 1 & 0 \end{bmatrix}, \quad \gamma^1_c = S\gamma^1_d S^{-1} = \begin{bmatrix} 0 & 1 \\ -1 & 0 \end{bmatrix}, \quad \text{in chiral basis.}$$

$$\left\{a_k, a^\dagger_{k'}\right\} = 2\pi\,\delta(k - k'), \quad \left\{b_k, b^\dagger_{k'}\right\} = 2\pi\,\delta(k - k'), \text{ other anticommutators are zero.}$$

$$\left\{a_n, a^\dagger_{n'}\right\} = \delta(n - n'), \quad \left\{b_n, b^\dagger_{n'}\right\} = \delta(n - n'), \text{ other anticommutators are zero.}$$

We will use $k = \frac{2\pi n}{L}$ for continuum limit($L \to \infty$) and n for quantization in a finite box of size L, where $n = n' + 1/2$ and $n' \in \mathbb{Z}$.

IV.B Spinors and transformation to chiral basis:

Taking constant mass m, we can easily find the boosted spinors, $u(k, m)$ and $v(k, m)$. For constant m, $\phi_{+p}(t) = e^{-i\omega t}$ and $\phi_{-m}(t) = e^{i\omega t}$. So from (IV.4),

$$\begin{aligned} U(x,t) &= \left[\gamma^0\partial_t - \gamma^1\partial_x - im\right] e^{-i\omega t + ikx} \begin{bmatrix} 1 \\ 0 \end{bmatrix} = i \begin{bmatrix} -(\omega + m) \\ k \end{bmatrix} e^{-ik\cdot x} \\ V(x,t) &= \left[\gamma^0\partial_t - \gamma^1\partial_x - im\right] \begin{bmatrix} 0 \\ 1 \end{bmatrix} e^{ik\cdot x} = i \begin{bmatrix} k \\ -(\omega + m) \end{bmatrix} e^{ik\cdot x} \end{aligned}$$

Hence, upto normalizations fixed by inner products, the boosted spinors are

$$u(k, m) = i \begin{bmatrix} -(\omega + m) \\ k \end{bmatrix}, \quad v(k, m) = i \begin{bmatrix} k \\ -(\omega + m) \end{bmatrix}$$

We have the adjoint spinors as,

$$\begin{aligned} \bar{u}(k, m) &= u^\dagger(k, m)\gamma^0 = -i \begin{bmatrix} -(\omega + m) & k \end{bmatrix} \begin{bmatrix} 1 & 0 \\ 0 & -1 \end{bmatrix} = i \begin{bmatrix} -(\omega + m) & -k \end{bmatrix} \\ \bar{v}(k, m) &= v^\dagger(k, m)\gamma^0 = -i \begin{bmatrix} k & -(\omega + m) \end{bmatrix} \begin{bmatrix} 1 & 0 \\ 0 & -1 \end{bmatrix} = i \begin{bmatrix} k & (\omega + m) \end{bmatrix} \end{aligned}$$

Now borrowing Peskin & Schroeder(P&S) conventions of spinors, we want to fix the inner products $\bar{u}(k, m)u(k, m) = 2m$ and $\bar{v}(k, m)v(k, m) = -2m$,

$$\begin{aligned} \bar{u}(k, m)u(k, m) &= \begin{bmatrix} -(\omega + m) & -k \end{bmatrix} \begin{bmatrix} -(\omega + m) \\ k \end{bmatrix} = 2m(\omega + m) \\ \bar{v}(k, m)v(k, m) &= \begin{bmatrix} k & (\omega + m) \end{bmatrix} \begin{bmatrix} k \\ -(\omega + m) \end{bmatrix} = -2m(\omega + m) \end{aligned}$$

So the normalized spinors are

$$\begin{aligned}
u(k,m) &= \frac{1}{\sqrt{(\omega+m)}}\begin{bmatrix}(\omega+m)\\ -k\end{bmatrix}, \quad v(k,m) = \frac{1}{\sqrt{(\omega+m)}}\begin{bmatrix}k\\ -(\omega+m)\end{bmatrix}\\
\bar{u}(k,m) &= \frac{1}{\sqrt{(\omega+m)}}\begin{bmatrix}(\omega+m) & k\end{bmatrix}, \quad \bar{v}(k,m) = \frac{1}{\sqrt{(\omega+m)}}\begin{bmatrix}k & (\omega+m)\end{bmatrix}
\end{aligned} \tag{IV.114}$$

The spinors with time-dependent mass $m(t)$ are obtained by just substituting $m(t)$ in the place of 'm' only inside the matrices, which is clearly seen from (IV.12) and (IV.13). The normalization cannot be changed to time-dependent mass else the spinors won't be solutions of the corresponding Dirac equation.

The transformation to chiral basis is accomplished by using the transformation matrix $S = \frac{1}{\sqrt{2}}\begin{bmatrix}1 & -1\\ 1 & 1\end{bmatrix}$. The mode expansion as in P&S is

$$\begin{aligned}
\Psi(x,t) &= \int \frac{dk}{2\pi}\frac{1}{\sqrt{2\omega}}\left[a_k u(k,m)e^{-ik\cdot x} + b_k^\dagger v(k,m)e^{ik\cdot x}\right]\\
&= \int \frac{dk}{2\pi}\frac{1}{\sqrt{2\omega}}\left[a_k\frac{1}{\sqrt{(\omega+m)}}\begin{bmatrix}(\omega+m)\\ -k\end{bmatrix}e^{-ik\cdot x} + b_k^\dagger\frac{1}{\sqrt{(\omega+m)}}\begin{bmatrix}k\\ -(\omega+m)\end{bmatrix}e^{ik\cdot x}\right]\\
&\xrightarrow{m\to 0} \int \frac{dk}{2\pi}\frac{1}{\sqrt{2}}\left[a_k\begin{bmatrix}1\\ -\mathrm{sgn}(k)\end{bmatrix}e^{-ik\cdot x} + b_k^\dagger\begin{bmatrix}\mathrm{sgn}(k)\\ -1\end{bmatrix}e^{ik\cdot x}\right]\\
&= \int \frac{dk}{2\pi}\frac{1}{\sqrt{2}}\begin{bmatrix}a_k e^{-ik\cdot x} + \mathrm{sgn}(k)b_k^\dagger e^{ik\cdot x}\\ -\mathrm{sgn}(k)a_k e^{-ik\cdot x} - b_k^\dagger e^{ik\cdot x}\end{bmatrix}
\end{aligned}$$

In the chiral basis,

$$\begin{aligned}
\Psi_c(x,t) &= S\cdot\Psi(x,t) = \frac{1}{\sqrt{2}}\begin{bmatrix}1 & -1\\ 1 & 1\end{bmatrix}\cdot\int \frac{dk}{2\pi}\frac{1}{\sqrt{2}}\begin{bmatrix}a_k e^{-ik\cdot x} + \mathrm{sgn}(k)b_k^\dagger e^{ik\cdot x}\\ -\mathrm{sgn}(k)a_k e^{-ik\cdot x} - b_k^\dagger e^{ik\cdot x}\end{bmatrix}\\
&= \int_{-\infty}^{\infty}\frac{dk}{2\pi}\frac{1}{2}\begin{bmatrix}(1+\mathrm{sgn}(k))(a_k e^{-ik\cdot x} + b_k^\dagger e^{ik\cdot x})\\ (1-\mathrm{sgn}(k))(a_k e^{-ik\cdot x} - b_k^\dagger e^{ik\cdot x})\end{bmatrix}
\end{aligned} \tag{IV.115}$$

Writing this as $\psi(x,t)$ and $\bar{\psi}(x,t)$,

$$\psi(x,t) = \int_0^{\infty}\frac{dk}{2\pi}(a_k e^{-ik\cdot x} + b_k^\dagger e^{ik\cdot x}) \tag{IV.116}$$

$$\bar{\psi}(x,t) = \int_{-\infty}^{0}\frac{dk}{2\pi}(a_k e^{-ik\cdot x} - b_k^\dagger e^{ik\cdot x}) \tag{IV.117}$$

IV.C Fermionic Boundary State

The action (IV.1) with $m(t) = 0$ in the chiral basis is

$$\begin{aligned}
S &= -\int dx^2\,\left[i\bar{\Psi}\gamma^\mu\partial_\mu\Psi + \Psi\gamma^\mu\partial_\mu\bar{\Psi}\right]\\
&= -\frac{i}{2}\int dw d\bar{w}\,\left(\psi^\dagger\bar{\partial}\psi + \bar{\psi}^\dagger\partial\bar{\psi} + \psi\bar{\partial}\psi^\dagger + \bar{\psi}\partial\bar{\psi}^\dagger\right)
\end{aligned}$$

On varying the action and collecting terms, we get the following

$$\delta S = \int d^2x \left(\delta\psi^\dagger\bar{\partial}\psi + \delta\psi\bar{\partial}\psi^\dagger + \delta\bar{\psi}^\dagger\partial\bar{\psi} + \delta\bar{\psi}\partial\bar{\psi}^\dagger\right) \tag{IV.118}$$

Given a boundary at $t = 0$, it will also have certain boundary terms, which we want to be zero.

$$\psi^\dagger\delta\psi + \psi\delta\psi^\dagger + \bar{\psi}^\dagger\delta\bar{\psi} + \bar{\psi}\delta\bar{\psi}^\dagger\Big|_{t=0} = 0 \tag{IV.119}$$

We impose this as an operator equation on the boundary state $|B\rangle$. The condition for a boundary state can be achieved via two identifications

$$\psi = i\bar{\psi}^\dagger, \quad \text{and} \quad \psi^\dagger = i\bar{\psi} \tag{IV.120}$$

$$\psi = -\bar{\psi}, \quad \text{and} \quad \psi^\dagger = \bar{\psi}^\dagger \tag{IV.121}$$

Now we impose the boundary conditions at $t = 0$ in terms of the mode expansions (IV.116) and (IV.117):

1. The boundary condition of (IV.120) gives $a_k \mp i a^\dagger_{-k} = 0$ for $k > 0$ and $b_k \mp i b^\dagger_{-k} = 0$ for $k < 0$. Similarly, the second condition is $a_k \pm i a^\dagger_{-k} = 0$ for $k < 0$ and $b_k \pm i b^\dagger_{-k} = 0$ for $k > 0$. Combining the separate conditions, we get $a_k \mp i\,\mathrm{sgn}(k) a^\dagger_{-k} = 0$ and $b_k \pm i\,\mathrm{sgn}(k) b^\dagger_{-k} = 0$. Hence, the boundary state corresponding to the first identification is
$$|N\rangle = \exp\left(\sum_k i\,\mathrm{sgn}(k)(a^\dagger_k a^\dagger_{-k} - b^\dagger_k b^\dagger_{-k})\right)|0\rangle \tag{IV.122}$$

2. The boundary condition (IV.121) is $a_k \mp \mathrm{sgn}(k) b^\dagger_{-k} = 0$ for $k > 0$, $a_k \pm b^\dagger_{-k} = 0$ for $k < 0$ and $b_k \pm a^\dagger_{-k} = 0$ for $k < 0$ and $b_k \mp a^\dagger_{-k} = 0$ for $k > 0$. The boundary state for the first identification is
$$|D\rangle = \exp\left(\sum_k \mathrm{sgn}(k) a^\dagger_k b^\dagger_{-k}\right)|0\rangle \tag{IV.123}$$

From the action S, we can find the non-zero components of the energy-momentum tensor $T = T_{ww}$ and $\bar{T} = T_{\bar{w}\bar{w}}$, and the components of the $U(1)$ current are $J_w = J$ and $J_{\bar{w}} = \bar{J}$,

$$T = \frac{i}{2}\left(\psi^\dagger\partial\psi + \psi\partial\psi^\dagger\right) \qquad \bar{T} = \frac{i}{2}\left(\bar{\psi}^\dagger\bar{\partial}\bar{\psi} + \bar{\psi}\bar{\partial}\bar{\psi}^\dagger\right) \tag{IV.124}$$

$$J = \psi^\dagger\psi \qquad \bar{J} = \bar{\psi}^\dagger\bar{\psi} \tag{IV.125}$$

The boundary conditions (IV.120) and (IV.121) satisfy the condition

$$T(w)|_{t=0} = \bar{T}(\bar{w})|_{t=0}, \qquad \text{on the cylinder.} \tag{IV.126}$$

$$\text{or,} \quad \left(z^2 T_{zz}(z)\right)|_{z(t=0)} = \left(\bar{z}^2 \bar{T}_{\bar{z}\bar{z}}(\bar{z})\right)|_{\bar{z}(t=0)}, \qquad \text{on the plane.} \tag{IV.127}$$

where $z = e^{2\pi(t-ix)/L}$ and $\bar{z} = e^{2\pi(t+ix)/L}$. Thus $|N\rangle$ and $|D\rangle$ are conformal invariant boundary states. It is also worth noting that the boundary conditions also satisfy

$$J(w)|_{t=0} = -\bar{J}(\bar{w})|_{t=0}, \qquad \text{on the cylinder.} \tag{IV.128}$$

$$\text{or,} \quad (zJ_z(z))\,|_{z(t=0)} = \left(\bar{z}\bar{J}_{\bar{z}}(\bar{z})\right)|_{\bar{z}(t=0)}, \qquad \text{on the plane.} \tag{IV.129}$$

Considering the zero modes in the cylinder, it means that the above boundary states are not charged. With $Q = J_0 + \bar{J}_0$,

$$Q|N\rangle = 0, \qquad Q|D\rangle = 0 \tag{IV.130}$$

Besides, specially for the state $|D\rangle$, $(J_0 - \bar{J}_0)|D\rangle = 0$. Hence

$$J_0|D\rangle = 0 \qquad \bar{J}_0|D\rangle = 0 \tag{IV.131}$$

IV.D Bosonised Boundary State

Consider a Dirichlet boundary state $\varphi\,|D\rangle = -\bar{\varphi}\,|D\rangle$. Using the bosonised fermions :

$$\psi = e^{-i\frac{\sqrt{\pi}}{4}\bar{P}} : e^{-i\sqrt{4\pi}\varphi(w)} : \qquad \psi^\dagger = e^{i\frac{\sqrt{\pi}}{4}\bar{P}} : e^{i\sqrt{4\pi}\varphi(w)} :$$

$$\bar{\psi} = e^{-i\frac{\sqrt{\pi}}{4}P} : e^{i\sqrt{4\pi}\bar{\varphi}(\bar{w})} : \qquad \bar{\psi}^\dagger = e^{i\frac{\sqrt{\pi}}{4}P} : e^{-i\sqrt{4\pi}\bar{\varphi}(\bar{w})} :$$

To translate the boson Dirichlet condition into the fermionic one, we get

$$\begin{aligned}
\psi\,|D\rangle &= e^{-i\frac{\sqrt{\pi}}{4}\bar{P}} : e^{-i\sqrt{4\pi}\varphi} : |D\rangle \\
&= e^{-\frac{\pi}{2}[Q,P]} e^{-i\frac{\sqrt{\pi}}{4}\bar{P}} e^{-i\frac{\sqrt{\pi}}{4}P} : e^{-i\sqrt{4\pi}\varphi} : |D\rangle \\
&= e^{-\frac{\pi}{2}[Q,P]} e^{-i\frac{\sqrt{\pi}}{4}\bar{P}} e^{-i\frac{\sqrt{\pi}}{4}P} : e^{i\sqrt{4\pi}\bar{\varphi}} : |D\rangle \\
&= e^{\frac{\pi}{2}([Q,P]-[\bar{P},\bar{Q}])}\ \bar{\psi}\,|D\rangle \\
&= e^{-i\pi}\ \bar{\psi}\,|D\rangle = -\bar{\psi}\,|D\rangle
\end{aligned}$$

where we have used the relation $e^x\,e^y = e^{y+[x,y]+\cdots}\,e^x$ and $[Q,P] = [\bar{Q},\bar{P}] = i$. We have also used (IV.131) which gives $P|D\rangle = J_0|D\rangle = 0$ and $\bar{P}|D\rangle = \bar{J}_0)|D\rangle = 0$.

Similarly, we can show that $(\psi^\dagger - \bar{\psi}^\dagger)\,|D\rangle$, $(\psi - i\bar{\psi}^\dagger)\,|N\rangle$ and $(\psi^\dagger - i\bar{\psi})\,|N\rangle$ vanish, where $|N\rangle$ is defined by $(\varphi - \bar{\varphi})\,|N\rangle = 0$ which is the Neumann boundary condition for scalar fields.

IV.E Baker-Campbell-Hausdorff(BCH) formula

Although we are interested in the 'out' massless oscillators, the BCH formula is valid for both massive and massless oscillators. So, we will suppress the 'in' or 'out' identification of the oscillators. Starting from

$$|\Psi\rangle = \exp\left(\sum_k \mathrm{sgn}(k)\gamma(k)a_k^\dagger b_{-k}^\dagger\right)|0\rangle \tag{IV.132}$$

we wish to obtain an expression of the form

$$|\psi\rangle = \exp\left(-\sum_k \kappa(k)(a_k^\dagger a_k + b_k^\dagger b_k)\right)\exp\left(\sum_k \mathrm{sgn}(k) a_k^\dagger b_{-k}^\dagger\right)|0\rangle \tag{IV.133}$$

Commuting $\exp\left(-\sum\limits_k \kappa(k)(a_k^\dagger a_k + b_k^\dagger b_k)\right)$ through $\exp\left(\sum\limits_k \mathrm{sgn}(k) a_k^\dagger b_{-k}^\dagger\right)$, we get

$$\exp\left(\sum_k \mathrm{sgn}(k) e^{-2\kappa(k)} a_k^\dagger b_{-k}^\dagger\right)|0\rangle$$

Thus,

$$\begin{aligned} &\mathrm{sgn}(k)\gamma(k) = e^{-2\kappa(k)}\,\mathrm{sgn}(k) \\ \Rightarrow\quad &\kappa(k) = -\frac{1}{2}\log(\gamma(k)) \end{aligned} \tag{IV.134}$$

IV.F Refermionization of bosonic bilinear $\mathcal{W}_4$

The bosonic(real scalar) bilinear $\mathcal{W}_4$ current [41, 26] is

$$\mathcal{W}_4(w) = 2\partial\phi\partial^3\phi - 3\partial^2\phi\partial^2\phi \tag{IV.135}$$

Using U(1) current relation $J = \psi^\dagger\psi = \frac{i}{\sqrt{4\pi}}\partial\phi$ and normal ordering gives the refermionized $\mathcal{W}_4$ current. Because of the fermionic anti-commutation relation most of the four fermion terms drop out and the only four fermion term that survives is $\partial\psi^\dagger\partial\psi\psi^\dagger\psi$. Finally, the expression is

$$\tilde{\mathcal{W}}_4(w) = \frac{7i}{6}\,\psi^\dagger\partial^3\psi + \frac{3i}{2}\,\partial^2\psi^\dagger\partial\psi - \frac{3i}{2}\,\partial\psi^\dagger\partial^2\psi - \frac{7i}{6}\,\partial^3\psi^\dagger\psi - 2\,\partial\psi^\dagger\partial\psi\psi^\dagger\psi \tag{IV.136}$$

And the corresponding charge is

$$\begin{aligned} \tilde{W}_4 = \frac{1}{4\pi}\Bigg(&\frac{14}{3}\int_{-\infty}^{\infty}\frac{dk}{2\pi}\,|k|^3\left[a_k^\dagger a_k + b_k^\dagger b_k\right] \\ &+ 2\int_{-\infty}^{\infty}\frac{dk_1dk_2dk_3dk_4}{(2\pi)^4}\,|k_1||k_2|\Big[a_{k_1}^\dagger a_{k_2}a_{k_3}^\dagger a_{k_4}\delta(k_1-k_2+k_3-k_4) + a_{k_1}^\dagger a_{k_2}b_{k_3}b_{k_4}^\dagger\delta(k_1-k_2-k_3+k_4) \\ &\quad - a_{k_1}^\dagger b_{k_2}^\dagger b_{k_3}a_{k_4}\delta(k_1+k_2-k_3-k_4) - b_{k_1}a_{k_2}a_{k_3}^\dagger b_{k_4}^\dagger\delta(-k_1-k_2+k_3+k_4) \\ &\quad + b_{k_1}b_{k_2}^\dagger a_{k_3}^\dagger a_{k_4}\delta(-k_1+k_2+k_3-k_4) + b_{k_1}b_{k_2}^\dagger b_{k_3}b_{k_4}^\dagger\delta(-k_1+k_2-k_3+k_4)\Big]\Bigg) \end{aligned} \tag{IV.137}$$

Bibliography

[1] G. Mandal, R. Sinha, and N. Sorokhaibam, *The inside outs of AdS(3)/CFT(2): Exact AdS wormholes with entangled CFT duals*, JHEP **1501** (2014) 036, [arXiv:1405.6695].

[2] G. Mandal, R. Sinha, and N. Sorokhaibam, *Thermalization with chemical potentials, and higher spin black holes*, JHEP **08** (2015) 013, [arXiv:1501.04580].

[3] G. Mandal, S. Paranjape, and N. Sorokhaibam, *Thermalization in 2D critical quench and UV/IR mixing*, arXiv:1512.02187.

[4] J. Maldacena and L. Susskind, *Cool Horizons for Entangled Black Holes*, Fortsch.Phys. **61** (2013) 781–811, [arXiv:1306.0533].

[5] J. M. Maldacena, *Eternal Black Holes in Anti-de Sitter*, JHEP **0304** (2003) 021, [hep-th/0106112].

[6] P. Calabrese and J. L. Cardy, *Time-dependence of correlation functions following a quantum quench*, Phys. Rev. Lett. **96** (2006) 136801, [cond-mat/0601225].

[7] T. Hartman and J. Maldacena, *Time Evolution of Entanglement Entropy from Black Hole Interiors*, JHEP **1305** (2013) 014, [arXiv:1303.1080].

[8] J. Cardy, *Quantum Quenches to a Critical Point in One Dimension: some further results*, arXiv:1507.07266.

[9] M. Banados, *Three-Dimensional Quantum Geometry and Black Holes*, hep-th/9901148.

[10] M. Banados, M. Henneaux, C. Teitelboim, and J. Zanelli, *Geometry of the (2+1) Black Hole*, Phys.Rev. **D48** (1993) 1506–1525, [gr-qc/9302012].

[11] M. Banados, C. Teitelboim, and J. Zanelli, *The Black hole in three-dimensional space-time*, Phys. Rev. Lett. **69** (1992) 1849–1851, [hep-th/9204099].

[12] V. Balasubramanian and P. Kraus, *A Stress Tensor for Anti-de Sitter Gravity*, Commun.Math.Phys. **208** (1999) 413–428, [hep-th/9902121].

[13] V. E. Hubeny, M. Rangamani, and T. Takayanagi, *A Covariant Holographic Entanglement Entropy Proposal*, JHEP **0707** (2007) 062, [arXiv:0705.0016].

[14] P. Caputa, G. Mandal, and R. Sinha, *Dynamical Entanglement Entropy with Angular Momentum and U(1) Charge*, JHEP **1311** (2013) 052, [arXiv:1306.4974].

[15] K. Skenderis and S. N. Solodukhin, *Quantum Effective Action from the AdS / CFT Correspondence*, Phys.Lett. **B472** (2000) 316–322, [hep-th/9910023].

[16] J. Louko, D. Marolf, and S. F. Ross, *On Geodesic Propagators and Black Hole Holography*, Phys.Rev. **D62** (2000) 044041, [hep-th/0002111].

[17] A. Polkovnikov, K. Sengupta, A. Silva, and M. Vengalattore, *Nonequilibrium dynamics of closed interacting quantum systems*, Rev.Mod.Phys. **83** (2011) 863, [arXiv:1007.5331].

[18] R. Nandkishore and D. A. Huse, *Many body localization and thermalization in quantum statistical mechanics*, Ann. Rev. Condensed Matter Phys. **6** (2015) 15–38, [arXiv:1404.0686].

[19] C. Gogolin and J. Eisert, *Equilibration, thermalisation, and the emergence of statistical mechanics in closed quantum systems*, tech. rep., arXiv:1503.07538, Mar., 2015.

[20] P. Calabrese and J. L. Cardy, *Evolution of entanglement entropy in one-dimensional systems*, J.Stat.Mech. **0504** (2005) P04010, [cond-mat/0503393].

[21] M. Rigol, V. Dunjko, V. Yurovsky, and M. Olshanii, *Relaxation in a completely integrable many-body quantum system: An Ab Initio study of the dynamics of the highly excited states of 1d lattice hard-core bosons*, Phys. Rev. Lett. **98** (Feb, 2007) 050405, [0604476].

[22] P. Calabrese, F. H. L. Essler, and M. Fagotti, *Quantum Quench in the Transverse-Field Ising Chain*, Physical Review Letters **106** (June, 2011) 227203, [arXiv:1104.0154].

[23] G. Mandal and T. Morita, *Quantum quench in matrix models: Dynamical phase transitions, Selective equilibration and the Generalized Gibbs Ensemble*, JHEP **10** (2013) 197, [arXiv:1302.0859].

[24] P. Di Francesco, P. Mathieu, and D. Senechal, *Conformal field theory*, . Springer, New York, USA, 890 p, ISBN: 038794785X.

[25] J. L. Cardy, *Conformal Invariance and Surface Critical Behavior*, Nucl.Phys. **B240** (1984) 514–532.

[26] C. Pope, *Lectures on W algebras and W gravity*, hep-th/9112076.

[27] P. Bouwknegt and K. Schoutens, *W symmetry in conformal field theory*, Phys.Rept. **223** (1993) 183–276, [hep-th/9210010].

[28] J. Cardy, *Thermalization and Revivals after a Quantum Quench in Conformal Field Theory*, Phys.Rev.Lett. **112** (2014) 220401, [arXiv:1403.3040].

[29] G. Festuccia and H. Liu, *The Arrow of time, black holes, and quantum mixing of large N Yang-Mills theories*, JHEP **0712** (2007) 027, [hep-th/0611098].

[30] D. Birmingham, I. Sachs, and S. N. Solodukhin, *Conformal field theory interpretation of black hole quasinormal modes*, Phys.Rev.Lett. **88** (2002) 151301, [hep-th/0112055].

[31] S. Datta and J. R. David, *Higher Spin Quasinormal Modes and One-Loop Determinants in the BTZ black Hole*, JHEP **1203** (2012) 079, [arXiv:1112.4619].

[32] M. R. Gaberdiel and R. Gopakumar, *An AdS_3 Dual for Minimal Model CFTs*, Phys.Rev. **D83** (2011) 066007, [arXiv:1011.2986].

[33] M. Gutperle and P. Kraus, *Higher Spin Black Holes*, JHEP **1105** (2011) 022, [arXiv:1103.4304].

[34] P. Kraus and E. Perlmutter, *Partition functions of higher spin black holes and their CFT duals*, JHEP **1111** (2011) 061, [arXiv:1108.2567].

[35] A. Cabo-Bizet, E. Gava, V. Giraldo-Rivera, and K. Narain, *Black Holes in the 3D Higher Spin Theory and Their Quasi Normal Modes*, JHEP **1411** (2014) 013, [arXiv:1407.5203].

[36] M. R. Gaberdiel, K. Jin, and E. Perlmutter, *Probing higher spin black holes from CFT*, JHEP **1310** (2013) 045, [arXiv:1307.2221].

[37] M. Beccaria and G. Macorini, *Resummation of scalar correlator in higher spin black hole background*, JHEP **1402** (2014) 071, [arXiv:1311.5450].

[38] M. Scully and M. Zubairy, Quantum Optics. Cambridge University Press, 1997.

[39] E. Tiesinga and P. R. Johnson, *Collapse and revival dynamics of number-squeezed superfluids of ultracold atoms in optical lattices*, Phys. Rev. A **83** (Jun, 2011) 063609.

[40] S. R. Das, D. A. Galante, and R. C. Myers, *Universality in fast quantum quenches*, JHEP **1502** (2015) 167, [arXiv:1411.7710].

[41] I. Bakas and E. Kiritsis, *Bosonic Realization of a Universal W Algebra and Z(infinity) Parafermions*, Nucl. Phys. **B343** (1990) 185–204. [Erratum: Nucl. Phys.B350,512(1991)].

[42] A. Duncan, *Explicit Dimensional Renormalization of Quantum Field Theory in Curved Space-Time*, Phys. Rev. **D17** (1978) 964.

[43] A. Perelomov, Generalized Coherent States and Their Applications. Modern Methods of Plant Analysis. Springer-Verlag, 1986.

[44] P. Calabrese and J. Cardy, *Time Dependence of Correlation Functions Following a Quantum Quench*, Physical Review Letters **96** (Apr., 2006) 136801, [cond-mat/0601225].

[45] E. Koelnik, *Scattering theory*, . Lecture notes, Section 4, http://www.math.ru.nl/ koelink/edu/LM-dictaat-scattering.pdf.

[46] A. Almheiri, D. Marolf, J. Polchinski, and J. Sully, *Black Holes: Complementarity or Firewalls?*, JHEP **1302** (2013) 062, [arXiv:1207.3123].

[47] A. Almheiri, D. Marolf, J. Polchinski, D. Stanford, and J. Sully, *An Apologia for Firewalls*, JHEP **1309** (2013) 018, [arXiv:1304.6483].

[48] S. L. Braunstein, S. Pirandola, and K. yczkowski, *Better Late than Never: Information Retrieval from Black Holes*, Phys.Rev.Lett. **110** (2013), no. 10 101301, [arXiv:0907.1190].

[49] S. H. Shenker and D. Stanford, *Black holes and the Butterfly Effect*, JHEP **1403** (2014) 067, [arXiv:1306.0622].

[50] M. Van Raamsdonk, *Evaporating Firewalls*, arXiv:1307.1796.

[51] D. Marolf and J. Polchinski, *Gauge/Gravity Duality and the Black Hole Interior*, Phys.Rev.Lett. **111** (2013) 171301, [arXiv:1307.4706].

[52] K. Papadodimas and S. Raju, *State-Dependent Bulk-Boundary Maps and Black Hole Complementarity*, Phys.Rev. **D89** (2014) 086010, [arXiv:1310.6335].

[53] K. Papadodimas and S. Raju, *The Black Hole Interior in AdS/CFT and the Information Paradox*, Phys.Rev.Lett. **112** (2014) 051301, [arXiv:1310.6334].

[54] S. H. Shenker and D. Stanford, *Multiple Shocks*, arXiv:1312.3296.

[55] S. G. Avery and B. D. Chowdhury, *No Holography for Eternal AdS Black Holes*, arXiv:1312.3346.

[56] V. Balasubramanian, M. Berkooz, S. F. Ross, and J. Simon, *Black Holes, Entanglement and Random Matrices*, arXiv:1404.6198.

[57] R. K. Gupta and A. Mukhopadhyay, *On the Universal Hydrodynamics of Strongly Coupled CFTs with Gravity Duals*, JHEP **0903** (2009) 067, [arXiv:0810.4851].

[58] T. Regge and C. Teitelboim, *Role of Surface Integrals in the Hamiltonian Formulation of General Relativity*, Annals Phys. **88** (1974) 286.

[59] S. Wadia, *Canonical Quantization of Non-Abelian Gauge Theory in the Schrodinger Picture: Applications to Monopoles and Instantons*, Ph.D. Thesis (1979).

[60] J.-L. Gervais, B. Sakita, and S. Wadia, *The Surface Term in Gauge Theories*, Phys.Lett. **B63** (1976) 55.

[61] J. D. Brown and M. Henneaux, *Central Charges in the Canonical Realization of Asymptotic Symmetries: An Example from Three-Dimensional Gravity*, Commun.Math.Phys. **104** (1986) 207–226.

[62] M. M. Roberts, *Time Evolution of Entanglement Entropy from a Pulse*, JHEP **1212** (2012) 027, [arXiv:1204.1982].

[63] S. Ryu and T. Takayanagi, *Holographic Derivation of Entanglement Entropy from AdS/CFT*, Phys.Rev.Lett. **96** (2006) 181602, [hep-th/0603001].

[64] S. Bhattacharyya, V. E. Hubeny, R. Loganayagam, G. Mandal, S. Minwalla, et al., *Local Fluid Dynamical Entropy from Gravity*, JHEP **0806** (2008) 055, [arXiv:0803.2526].

[65] S. Bhattacharyya, V. E. Hubeny, S. Minwalla, and M. Rangamani, *Nonlinear Fluid Dynamics from Gravity*, JHEP **0802** (2008) 045, [arXiv:0712.2456].

[66] J. L. Cardy, *Operator Content of Two-Dimensional Conformally Invariant Theories*, Nucl.Phys. **B270** (1986) 186–204.

[67] A. Maloney and E. Witten, *Quantum Gravity Partition Functions in Three Dimensions*, JHEP **1002** (2010) 029, [arXiv:0712.0155].

[68] M. R. Gaberdiel, *Constraints on Extremal Self-Dual CFTs*, JHEP **0711** (2007) 087, [arXiv:0707.4073].

[69] H. Afshar, A. Bagchi, S. Detournay, D. Grumiller, S. Prohazka, et al., *Holographic Chern-Simons Theories*, arXiv:1404.1919.

[70] E. Witten, *(2+1)-Dimensional Gravity as an Exactly Soluble System*, Nucl.Phys. **B311** (1988) 46.

[71] A. Campoleoni, S. Fredenhagen, S. Pfenninger, and S. Theisen, *Asymptotic symmetries of three-dimensional gravity coupled to higher-spin fields*, JHEP **1011** (2010) 007, [arXiv:1008.4744].

[72] M. Ammon, A. Castro, and N. Iqbal, *Wilson Lines and Entanglement Entropy in Higher Spin Gravity*, JHEP **1310** (2013) 110, [arXiv:1306.4338].

[73] J. de Boer and J. I. Jottar, *Entanglement Entropy and Higher Spin Holography in* AdS_3, arXiv:1306.4347.

[74] T. Ugajin, *Two dimensional quantum quenches and holography*, arXiv:1311.2562.

[75] V. Balasubramanian, P. Kraus, and A. E. Lawrence, *Bulk versus Boundary Dynamics in Anti-de Sitter Space-Time*, Phys.Rev. **D59** (1999) 046003, [hep-th/9805171].

[76] V. Balasubramanian, A. Bernamonti, J. de Boer, N. Copland, B. Craps, et al., *Thermalization of Strongly Coupled Field Theories*, Phys.Rev.Lett. **106** (2011) 191601, [arXiv:1012.4753].

[77] H. Liu and S. J. Suh, *Entanglement growth during thermalization in holographic systems*, Phys. Rev. **D89** (2014), no. 6 066012, [arXiv:1311.1200].

[78] S. Bhattacharyya and S. Minwalla, *Weak Field Black Hole Formation in Asymptotically AdS Spacetimes*, JHEP **0909** (2009) 034, [arXiv:0904.0464].

[79] E. Caceres, A. Kundu, J. F. Pedraza, and D.-L. Yang, *Weak Field Collapse in AdS: Introducing a Charge Density*, arXiv:1411.1744.

[80] P. Bizon and A. Rostworowski, *On weakly turbulent instability of anti-de Sitter space*, Phys.Rev.Lett. **107** (2011) 031102, [arXiv:1104.3702].

[81] O. J. Dias, G. T. Horowitz, and J. E. Santos, *Gravitational Turbulent Instability of Anti-de Sitter Space*, Class.Quant.Grav. **29** (2012) 194002, [arXiv:1109.1825].

[82] V. Balasubramanian, A. Buchel, S. R. Green, L. Lehner, and S. L. Liebling, *Holographic Thermalization, stability of AdS, and the Fermi-Pasta-Ulam-Tsingou paradox*, Phys.Rev.Lett. **113** (2014) 071601, [arXiv:1403.6471].

[83] P. Basu, C. Krishnan, and A. Saurabh, *A Stochasticity Threshold in Holography and and the Instability of AdS*, arXiv:1408.0624.

[84] B. Craps, O. Evnin, and J. Vanhoof, *Renormalization group, secular term resummation and AdS (in)stability*, JHEP **1410** (2014) 48, [arXiv:1407.6273].

[85] B. Craps, O. Evnin, and J. Vanhoof, *Renormalization, averaging, conservation laws and AdS (in)stability*, arXiv:1412.3249.

[86] S. Datta, J. R. David, M. Ferlaino, and S. P. Kumar, *Universal correction to higher spin entanglement entropy*, Phys.Rev. **D90** (2014), no. 4 041903, [arXiv:1405.0015].

[87] P. Calabrese and J. Cardy, *Quantum quenches in extended systems*, Journal of Statistical Mechanics: Theory and Experiment **6** (June, 2007) 8, [arXiv:0704.1880].

[88] G. Mandal and N. Sorokhoibam, *In preparation*, .

[89] G. Mandal and S. Thakur, *In preparation*, .

[90] P. Calabrese and J. Cardy, *Entanglement and correlation functions following a local quench: a conformal field theory approach*, Journal of Statistical Mechanics: Theory and Experiment **10** (Oct., 2007) 4, [arXiv:0708.3750].

[91] M. Nozaki, T. Numasawa, and T. Takayanagi, *Holographic Local Quenches and Entanglement Density*, JHEP **1305** (2013) 080, [arXiv:1302.5703].

[92] G. Mandal, R. Sinha, and T. Ugajin, *Quantum quench with defects and its holographic dual*, . In preparation.

[93] P. Calabrese and J. L. Cardy, *Entanglement entropy and quantum field theory*, J. Stat. Mech. **0406** (2004) P06002, [hep-th/0405152].

[94] P. Calabrese, J. Cardy, and E. Tonni, *Entanglement Entropy of Two Disjoint Intervals in conformal field theory II*, J.Stat.Mech. **1101** (2011) P01021, [arXiv:1011.5482].

[95] P. M. Chesler and L. G. Yaffe, *Horizon formation and far-from-equilibrium isotropization in supersymmetric Yang-Mills plasma*, Phys. Rev. Lett. **102** (2009) 211601, [arXiv:0812.2053].

[96] S. R. Das, T. Nishioka, and T. Takayanagi, *Probe Branes, Time-dependent Couplings and Thermalization in AdS/CFT*, JHEP **07** (2010) 071, [arXiv:1005.3348].

[97] V. Balasubramanian, A. Bernamonti, J. de Boer, N. Copland, B. Craps, E. Keski-Vakkuri, B. Muller, A. Schafer, M. Shigemori, and W. Staessens, *Holographic Thermalization*, Phys. Rev. **D84** (2011) 026010, [arXiv:1103.2683].

[98] F. H. L. Essler, G. Mussardo, and M. Panfil, *Generalized Gibbs Ensembles for Quantum Field Theories*, Phys. Rev. **A91** (2015), no. 5 051602, [arXiv:1411.5352].

[99] P. Calabrese, F. H. L. Essler, and M. Fagotti, *Quantum quenches in the transverse field Ising chain: II. Stationary state properties*, Journal of Statistical Mechanics: Theory and Experiment **7** (July, 2012) 22, [arXiv:1205.2211].

[100] T. Barthel and U. Schollwöck, *Dephasing and the Steady State in Quantum Many-Particle Systems*, Physical Review Letters **100** (Mar., 2008) 100601, [arXiv:0711.4896].

[101] M. Cramer, C. M. Dawson, J. Eisert, and T. J. Osborne, *Exact Relaxation in a Class of Nonequilibrium Quantum Lattice Systems*, Physical Review Letters **100** (Jan., 2008) 030602, [cond-mat/0703314].

[102] M. Rigol, V. Dunjko, and M. Olshanii, *Thermalization and its mechanism for generic isolated quantum systems*, Nature **452** (Apr., 2008) 854–858, [arXiv:0708.1324].

[103] A. Iucci and M. A. Cazalilla, *Quantum quench dynamics of the Luttinger model*, Physical **80** (2009) 063619, [arXiv:1003.5170].

[104] D. Fioretto and G. Mussardo, *Quantum quenches in integrable field theories*, New Journal of Physics **12** (May, 2010) 055015, [arXiv:0911.3345].

[105] P. Calabrese, F. H. L. Essler, and M. Fagotti, *Quantum quench in the transverse field Ising chain: I. Time evolution of order parameter correlators*, Journal of Statistical Mechanics: Theory and Experiment **7** (July, 2012) 16, [arXiv:1204.3911].

[106] B. Bertini, D. Schuricht, and F. H. L. Essler, *Quantum quench in the sine-Gordon model*, Journal of Statistical Mechanics: Theory and Experiment **10** (Oct., 2014) 35, [arXiv:1405.4813].

[107] S. R. Das, D. A. Galante, and R. C. Myers, *Universal scaling in fast quantum quenches in conformal field theories*, Phys.Rev.Lett. **112** (2014) 171601, [arXiv:1401.0560].

[108] N. Birrell and P. Davies, Quantum Fields in Curved Space. Cambridge Monographs on Mathematical Physics. Cambridge University Press, 1984.

[109] D. Das and S. Das, *Unpublished*, .

[110] S. R. Das, D. A. Galante, and R. C. Myers, *Smooth and fast versus instantaneous quenches in quantum field theory*, JHEP **08** (2015) 073, [arXiv:1505.05224].

[111] S. Sotiriadis and J. Cardy, *Quantum quench in interacting field theory: A Self-consistent approximation*, Phys. Rev. **B81** (2010) 134305, [arXiv:1002.0167].

[112] M. Abramowitz and I. Stegun, Handbook of Mathematical Functions. Dover Publications, 1965.

[113] L. Landau and E. Lifshit s, Quantum Mechanics: Non-relativistic Theory. Butterworth Heinemann. Butterworth-Heinemann, 1977.

[114] M. V. Berry, *Semiclassically weak reflections above analytic and non-analytic potential barriers*, Journal of Physics A: Mathematical and General **15** (1982), no. 12 3693.

[115] S. D. Mathur, *Is the Polyakov path integral prescription too restrictive?*, hep-th/9306090.

[116] B. Craps, D-branes and boundary states in closed string theories. PhD thesis, Leuven U., 2000. hep-th/0004198.

[117] E. Bergshoeff, C. N. Pope, L. J. Romans, E. Sezgin, and X. Shen, *The Super W(infinity) Algebra*, Phys. Lett. **B245** (1990) 447–452.

[118] M. Fagotti and P. Calabrese, *Evolution of entanglement entropy following a quantum quench: Analytic results for the xy chain in a transverse magnetic field*, Phys. Rev. A **78** (Jul, 2008) 010306.

[119] J. Schachenmayer, B. P. Lanyon, C. F. Roos, and A. J. Daley, *Entanglement growth in quench dynamics with variable range interactions*, Phys. Rev. X **3** (Sep, 2013) 031015.

[120] M. Ghasemi Nezhadhaghighi and M. A. Rajabpour, *Entanglement dynamics in short and long-range harmonic oscillators*, Phys. Rev. **B90** (2014), no. 20 205438, [arXiv:1408.3744].

[121] A. Nahum, J. Ruhman, S. Vijay, and J. Haah, *Quantum Entanglement Growth Under Random Unitary Dynamics*, arXiv:1608.06950.

[122] J. S. Cotler, M. P. Hertzberg, M. Mezei, and M. T. Mueller, *Entanglement Growth after a Global Quench in Free Scalar Field Theory*, arXiv:1609.00872.

[123] J. Abajo-Arrastia, J. Aparicio, and E. Lopez, *Holographic Evolution of Entanglement Entropy*, JHEP **11** (2010) 149, [arXiv:1006.4090].

[124] S. Kundu and J. F. Pedraza, *Spread of entanglement for small subsystems in holographic CFTs*, arXiv:1602.05934.

[125] X. Bai, B.-H. Lee, L. Li, J.-R. Sun, and H.-Q. Zhang, *Time Evolution of Entanglement Entropy in Quenched Holographic Superconductors*, JHEP **04** (2015) 066, [arXiv:1412.5500].

[126] C. Holzhey, F. Larsen, and F. Wilczek, *Geometric and renormalized entropy in conformal field theory*, Nucl. Phys. **B424** (1994) 443–467, [hep-th/9403108].

[127] H. Casini, C. D. Fosco, and M. Huerta, *Entanglement and alpha entropies for a massive Dirac field in two dimensions*, J. Stat. Mech. **0507** (2005) P07007, [cond-mat/0505563].

[128] D. Senechal, *An Introduction to bosonization*, in CRM Workshop on Theoretical Methods for Strongly Correlated Fermions Montreal, Quebec, C 1999. cond-mat/9908262.

[129] J. von Delft and H. Schoeller, *Bosonization for beginners: Refermionization for experts*, Annalen Phys. **7** (1998) 225–305, [cond-mat/9805275].